1.0

1.1

1.25   1.4   1.6

2.8   2.5

3.2   2.2

3.6

4.0   2.0

1.8

MICROCOPY RESOLUTION TEST CHART

AFFDL-TR-77-21

② **LEVEL** II

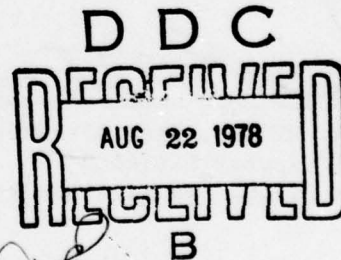# INTEGRATION OF AIR CUSHION LANDING SYSTEM TECHNOLOGY INTO THE JINDIVIK REMOTELY PILOTED VEHICLE

BOEING AEROSPACE COMPANY
P. O. BOX 3999
SEATTLE, WASHINGTON 98124

MARCH 1978

D D C

RECEIVED

AUG 22 1978

B

TECHNICAL REPORT AFFDL-TR-77-21
Final Report for Period April 1975 — January 1977

AIR FORCE FLIGHT DYNAMICS LABORATORY
AIR FORCE WRIGHT AERONAUTICAL LABORATORIES
AIR FORCE SYSTEMS COMMAND
WRIGHT-PATTERSON AIR FORCE BASE, OHIO 45433

78 08 04 005

JAMES T. STEIGER
Project Engineer

AIVARS V. PETERSONS, Actg Chief
Mechanical Branch
Vehicle Equipment Division
Air Force Flight Dynamics Laboratory

FOR THE COMMANDER

SOLOMON R. METRES, Actg Director
Vehicle Equipment Division
Air Force Flight Dynamics Laboratory

AIR FORCE/56780/26 July 1978 — 250

REPORT DOCUMENTATION PAGE	READ INSTRUCTIONS BEFORE COMPLETING FORM

1. REPORT NUMBER	2. GOVT ACCESSION NO.	3. RECIPIENT'S CATALOG NUMBER
AFFDL-TR-77-21		

4. TITLE (and Subtitle)	5. TYPE OF REPORT & PERIOD COVERED
INTEGRATION OF AIR CUSHION LANDING SYSTEM TECHNOLOGY INTO THE JINDIVIK REMOTELY PILOTED VEHICLE.	FINAL TECHNICAL REPORT APRIL 1975 - JAN. 1977
	6. PERFORMING ORG. REPORT NUMBER

7. AUTHOR(s)	8. CONTRACT OR GRANT NUMBER(s)
A. J. P. Lloyd, J. J. McAvoy, V. K. Rajpaul	F33615-75-C-3088

9. PERFORMING ORGANIZATION NAME AND ADDRESS	10. PROGRAM ELEMENT, PROJECT, TASK AREA & WORK UNIT NUMBERS
Boeing Aerospace Company P.O. Box 3999 Seattle, Washington 98124	24630111 04

11. CONTROLLING OFFICE NAME AND ADDRESS	12. REPORT DATE
Air Force Flight Dynamics Laboratory Air Force Systems Command Wright Patterson Air Force Base, Ohio 45433	March 1978
	13. NUMBER OF PAGES
	310 p.

14. MONITORING AGENCY NAME & ADDRESS(if different from Controlling Office)	15. SECURITY CLASS. (of this report)
	Unclassified
	15a. DECLASSIFICATION/DOWNGRADING SCHEDULE

16. DISTRIBUTION STATEMENT (of this Report)

62201F

Approved for public release; distribution unlimited

17. DISTRIBUTION STATEMENT (of the abstract entered in Block 20, if different from Report)

Final rept. Apr 75-Jan 77,

18. SUPPLEMENTARY NOTES

19. KEY WORDS (Continue on reverse side if necessary and identify by block number)

Air Cushion Landing Systems
RPV
Launch
Recovery

20. ABSTRACT (Continue on reverse side if necessary and identify by block number)

Studies have been conducted on an Air Cushion Landing System for the Australian Jindivik target drone aircraft. Analyses are presented of the airflow and yaw thruster control systems, and the vehicle stability with a deployed recovery trunk is assessed. The vehicle touchdown and slideout on a recovery trunk are presented, and the design of an improved retention/release system is shown.

DD FORM 1473 EDITION OF 1 NOV 63 IS OBSOLETE
1 JAN 73

78 08 04 005

059610

FOREWORD

This report presents the results of work conducted by the Boeing
Aerospace Company, P.O. Box 3999, Seattle, Washington 98124, on
the Integration of an Air Cushion Landing System into the
Australian Jindivik target drone. Contract number was F33615-
75-C-3088, Project Number was 2402, and the Task Number was 01.
The contract was conducted under the sponsorship of the Air
Force Flight Dynamics Laboratory. Project Engineers during the
course of the contract were L/Col. J. C. Vaughan, Capt. J. R.
Cooper, G. J. Shumaker and J. T. Steiger (AFFDL/FEM).

The work reported herein was conducted between April 1975 and
January 1977. This report was submitted by the authors in
August 1977.

iii

TABLE OF CONTENTS

TABLE OF CONTENTS (Continued)

LIST OF ILLUSTRATIONS

LIST OF ILLUSTRATIONS (Continued)

LIST OF TABLES

LIST OF ABBREVIATIONS AND SYMBOLS

ABBREVIATIONS

ACLS	Air Cushion Landing System
ACRS	Air Cushion Recovery System
ACTS	Air Cushion Takeoff System
AFFDL	Air Force Flight Dynamics Laboratory
BAC	Boeing Aerospace Company
DOF	Degrees of Freedom
GAF	Government Aircraft Factory
IGE	In Ground Effect
LaRC	Langley Research Center
LeRC	Lewis Research Center
MMRPV	Multi-Mission Remotely Piloted Vehicle
NASA	National Aeronautics and Space Administration
OGE	Out of Ground Effect
RPV	Remotely Piloted Vehicle
TVCS	Thrust Vector Control System

SYMBOLS

A	Area	sq. in.
A_b	Effective cross sectional area of bottom of trunk	sq. ft.
A_c	Cushion area	sq. in.
A_{cc}	Cross sectional area of cushion volume	sq. in.
A_f	Frontal area of trunk	sq. ft.
A_{fp}	Footprint area of trunk	sq. ft.
A_g	Area of gap under trunk	sq. ft.
A_j	Trunk peripheral air jet orifice area	sq. ft
A_n	Engine compressor bleed port area	sq. in.
A_{rel}	Relief valve area	sq. in.

xvi

SYMBOLS

A_s	Area of sector of trunk element	ft^2
A_t	Trunk foot print area	sq. in.
AZI	Azimuth	deg.
a	Acceleration	
b	Wing span	ft.
c or $\bar{c}$	Mean aerodynamic chord	ft.
C	Trunk element chord length	ft.
CA_t	Cross sectional area of trunk element	sq. ft.
cb	Center of braking	---
cd	Center of aero drag	---
C_D	Coefficient of drag or orifice discharge coefficient	---
cg	Center of gravity	---
C_ℓ	Aerodynamic roll moment coefficient	---
$C_{L\alpha_H}$	Horizontal tail lift coefficient	---
C_{ℓ_β}	Roll moment coefficient slope due to side slip	---
C_{ℓ_ζ}	Roll moment coefficient slope due to ailerons	---
C_L	Aerodynamic coefficient of lift	---
C_m	Aerodynamic pitch moment coefficient	---
$C_{m_{q_H}}$	Damping coefficient due to horizontal tail	---
C_{m_η}	Pitch moment slope due to elevator	---
C_n	Aerodynamic yaw moment coefficient	---
C_{n_β}	Yaw moment coefficient slope due to side slip	---
cp	Center of cushion pressure	---
C_Y	Aerodynamic side force coefficient	---
C_{Y_β}	Side force coefficient slope due to side slip	---
C_θ	Pitch damping coefficient	ft-lbs-sec/deg
C_ϕ	Roll damping coefficient	ft-lbs-sec/deg

xvii

SYMBOLS

$(C_\psi)_{ac}$	Engine gyro couple coefficient	ft-lbs-sec/deg
d	Deflection	in.
D	Trunk element OGE diameter	ft.
E	Modulus of elasticity	lbs/sq. in.
F	Force	lbs.
F_c	Cable force	lbs.
F_d	Drag force	lbs.
F_ℓ	Lift force	lbs.
F_{ℓ_n}	Perpendicular force on trunk	lbs.
F_p	Parallel force on trunk	lbs.
F_x	Longitudinal Component of force	lbs.
F_{td}	Trunk braking force	lbs.
F_{th}	Engine thrust	lbs.
F_{tv}	Vectored thrust	lbs.
F_y	Lateral Component of force	lbs.
F_μ	Frictional force	lbs.
f_m	Momentum factor for jetted air at trunk ground interface	---
g	Acceleration due to gravity	ft/sec^2
H_a	Aileron Hinge Moment	ft-lbs
H_e	Elevator Hinge Moment	ft-lbs
h_{cg}	Height of aircraft center of gravity	ft.
I_a	Aileron rotational moment of inertia	$slug-ft^2$
I_e	Elevator rotational moment of inertia	$slug-ft^2$
I_{xx}	Aircraft roll moment of inertia	$slug-ft^2$
I_{yy}	Aircraft pitch moment of inertia	$slug-ft^2$
I_{zz}	Aircraft yaw moment of inertia	$slug-ft^2$
K	Pressure drop K-factor	---
K_ϕ	Roll Stiffness coefficient	ft-lbs/deg
K_θ	Pitch stiffness coefficient	ft-lbs/deg
L	Aerodynamic lift	lbs.
ℓ	length	ft. or in.
ℓ_{cb}	Distance between aircraft CG and	

SYMBOLS

	center of drag	ft.
M_x	Roll moment	ft-lbs
M_y	Pitch moment	ft-lbs
M_z	Yaw moment	lbs
m	Air mass	lbs
N	Engine compressor speed	RPM
N_D	Engine compressor maximum design speed	RPM
P	Cable Tension	lbs.
P_1	Compressor inlet pressure	psia
P_{2S}	Compressor outlet static pressure	psia
P_B	Bleed air total pressure down-steam of port	psia
P_t	Trunk air pressure	psig
P_c	Cushion air pressure	psig
q	Air flow velocity head or aircraft pitch rate	psig deg/sec
r	Trunk side element inner radius	ft.
r_d	Trunk side element out of ground effect radius	ft.
S	Aircraft wing reference area or stroke of trunk element	sq. ft. ft.
S_H	Horizontal tail area	sq. ft.
T_1	Compressor inlet temperature	$^\circ R$
T_2	Compressor outlet temperature	$^\circ R$
V	Velocity	ft.sec or knots
V_c	Cushion volume	cu ft.
V_H	Horizontal tail volume coefficient	---
V_r	ACTS trunk release velocity	ft/sec
V_t	Trunk volume	cu ft.
V_{to}	Aircraft takeoff velocity	ft/sec
V_x	Velocity of aircraft parallel to runway	ft/sec
W	Air flow rate	lbs/sec
W_a	Aircraft weight	lbs.
W_b	Bleed air flow rate	lbs/sec

SYMBOLS

W_t	Trunk weight	lbs.
X_H	Distance from aircraft cg to horizontal tail	ft.
X_t	Axial distance from aircraft cg to trunk element	ft.
Y_a	Lateral distance from trunk element lower attachment point to aircraft centerline	ft.
Y_c	Lateral distance from trunk element lower attachment point to center of flattened area	ft.
Y_f	Width of trunk element flattened area	ft.
Y_t	Lateral distance from aircraft cg to trunk element lowermost point	ft.
y	Lateral drift	ft.
z	Distance between cg and ground	ft.
z_a	Vertical distance from aircraft cg to trunk lowermost attachment point	ft.
z_{cg}	Vertical distance between aircraft cg and flattened area of trunk element	ft.
z_t	Vertical distance between lowermost attachment point and lowermost point of OGE trunk element	ft.
z_0	Vertical distance between lowermost attachment point and lowermost point of trunk element	ft.
z_∞	Vertical distance between lowermost attachment point and lowermost point of OGE trunk element (used in ratio z_0/z_∞)	ft.
α	Aircraft angle of attack	deg.

SYMBOLS

β	Aircraft aerodynamic side slip	deg.
γ	Angle of relative wind direction relative to runway centerline	deg.
	or adiabatic gas constant	---
δ	Air pressure ratio	---
δ_a	Aileron deflection	deg.
δ_e	Elevator delfection	deg.
δ_f	Flap deflection	deg.
ζ	Aircraft course angle relative to runway centerline	deg.
η_H	Dynamic pressure ratio for horizontal tail	---
θ	Temperature ratio	---
	or aircraft pitch angle	deg.
θ_c	Chord angle	deg.
θ_s	Auto pilot set pitch angle	deg.
λ_H	Horizontal tail taper ratio	---
Λ	Wing sweep angle	deg.
μ	Coefficient of friction	---
μ_t	Trunk drag coefficient of friction	---
ρ	Density	lbs/cu ft.
τ	Time	sec.
ϕ	Aircraft roll angle	deg.
ϕ_s	Auto pilot set roll angle	deg.
ϕ_{sc}	Skid contact roll angle	deg.
ψ	Aircraft yaw angle	deg.

SYMBOLS

ψ_r	Yaw gyro reference angle	deg.

SUBSRIPTS

amb	Ambient
c	Cushion
cb	Center of braking
f	Flattened
gc	Gyro coupler
i	ith element
l	Left side
o	Non flattened
r	Right side
ram	Ram air
t	Trunk
tv	Thrust vector
ws	Wing tip skid
x	Axial component
y	Lateral component

SUPERSCRIPT

	Differential with respect to time sec^{-1}

SUMMARY

This report describes progress in the development of an ACLS for
the Jindivik target drone in the period April 1975 to January
1977. The major activities in this time period were a series of
ground tests at the Avalon Field test facility of GAF, the
testing of the retention/release system at NASA/LaRC, and the
running of wind tunnel tests of Jindivik with a deployed
recovery trunk at the Australian Aeronautical Research
Laboratories. Boeing, as a technical consultant to AFFDL,
conducted detailed analyses of the airflow system and yaw
thruster directional control system, monitored the ground tests,
simulated the approach and landing of Jindivik on the recovery
trunk, redesigned the retention/release system, and evaluated
the effect of the ACLS on the aerodynamic stability of Jindivik.

Section 2 of this report evaluates the performance of the
airflow system, compares test data and analytical predictions,
and makes recommendations for improving the system. Section 3
presents an analysis of the performance of the yaw thruster
control system on both the takeoff and recovery trunk. The
effect of the ground controller (or "batsman") on the vehicle
directional control during a takeoff roll is assessed. Section
4 evaluates the aerodynamic stability of Jindivik with a
deployed recovery trunk, and makes recommendations for further
wind tunnel testing. The basic vehicle is unstable with a
deployed trunk, and hence modifications will be required.
Section 5 presents the results of a six degrees of freedom
computer analysis of landing and slideout on the recovery trunk.
Forward pitching immediately following touchdown was determined
to be a potential problem area. Section 6 presents the analysis
and design of a positive retention/release system to replace the
current velcro design. The latter was found to be potentially

unsatisfactory in that some separation occurred during ACTS deceleration in the ground tests, and also because testing at NASA/LaRC showed that inflight separation did not occur uniformly and repeatably. Section 7 presents an overview of the ground testing conducted at the GAF Avalon Field facility, and Section 8 presents the overall conclusions and recommendations arising from this phase of the development of an ACLS for Jindivik.

SECTION 1

INTRODUCTION

The role of RPV's in performing combat, reconnaissance, and electronic surveillance for the Air Force is an expanding one, limited only by the ability to perform the various missions on a cost effective basis using available technology. This is motivating the exploration of technologies by which costs of present RPV systems can be reduced or their mission roles expanded in terms of operational flexibility. The future missions performed using advanced RPV systems will be largely determined by the total life cycle costs of these systems.

A significant portion of the RPV life cycle costs is due to the launch and recovery methods. Substantial costs are attributable to disposable hardware such as rocket motors and high density pre-packed parachutes. These costs are lowered when the launch and recovery system permits a reduction in the number of required vehicles and personnel due to reduced turn-around time and simpler maintenance. A recovery system having positive vehicle control (as opposed to a parachute system) reduces the rate of attrition and hence the total number of vehicles procured. Reduced launch and recovery costs also increase the operational readiness of a squadron by encouraging more actual training flights and less simulator training.

There are many options available for launch and recovery. Launch can be effected by catapult or rocket assist, conventional self-propelled methods using wheels, air drops from carrier aircraft, etc. The recovery options include mid-air retrieval by helicopters, mid-air docking, parachute descent, or skid landing on prepared runways. A highly desirable method of launch and recovery would be a common system for both takeoff or landing, which would be low in cost per sortie, reduce

1

dependence on paved runways, have a long life, and which would minimize weight, volume, and operating penalty for the air vehicle. A system potentially offering these specific advantages over many other currently used lauch and recovery methods is now accepted to be that based on air cushion technology.

The air cushion launch and recovery systems (ACLS), though not completely developed into a mature technology, hold great promise in providing the solution to existing costly or complicated launch and recovery techniques. It is perfectly conceivable that with a reasonable amount of engineering developmental effort over the next few years, ACLS could provide landing or takeoff capability from unprepared terrain or water, be low in penalty to the vehicle performance, and provide substantially improved life cycle costs. This technology would then be of great benefit to the definition of multi-mission operational roles of future RPV's.

The Air Force Flight Dynamics Laboratory (AFFDL) has recognized the potential of ACLS technology, and has pioneered its development through both contracted and in-house programs. AFFDL has selected the Jindivik, an Australian target drone manufactured by GAF, as a test vehicle for developing ACLS technology for direct application to future RPV's, such as the USAF MMRPV program.

The Jindivik ACLS includes many promising new ACLS concepts which require testing. These include:

o Use of the main engine as a source of air for the ACLS
o Incorporation of a hub driven fan to augment the flow, thereby providing a match between the high pressure low flow source, and the low pressure high flow requirement of the ACLS

2

o Use of inexpensive, inelastic trunk materials for the ACLS
  trunks
o Separate takeoff and landing trunks, with the takeoff trunk
  being jettisoned following takeoff, to eliminate the inflight
  retraction problem
o Rapid braking capability provided by the recovery trunk
  design, thereby reducing landing field length
o Simple engine exhaust deflector system, using the Coanda
  effect on nozzle mounted end plates, to provide yaw control
  during ground operation

Many organizations have been involved in this phase of the
development of the Jindivik ACLS. AFFDL has been prime
contractor with overall program direction and control. B. F.
Goodrich has built the trunks, and Chandler-Evans the yaw
thruster directional control system. The latter has been tested
at NASA/LaRc. Tech Development Inc. has built the hub driven
turbofan. NASA/LaRc has tested the retention/release system.
GAF has assembled the ACLS on the Jindivik test vehicle, and has
conducted the ground tests in Australia. Boeing Aerospace
Company (BAC) has acted as consultants to AFFDL.

This report describes work conducted by BAC during the period
April 1975 through January 1977. The major tasks originally
assigned to BAC were:

(1) To monitor the ground tests run by GAF
(2) To evaluate GAF wind tunnel data
(3) To develop plans for a flight test program
(4) To evaluate flight test data obtained by GAF
(5) To determine any additional technology needed to
     transition the new technology to a current or
     proposed USAF RPV.

Various developmental problems, typical of a new technology and
described elsewhere in this report, were encountered by GAF

during the ground tests. As a result, these tests were only partially complete when they were terminated in mid 1976, a year behind schedule. Consequently, it was not possible to complete the required analyses and planning for subsequent flight testing in Australia within the time constraints of this contract. Significant progress has, however, been made. The yaw thruster directional control system has been analyzed and tested, and appears to work satisfactorily. The effect of the recovery trunk on the aerodynamic characteristics of the Jindivik vehicle has been determined, based on wind tunnel data supplied by GAF. Recommendations for further wind tunnel testing have been made. A new retention/release system has been analyzed and designed for the takeoff trunk, and six degrees of freedom computer analyses have been run on touchdown and slideout on the ACRS trunk.

4

SECTION 2

AIRFLOW ANALYSIS

2.1 SYSTEM DESCRIPTION

Figure 1 shows schematics of the airflow system for the
Jindivik ACRS and ACTS. Air is bled from a tapping on the
delivery casing of the Bristol Siddeley (now Rolls Royce Ltd.)
Viper 11/201 turbojet engine. The bleed air flows through a
bleed port fitting which penetrates the vehicle fuselage, and
thence forward through a flexible duct mounted externally on
the fuselage. The ducting then reenters the fuselage, and the
flow splits at a Y junction. For the ACRS, one branch supplies
direct bleed air to the trunk, while the other branch supplies
air to the hub section of a hub driven turbofan. Motor
operated shutoff valves are installed in both lines.
Overpressurization of the trunk is prevented by a relief valve
which exhausts to ambient. For the ACTS, the valve in the line
supplying the ACRS trunk (#1 in Figure 1) is closed, and all
the bleed air flows into the turbofan. The augmented air
exiting the turbofan is discharged through a transition section
into the trunk. An approximate layout of the airflow system is
shown in Figure 2.

The Jindivik airflow system has several significant innovations
in ACLS technology. Integration of the system with the main
engine results in considerable costs and weight savings over
systems with separate air sources such as on the Buffalo CC-115
aircraft. The use of a hub driven turbofan results in a
relatively efficient match between the high flow, low pressure
demand of the ACLS, and the low flow, high pressure capability
of the Viper 11/201 engine. On the ACTS the cushion air is
supplied by inward facing nozzles (45° to the vertical) on the

5
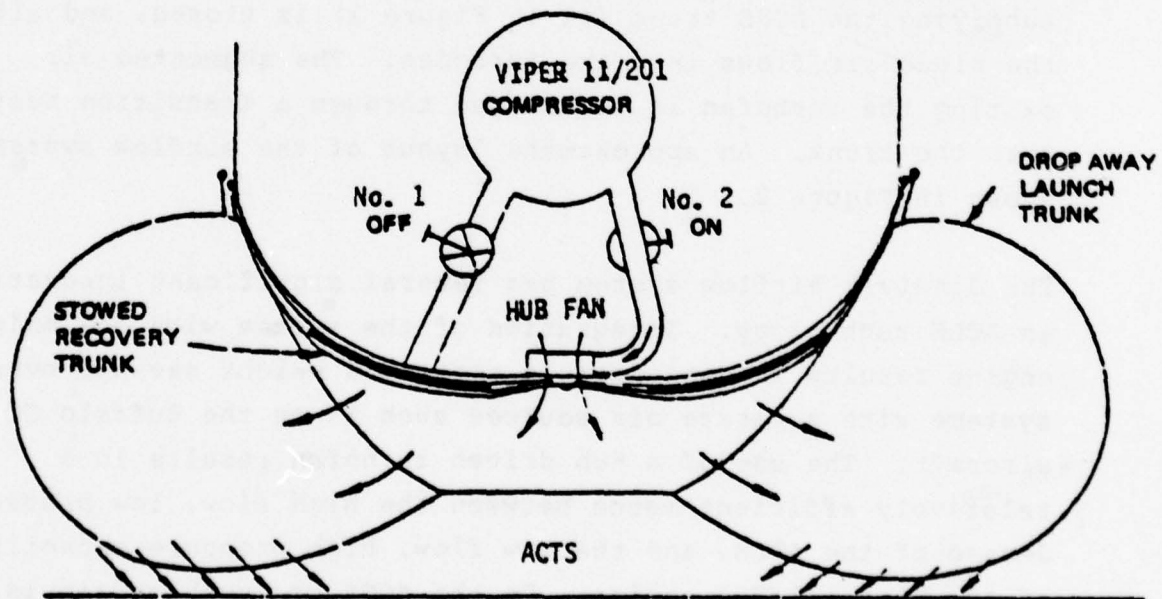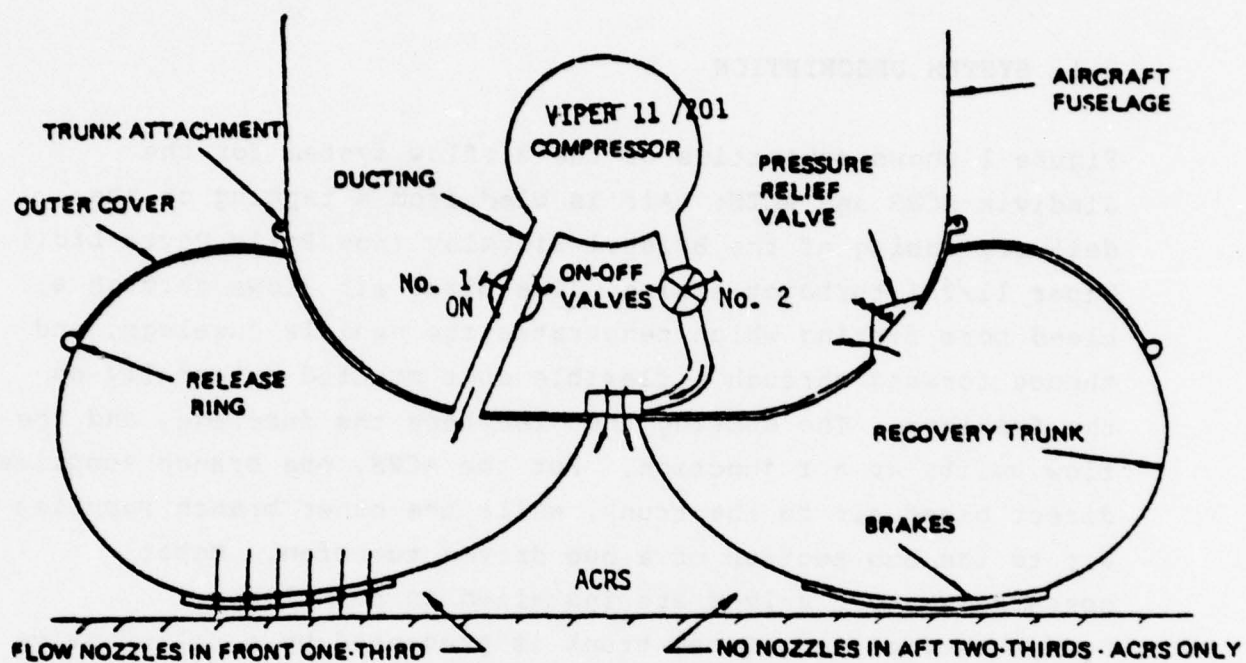
Figure 1   ACTS and ACRS Airflow Schematic

BLEED PORT FITTING

SIDE VIEW

BLOW UP OF BLEED
PORT FITTING

TOP VIEW

FLEXIBLE DUCTING

Y-JUNCTION

MOTOR OPERATED
SHUTOFF VALVES

TRANSITION SECTION

TURBOFAN
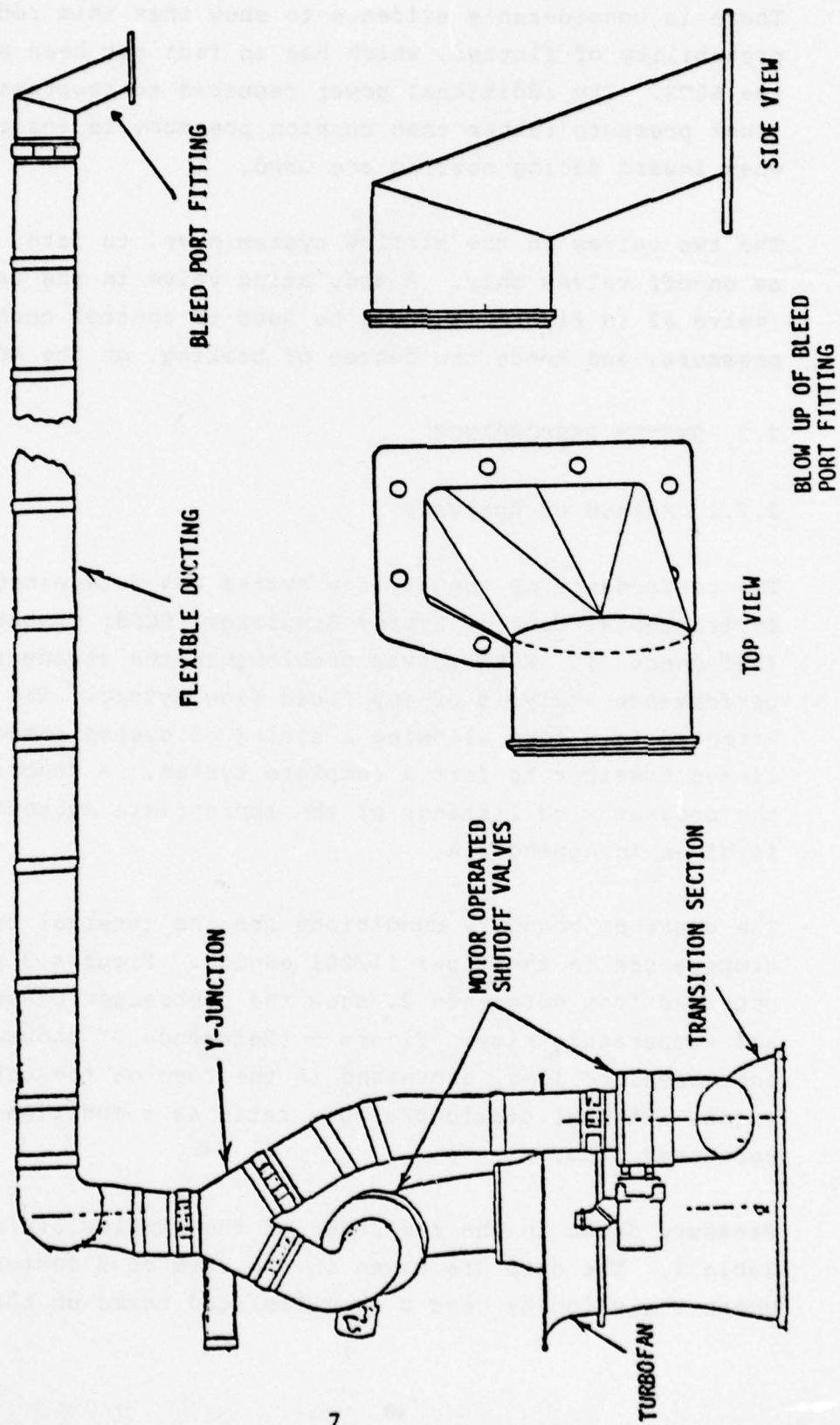
Figure 2   Airflow System Layout

7

trunk, rather than by direct discharge into the cushion volume. There is considerable evidence to show that this reduces the probability of flutter, which has in fact not been a problem on the ACTS. The additional power required to compress the air to trunk pressure rather than cushion pressure is insignificant when inward facing nozzles are used.

The two valves in the airflow system have, to date, been used as on-off valves only. A modulating valve in the fan line (valve #2 in Figure 1) could be used to control cushion pressure, and hence the degree of braking, on the ACRS.

2.2 SYSTEM PERFORMANCE

2.2.1 Method of Analysis

The performance of the airflow system was determined using the Environmental Control System Simulator (ECSS) Computer Program (Reference 1). ECSS solves problems in the steady state performance analysis of any fluid flow system. The program is arranged in a form allowing a series of system components to be linked together to form a complete system. A description of the program with listings of the appropriate subroutines is given in Appendix A.

The upstream boundary conditions are the internal pressures and temperature in the Viper 11/201 engine. Figures 3 and 4, obtained from Reference 2, show the compressor pressure ratio and temperature rise. Figure 5 (Reference 3) shows the bleed port pressure loss, expressed in the form of the ratio of engine internal static pressure ratio as a function of corrected flow.

Pressure drops in the remainder of the airflow are defined in Table 1. The data are given in the form of K factors ($K = \Delta P/q$) where the velocity head q is calculated based on the given

8

COMPRESSOR PRESSURE RATIO $\frac{P_{25}}{P_1}$

T_1 COMPRESSOR INLET TEMPERATURE, °R

P_1 COMPRESSOR INLET PRESSURE, PSIA

P_{25} COMPRESSOR OUTLET STATIC PRESSURE, PSIA

$\frac{N}{N_D}$ $\dfrac{\text{COMPRESSOR SPEED}}{\text{ENGINE COMPRESSOR MAXIMUM DESIGN SPEED}}$

MACH NO. = 0
NO INTAKE LOSSES

ENGINE RELATIVE SPEED $\quad \frac{N}{N_D} \sqrt{\frac{518.7}{T_1}}$
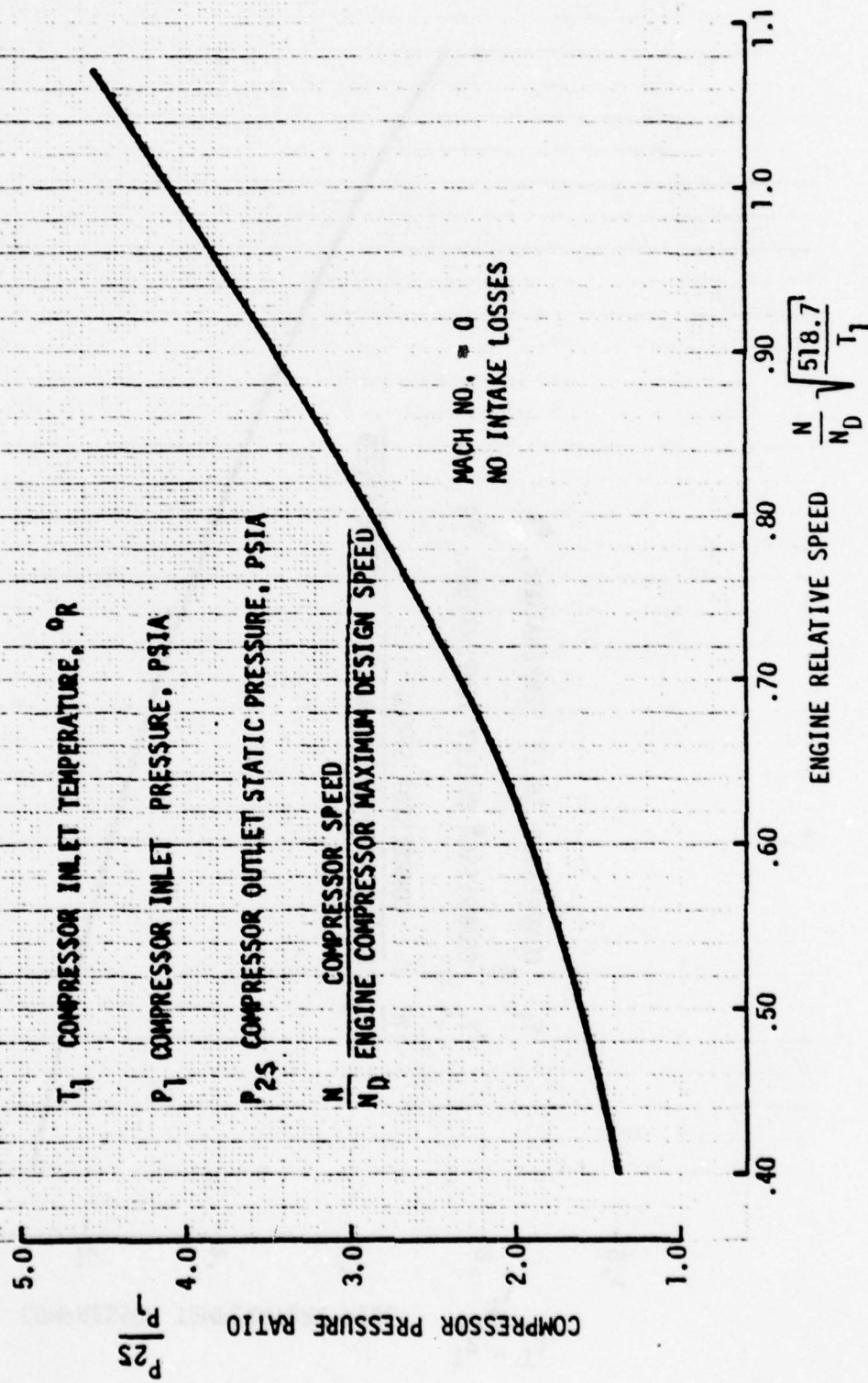
Figure 3 Engine Compressor Ratio

6

T_1 COMPRESSOR INLET TEMPERATURE, °R

T_2 COMPRESSOR OUTLET TEMPERATURE, °R

$\dfrac{N}{N_D}$ $\dfrac{\text{COMPRESSOR SPEED}}{\text{ENGINE COMPRESSOR MAXIMUM DESIGN SPEED}}$

COMPRESSOR TEMPERATURE RISE $\dfrac{T_2 - T_1}{T_1}$

ENGINE RELATIVE SPEED $\dfrac{N}{N_D}\sqrt{\dfrac{518.7}{T_1}}$
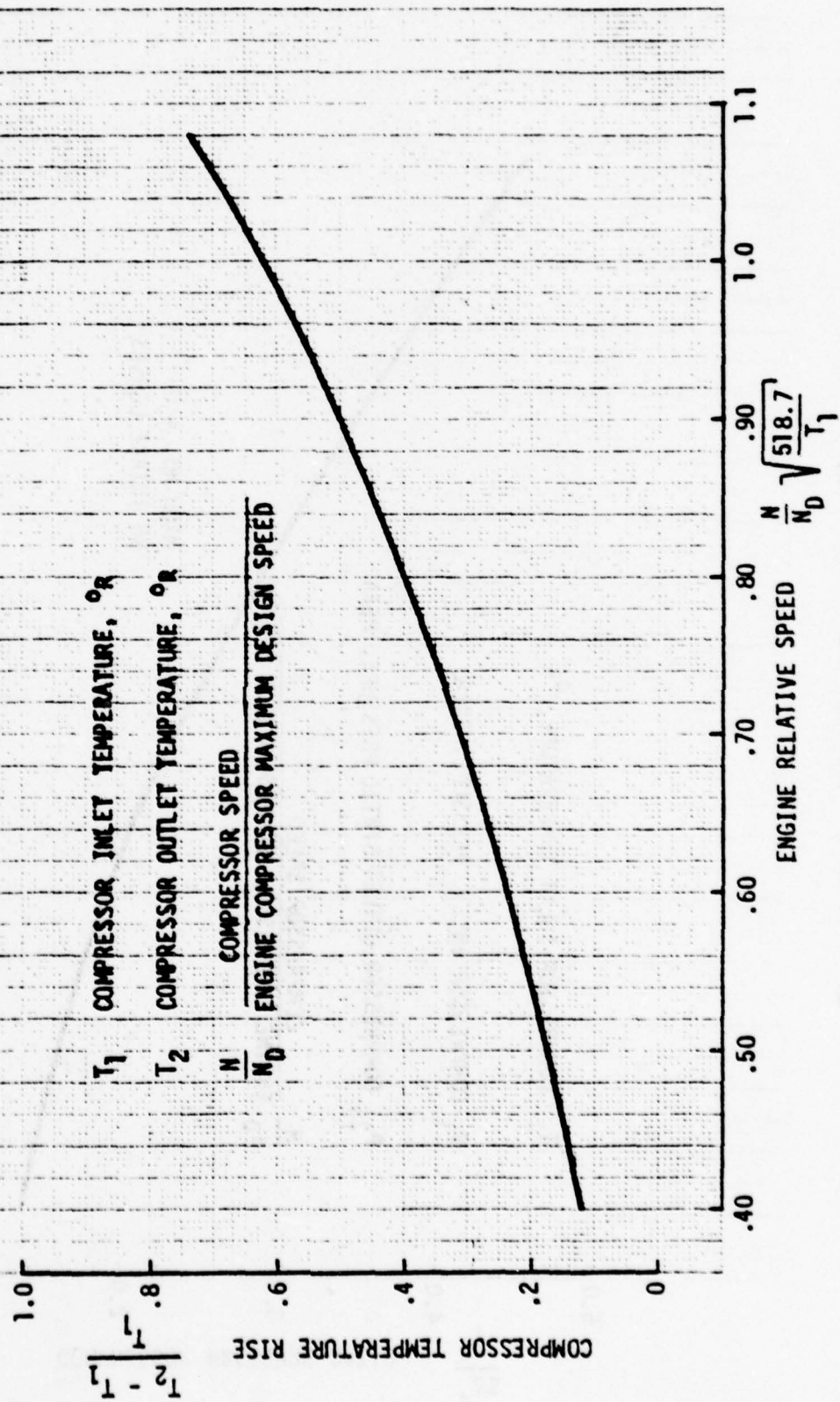
Figure 4 Engine Compressor Temperature Rise

W_b - BLEED AIR FLOW RATE, LBS/SEC

T_2 - COMPRESSOR OUTLET TEMP, °R

P_{2S} - COMPRESSOR OUTLET STATIC PRESSURE, PSIA

P_B - BLEED AIR TOTAL PRESSURE DOWNSTREAM OF PORT, PSIA
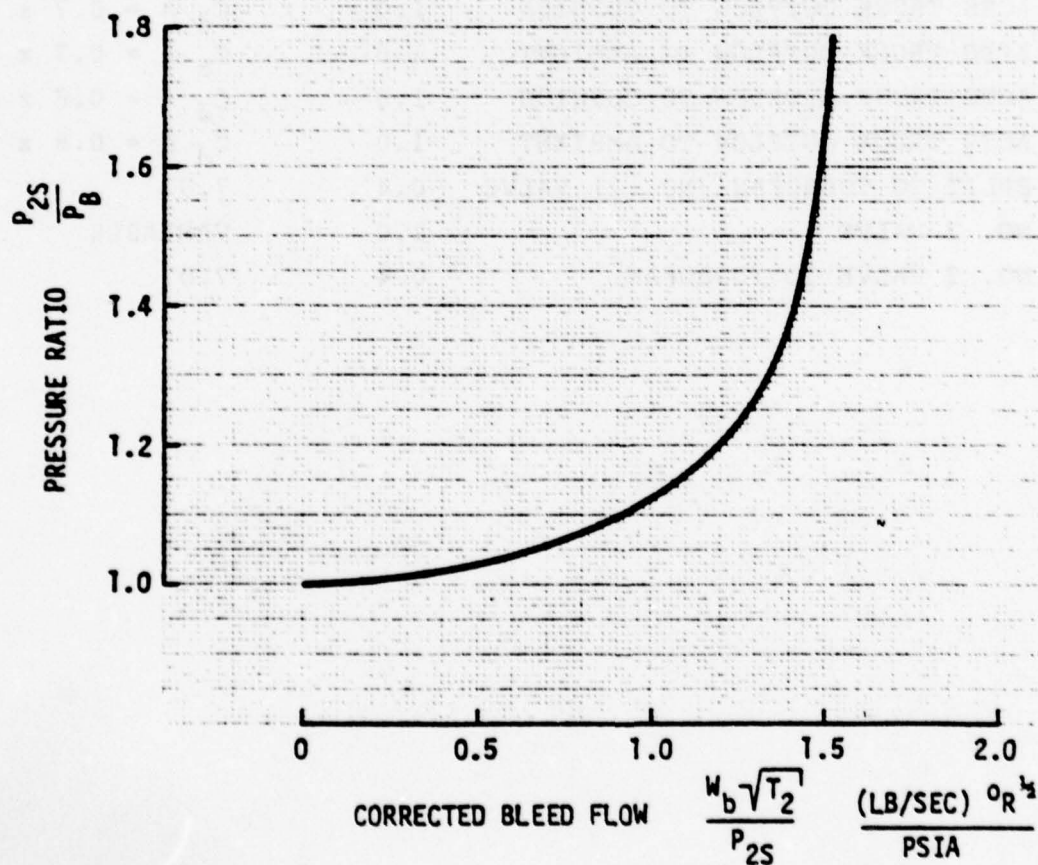
Figure 5   Engine Port Pressure Drop Characteristics

11

TABLE 1 SYSTEM PRESSURE DROP CHARACTERISTICS

SECTION	K FACTOR	EFFECTIVE AREA (IN^2)
BLEED PORT FITTING	1.	3.50
BLEED PORT FITTING TO SPLIT	1.07	7.07
SPLIT TO TRUNK (NO. 1) VALVE	0.18	7.07
NO. 1 VALVE	1.0	VARIABLE
NO. 1 VALVE TO TRUNK	1.02	7.07
ACRS TRUNK OUTFLOW TO CUSHION	1.0	$C_d A = 0.7 \times 2.42$
ACRS TRUNK OUTFLOW TO AMBIENT	1.0	$C_d A = 0.7 \times 2.42$
ACTS TRUNK OUTFLOW TO CUSHION	1.0	$C_d A = 0.8 \times 57.7$
ACTS TRUNK OUTFLOW TO AMBIENT	1.0	$C_d A = 0.8 \times 28.9$
SPLIT TO TURBOFAN (NO. 2) VALVE	0.4	7.07
NO. 2 VALVE	1.0	VARIABLE
NO. 2 VALVE TO TURBOFAN	0.4	7.07

value of effective area.

Figure 6 shows the performance of the turbofan, obtained from Reference 4. Reference 4 also included data showing the turbine (or drive) flow for each test condition. Several problems were encountered in trying to use this fan data for analyzing the system performance namely:

1. Turbine flow is normally correlated by plotting corrected flow ($\frac{W\sqrt{\theta}}{\delta}$ or $\frac{W\sqrt{\theta}}{A_\eta \delta}$) as a function of pressure ratio. A single curve should be obtained, irrespective of turbine speed. However, when this correlation was attempted, considerable data scatter was observed, as shown in Figure 7. The relationship between corrected flow and pressure ratio has a significant impact on system performance. For example, changing from the basic curve to the lower limit curve of Figure 7 results in a higher drive pressure and hence, from Figure 6, in improved turbofan performance.

2. Figure 6 shows performance for drive pressures ranging from 35 to 17.5 psia. However, in many cases, and particularly with the ACRS at part power, lower drive pressures are observed.

3. Reference 4 has no information on the performance of the fan in the stall region.

As a consequence of these problems, further tests were run on the turbofan as reported in Reference 6.

The revised fan map, obtained from Reference 6, is shown as Figure 8. This map covers the complete range of drive pressures. Furthermore, the turbine flow data shows an excellent correlation as shown in Figure 9.

13
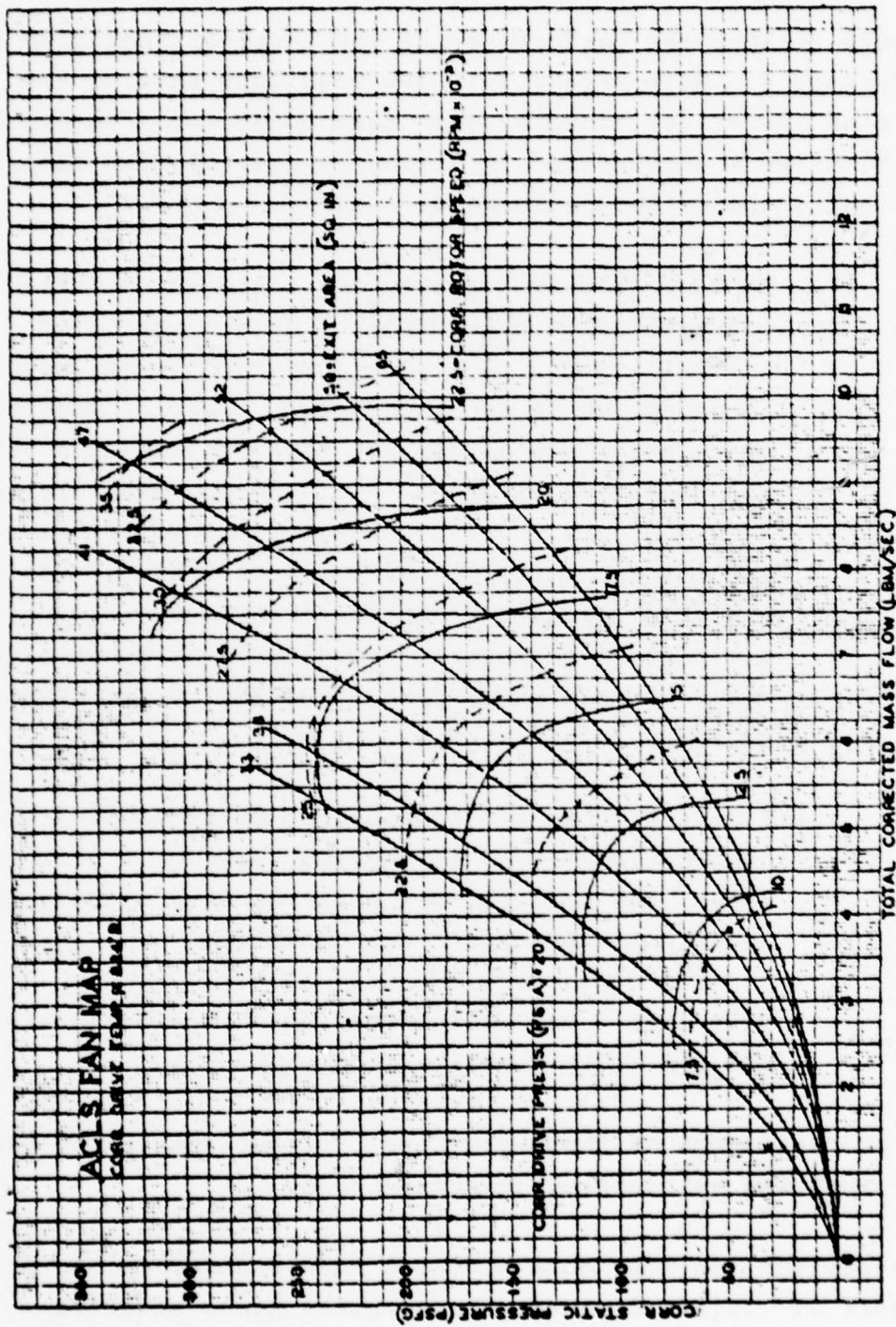
Figure 6 Original Fan Performance Map

14
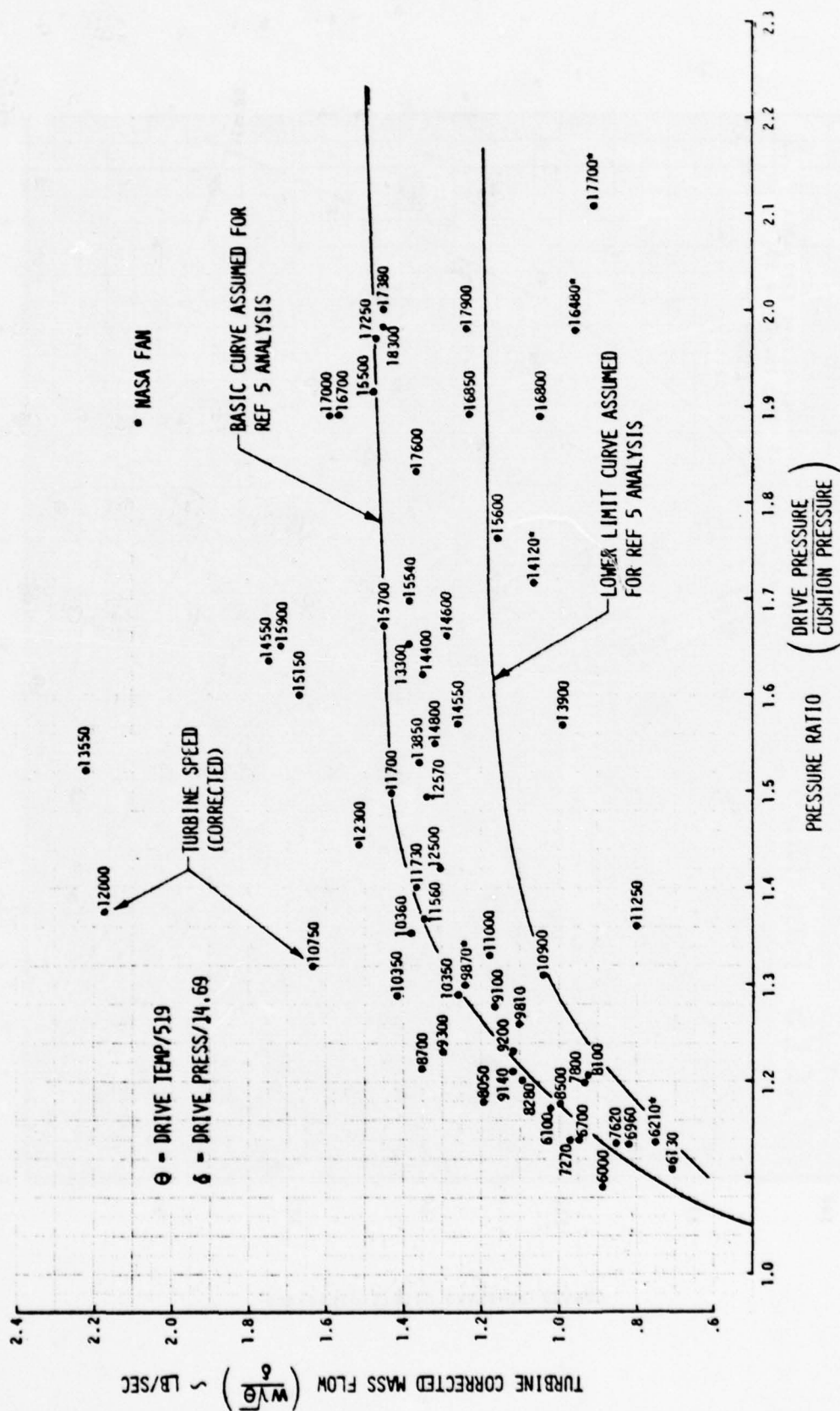
Figure 7 Turbine Flow Characteristics

15

TOTAL CORRECTED MASS FLOW (LBM/SEC)
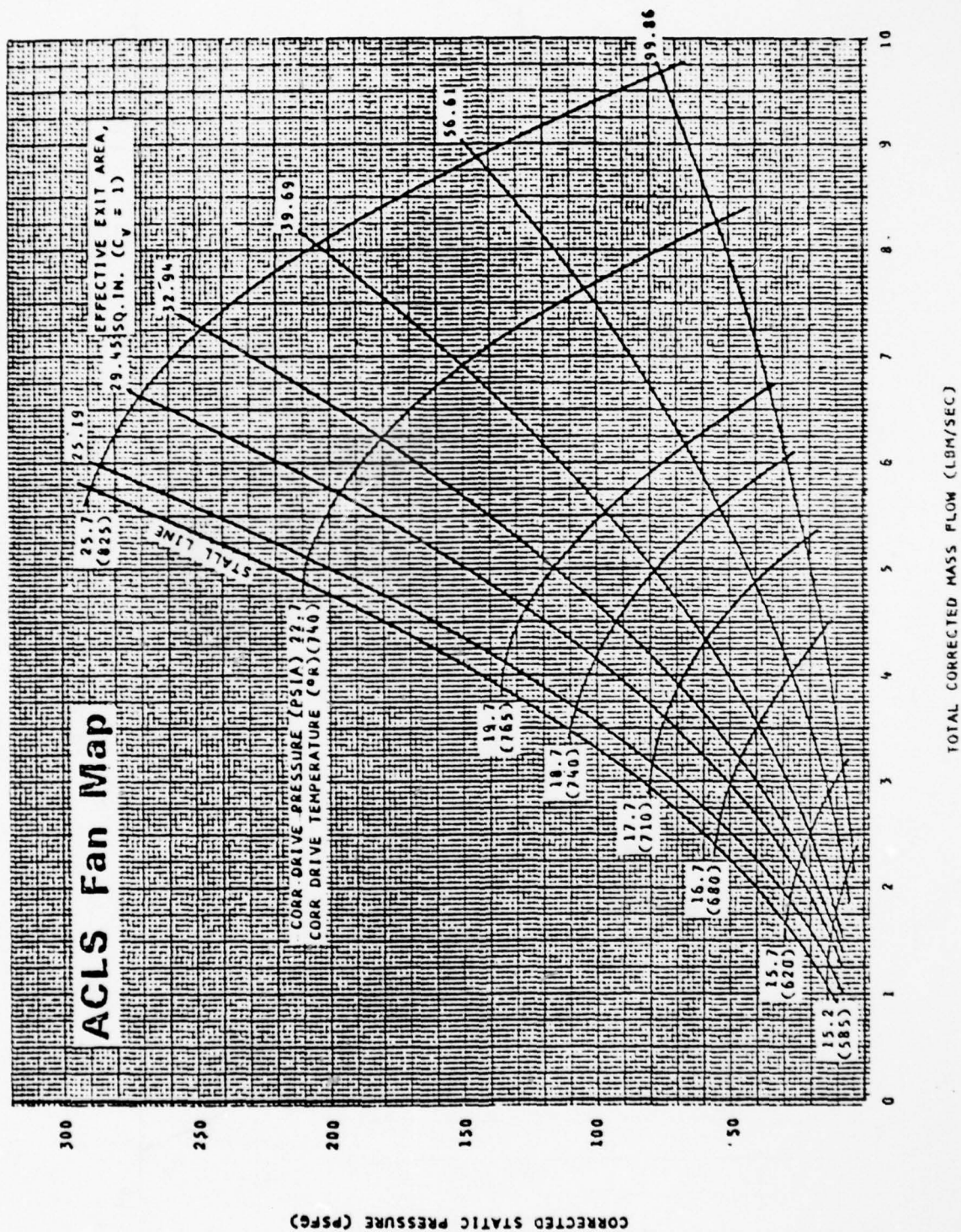
Figure 8   Revised Fan Performance Map

16
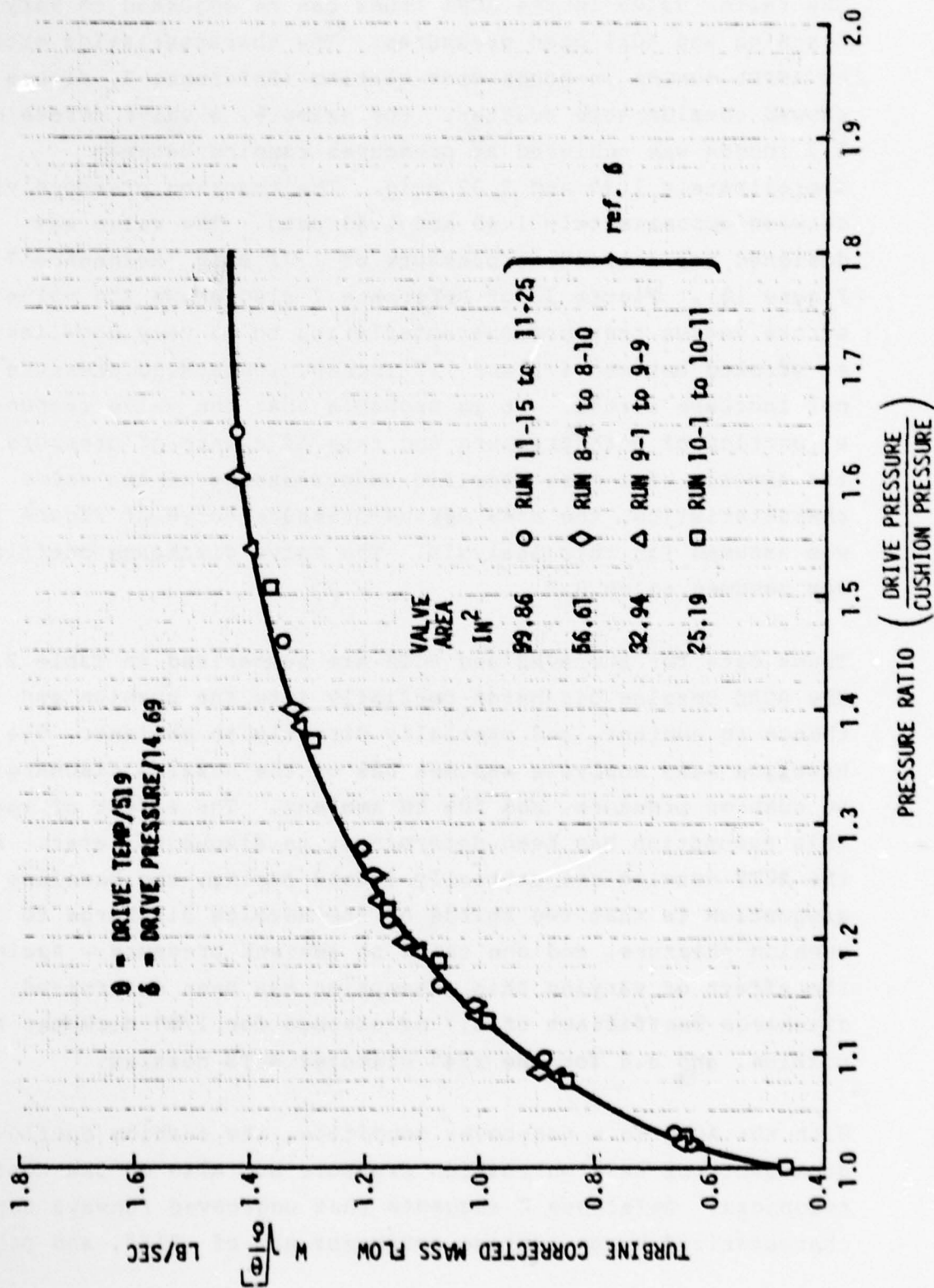
Figure 9 Revised Turbine Flow Characteristics

17

The relief valve in the ACRS trunk can be adjusted to vary the cracking and full open pressures. The characteristics obtained by AFFDL during in-house drop testing (Reference 7, Figure 33) showed considerable scatter. For example, a valve stroke of 1.2 inches was achieved at pressures ranging between approximately 1.95 and 2.32 psig. The cracking pressure varied between approximately 1.45 and 1.63 psig. The valve was designed for a cracking pressure of 1.71 psig (Reference 7, Figure 10). Figure 33 of Reference 7 also shows the valve stroke versus pressure characteristics to be very non-linear; at strokes between 1.3 and 1.5 inches, increasing pressure does not increase stroke. It is probable that the valve response is a function of both pressure and rate of change of pressure. In the absence of a more specific understanding of the valve characteristics, the area versus pressure curve of Figure 10 was assumed for this analysis. The valve discharge coefficient was assumed to be 0.9.

Trunk data for the ACRS and ACTS are summarized in Table 2. The ACRS nozzles discharge partially into the cushion and thence to ambient, and partially directly to ambient. The baseline ACRS analysis assumes 50% of the nozzles discharging to cushion pressure, and 50% to ambient. The effect of varying this assumption has been determined, as discussed later. As the ACTS nozzles are partially inward facing, the baseline assumption is that two thirds of the nozzles discharge to cushion pressure, and one third to ambient pressure. Again, the effect of varying this assumption has been determined. A discharge coefficient of 0.7 is assumed for 1/8" diameter ACRS nozzles, and 0.8 for the 1/4" diameter ACTS nozzles.

With the ACLS in a non-hover condition, the cushion outflow is dependent not only on cushion pressure but also on the surface roughness. Reference 8 suggests that ungrooved runways can be characterized by an average roughness gap of .016", and grooved
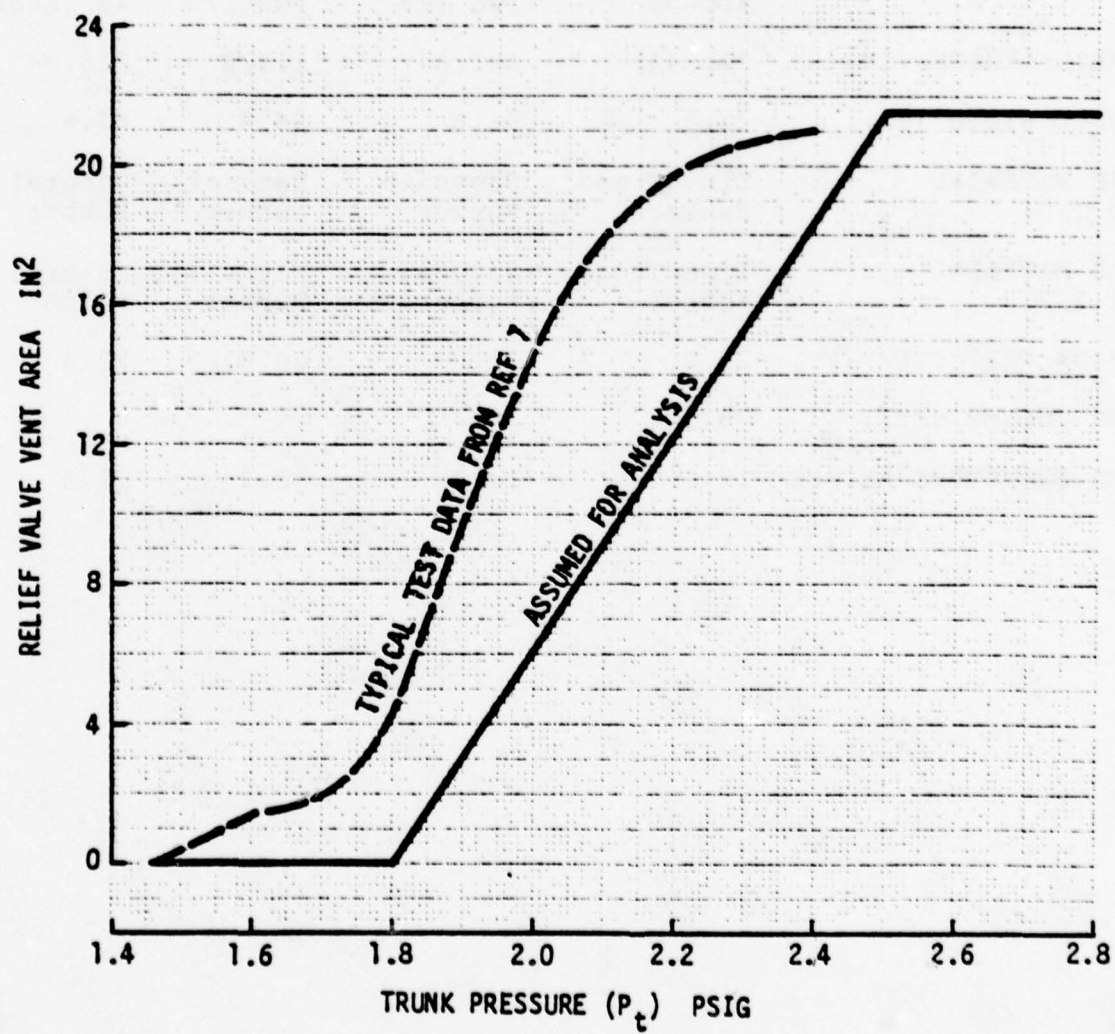
Figure 10 Relief Valve Characteristics

19

Table 2   ACRS and ACTS Trunk Data

	LAB TEST AFFDL-TR-74-64	ACRS#2 5X2027	ACRS#3 5X2064	ACTS#1 5X2024
CUSHION AREA (IN^2)	2346	3812	3298	3988
CP FWD OF CG (IN)	9.0	5.95	4.15	5.95
AREA OF TREAD (IN^2)	2200	2478	2364	2505
HOLES	1182,1/8" dia. all around	394,1/8" dia. fwd 1/3	394,1/8" dia. fwd 1/3	1764,1/4" dia. 45°,A=86.6
OVERALL LENGTH (IN)	121.44	121.87	111.5	125.94
OVERALL WIDTH (IN)	53.3	66.6	55.8	67.6
TREAD MATERIAL (FWD 1/3)	Tire Tread Rubber	Neoprene Rubber	Natural Rubber	Natural Rubber
TREAD MATERIAL (AFT 2/3)	Tire Tread Rubber	Natural Rubber	Natural Rubber	Natural Rubber
CUSHION PERIMETER (FT)	21.2	22.0	20.85	22.4
TRUNK VOLUME (FT^3)	39.1			
HOVER STRUCTURE HEIGHT (IN)	12.	14.3	11.0	12.5

Table 2 (Continued)

PERFORMANCE CHARACTERISTICS   (REFERENCE 7)

HOVER P_t (PSIG)	1.39-1.93	1.8-2.1	0.93-1.3
ROLL STIFFNESS (FT-LB/DEG)	36-70	98(static) 90(dynamic)	31(dynamic)
ROLL NATURAL DAMPED FREQUENCY (CPS)	0.21-0.29	0.33	0.19
ROLL DAMPING RATIO	0.057-0.069	0.081	0.17
ROLL DAMPER COEFFICIENT(FT-LB-SEC/DEG)	3.7-4.4	7.05	8.9
PITCH STATIC STIFFNESS (FT-LB/DEG)	980	1030	
PITCH DYNAMIC STIFFNESS (FT-LB/DEG)	953-1370	1250	
PITCH NATURAL DAMPED FREQUENCY (CPS)	0.87-1.05	1.00	
PITCH DAMPING RATIO	0.038-0.051	0.062	
PITCH DAMPER COEFFICIENT (FT-LB-SEC/DEG)	17-20	25	
HEAVE STATIC STIFFNESS (LB-IN)	725-870	775-1060	
HEAVE DYNAMIC STIFFNESS (LB/IN)	800-1350	1095	
HEAVE NATURAL DAMPED FREQUENCY (CPS)	1.7-2.2	1.94	
HEAVE DAMPING RATIO	0.18-0.35	0.266	
HEAVE DAMPER COEFFICIENT (LB-SEC/IN)	31-65	57.5	

21

runways by a gap of .063". The corresponding cushion pressure versus flow characteristics for ACRS #3 are shown in Figure 11. It is shown later that because of the flat fan pressure rise versus flow characteristics, the assumption of the average gap in non-hover conditions is not very critical.

The airflow system performance discussed below includes one further correction to the data assumed in the Reference 5 analysis. Ground testing of the Jindivik ACLS in Australia showed the engine static pressure, obtained by measuring port pressure at zero flow, to be less than engine manufacturer's data as shown in Figure 12. Although the test data is from one engine only, and is not necessarily typical of the average Viper 11/201 engine, it has been used in the analysis. Experience has shown that engine pressures less than manufacturers' brochure values are the norm rather than the exception.

2.2.2 ACRS Airflow System Performance

Fan off Performance - During touchdown and slideout it is currently envisaged that the ACRS will operate with the fan valve closed. Figure 13 shows trunk pressure on a standard day as a function of engine relative speed. The trunk pressure increases rapidly until the relief valve cracking point is reached, at a engine relative speed of 52%. Above this point the increase of trunk pressure with speed is quite modest. Figure 14 shows the thrust of the Viper 11/201 engine as a function of relative engine speed and Mach number on a standard day (Reference 2). Assuming that a trunk pressure on the order of 1.8 psig is required to give adequate trunk stiffness, Figures 13 and 14 show that the maximum required relative engine speed is 52% and resulting thrust is on the order of 200-350 pounds. The approach engine speed is expected to be around 54 to 58%, and thus trunk stiffness will be adequate at touchdown. The thrust level of 200-350 pounds during slideout will not significantly affect braking performance.

22
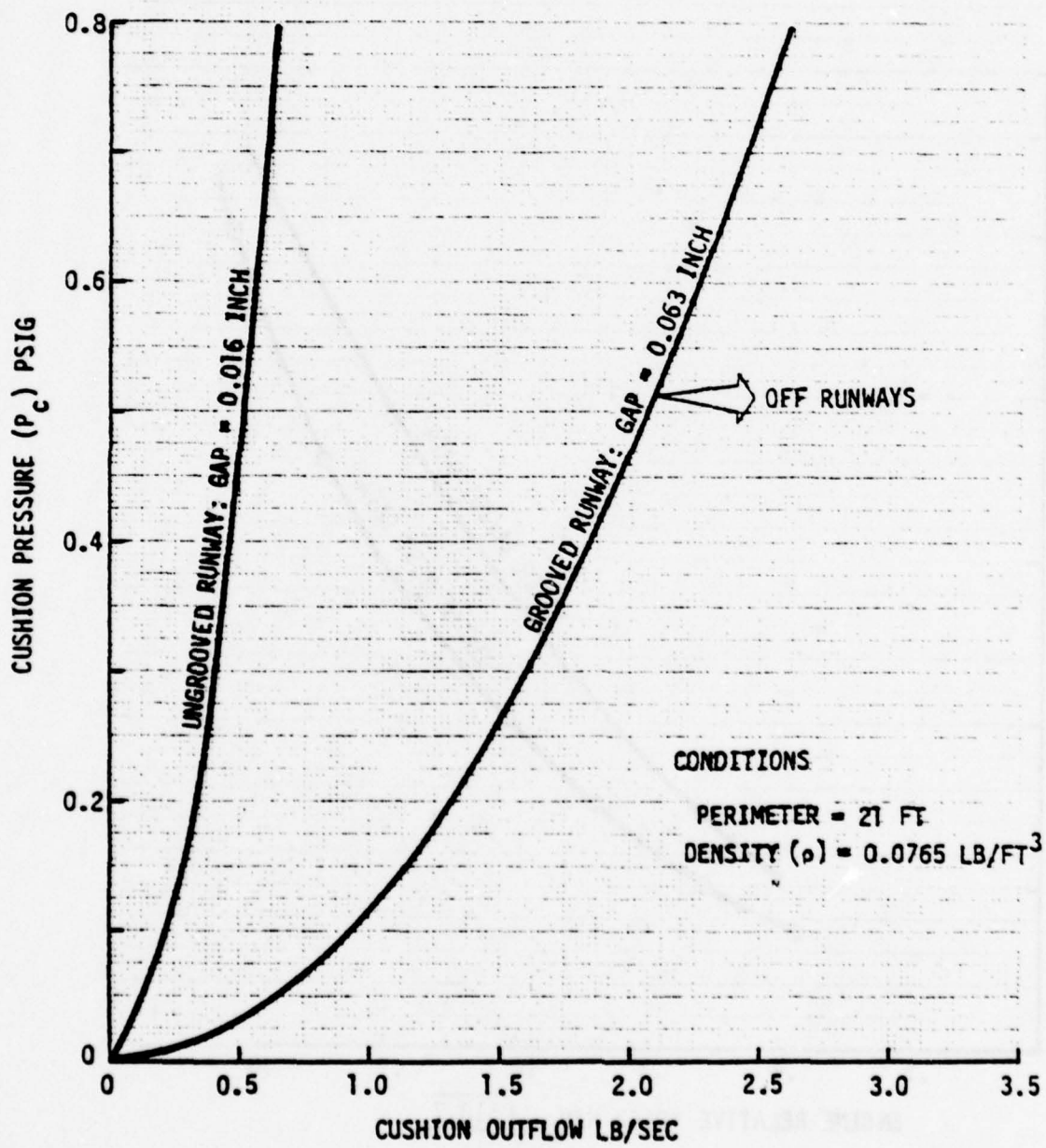
Figure 11 Cushion Outflow During Non Hover Conditions
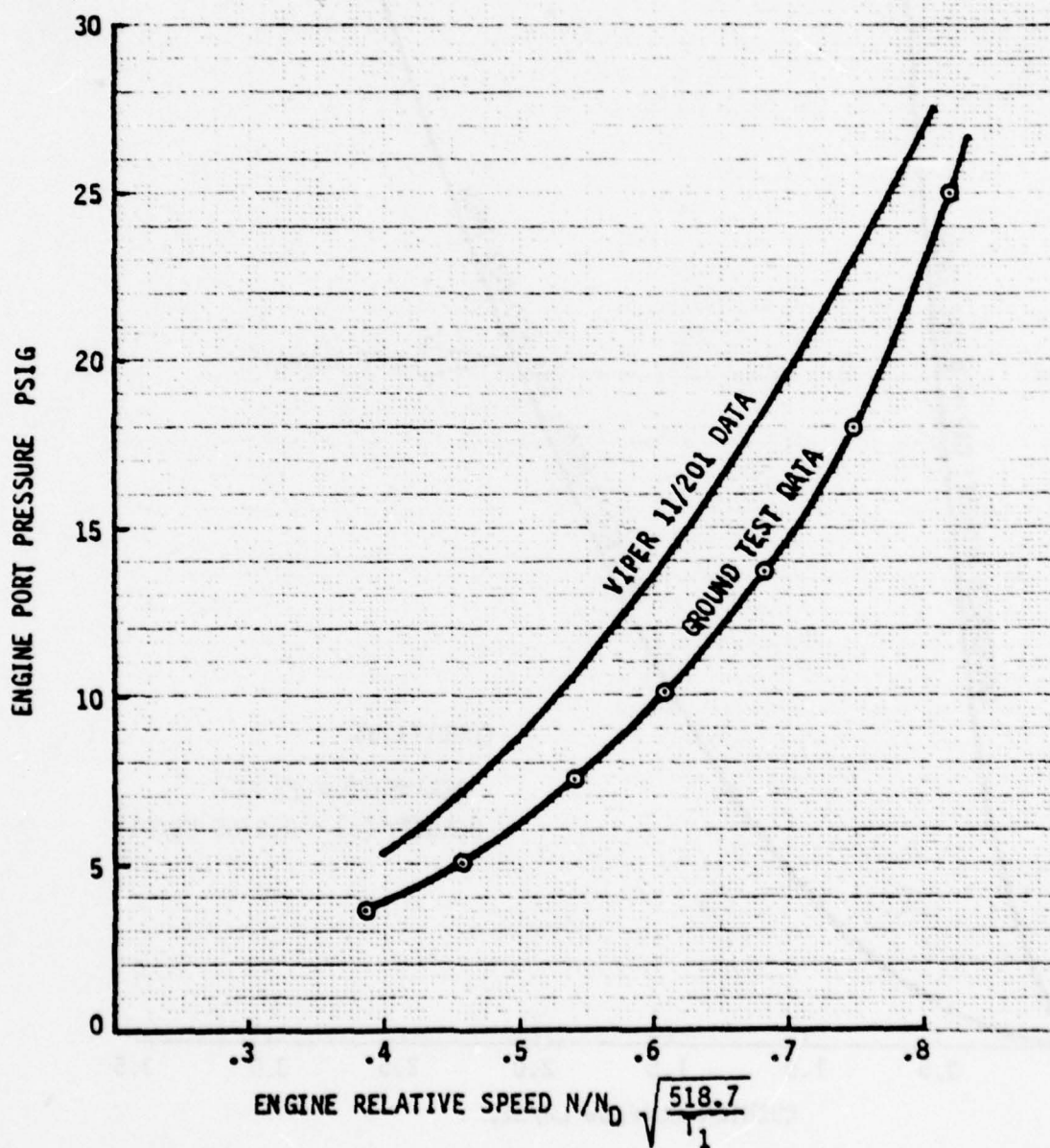
Figure 12 Engine Bleed Port Pressure

24
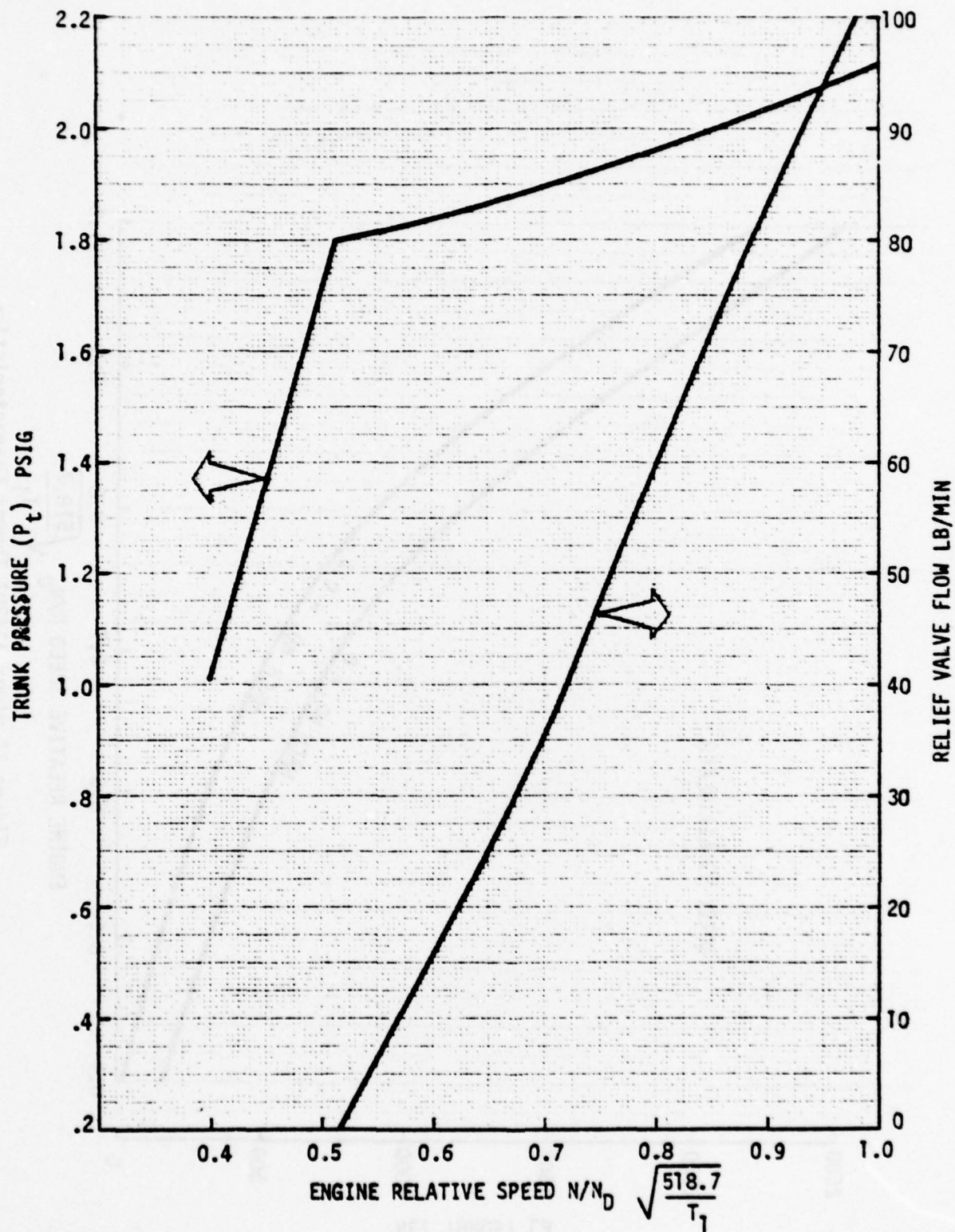
Figure 13 ACRS Performance - Fan Off

25

NET THRUST LB

ENGINE RELATIVE SPEED N/N$_D$ $\sqrt{\dfrac{518.7}{T_1}}$

MACH NO. = 0.3

MACH NO. = 0

NOTE: NO AIR BLEED
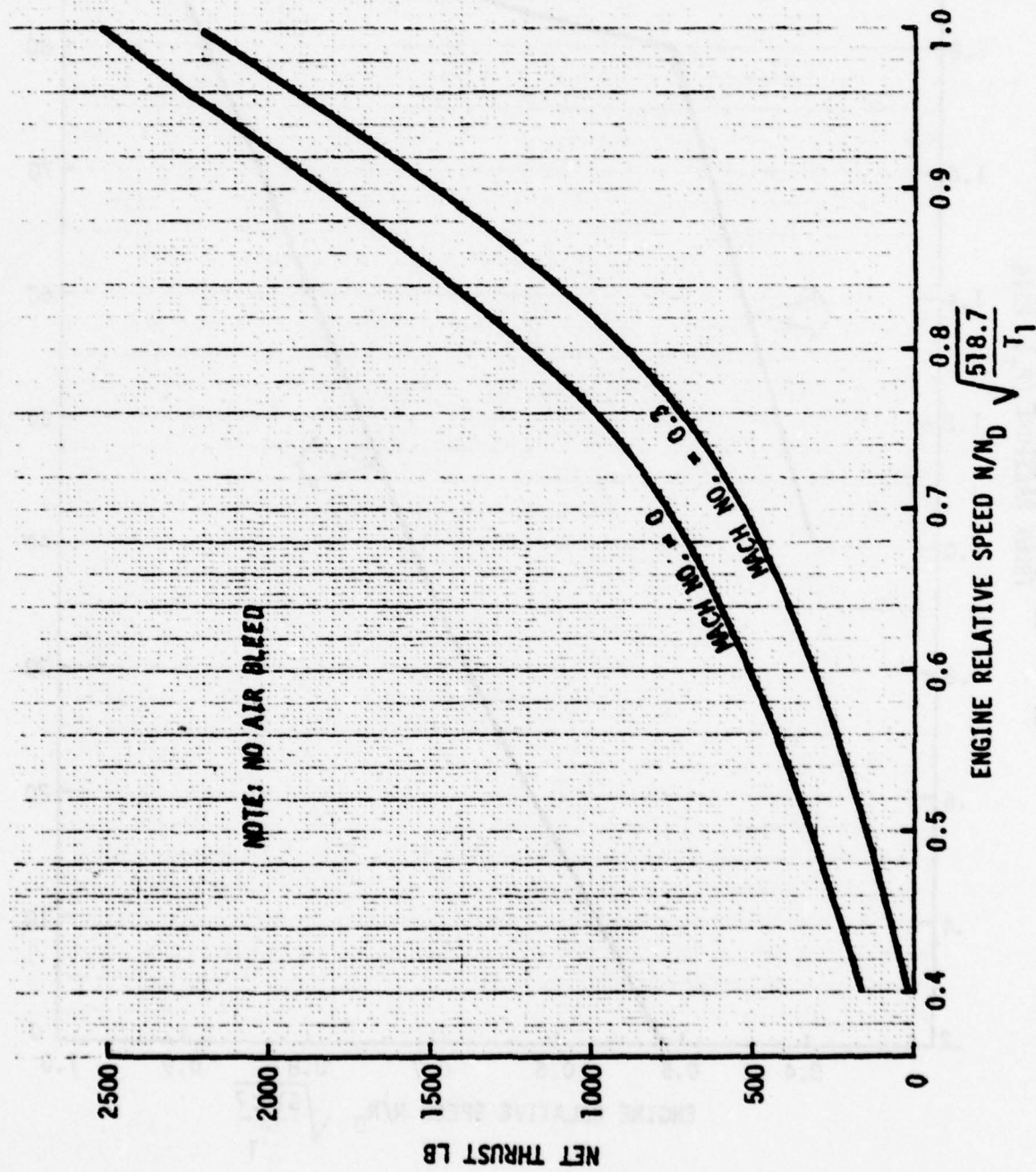
Figure 14 Viper 11/201 Thrust Characteristics

Figure 13 shows that the trunk pressure at 100% nominal engine speed is 2.1 psig, corresponding to a relief valve opeing of 42% (Figure 10). Thus there appears to be adequate margin in the relief valve to handle dynamic pressure fluctuations during touchdown and slideout.

The cushion pressure generated during fan off operation is very small, since the inflow is only 21 lb/min at 100% engine speed, and the cushion cavity is vented through the fan. Hence, Figure 13 is applicable to rough or smooth surfaces, or for out of ground effect operation.

Fan-On Performance - Numerous conditions of ACRS operation with the fan on have been analyzed. The baseline conditions can be summarized as follows:

o Cushion Hover Pressure = 0.65 psig
o Standard day
o Trunk discharge coefficient = 0.7
o 50% of trunk nozzles discharging to cushion, 50% to ambient
o Rough runway as in Figure 11
o Relief valve characteristics as in Figure 10
o Engine bleed pressure as in Figure 12
o "Revised" fan map as in Figure 8
o Both valves fully open

Figures 15 and 16 show the performance of the baseline system. Figure 15 shows trunk and cushion pressure, and it can be seen that a hover condition is not reached until engine speed is close to nominal. Assuming again that a trunk pressure of 1.8 psig is required for adequate pitch and roll stiffness, a relative engine speed of approximately 80% is required. This can be contrasted with Figure 13, which shows that the same trunk pressure is achieved at 52% engine speed with fan off.

27
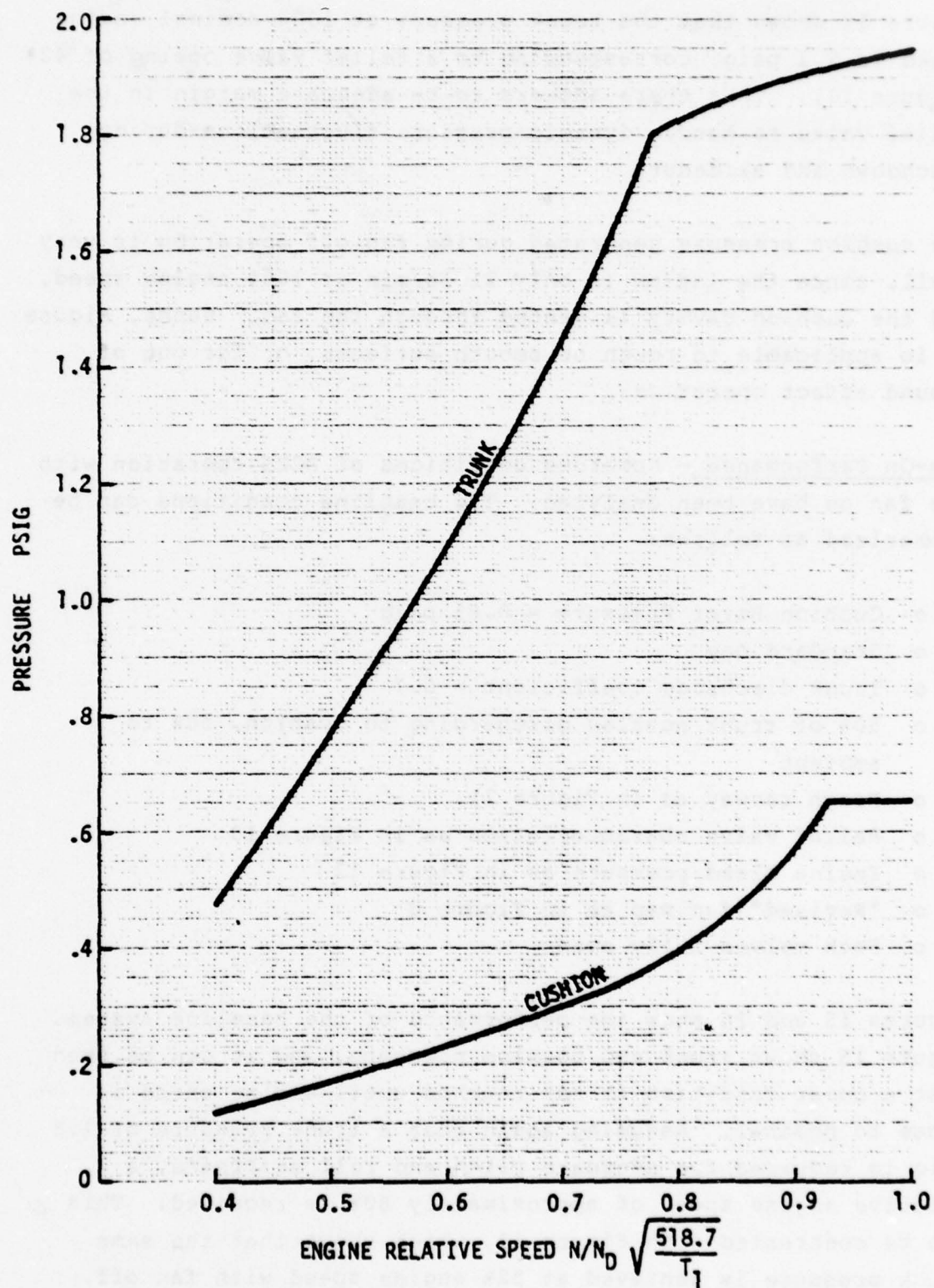
Figure 15 ACRS Baseline System - Trunk and Cushion Pressures
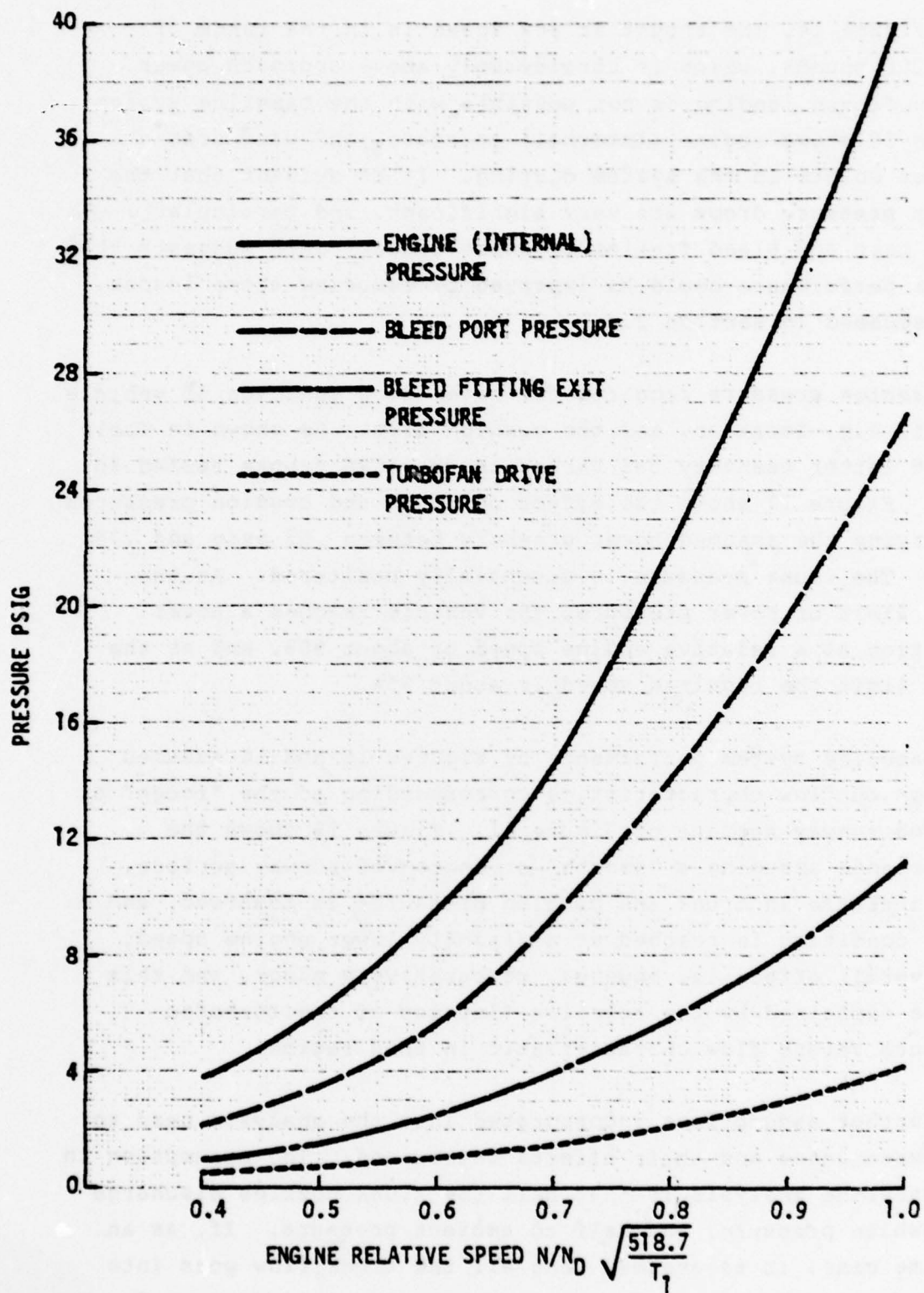
Figure 16   ACRS Baseline System Pressures

From Figure 14, the thrust at 80% speed is in the range of
900-1200 pounds, which is considerably above approach power.
Thus a fan-on landing is not possible with the baseline system.
Figure 16 shows engine (internal) pressure, and pressures at
various points in the system ducting. It is evident that the
system pressure drops are very significant, and particularly the
bleed port and bleed fitting pressure drops. This suggests that
system performance could be improved by reducing these losses,
as discussed in Section 2.4.

The cushion pressure required for hover is a function of vehicle
weight, c.g. location, and the cushion area. As shown in Table
2, the latter quantity has varied in the ACRS trunks tested to
date. Figure 17 shows the effect on trunk and cushion pressures
of varying the assumed hover pressure between .55 psig and .75
psig. The trunk pressure is essentially unaltered. At the
lower limit of hover pressure, the vehicle reaches a hover
condition at a relative engine speed of about 90%, and at the
upper limit the required speed is about 95%.

The baseline system performance of Figures 15 and 16 assumes
cushion outflow characteristics corresponding to the "rough" or
grooved runway surface of Figure 11. Figure 18 shows the
performance assuming a "smooth" or ungrooved runway surface.
Some increase in trunk and cushion pressures is observed, and a
hover condition is reached at a slightly lower engine speed.
The overall effect is, however, comparatively minor, and this
can be explained by the relative flatness of the turbofan
pressure versus flow characteristic in this region.

Two further assumptions incorporated into the analysis need to
be investigated and their effects determined. The assumption in
the baseline analysis is that half the trunk nozzles discharge
to cushion pressure, and half to ambient pressure. If, as an
extreme case, it is assumed that all the trunk flow goes into
the cushion, the result is that trunk pressure is increased,

30
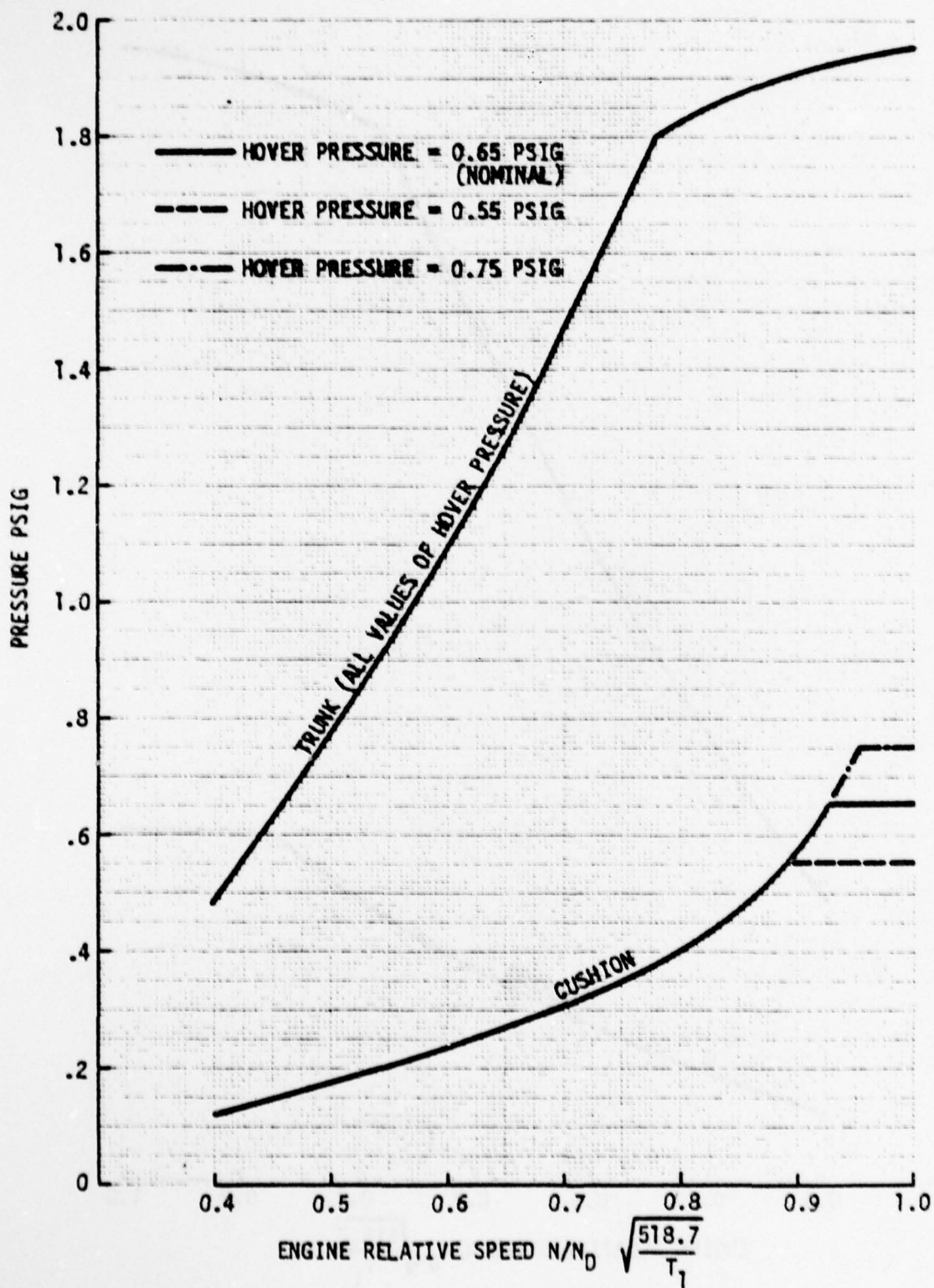
Figure 17   Effect of Hover Pressure on ACRS
Trunk and Cushion Pressures
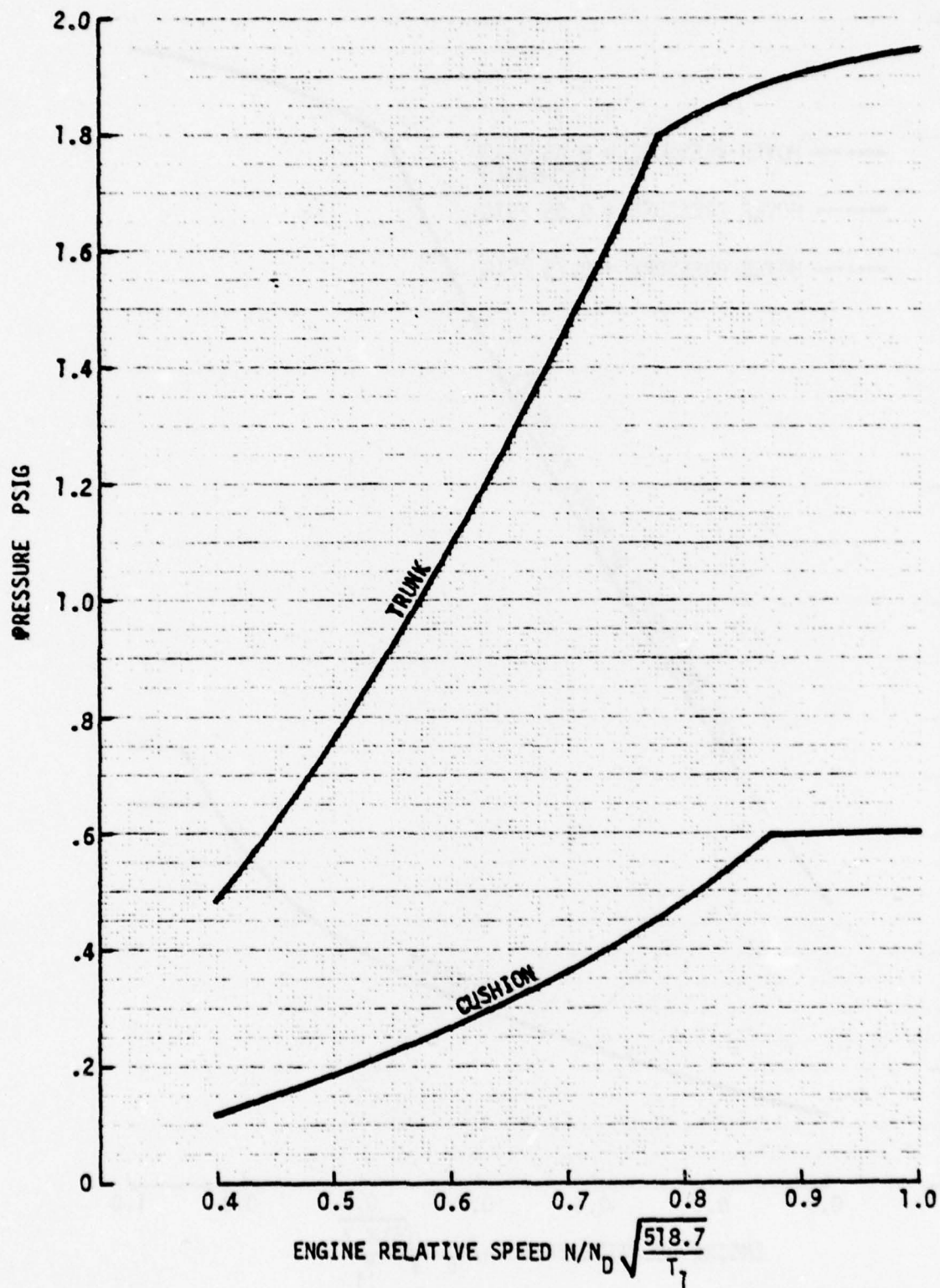
Figure 18   ACRS Trunk and Cushion Pressures - "Smooth" Runway

because of the higher back pressure. Cushion pressure is also increased, because of the higher inflow. Results are shown in Figure 19 and comparison with Figure 15 indicates that the effects are comparatively small. Figure 20 shows the effect of increasing the trunk nozzle discharge coefficient from 0.7 to 0.8. This increases trunk outflow, and trunk pressures are affected to some extent. For example, at 60% relative engine speed, trunk pressure decreases from 1.09 psig to 0.96 psig. Cushion pressure, on the other hand, is essentially unaltered.

The fan-on operation out of ground effect of the ACRS airflow system is of interest, since this is a condition which is convenient to test in order to compare test and analysis. Trunk pressures are reduced, and are virtually identical with those shown in Figure 20. It should be noted that at an approach engine speed of 60%, the trunk pressure is less than 1 psig, which might not even be high enough to deploy the trunk satisfactorily. This confirms that with the current system, approach should be in a fan off condition, when the corresponding trunk pressure is above 1.8 psig (Figure 13).

The performance of the system is relatively unaffected by ambient temperature. On a MIL-STD-210A Hot Day, trunk pressures are typically .05 psig lower, and cushion pressure .02 psig lower. A potential problem exists with trunk and fan bearing over temperature during prolonged Hot Day high power operation on the ACRS. Bleed air temperatures for various engine speeds and thrusts on a Hot Day at zero forward speed are as follows:

RELATIVE SPEED %	THRUST POUNDS	BLEED TEMPERATURES (^{O}F)	
		ENGINE	FAN OR TRUNK INLET (ESTIMATED)
80	1050	312	291
87	1440	348	324
100	2230	407	377
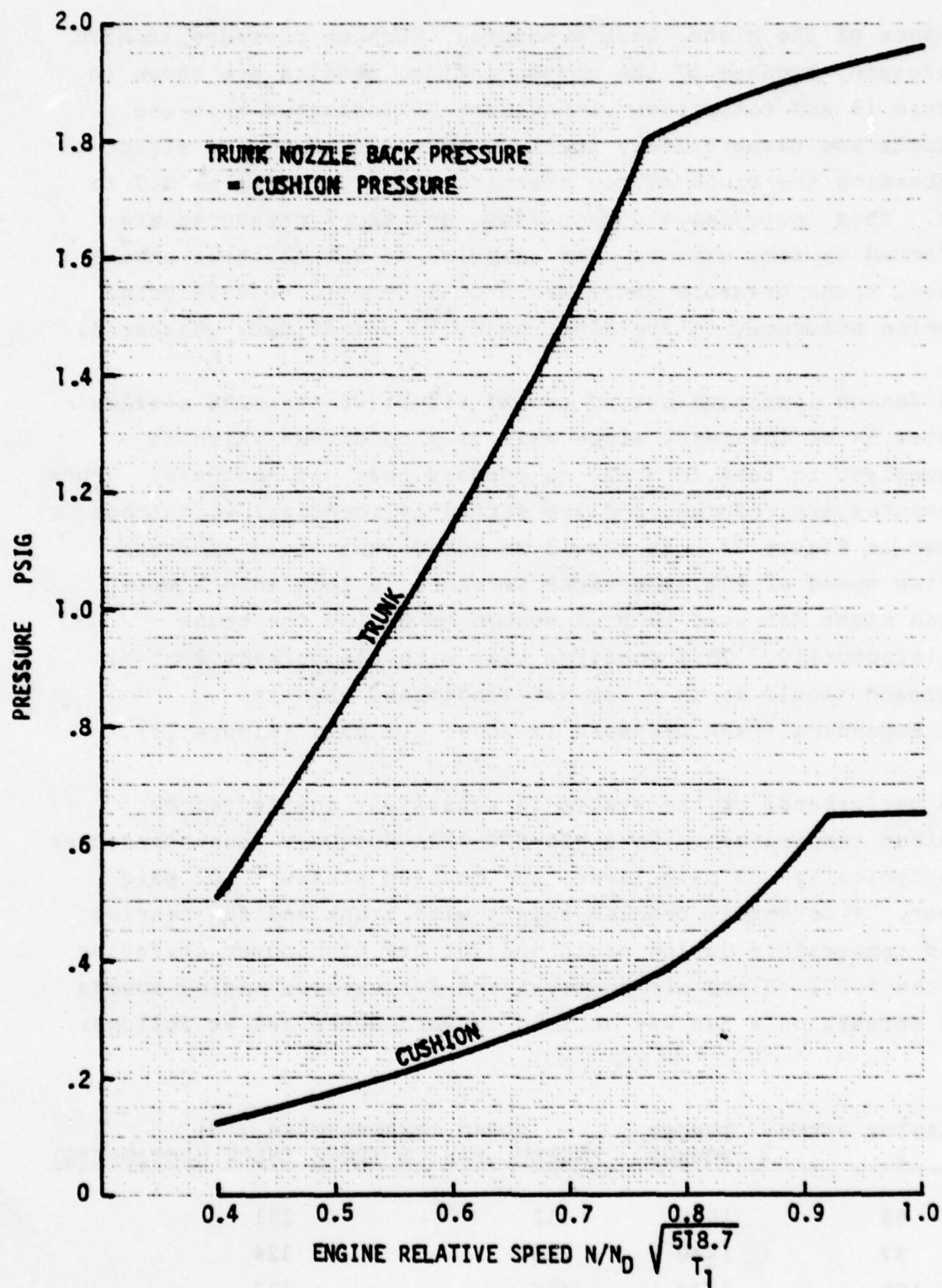
Figure 19   ACRS Trunk and Cushion Pressures - Effect of
             Trunk Nozzle Back Pressure

34
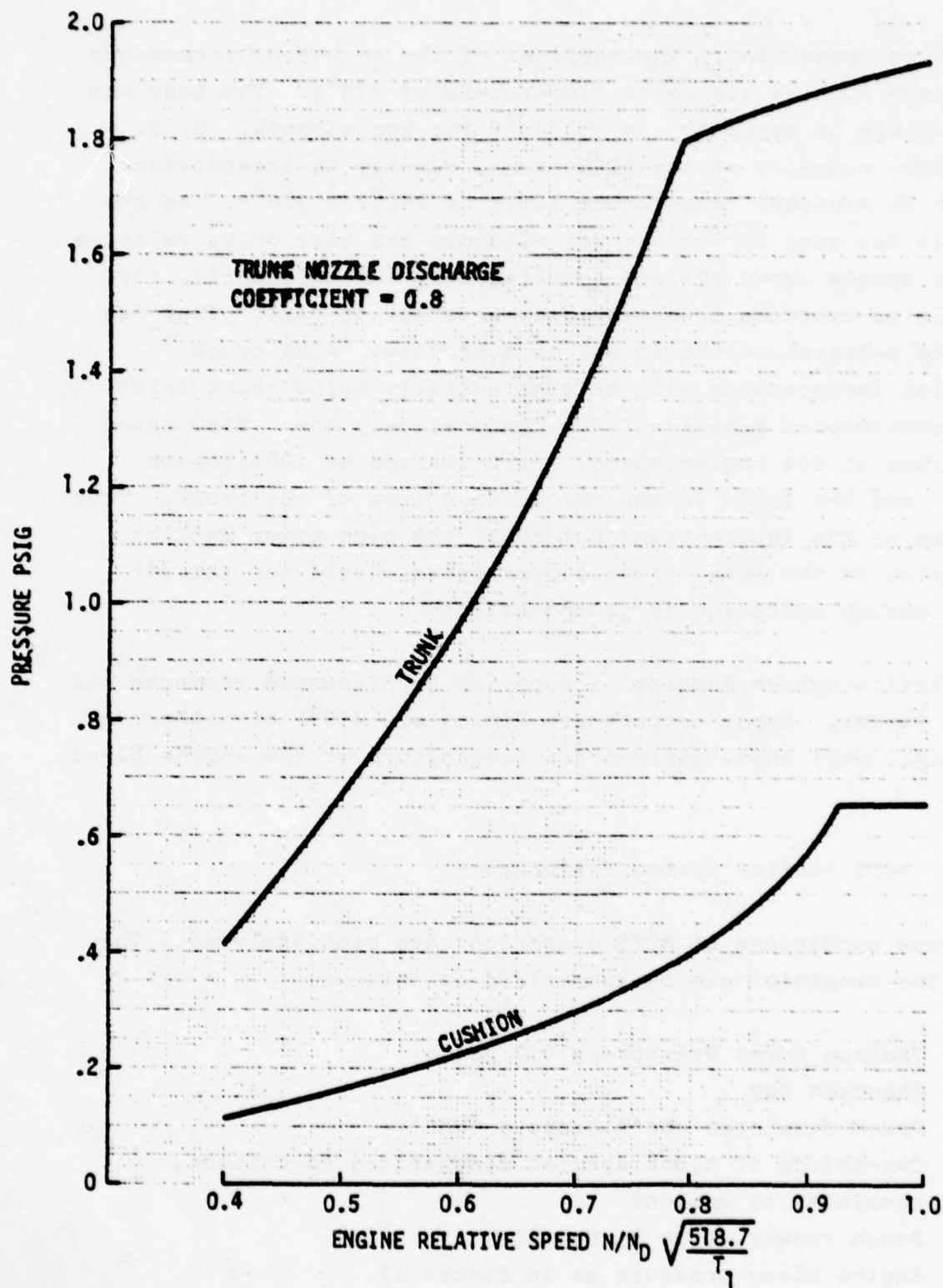
Figure 20   ACRS Trunk and Cushion Pressures - Effect of
             Nozzle Discharge Coefficient

Tech Development Inc., the supplier of the turbofan, recommends
a maximum turbine air inlet temperature of 375°F. The bearings
are capable of operation up to 380°F for ten minutes. B. F.
Goodrich, supplier of the ACRS trunk, specify an intermittent
(20 to 30 minutes) temperature limit of 250°F - 300°F. As the
ACRS is designed for touchdown, slideout and taxi only, relative
engine speeds above 80% are required only intermittently, for
example to overcome breakaway drag at start of taxi. Thus fan
bearing temperature should not be a problem. ACRS trunk
material temperatures will be substantially below trunk inlet
air temperatures because of the comparatively low flow rates
(1 lb/sec at 80% engine speed, 1-1/2 lbs/sec at 100% engine
speed),and the large volume and surface area of the trunk. Thus
because of the intermittant nature of the high power setting
operation on the ACRS, trunk temperatures should not exceed
250°F during operation in ground effect.

The airflow system ducting is supplied by Arrowhead Products and
H. K. Porter. Upper temperature limits are 450°F or higher (at
60 psig), well above maximum air temperature at the engine bleed
port.

2.2.3 ACTS Airflow System Performance

Numerous conditions of ACTS operation have been analyzed. The
baseline condition can be summarized as follows:

o Cushion Hover Pressure = 0.7 psig
o Standard Day
o Trunk discharge coefficient = 0.8
o Two-thirds of trunk nozzles discharging to cushion,
   remainder to ambient
o Rough runway as in Figure 11
o Engine bleed pressure as in Figure 12
o Revised fan map as in Figure 8

36

o   ACRS trunk valve (Number 1, Figure 1) fully closed

o   Fan valve fully open

The higher hover pressure assumed for the ACTS is based on the
fact that the vehicle will be heavier at takeoff than at
landing. The higher trunk nozzle discharge coefficient (0.8
versus 0.7 for the ACRS) results from the larger hole size (1/4"
diameter versus 1/8" diameter for the ACRS). The assumption of
two thirds of the nozzles "seeing" cushion pressure and one
third ambient pressure is somewhat arbitrary, but appears
reasonable as the ACTS nozzles are inward facing at an angle of
45°.

As with the ACRS analysis, the effects of the various
assumptions have been investigated parametrically, and similar
trends are observed. The effects of various parameter changes
are summarized in Figures 21 and 22, showing trunk and cushion
pressures respectively. The figures show the baseline
assumptions to be the most conservative, in that they result in
the lowest trunk and cushion pressures. Vehicle hover is
achieved at engine speeds between 68% and 78%, which is
satisfactory. A maximum hover pressure of 0.8 psig, which
corresponds to a vehicle weight of over 3200 lbs, could be
reached at an engine speed of 80% with the baseline system.
Insufficient test data are available to assess the adequacy of
the trunk pressure in terms of providing adequate pitch and roll
stiffness. It should be remembered that the parking bladders
also contribute to the ACTS trunk stiffness.

2.3   COMPARISON OF TEST AND ANALYSIS

During ground testing of the Jindivik at the Government Aircraft
Factory facility at Avalon Field, some pressures in the airflow
systems were recorded. During initial testing on the ACTS and
ACRS in October, 1975, some trunk and drive pressures were
recorded. However, considerable difficulty was experienced with
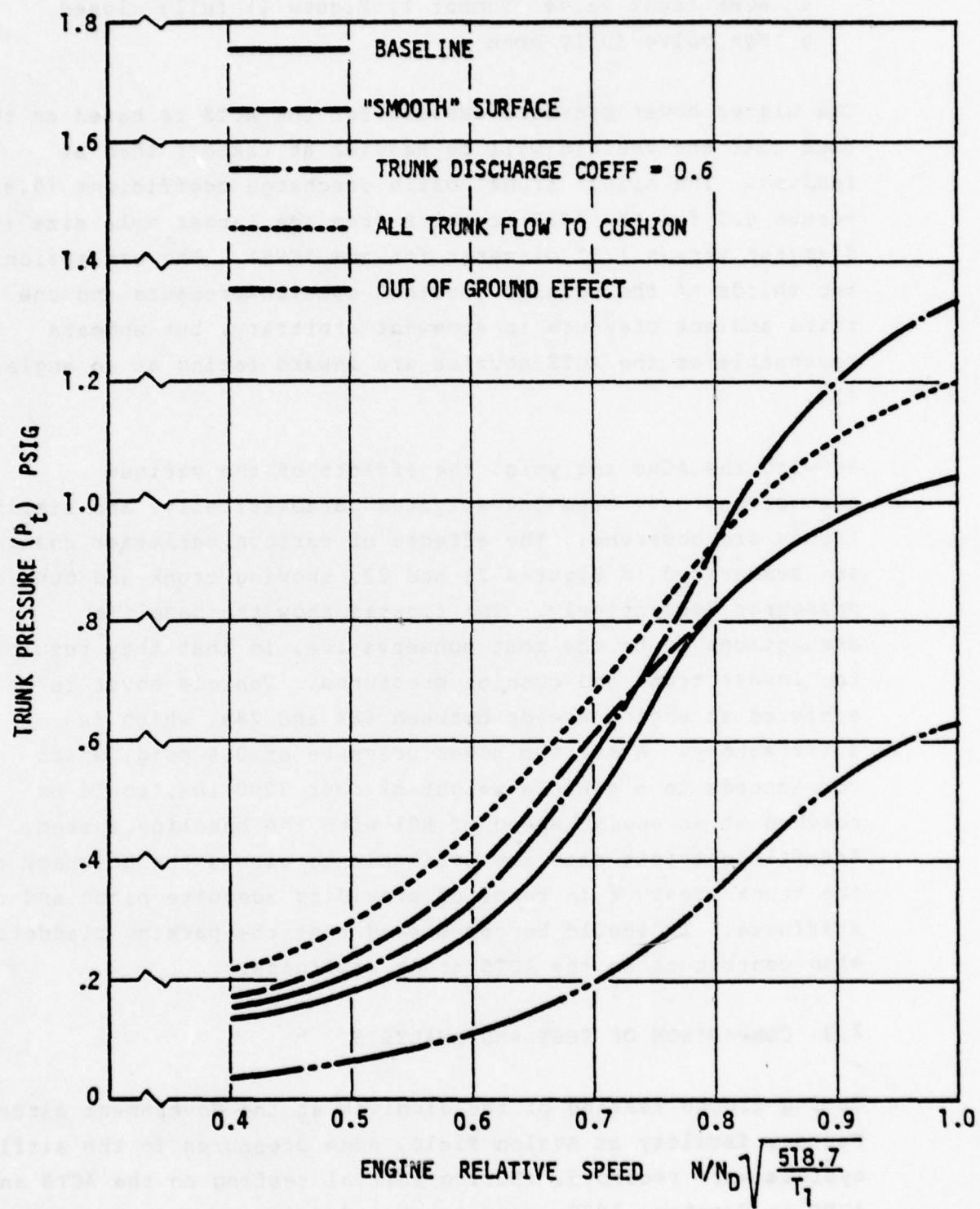
Figure 21 ACTS Trunk Pressures
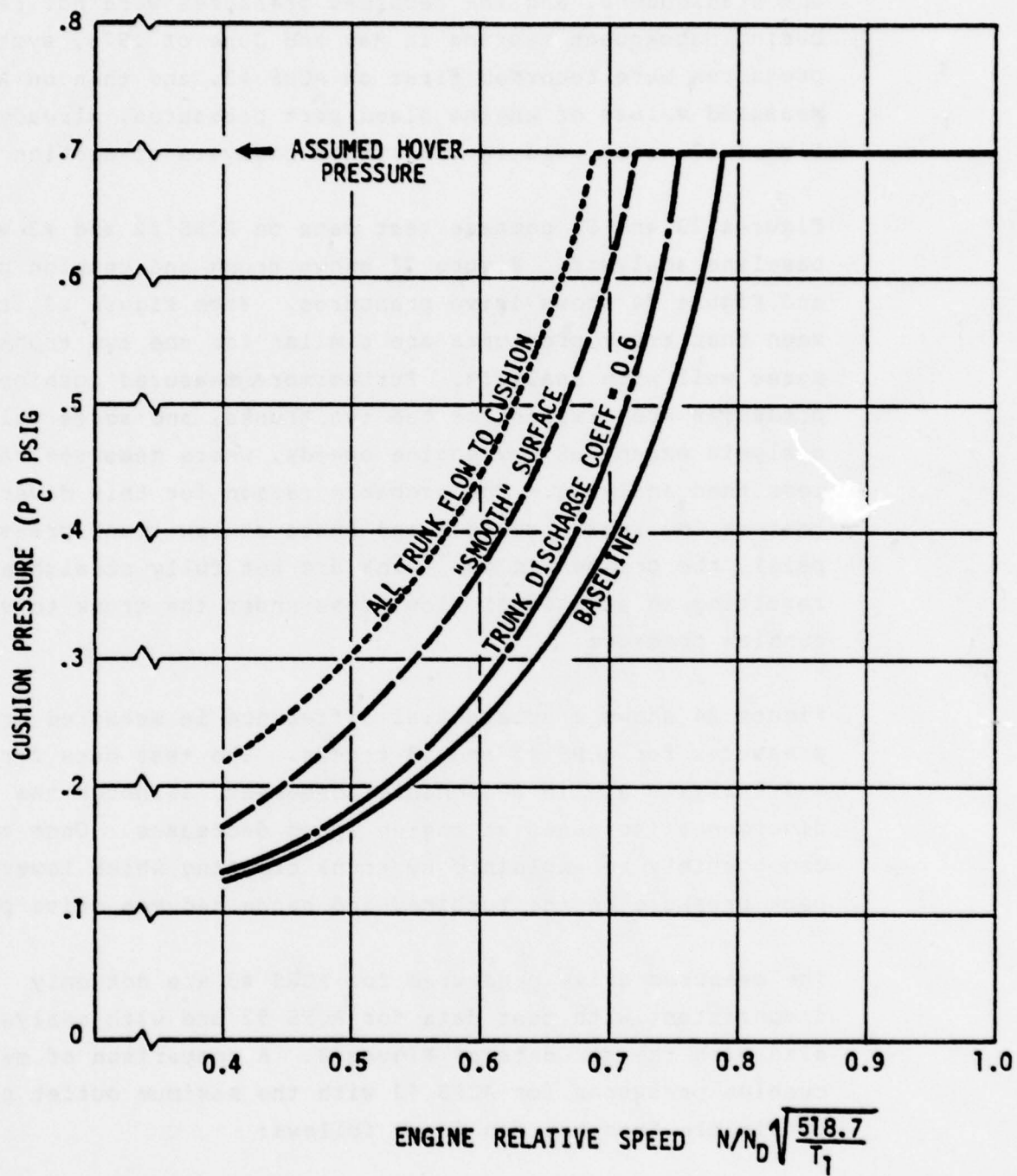
Figure 22 ACTS Cushion Pressure

the transducers, and the recorded pressures were not reliable. During subsequent testing in May and June of 1976, system pressures were recorded first on ACRS #3, and then on ACRS #2. Measured values of engine bleed port pressures, already shown in Figure 12, were used in the system analysis of Section 2.2.

Figures 23 and 24 compare test data on ACRS #2 and #3 with the baseline analysis. Figure 23 shows trunk and cushion pressures, and Figure 24 shows drive pressures. From Figure 23 it can be seen that trunk pressures are similar for the two trunks, and agree well with analysis. Furthermore, measured cushion pressures are similar for the two trunks, and agree well with analysis except at low engine speeds, where measured values are less than analysis. The probable reason for this divergence is that at low engine speeds, and hence at low trunk pressure (<0.7 psig), the creases in the trunk are not fully straightened out, resulting in additional flow areas under the trunk to vent the cushion pressure.

Figure 24 shows a substantial difference in measured drive pressures for ACRS #2 and #3 trunks. The test data for ACRS #2 and analysis are in reasonable agreement, although the divergence increases as engine speed decreases. Once again this can possibly be explained by trunk creasing which lowers the back pressure on the turbine, and hence reduces drive pressure.

The measured drive pressures for ACRS #3 are not only inconsistent with test data for ACRS #2 and with analysis, but also with the fan data of Figure 8. A comparison of measured cushion pressures for ACRS #3 with the maximum outlet pressure obtainable from the fan is as follows:

40
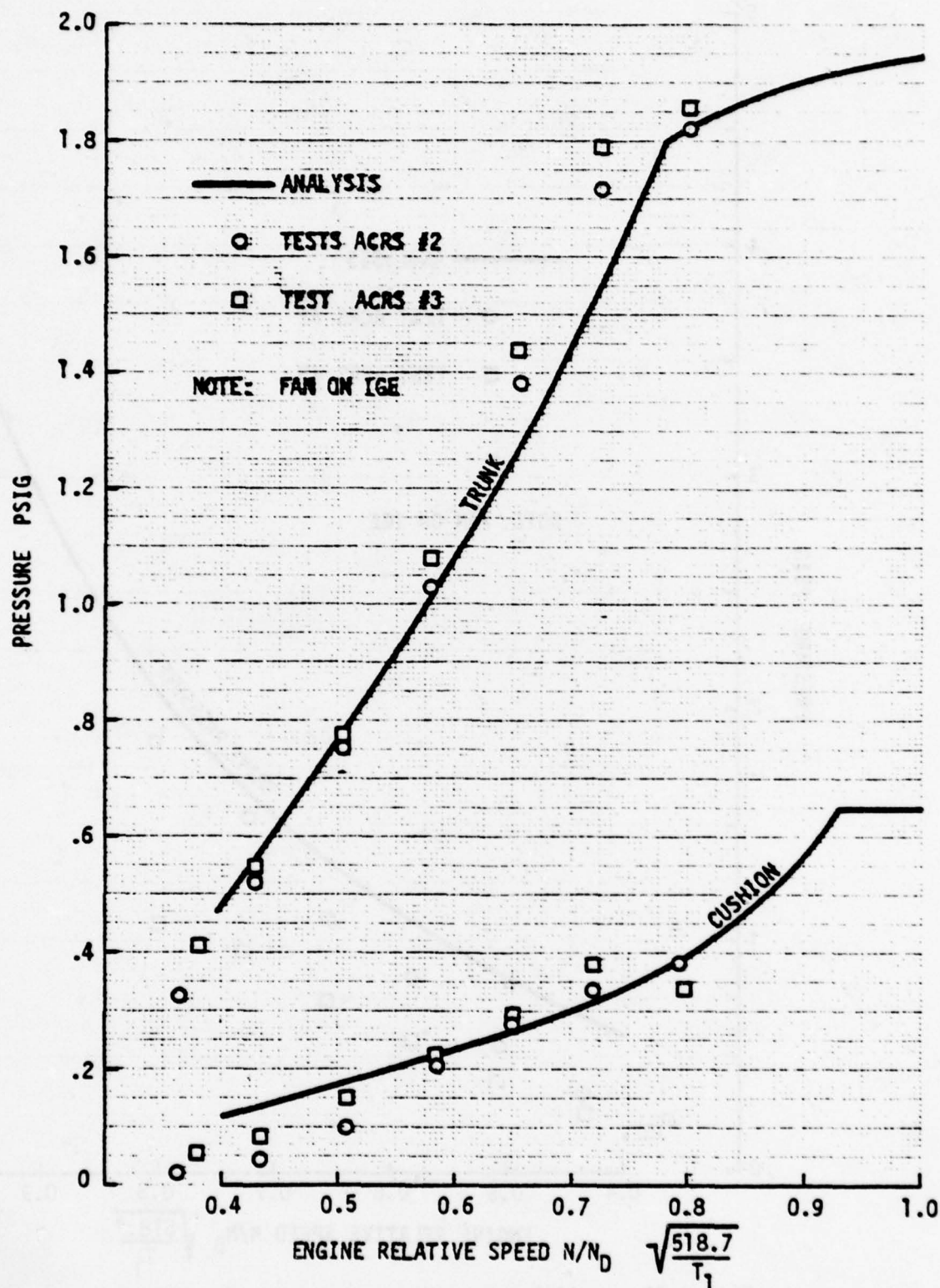
Figure 23   ACRS Trunk and Cushion Pressures -
              Comparison of Test and Analysis

41
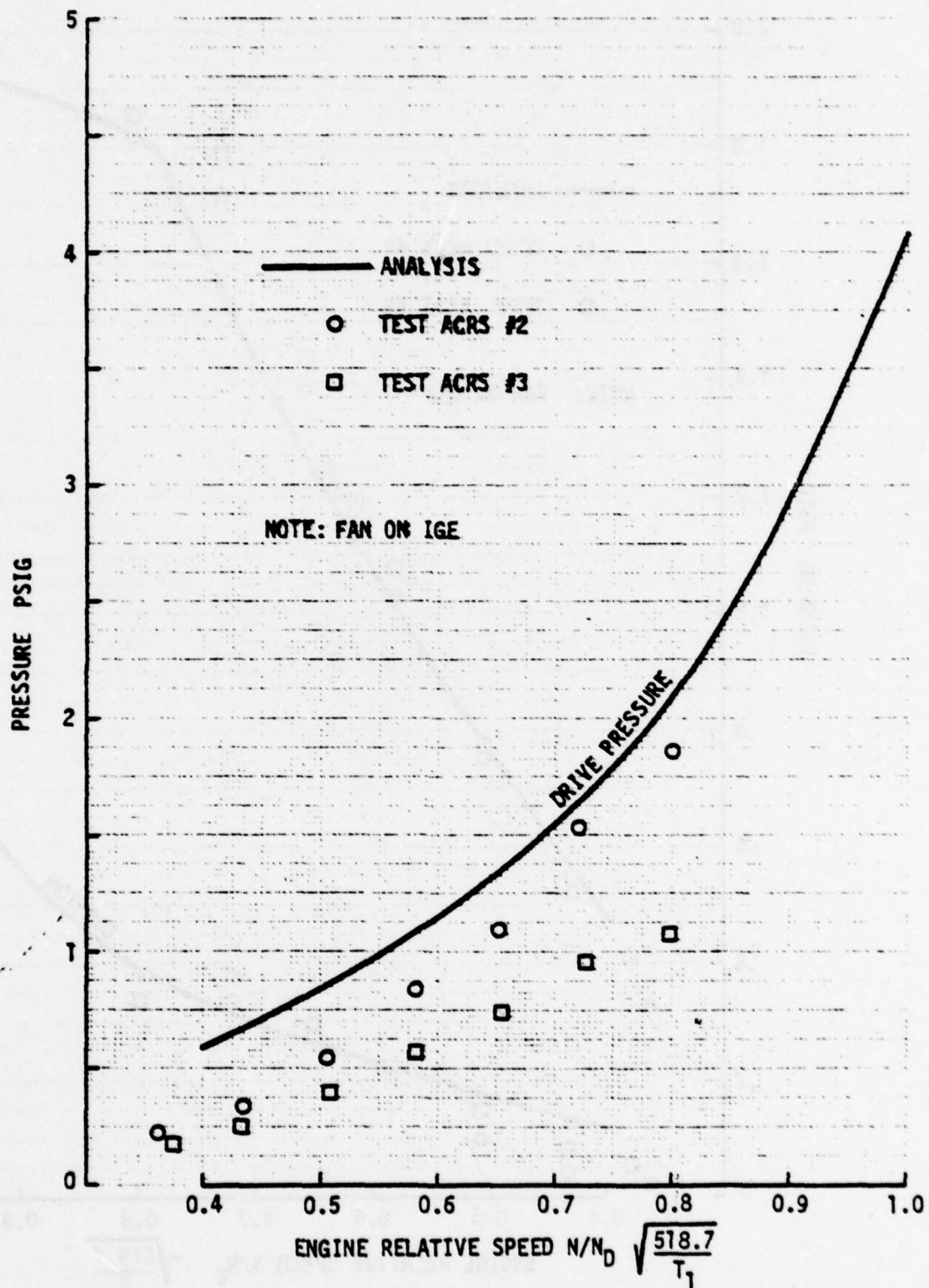
Figure 24   ACRS Drive Pressure - Comparison of
Test and Analysis

42

ENGINE RELATIVE SPEED %	DRIVE PRESSURE PSIA	MEASURED CUSHION PRESSURE PSIG	MAXIMUM FAN OUTLET PRESSURE PSIG (from map)
40	14.9	.07	–
50	15.1	.15	.08
60	15.3	.24	.11
70	15.55	.31	.17
80	15.8	.35	.22

The measured cushion pressures are substantially above the fan outlet pressures at the stall point, which generally are the maximum obtainable outlet pressures. Thus, there is considerable evidence to suggest that measured drive pressures on ACRS #3 are in error.

In conclusion, agreement between test and analysis on the ACRS appears good, and thus the analytically calculated performance figures at higher engine powers, not tested to date, can be used with reasonable confidence. Test data is still required to validate the ACTS airflow model.

2.4 SYSTEM EVALUATION

The lack of ground test data on the ACTS make it difficult to evaluate the adequacy of the system with confidence. Hover pressure is achieved at an engine relative speed of 80%, which is satisfactory. The major concern is whether trunk pressures are high enough to provide sufficient pitch and roll stiffness, particularly during deceleration on the ACTS. This question can only be resolved by future testing.

With the current ACRS system, and assuming that a trunk pressure of approximately 1.8 psig is required to give sufficient pitch and roll stiffness, the minimum engine speed for fan-on operation is around 77%. The corresponding thrust is between 750-1000 lbs. Such a thrust level is higher than that

anticipated during approach, and certainly unacceptably high for slideout. Thus approach and slideout are currently envisaged as being with the fan off.

A current concern about Jindivik is the high drag loads, and resulting pitch moments, which would occur during a fan-off landing. As discussed in Section 5, the Jindivik landing system is unlike any ACLS that has been tested to date, in that there is no cushion pressure to absorb part of the vertical load and only part of the trunk is lubricated. Imposition of the high drag loads, and resulting forward pitching moments, on a system with limited pitch stiffness, could cause unacceptable pitch oscillation and contact of the fuselage with the ground.

For demonstration landings, an obvious way to alleviate this problem is to select a low friction surface such as wet grass. The alternative approach is to modify the airflow system to permit fan-on landings. Referring to Figure 16, it can be seen that the major contributors to pressure drop in the system are the bleed port and the bleed port fitting. The pressure drop in the latter can certainly be reduced by an improved design. System pressure drops can also be reduced by replacing the flexible ducting running external to the Jindivik fuselage with smooth ducting. Figure 25 shows trunk and cushion pressure, assuming a bleed port fitting K factor of 2, based on an area of 7.07 square inches. The figure also shows the effect of turbofan valve angles of 90° (full open), 45°, 30° and 0° (full closed). As the turbofan valve is closed, trunk pressure is increased at the expense of cushion pressure. Assuming a requirement to maintain a trunk pressure of at least 1.8 psig at an engine speed of 60%, the fan valve angle can be set at 45°. This gives an equilibrium cushion pressure of 0.2 psig, resulting in significantly lower drag and pitching moments. An alternate approach is to control the fan valve angle as a function of engine speed. Figure 26 shows a suitable control law for the valve, and Figure 27 the resulting trunk and cushion

44
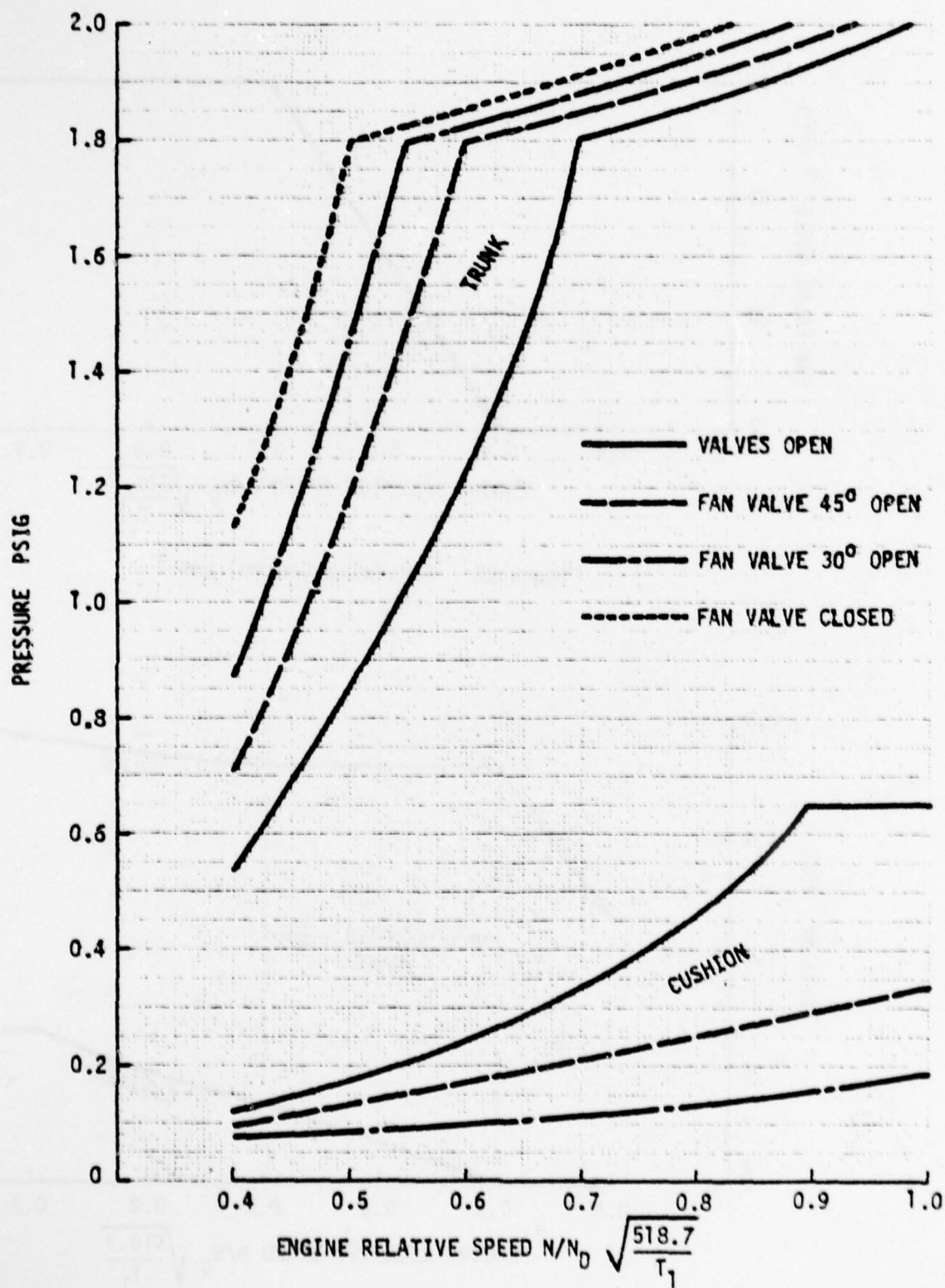
Figure 25   ACRS Trunk and Cushion Pressures
- Reduced Port Fitting Losses
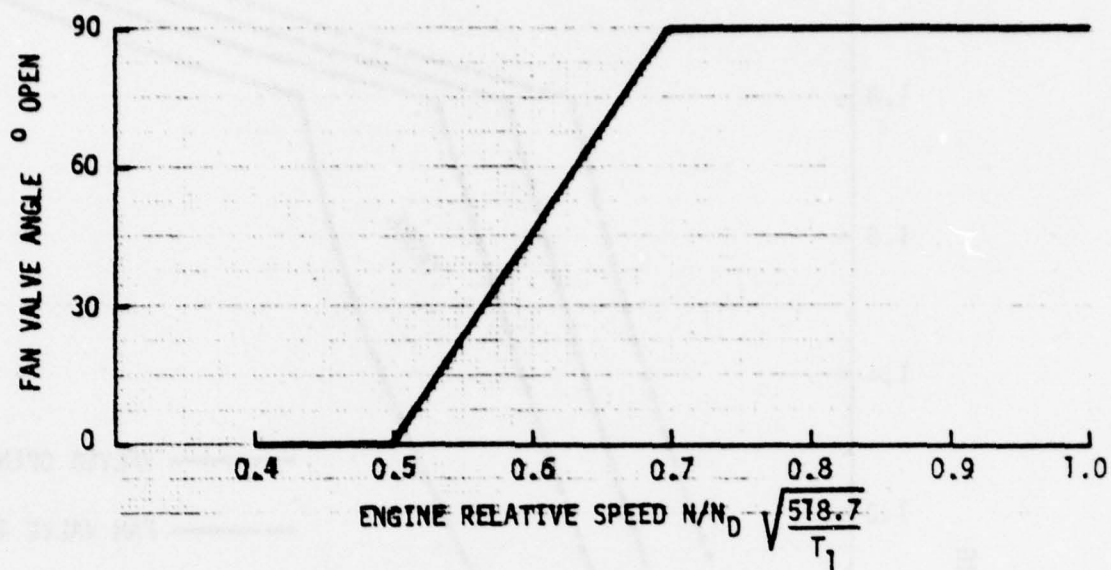
Figure 26   Fan Valve Control Law
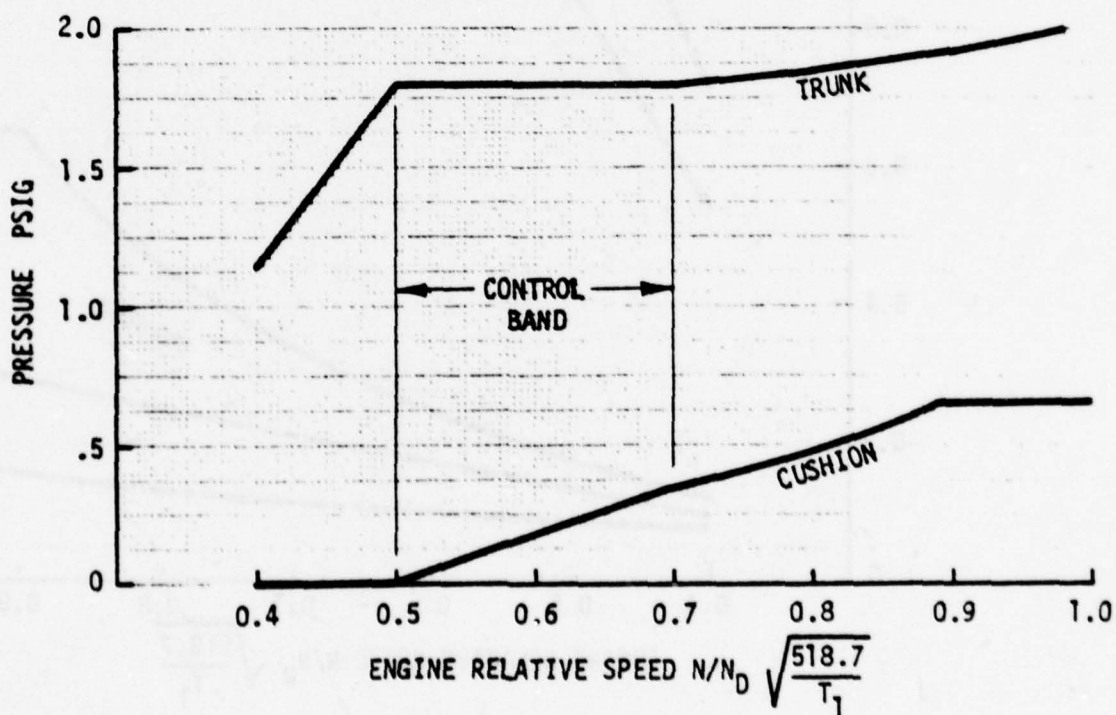
Figure 27   ACRS Trunk and Cushion Pressures -
Controlled Fan Valve

46

pressures. Figure 16 indicates that the second major contributor to system pressure drops is the engine bleed port. Bleed port losses could be substantially reduced by using a Viper 522 center section, giving a choked corrected flow at the ports of 2.7 $\frac{lbs/sec \ ^{\circ}R^{1/2}}{psia}$,as opposed to 1.5 for the Viper 11/201 center section. With the Viper 522 center section port characteristics, and the improved bleed port fitting, trunk cushion pressures are approximately as shown as Figure 28. With the fan valve fully open, the calculated trunk pressure is 1.81 psig and cushion pressure .34 psig at an engine speed of 60%. Thus fan-on approach, landing and slideout would be possible. During fan off operation, a maximum trunk pressure of 2.19 psig is achieved and the relief valve still should have adequate margin to absorb pressure transients.

The Viper 522 center section also benefits ACTS airflow performance. For example at an engine speed of 70%, trunk pressure is increased from .5 to .8 psig, and cushion pressure from .4 to .7 psig (hover condition).

The Viper 11/201 manual recommends that bleed flows "should not exceed 6 1/2% of the air mass flow, but higher bleeds can be accommodated". Figure 29 compares bleed flows for the ACRS (fan-on and fan-off) and the ACTS with this limit. Highest flows are with ACRS fan-on operation. With the baseline system, the recommended bleed extraction rate is not exceeded. With the new center section, the bleed flow at a relative speed of 100% is 237 lb/min. This is 9% of the Viper 11/201 core flow, but only 7.5% of the 522 center section core flow. Thus overbleeding is unlikely to be problem with a new center section.

In conclusion, there is the potential for considerable improvement in airflow system performance. Redesign of the bleed port fitting and system ducting produces a worthwhile

47
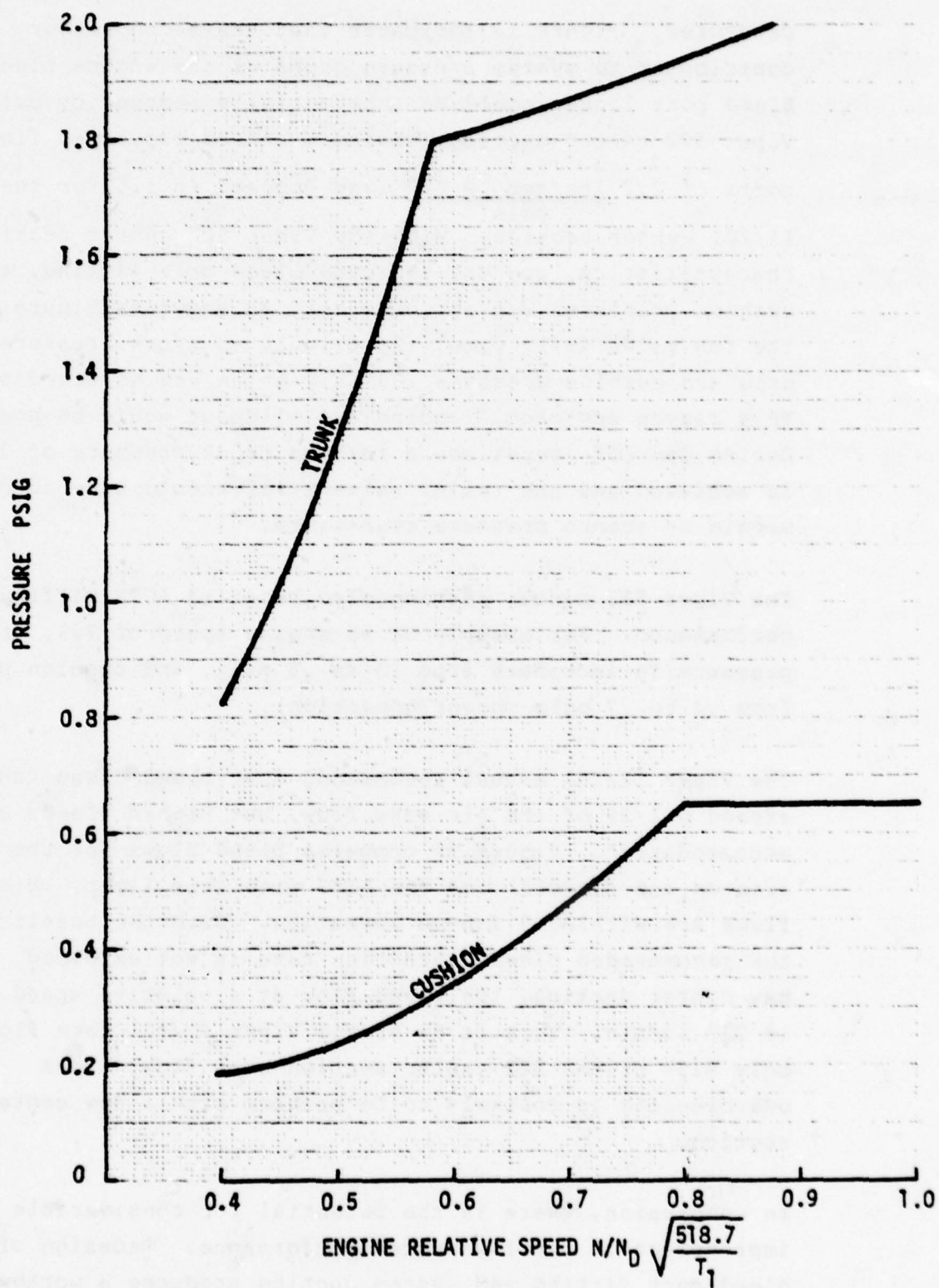
Figure 28   ACRS Trunk and Cushion Pressures —
              Viper 522 Center Section

48

240 ─

220 ─

200 ─

180 ─

160 ─

140 ─

120 ─

100 ─

80 ─

60 ─

40 ─

BLEED AIR FLOW RATE $(W_b \times 60)$ LBS/MIN

──────── RECOMMENDED LIMIT, VIPER 11/20 I

─ ─ ─ ─ ACRS FAN ON ⎫
                    ⎬ NEW PORT,
─ ·─ ·─   ACTS   ⎭ NEW FITTING

············ ACRS FAN ON, BASELINE SYSTEM

0.4   0.5   0.6   0.7   0.8   0.9   1.0

ENGINE RELATIVE SPEED $N/N_D \sqrt{\dfrac{518.7}{T_I}}$
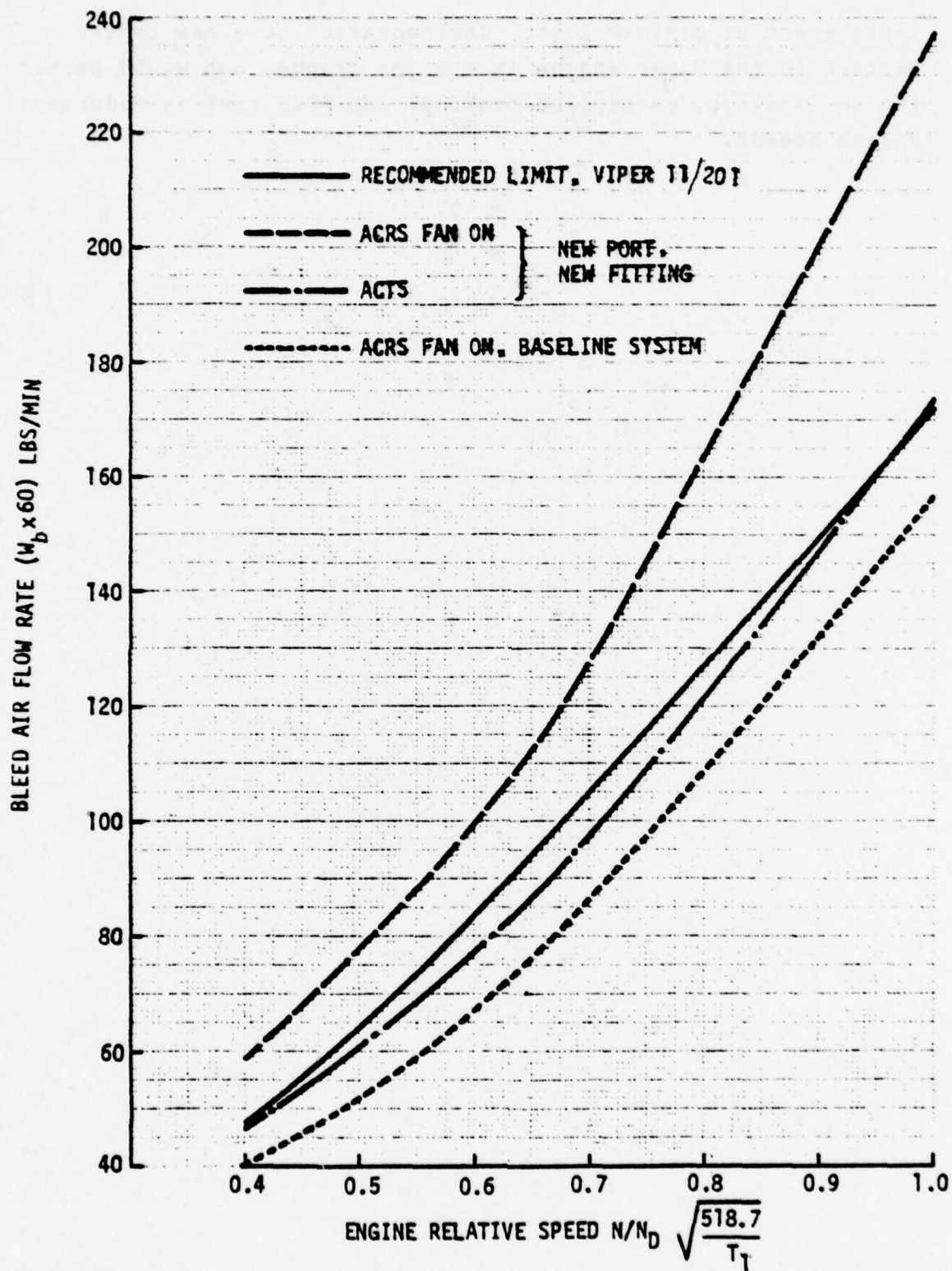
Figure 29   Comparison of Actual and Recommended
Bleed Flow Rates

49

improvement at minimum cost. Incorporation of a new center
section in the Viper engine is a major change, but would permit
fan on landings, controlled braking, and ACRS taxi at reduced
engine speeds.

50
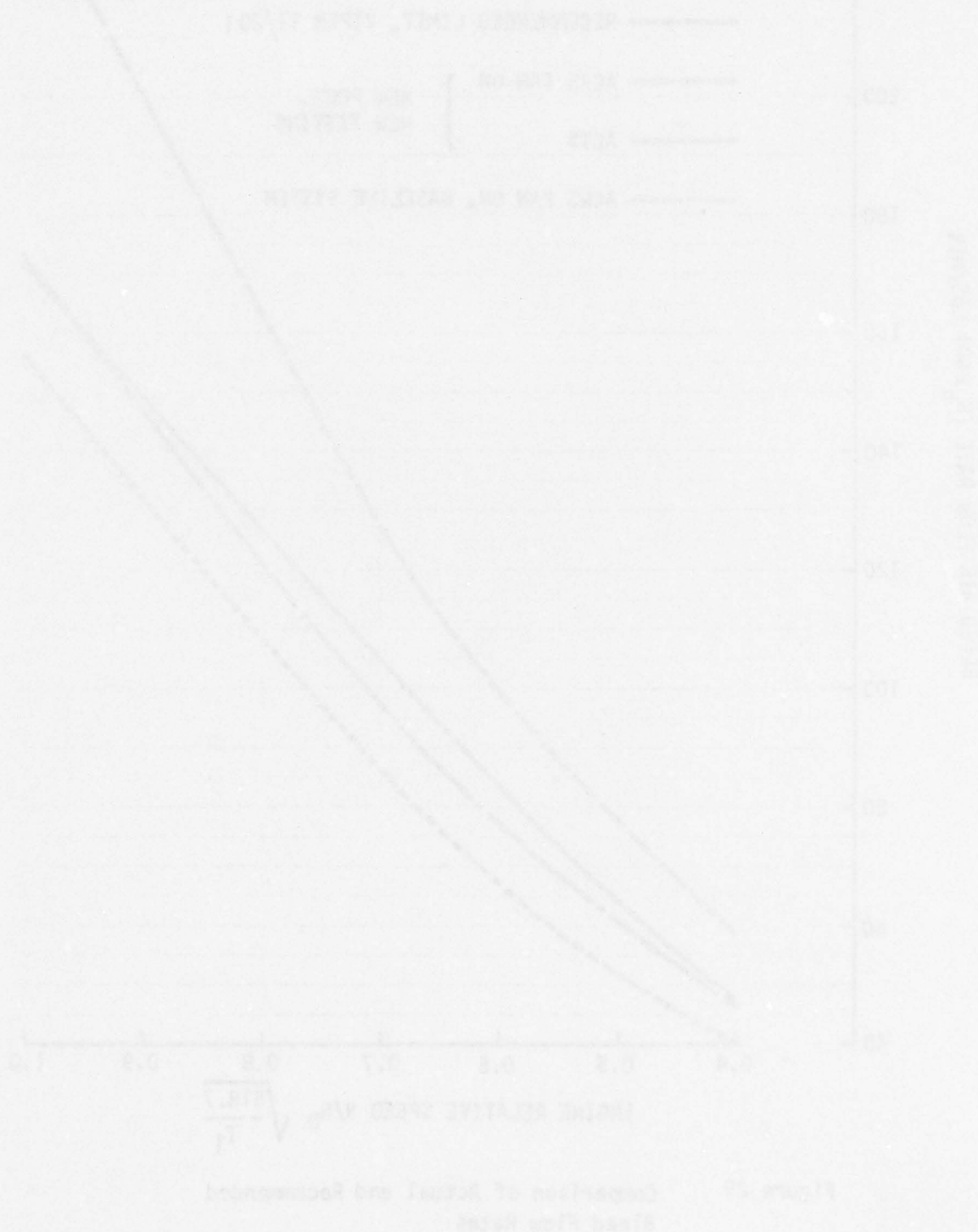
YAW THRUSTER CONTROL ANALYSIS

This section contains a description of the Jindivik yaw control
system and its performance under static and dynamic conditions
at high engine power settings for the ACTS and ACRS. The
response of the vehicle to disturbances generated by side wind,
gusts and runway crown is evaluated.

3.1 YAW THRUSTER DESCRIPTION

The Jindivik autopilot, consisting of roll, pitch and yaw gyros,
positions the elevator and ailerons to maintain the flight
attitude. The Jindivik has no rudder; turns during flight are
performed through rolling maneuvers initiated by the ailerons.

The Jindivik normally utilizes a tricycle trolley for launch.
During launch, the yaw gyro commands bypass the ailerons and
instead control the trolley front wheel steering angle. The
autopilot does not sense lateral drift. The "batsman" located
on the runway centerline sights the Jindivik through binoculars
and steers by rotating the yaw gyro reference angle by radio
control. The autopilot senses an error in the yaw angle and
commands a steering adjustment. The maximum rate of reference
angle change is 10 degrees per second. The difference between a
gyro reference angle and the actual aircraft attitude is called
the reference angle error. The maximum reference angle error is
30 degrees.

At liftoff the Jindivik separates from the trolley, and yaw
control is transferred to the ailerons. Control of the aircraft
during flight is also achieved by resetting the gyro reference
angles.

51

For taxi or takeoff on the ACTS or taxi on the ACRS, yaw control is provided by yaw thrusters, as shown in Figure 30. The mechanism (Figure 31) consists of a solenoid valve that opens and closes an air passage between the exhaust side and the ambient air side. When the solenoid valve is closed, the jet stream reduces the pressure on the turning wall, and hence the jet stream becomes attached to the turning wall (the Coanda effect). When the valve is opened, the vacuum is relieved and thus the jet stream becomes detached from the turning wall.

Operation of the yaw thrusters is controlled by a Pulse Ratio Modulator (Reference 9), which receives the reference angle error as an input from the yaw gyro. The Pulse Ratio Modulator will provide for modulated vectored thrust by oscillating the solenoid valve at 3 Hz. The maximum lateral force of the vectored thrust is 110 lbs at takeoff thrust.

3.2 SYSTEM PERFORMANCE

The purpose of the yaw thruster control system is to provide a means of directional control for the ACLS equipped Jindivik. As the thrusters operate by diverting part of the engine thrust, it is apparent that the control system will be ineffective during conditions of low engine thrust, and in particular during braking on the ACRS and ACTS. In this section, the performance of the system is evaluated for both trunks for engine speed ranging from 60% to 100%, corresponding to taxi and takeoff conditions. The effectiveness of the system is determined for various disturbances such as side winds (steady and gusts) and runway crown effects.

For the system performance analysis, certain assumptions, described in detail in the following sections, were made concerning ACRS and ACTS trunk and cushion pressures as a function of engine speed. Initial ground testing in Australia

CONTROL PORTS

SOLENOID
VALVE
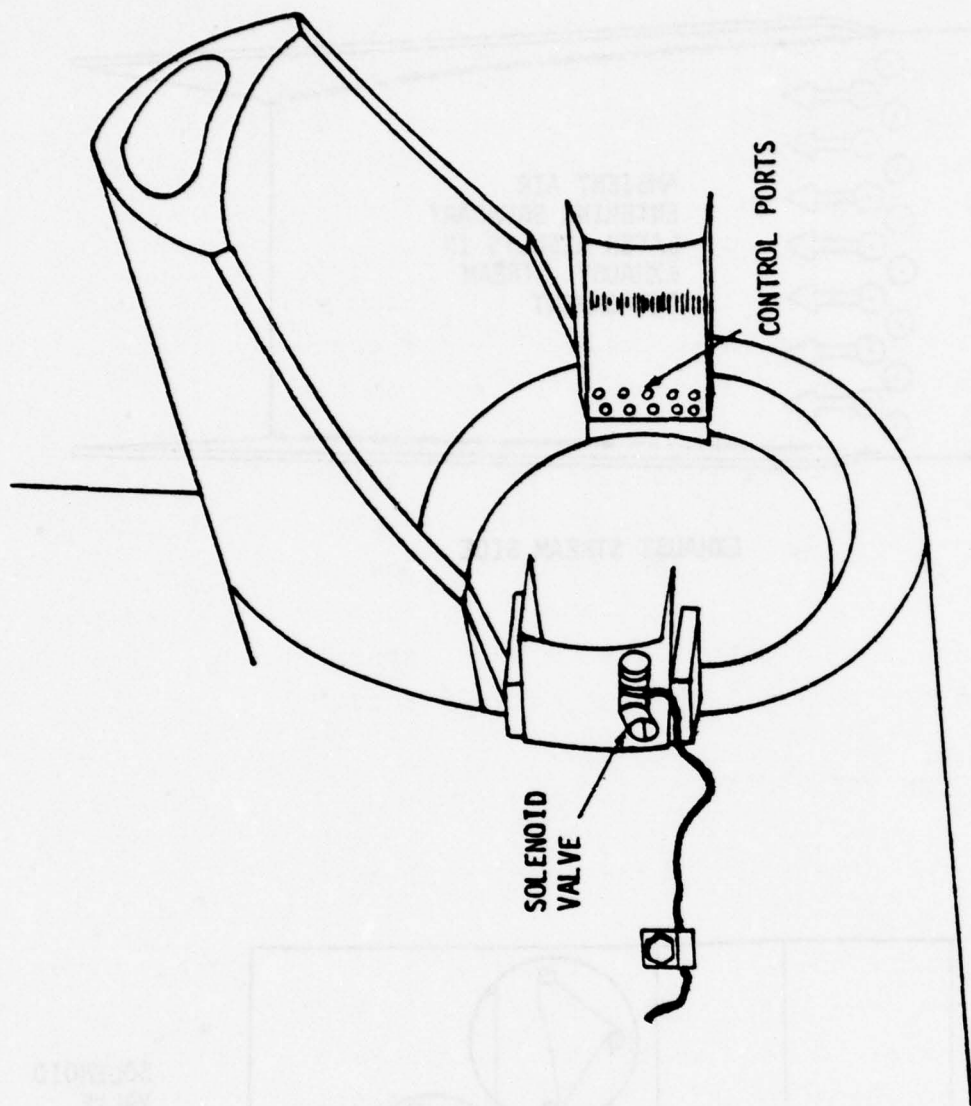
Figure 30 Thrust Vector Control System Installation

AMBIENT AIR
ENTERING BOUNDARY
LAYER RESULTS IN
EXHAUST STREAM
DETACHMENT

EXHAUST STREAM SIDE

SOLENOID
VALVE
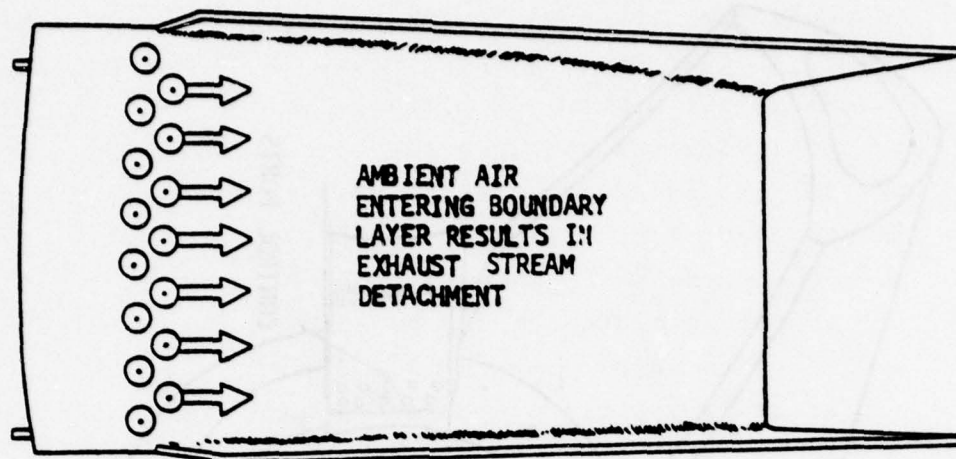
AMBIENT AIR
(VALVE OPEN)
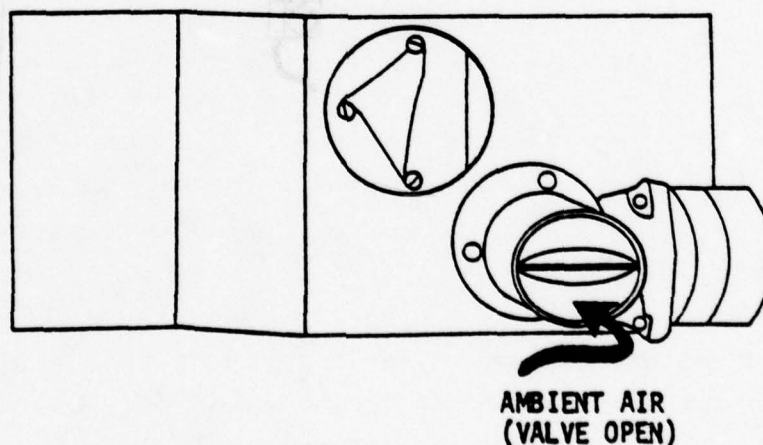
AMBIENT AIR SIDE

Figure 31 Thrust Vector Control System Mechanism

54

showed actual trunk and cushion pressures to be substantially
lower, as discussed in Section 2. Thus, the analysis reported
herein is not directly applicable to the vehicle configuration
tested in Australia, since the higher trunk and cushion
pressures assumed for the analysis result in trunk drags low
enough to be comparatively unimportant. Various recommendations
have been made in Sections 2 and 8 of this report for ways to
improve the performance of the airflow system. It will be
necessary to adopt some or all of these recommendations to give
satisfactory vehicle performance, and trunk and cushion
pressures will be improved over values experienced in Australia.
When test data on the improved system becomes available, it will
be possible to assess the applicability of the results in this
section by comparing trunk and cushion pressures with the values
assumed for this analysis. If there is still a significant
discrepancy, the analysis should be updated to reflect the
latest airflow system performance.

3.2.1 Method of Analysis

The effectiveness of the thruster system was investigated
through both steady state and dynamic analyses. In the steady
state analysis, a disturbing force such as a side wind is
defined. For the vehicle to be at steady state, both lateral
forces and moments must be in balance. The analysis determines
the percentage of available side force from the yaw thruster,
and the vehicle yaw angle, at which such a balance is achieved.
The analysis is then repeated first at different engine speeds
(or thrusts) and vehicle speeds, and then for different
disturbances. In the dynamic analysis, the directional control
performance is evaluated during a vehicle run such as a takeoff
roll. The criterion of performance is the vehicle drift from
the runway centerline. The dynamic analysis introduces another
variable, namely the response of the "batsman" who controls the
yaw gyro setpoint. The batsman is assumed to respond to lateral
drift and not to vehicle heading. The two parameters

55

determining the role of the batsman are assumed to be the drift at which the batsman starts to respond (i.e. the deadband), and the amount by which he resets the heading for a drift exceeding the threshold (i.e. the gain).

The evaluation of yaw thruster effectiveness, both steady state and dynamic, was accomplished using a four degrees of freedom (4 DOF) computer program (Reference 10). The degrees of freedom are longitudinal and lateral motion, yaw and roll. Yaw must be included as a degree of freedom because the aerodynamic side force is potentially the highest force acting on an aircraft during slideout and taxi, and is extremely sensitive to the angle of aerodynamic sideslip β. Roll is required to include wing tip skid and asymmetrical trunk drag influences.

For operation on the ACRS at low engine power settings such as in taxi operation, the vehicle pitch angle will influence trunk drag as only the forward one third of the trunk is lubricated. Consequently for ACRS analysis, the pitch angle was calculated on a quasi steady-state basis. As trunk drag was considered to be significant only for the low engine power (and hence low speed) cases, the effect of elevator moments on the pitch angle was not included. Pitch angles were not determined for the ACTS analysis.

Forces and moments acting on the vehicle are shown as Figures 32 and 33 respectively, and include the effect of the following:

- o Crosswind velocity
- o Vehicle moments of inertia
- o Trunk induced forces and moments
- o Wing tip skid induced forces and moments
- o Yaw thruster forces and moments
- o Taxiway crown or slope
- o Engine thrust
- o Engine gyro coupling effects
- o Aerodynamic forces and moments (including ailerons)

56
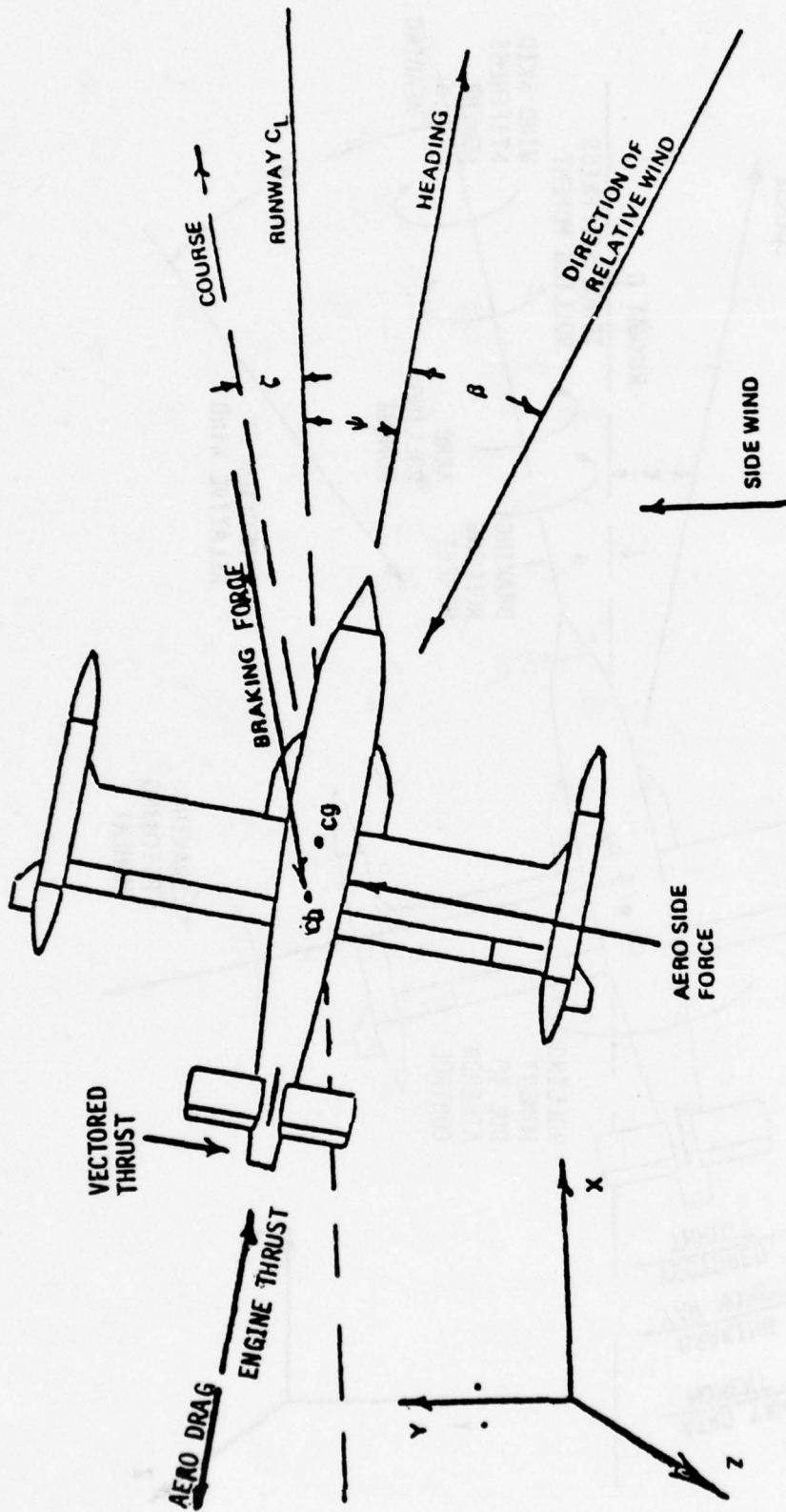
Figure 32 Force Diagram X-Y Plane
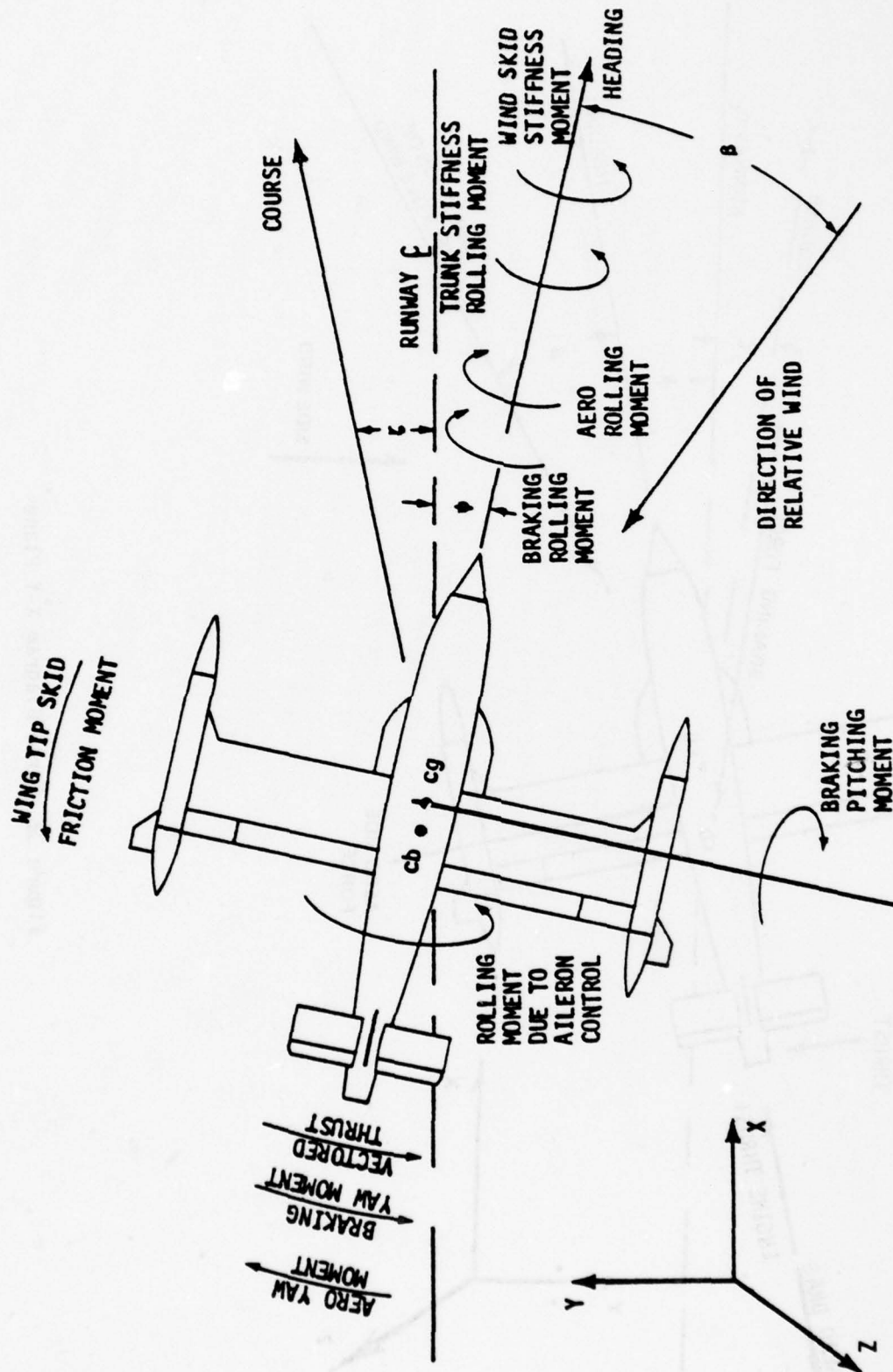
Figure 33 Moment Diagram

58

Basic vehicle data assumed for the analysis is summarized in Table 3.

The equations expressing the forces and moments acting on the vehicle are derived in the following paragraphs.

ACTS Trunk. The frictional drag of the ACTS trunk which is assumed to have a uniform coefficient of friction fore and aft is given by:

$$F_{td} = \mu_t A_t P_t \tag{1}$$

where the ACTS trunk pressure P_t versus engine RPM is shown in Figure 34. The P_t - RPM relationship was determined by the airflow system analysis of Reference 5. As discussed in Section 3.2, the assumed trunk and cushion pressures in this analysis are higher than values observed during the ground tests. They are also higher than values calculated in Section 2, since those calculations were updated following the ground tests. The trunk-ground reaction force $A_t P_t$ in equation (1) is net force of the aircraft weight, W_a, aerodynamic lift, L, and the force of air cushion lift, $P_c A_c$. The flattened area of the trunk is thus:

$$A_t = (W_a - L - P_c A_c)/P_t \quad \text{(Equilibrium)} \tag{2}$$

The cushion area is assumed constant and the cushion air pressure is assumed to vary with engine RPM and the aircraft weight-lift differential as shown in Figure 35.

TABLE 3 - AIRCRAFT DATA

WEIGHT	3400 LBS
MOMENTS OF INERTIA	
I_{xx} (ROLL)	2414 SLUG-FT^2
I_{zz} (YAW)	4082 SLUG-FT^2
CG HEIGHTS	
ACRS	2.8 FT
ACTS	3.1 FT
MAX ENGINE THRUST	2500 LBS
ENGINE RPM FOR TAKEOFF	
0 KNOTS	87%
40 KNOTS	100%
ENGINE GYRO COUPLING COEFFICIENT	21.8 FT-LB-SEC/DEG
WING TIP SKID AND WING ROLL STIFFNESS	6300 FT-LB-DEG
WING REFERENCE AREA	76 SQ. FT.
WING SPAN	18 FT.
ACTS TRUNK	
CUSHION AREA	3988 SQ. IN.
ROLL STIFFNESS	31 FT-LBS/DEG
PITCH STIFFNESS	1000 FT-LBS/DEG
ROLL DAMPING	8.9 FT-LB-SEC/DEG
ACRS TRUNK	
CUSHION AREA	3812 SQ. IN.
▷1 ROLL STIFFNESS	98 FT-LBS/DEG (STATIC)
	90 FT-LBS/DEG (DYNAMIC)
▷2 PITCH STIFFNESS	1030 FT-LBS/DEG (STATIC)
	1250 FT-LBS/DEG (DYNAMIC)
ROLL DAMPING	7.05 FT-LBS-SEC/DEG

▷1 95 FT-LBS/SEC USED IN ANALYSIS
▷2 1030 FT-LBS/DEG USED IN ANALYSIS

Figure 34   ACTS Trunk Pressure

Figure 35   ACTS Cushion Pressure

Figure 36   ACTS Trunk Center of Braking

61
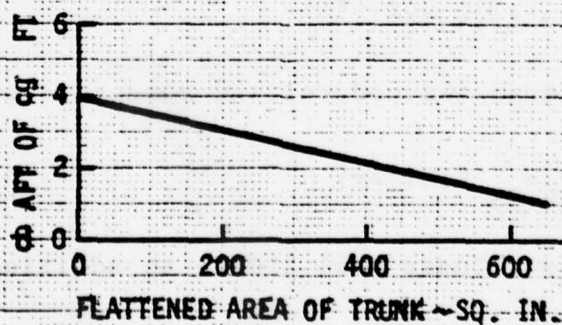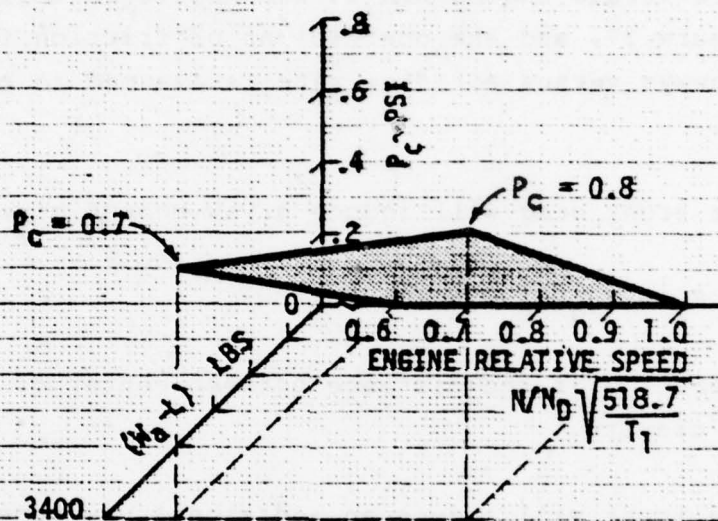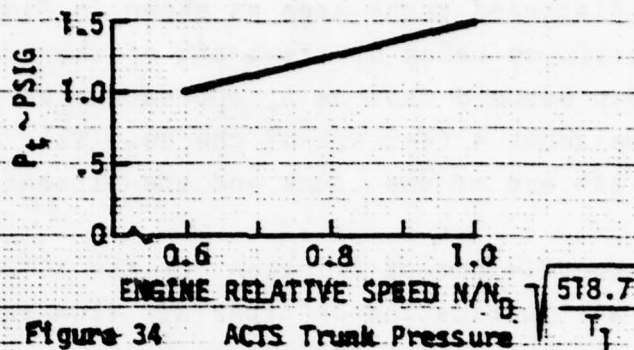
The center of braking for the ACTS trunk is assumed to vary with the flattened trunk area as shown in Figure 36. With the aircraft cg being 0.5 feet aft of the trunk center of pressure, it was assumed that as A_t approaches zero, the center of braking moves about 4 feet aft of the cg. This is the distance between the aft end of the trunk and the aircraft cg.

The coefficient of friction for the ACTS trunk is dependent on the air lubrication or trunk air flow rate. The trunk air flow rate versus engine RPM is assumed to be defined as shown in Figure 37, and the coefficient of friction for wet and dry runways versus air flow rate is assumed to be as shown in Figure 38.

The trunk drag will induce a yaw moment given by:

$$M_z = F_{td} \ell_{cb} \, \text{Sin} \, (\psi + \zeta) \tag{3}$$

Where ℓ_{cb} is the distance between center of braking and center of gravity.

The trunk will induce an additional yaw moment when in a rolled attitude, given by:

$$M_z = (K_\phi)_t \phi \mu_t \, \text{Cos}(\psi + \zeta) \tag{4}$$

The trunk drag induced rolling moment is given by:

$$M_x = F_{td} h_{cg} \, \text{Sin}(\psi + \zeta) \tag{5}$$

The trunk stiffness will induce an additional rolling moment given by:

$$M_x = (K_\phi)_t \phi \tag{6}$$

The rolling motion is damped by:

62
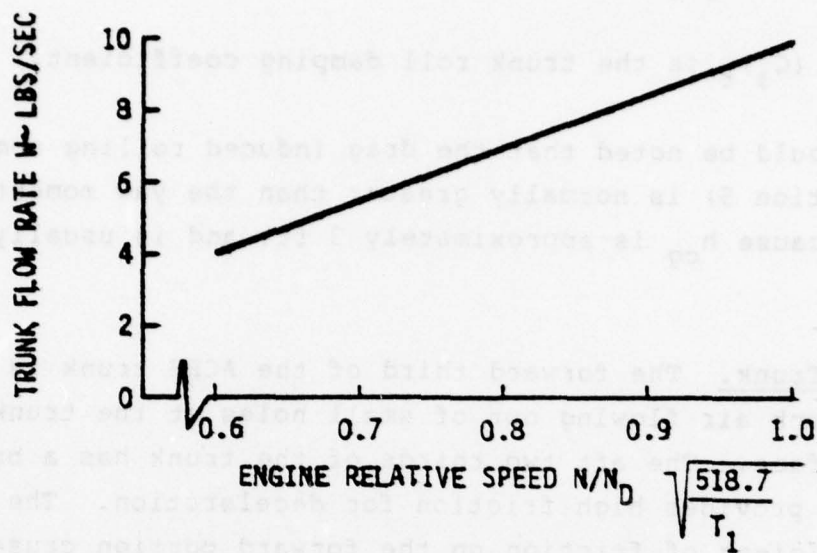
Figure 37   ACTS Trunk Air Flow Rate
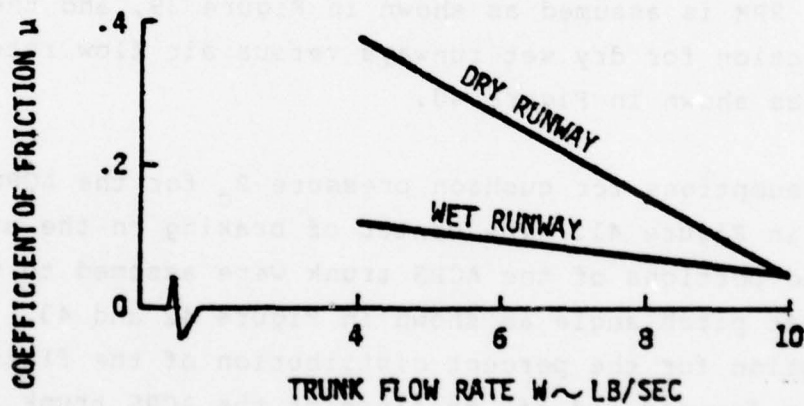
Figure 38 ACTS Trunk Coefficient of
Friction Versus Air Flow Rate

63

$$M_x = -(C_\phi)_t \dot{\phi} \qquad\qquad (7)$$

Where $(C_\phi)_t$ is the trunk roll damping coefficient.

It should be noted that the drag induced rolling moment (Equation 5) is normally greater than the yaw moment (Equation 3) because h_{cg} is approximately 3 ft. and is usually larger than ℓ_{cb}.

ACRS Trunk. The forward third of the ACRS trunk is lubricated by trunk air flowing out of small holes at the trunk ground interface. The aft two thirds of the trunk has a brake tread which provides high friction for deceleration. The lower coefficient of friction on the forward portion causes the center of drag to be aft of the cg and thus directional stability is provided. The coefficient of friction for the aft two thirds is assumed to be 0.9 and 0.3, respectively, for dry and wet runways. The coefficient of friction for the forward portion is dependent on the air flow rate. The trunk air flow rate versus engine RPM is assumed as shown in Figure 39, and the coefficient of friction for dry wet runways versus air flow rate is assumed to be as shown in Figure 40.

The assumptions for cushion pressure P_c for the ACRS trunk is given in Figure 41. The center of braking on the aft and forward portions of the ACRS trunk were assumed to vary with the aircraft pitch angle as shown in Figure 42 and 43. The assumption for the percent distribution of the flattened area for the forward and aft portions of the ACRS trunk is shown in Figure 44.

Assuming that in the calculation of pitch angle the distribution between forward and aft flattened areas corresponds to the 0° pitch point of Figure 44, the pitch angle θ is approximated (Figure 45) by:

64
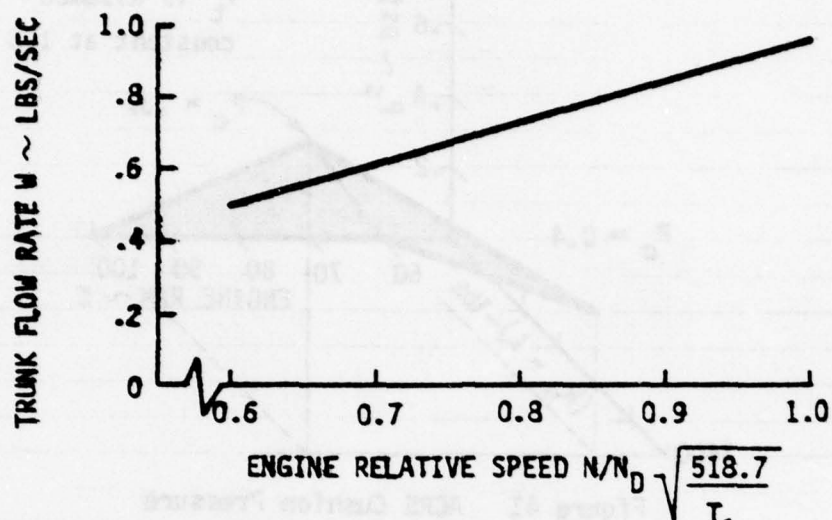
Figure 39   ACRS Trunk Air Flow Rate - Fan Off[1]
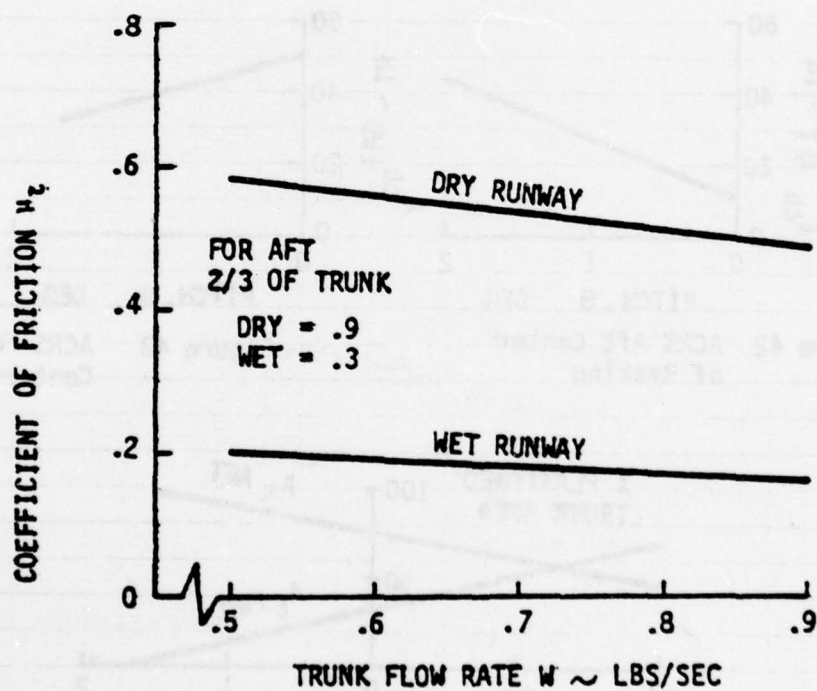
Figure 40   Forward ACRS Trunk Coefficient of
Friction vs Air Flow Rate
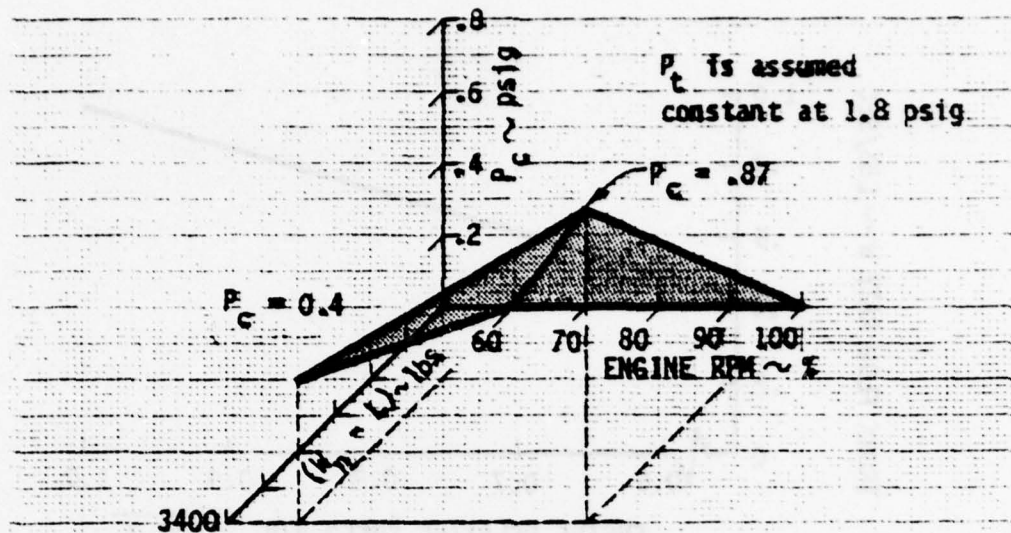
Figure 41   ACRS Cushion Pressure
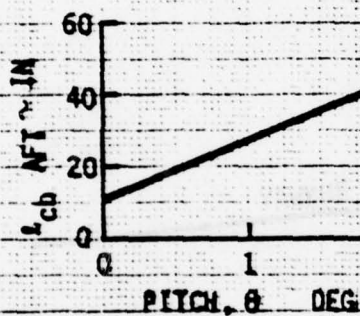
Figure 42   ACRS Aft Center
of Braking
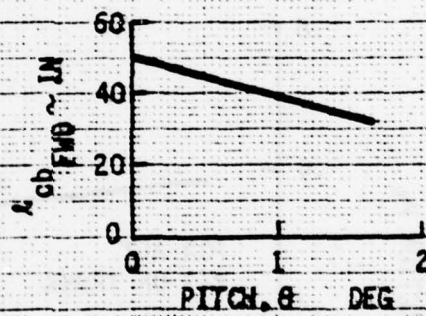
Figure 43   ACRS Forward
Center of Braking
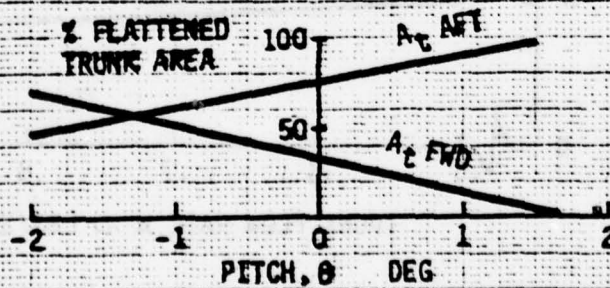
Figure 44   Percent Flattened Areas of ACRS Trunk

66

CENTER OF CUSHION PRESSURE MOMENT

TRUNK STIFFNESS MOMENT

TRUNK DRAG MOMENT

DRAG

h_{cg}

.5 FT

CG

CP
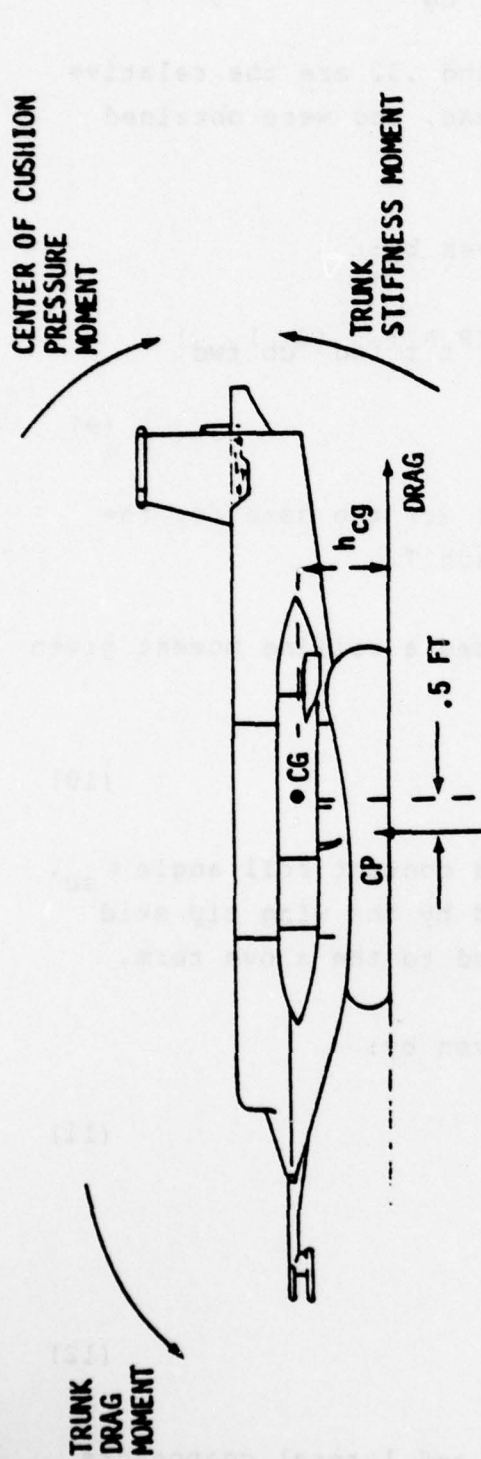
TRUNK STIFFNESS MOMENT $= K_\theta \theta$

TRUNK DRAG MOMENT $= (.68 \, (\mu_t)_{aft} + .32 \, (\mu_t)_{fwd}) \, A_t P_t h_{cg} \, \text{Cos} \, (\psi + \zeta)$

CENTER OF CUSHION PRESSURE MOMENT $= .5 \, A_c P_c$

$\sum M_Y = K_\theta \theta + (.68 \, (\mu_t)_{aft} + .32 \, (\mu_t)_{fwd}) \, A_t P_t h_{cg} \, \text{Cos} \, (\psi + \zeta) + .5 \, A_c P_c = 0$

THUS

$\theta = -\left[.5 A_c P_c + (.68 \, (\mu_t)_{aft} + .32 \, (\mu_t)_{fwd}) \, A_t P_t h_{cg} \, \text{Cos} \, (\psi + \zeta) \right] / \, K_\theta$

Figure 45 Balance of Pitching Moments

67

$$\theta = - [.5A_c P_c + (.68(\mu_t)_{aft} + .32(\mu_t)_{fwd})A_t P_t h_{cg} Cos(\psi+\zeta)]/K_\theta \qquad (8)$$

In the above equation the factors .68 and .32 are the relative non-lubricated and lubricated trunk areas, and were obtained from the appropriate drawings.

The yaw moment due to trunk drag is given by:

$$M_z = [(\mu_t)_{aft}(P_t A_t)_{aft}(\ell_{cb})_{aft} - (\mu_t)_{fwd}(P_t A_t)_{fwd}(\ell_{cb})_{fwd}]$$

$$x \quad sin(\psi+\zeta) \qquad (9)$$

The remaining yaw and roll moment terms are the same for the ACTS and are given in equations 4 through 7.

Wing Tip Skid. The wing tip skid induces a rolling moment given by:

$$M_x = - (K_\phi)_{ws} (\phi \pm \phi_{sc}) \qquad (10)$$

for roll angles ϕ greater than the skid contact roll angle ϕ_{sc}. An additional rolling moment is induced by the wing tip skid frictional forces, but is small compared to the above term.

Similarly, a yaw moment is induced, given by:

$$M_z = (K_\phi)_{ws} (\phi \pm \phi_{sc}) \mu_{ws} Cos (\psi+\zeta) \qquad (11)$$

The skid friction is given by:

$$F_\mu = \frac{2}{b} (K_\phi)_{ws} (\phi \pm \phi_{sc}) \mu_{ws} \qquad (12)$$

This can be resolved into longitudinal and lateral components given by:

68

$$F_x = F_\mu \; \cos (\psi + \zeta) \tag{13}$$

$$F_y = F_\mu \; \sin (\psi + \zeta)$$

<u>Yaw Thruster.</u> The yaw thruster produces a yaw moment given by:

$$M_z = F_{tv} \; \ell_{tv} \tag{14}$$

where ℓ_{tv} is the distance between the thrusters and the cg. The yaw thruster force can be resolved into longitudinal and lateral components given by:

$$F_x = F_{tv} \; \sin \psi$$
$$\tag{15}$$
$$F_y = F_{tv} \; \cos \psi$$

The vectored thrust F_{tv} is determined by the demand from the yaw gyro reference angle error, and the maximum available vectored thrust and the resulting thrust loss versus engine RPM are shown respectively in Figures 46 and 47. The engine thrust for various Mach numbers, and at different engine RPM, is shown in Figure 14 (Reference 2). In the analysis the percentage drop in engine thrust due to a higher Mach number is evaluated and applied to the vectored thrust and drag data of Figures 46 and 47.

The yaw gyro demand for vectored thrust was simulated by the assumed control relationship of Figure 48. Although the autopilot will sense directional errors, it will not sense lateral drift from the runway centerline, this function being performed by the batsman located at the end of the runway. The batsman control, namely shifting the yaw gyro reference angle, was simulated by the assumed relationship shown on Figure 49.

69
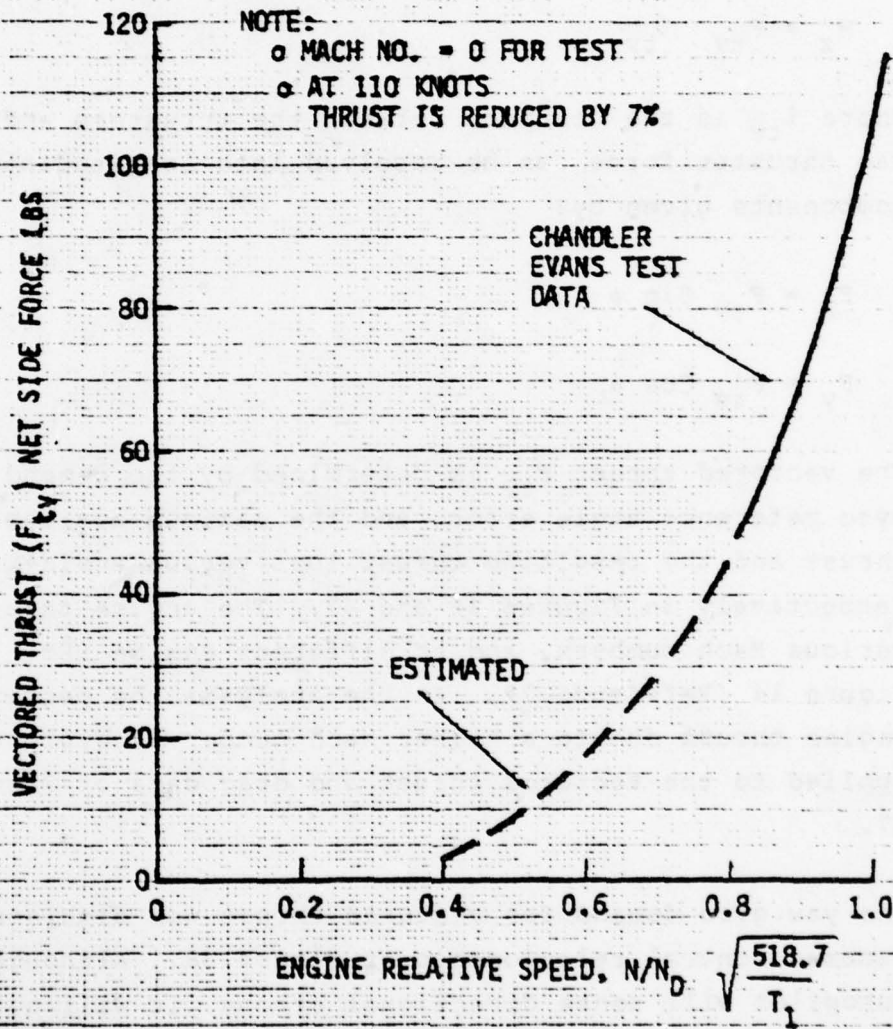
Figure 46   Maximum Available Vectored Thrust
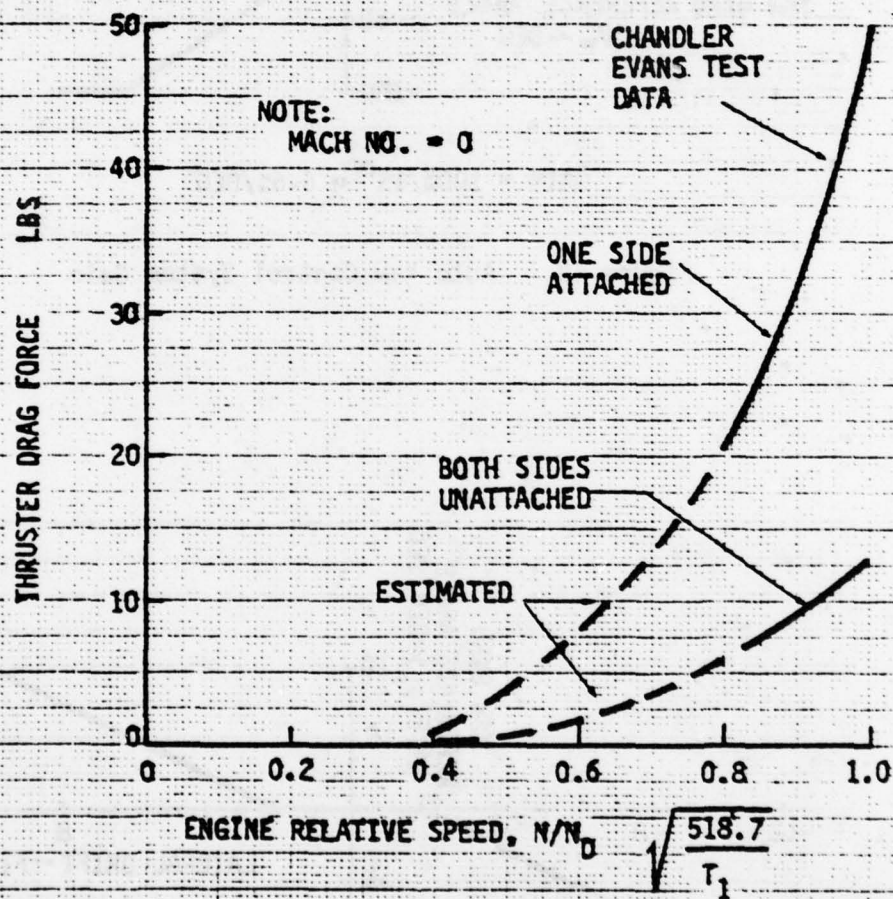
Figure 47   Maximum Thrust Vector Control System Drag
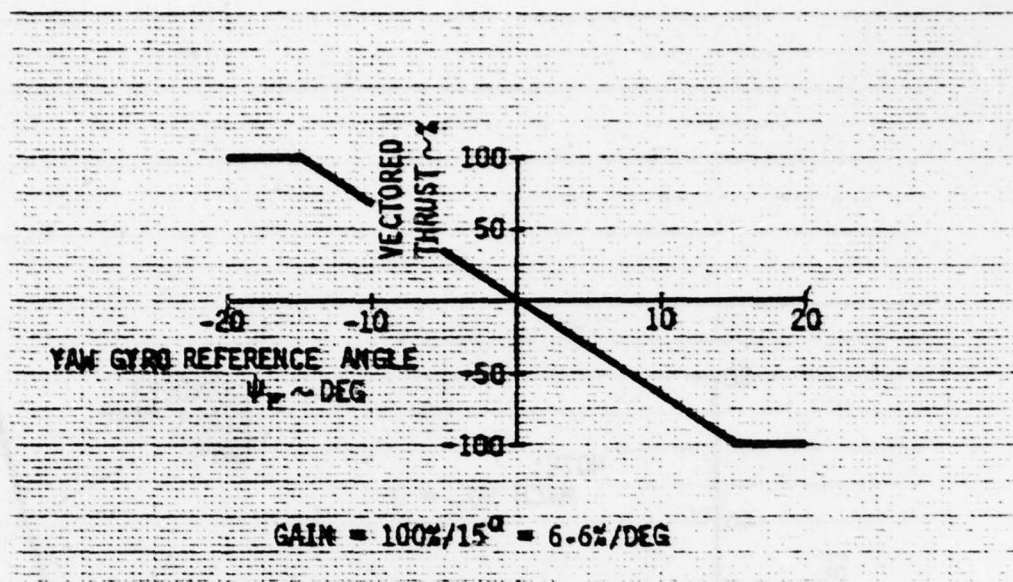
Figure 48   Auto Yaw Control System Gain
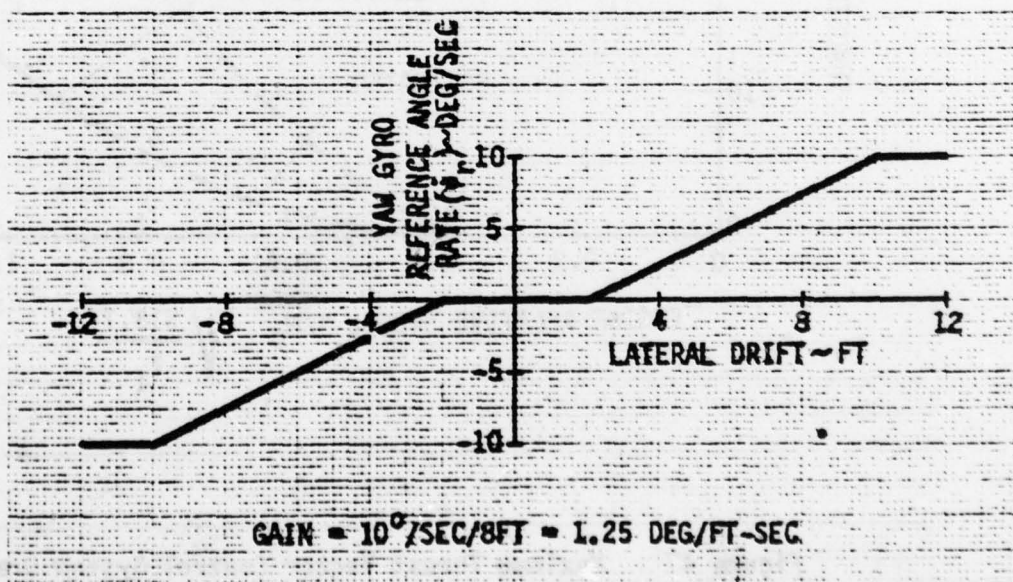
Figure 49   Ground Based Pilot Control of Yaw-Gyro

72

1.0

1.1

1.25 1.4 1.6

1.8

2.0

2.2

2.5

.28

.25

MICROCOPY RESOLUTION TEST CHART
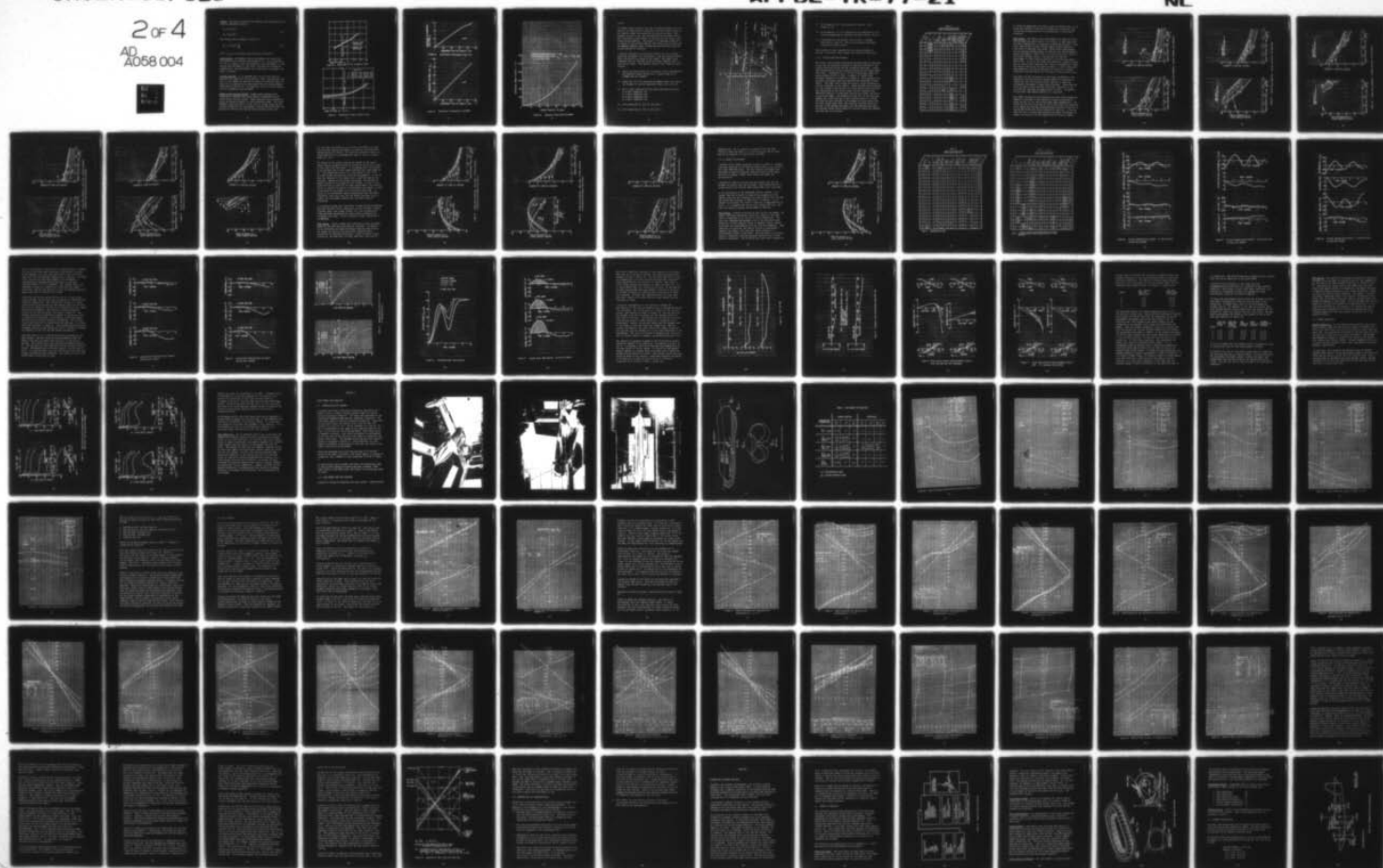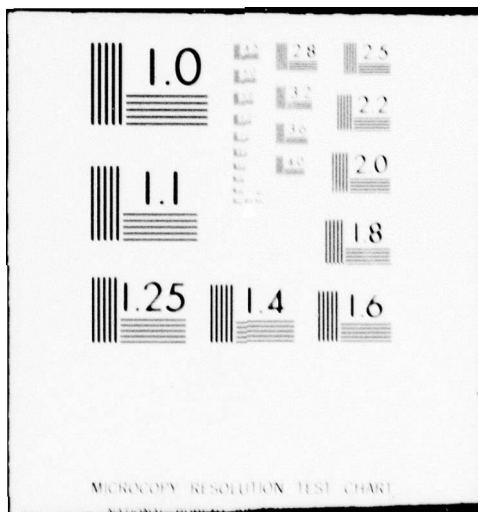
Engine. The engine thrust can be resolved into longitudinal and lateral components given by:

$$F_x = F_{th} \cos \psi$$

$$F_y = F_{th} \sin \psi$$

(16)

The engine gyro yaw moment is given by:

$$M_z = -(C_\psi)_{gc} \, \dot{\psi} \, \frac{N}{N_D}$$

(17)

where $(C_\psi)_{gc}$ is the engine gyro coupling coefficient.

Aerodynamics. Aerodynamic forces and moments are calculated from coefficients obtained from Reference 11. The coefficients of lift C_L, drag C_D, aero side force C_Y, aero yaw moment C_n, and aileron rolling moment C_ℓ are shown in Figures 50 through 54, respectively. The aerodynamic roll coefficient is constant and equal to 0.00125.

Aileron Controls. It is assumed that the roll gyro acts to maintain roll stability of the vehicle. Thus, the ailerons will exert a roll moment as required to attempt to maintain zero roll angle up to a maximum value determined from the rolling moment coefficient of Figure 54. The dynamics of the roll gyro system are not included in this analysis.

Steady State Analysis Method. Steady state analysis were conducted to determine the force balance limitations of the thrust vector control system. These analysis were conducted by using the dynamic program in a non-integrating mode. For given boundary conditions such as cross wind or runway crown and the aircraft conditions of longitudinal velocity and engine RPM, the percent of vehicle crab and available vectored thrust were

73
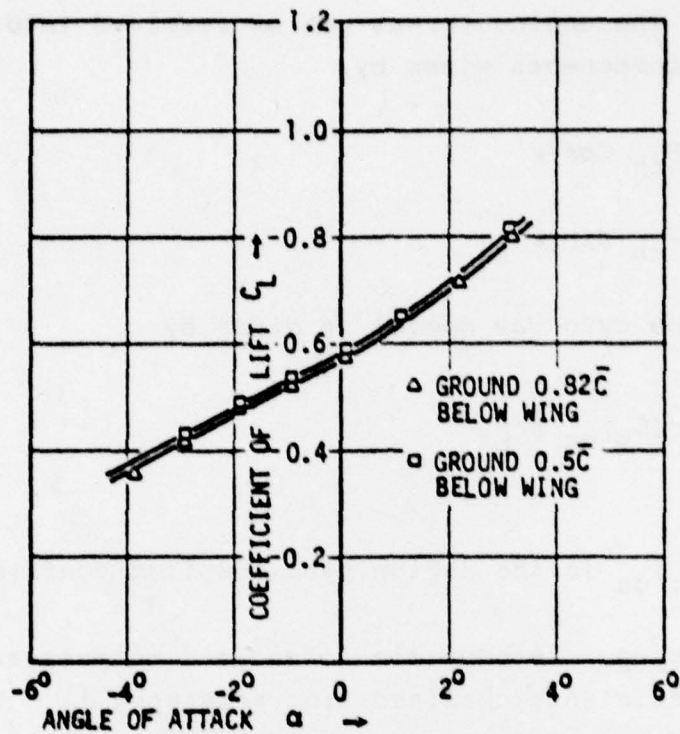
Figure 50   Coefficient of Lift vs Angle of Attack
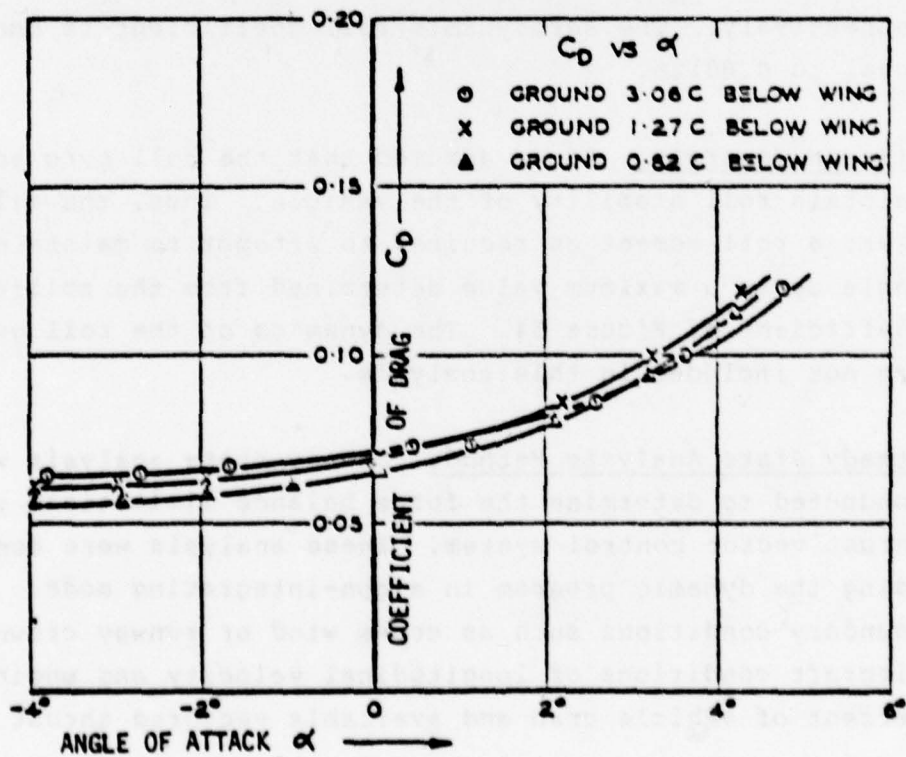
Figure 51   Coefficient of Drag vs Angle of Attack

74
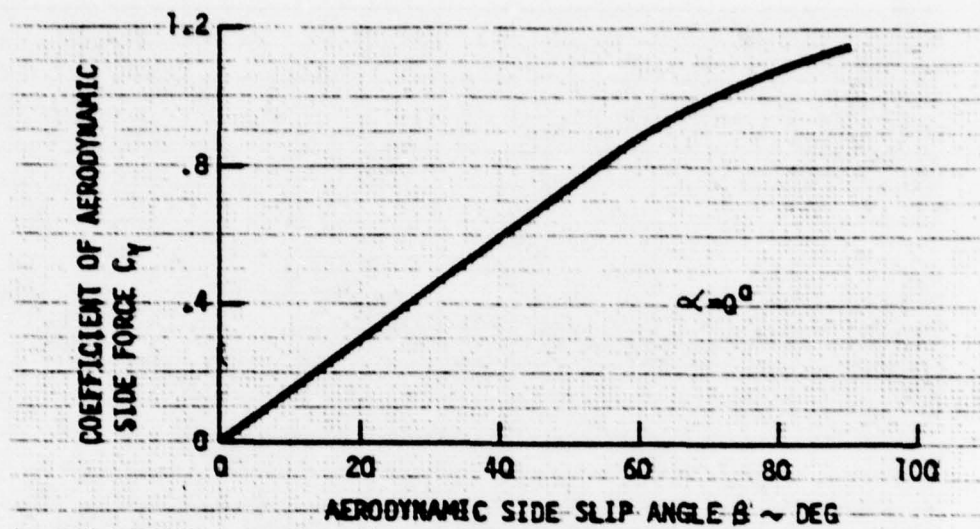
Figure 52   Coefficient of Aerodynamic Side Force
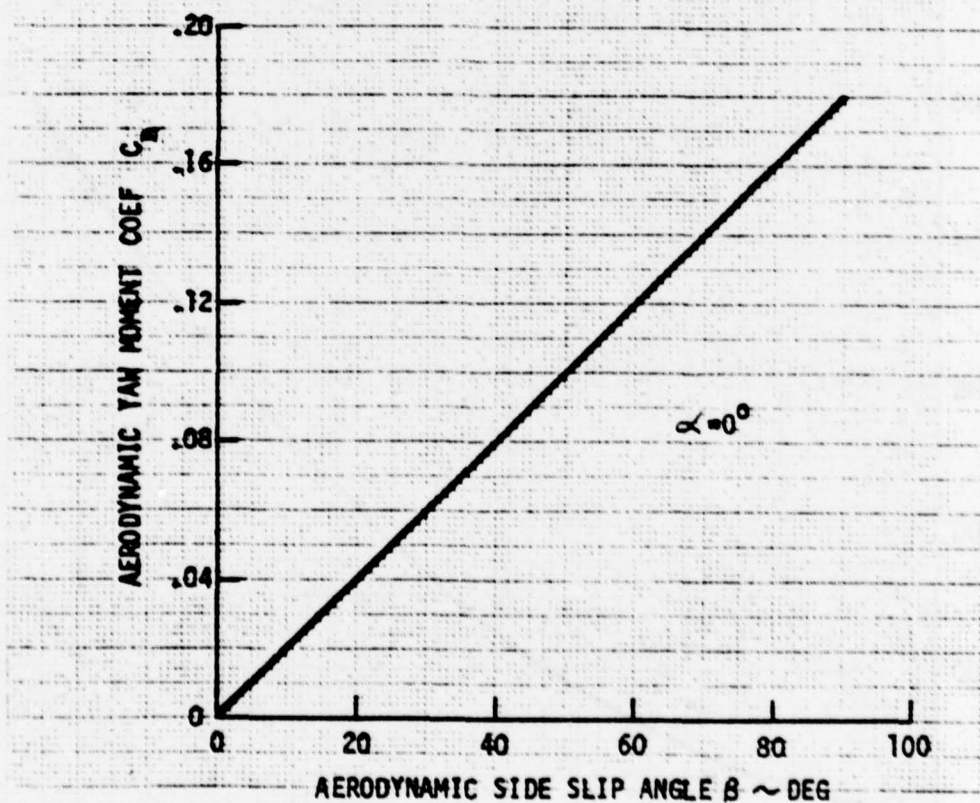
Figure 53   Coefficient of Aerodynamic Yaw Moment

75
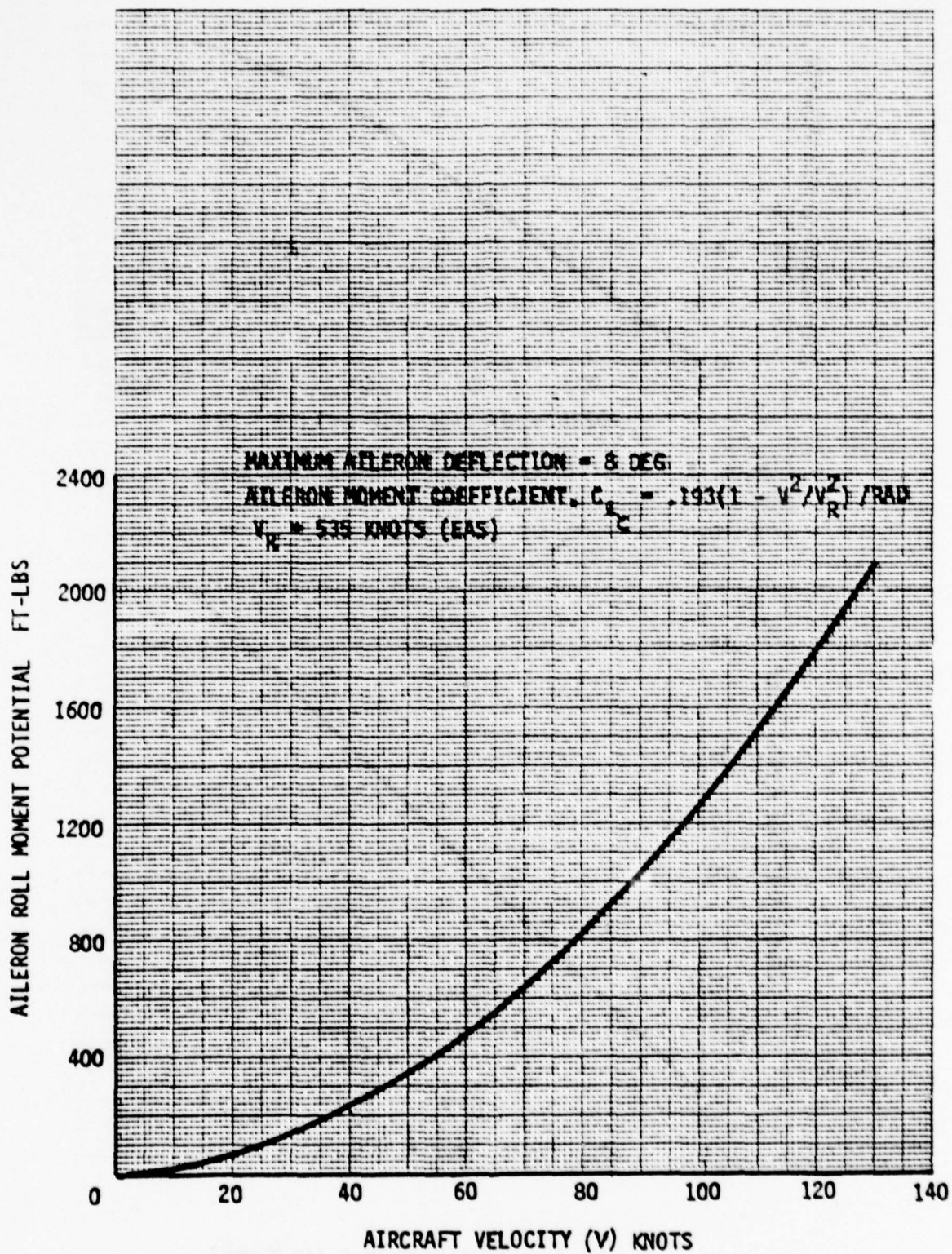
Figure 54   Potential Aileron Rolling Moment

76

varied.

The steady state condition for taxi or takeoff assumes that the velocity or acceleration is parallel with the runway centerline. The lateral linear and rotational velocities are zero. The problem is thus to find the required crab and vectored thrust, both expressed as percentages, to balance out the lateral side forces and yaw moments. The method is illustrated graphically in Figure 55, which shows lateral side forces (solid lines) and yaw moments (dashed lines) plotted against vectored thrust for various amounts of crabbing.

A computer subroutine was written to store the total lateral force and yaw moment for variations in crab and vectored thrust. These data points are shown on the figure. The sample case presented does not consider trunk frictional moments, and is thus fairly linear. The computer steps of the technique are as follows:

(a) Search the stored data for the percent crab giving positive and negative lateral forces (e.g., solid lines at 0% crabbed and 20% crabbed)

(b) Search for the first positive yaw moment along the line of the largest of the two crab angle lines (e.g., point f)

(c) Write linear equations of the lines intersecting points:
1) a and b (Equation (1))
2) c and d (Equation (2))
3) e and f (Equation (3))
4) g and h (Equation (4))

(d) Solve Equations (1) and (4) for point i

(e) Solve Equations (2) and (3) for point j

Figure 55: Solution Technique for Steady State Conditions

(f)   Write equation for line intersecting points i and j
      (Equation (5))

(g)   Solve Equation (5) for intersection with abscissa for the
      required percentage of available vectored thrust. (Point k)

(h)   Interpolate for the percent crab of point k between
      Equations (1) and (2). This is the percent crab angle
      required for steady state.

The procedure is then repeated for any required range of
aircraft velocities, engine speeds and side wind velocities.

3.2.2 Steady State Performance

The steady state analysis determines the percentage of available
thrust and the yaw angle required to keep the aircraft on the
runway centerline during various crosswind conditions. Values
were determined for various vehicle velocities and engine power
conditions. Crosswinds of 10, 20 and 30 knots were used, and
engine speeds of 60% to 100%. A summary of steady state
analyses conducted is presented in Table 4. Only analyses that
provided significant data are presented and discussed in this
report. The right hand column also gives a cross reference to
figures contained in this report. These analyses were conducted
for the purpose of determining the force balance characteristics
and limitations of the thrust vector control system on the
ACTS/ACRS Jindivik in conditions such as side winds, and with a
runway crown angle. The effects of wing tip skid friction and
symmetrical trunk drag due to the aircraft being in a rolled
attitude are also included in all except the first three runs.
For each steady state case, the required vectored thrust as a
percent of the maximum available, and the required yaw angle,
are plotted versus engine speed for aircraft velocities ranging
from one knot to 120 knots.

79

TABLE 4
THRUST VECTOR CONTROL SYSTEM
STEADY STATE ANALYSES RUN MATRIX

RUN NO	ACTS	ACRS	SIDE WIND SPEED KTS	RUNWAY CROWN %	RUNWAY CONDITION	SKID/TRUNK INDUCED YAW MOMENTS	NO TRUNK. OR SKID DRAG FRICTION LOSS	FIGURE NO.
1	EITHER		10	NONE	DRY	NONE	•	56
2	EITHER		20	↑	↑	↑	•	57
3	EITHER		30				•	58
4	•		10					59
5	•		20					60
6	•		30					61
7		•	10					
8		•	20		↓			
9		•	30		DRY			
10	•		10		WET	↓		
11		•	10		WET	NONE		
12	•		10		DRY	SKID GAP 3"		
13	•		20			3"		
14		•	10	↓		6"		64
15		•	20	NONE		SKID GAP 6"		
16	•		10	2		NONE		
17	•		10	2		SKID GAP 3"		62
18	•		20	2		SKID GAP 3"		63
19		•	20	2		NONE		
20		•	10	2	↓	SKID GAP 6"		65
21		•	20	2	DRY	SKID GAP 6"		

It should be emphasized that these cases are steady state in the sense that lateral forces and all moments are in balance; the vehicle may be accelerating (or decelerating) in the forward direction.

ACTS System. The steady state requirements for vectored thrust and yaw angle for conditions of 10, 20 and a 30 knot side wind are shown respectively in Figures 56 through 58 for ACTS. These three cases do not include the yaw moment effects resulting from wing tip skid and trunk drag. These three cases present the yaw thruster effectiveness in reacting only the aerodynamic forces and moments. Note that in a 10 knot side wind, there is sufficient vectored thrust. The maximum yaw thruster requirement is 79% at vehicle velocity of 40 knots and engine RPM of 60%. In the 20 knot side wind condition, Figure 57 shows that at engine RPM's less than 75%, there is insufficient thrust for vehicle velocities less than 60 knots. In the 30 knot side wind condition, 95% engine RPM would be required to provide sufficient vectored thrust for the range of vehicle velocities.

The effect of the low levels of trunk drag considered in this analysis or of wing tip skid induced moments is generally to reduce the level of vectored thrust required to react the aerodynamic yaw moment in side wind conditions. Trunk drag and wing tip skid friction provide directional stability to the aircraft and thus less vectored thrust is required to prevent the aircraft from weather-cocking in a side wind.

The effect of wing tip skid friction and trunk drag induced yaw moments is included in the results of Figures 59 through 61 which are for 10, 20, and 30 knot side winds respectively. The effect of skid and trunk drag in the 10 knot side wind condition is to reduce the required vectored thrust from 47% to 31% for an engine RPM of 60% and vehicle velocity of one knot. It can be seen that for a 20 knot side wind the yaw angle requirement is higher, and thus the rolling moments due to drag are higher.

81
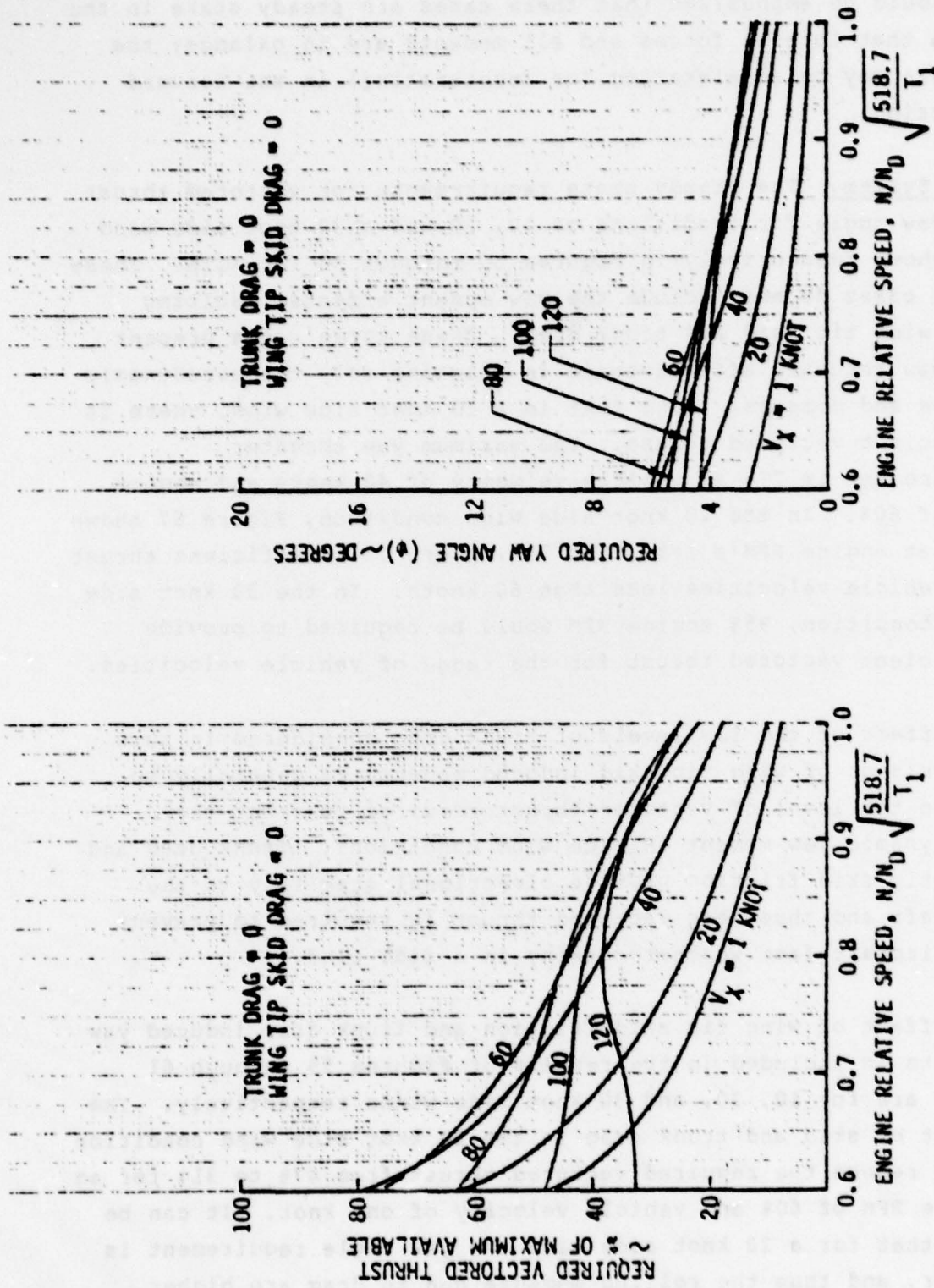
Figure 56   Steady State Conditions - 10 Knot Sidewind - No Trunk Drag

82
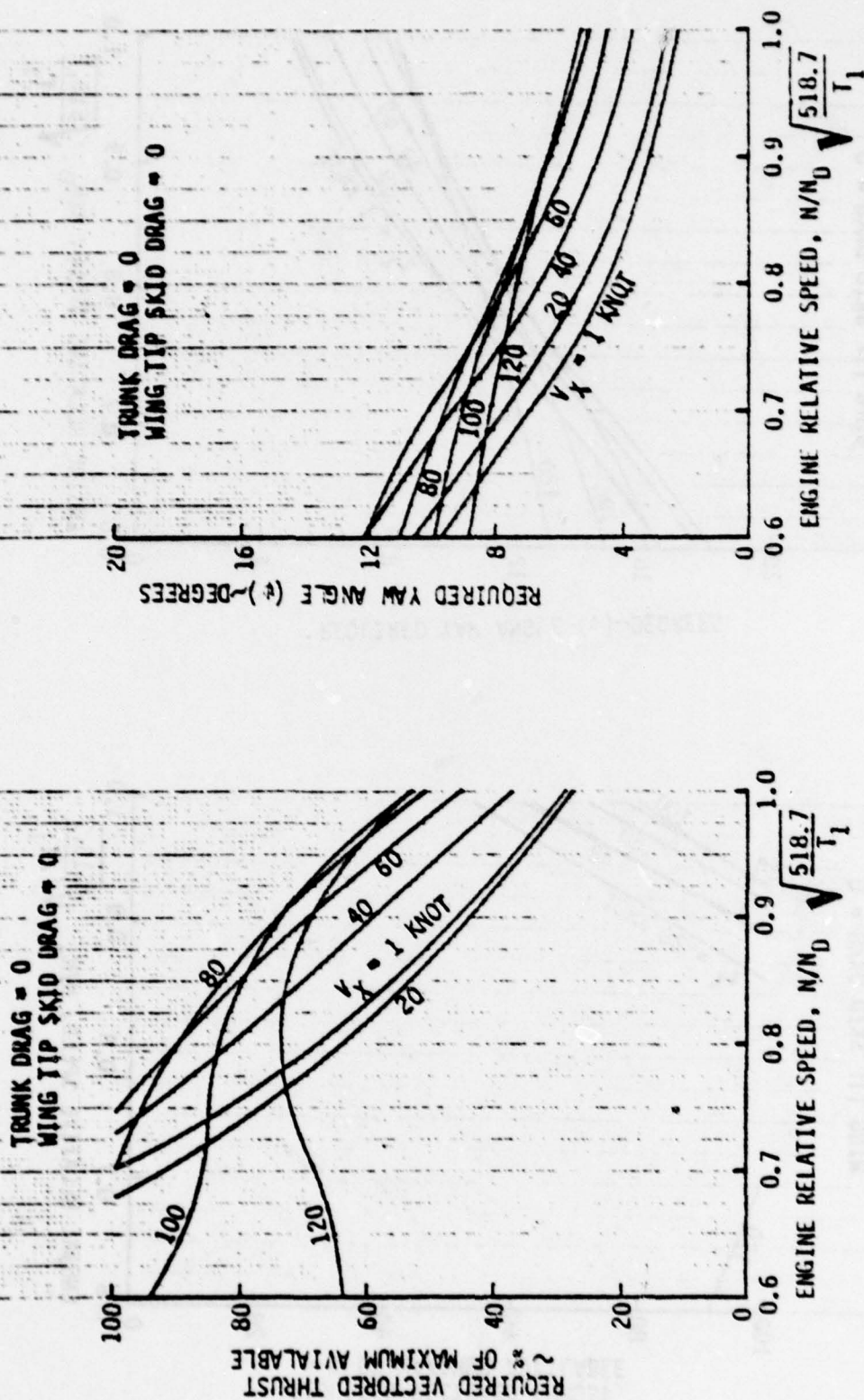
Figure 57   Steady State Conditions - 20 Knot Side Wind - No Trunk Drag

83
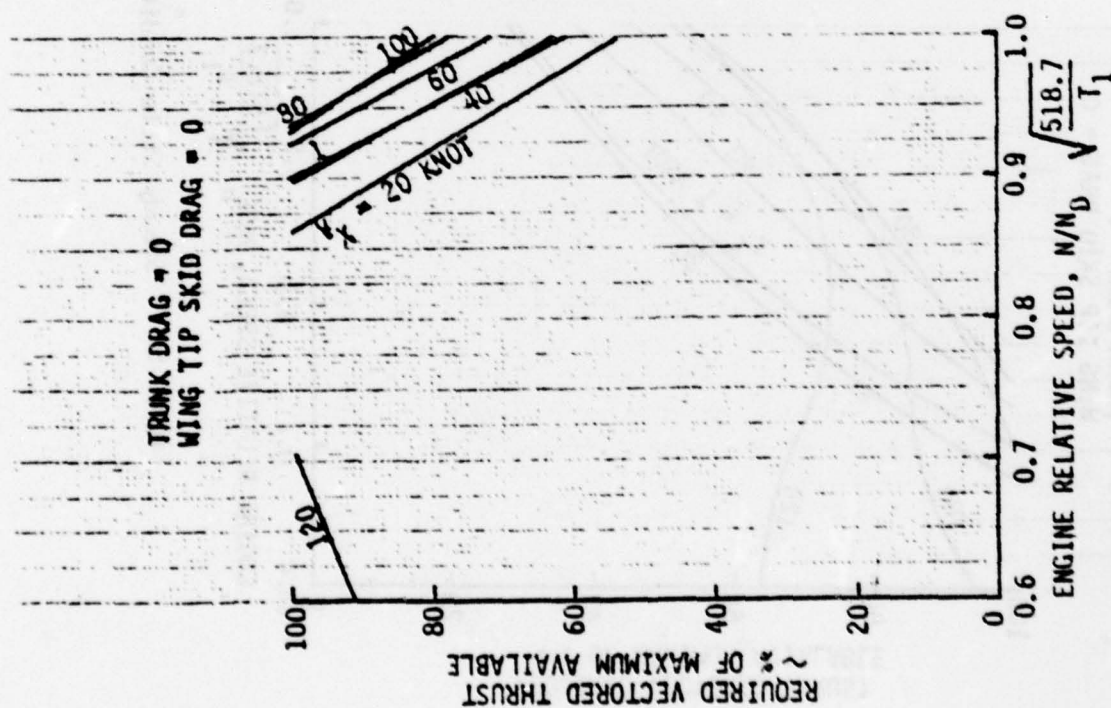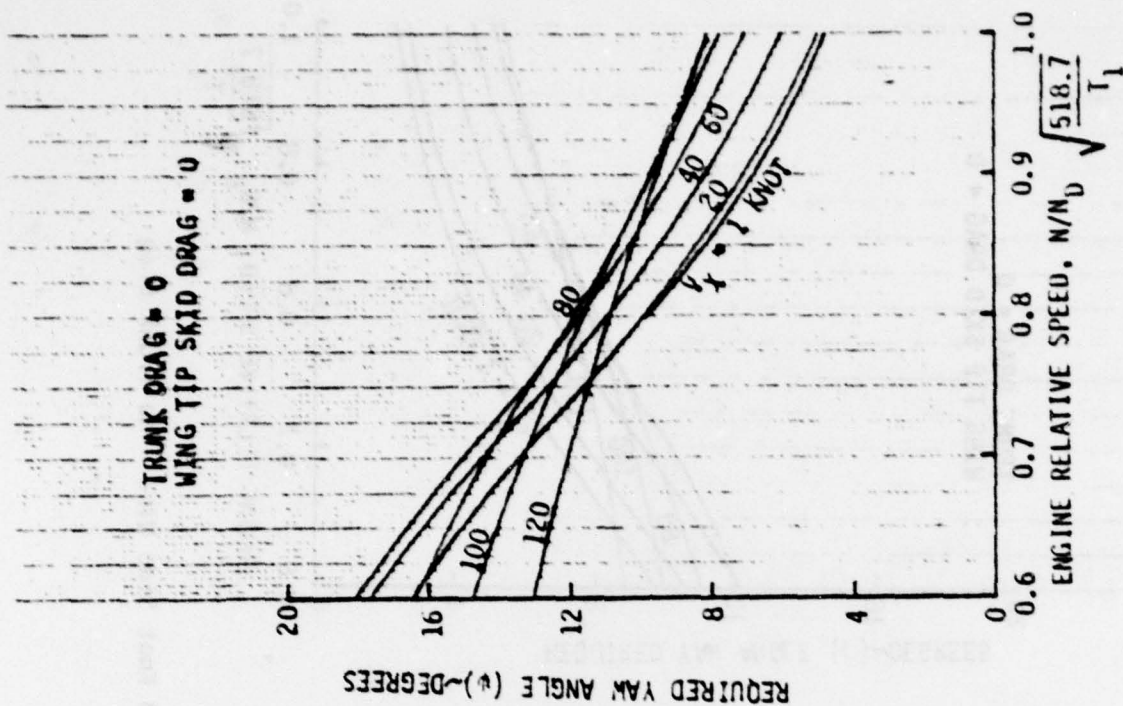
Figure 58   Steady State Conditions - 30 Knot Side Wind - No Trunk Drag

84
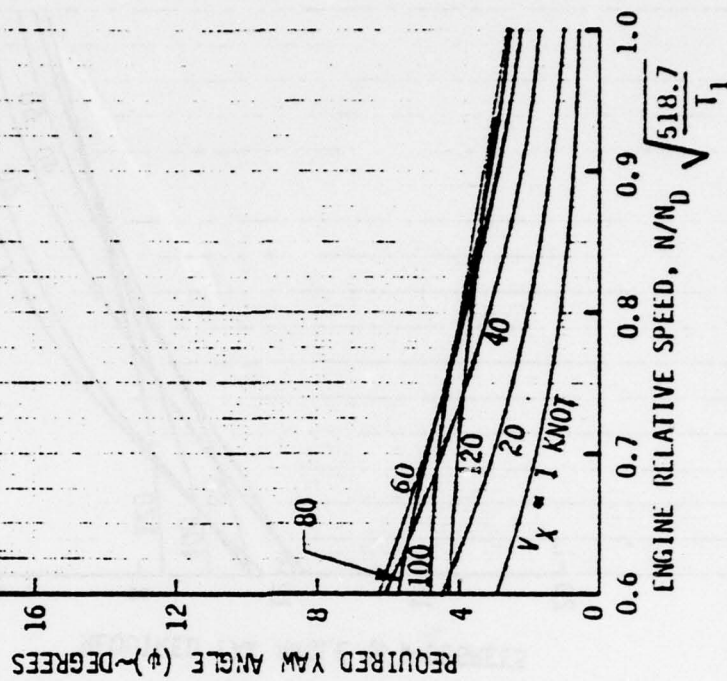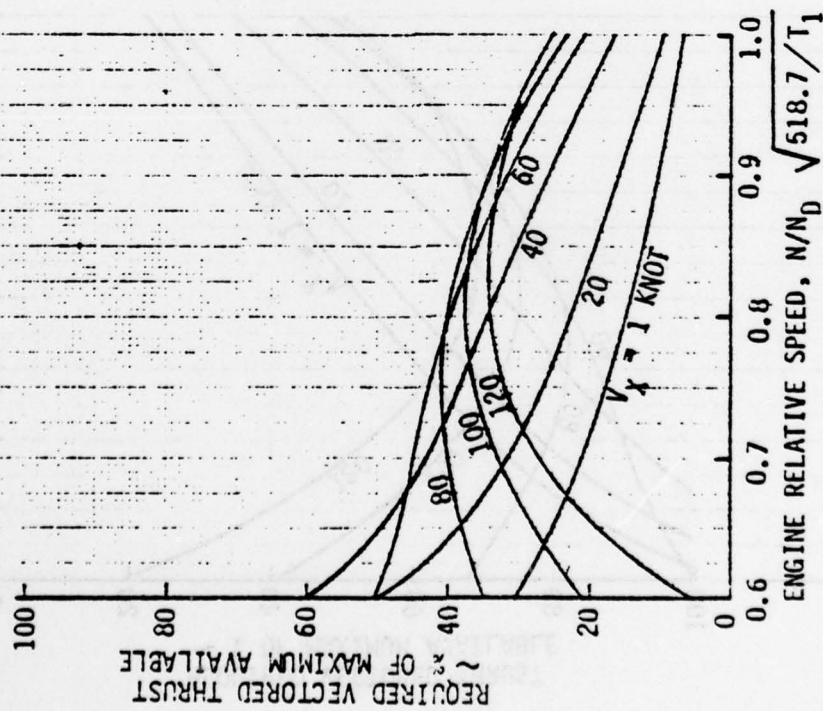
Figure 59   Steady State Conditions - ACTS Trunk - 10 Knot Side Wind,
Including Trunk Drag and Wing Tip Skid Effects

85
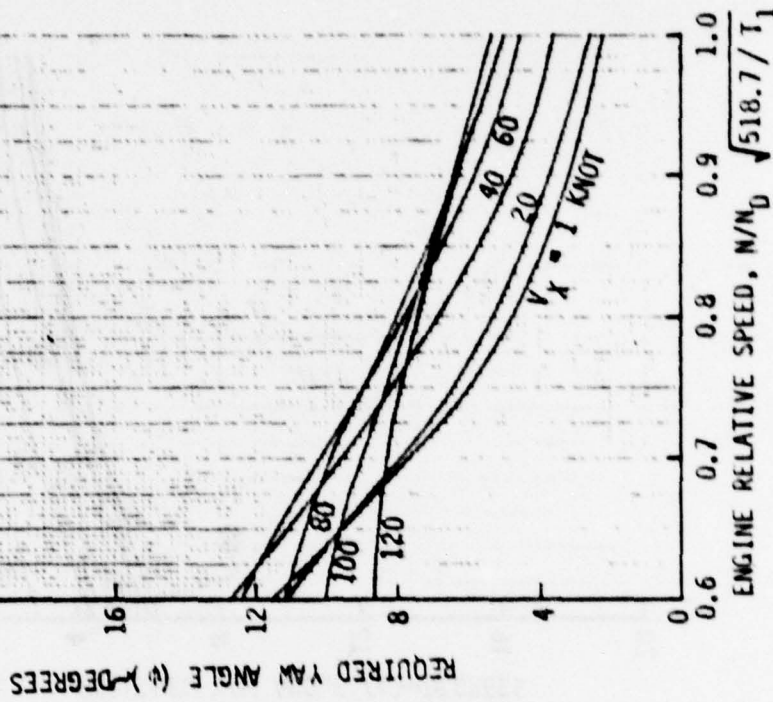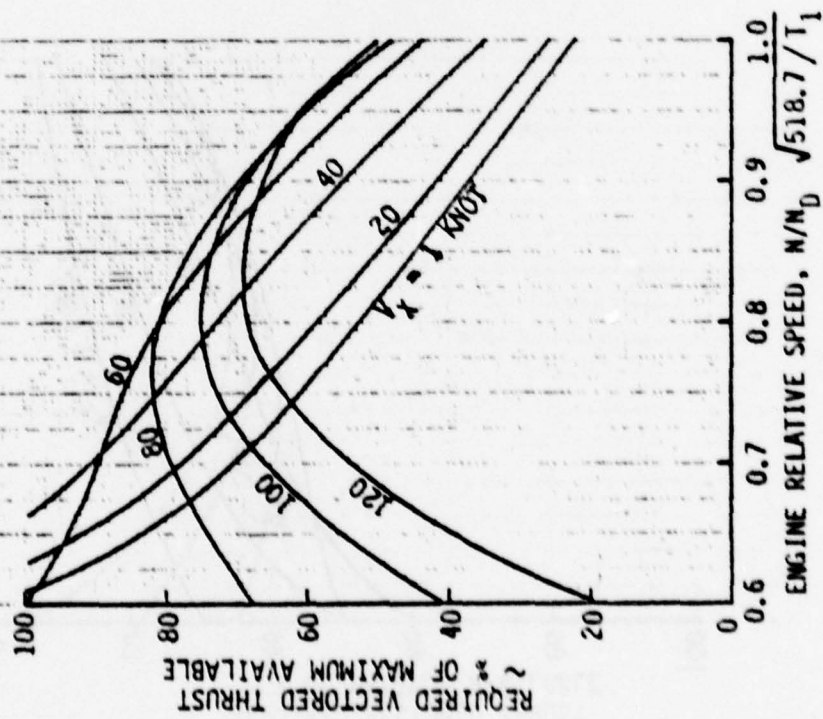
Figure 60   Steady State Conditions - ACTS Trunk - 20 Knot Side Winds,
Including Trunk Drag and Wing Tip Skid Effects

86

REQUIRED YAW ANGLE (ϕ) ~ DEGREES

$V_X = 1$ KNOT

20 16 12 8 4 0

60 40 20 100 80 120

ENGINE RELATIVE SPEED, $N/N_D \sqrt{518.7/T_1}$

0.6 0.7 0.8 0.9 1.0

REQUIRED VECTORED THRUST ~ % OF MAXIMUM AVAILABLE

100 80 60 40 20

100 80 120 60 40 20

$V_X = 1$ KNOT

ENGINE RELATIVE SPEED, $N/N_D \sqrt{518.7/T_1}$

0.6 0.7 0.8 0.9 1.0
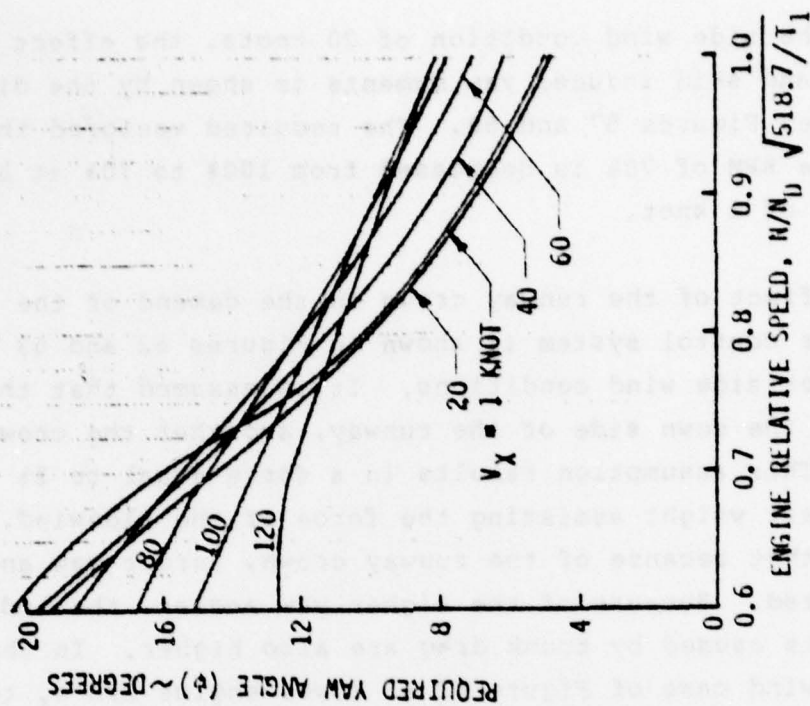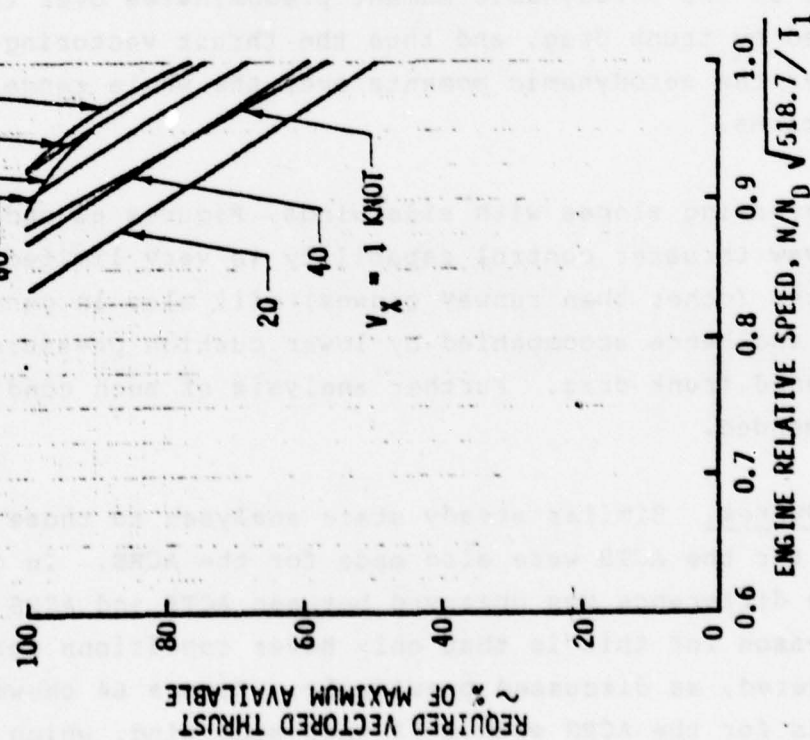
Figure 61   Steady State Conditions - ACTS Trunk - 30 Knot Side Winds,
Including Trunk Drag and Wing Tip Skid Effects

87

For the side wind condition of 20 knots, the effect of trunk drag and skid induced yaw moments is shown by the difference between Figures 57 and 60. The required vectored thrust at an engine RPM of 70% is decreased from 100% to 70% at a vehicle speed of 1 knot.

The effect of the runway crown on the demand of the thrust vector control system is shown in Figures 62 and 63 for 10 and 20 knot side wind conditions. It is assumed that the aircraft is on the down side of the runway, and that the crown slope is 2%. This assumption results in a force equal to 2% of the aircraft weight assisting the force of the sidewind. It can be seen that because of the runway crown, larger yaw angles are required. Because of the higher yaw angles, the induced yaw moments caused by trunk drag are also higher. In the 10 knot side wind case of Figure 62 at lower engine RPM's, the vectored thrust is required to assist the aerodynamic yaw moment in order to overcome the yaw moment due to skid and trunk drag. In Figure 63 the aerodynamic moment predominates over the moment induced by trunk drag, and thus the thrust vectoring acts to counter the aerodynamic moments over the whole range of conditions.

In traversing slopes with side winds, Figures 62 and 63 indicate that yaw thruster control capability is very limited. Sloping surfaces (other than runway crowns) will also in general be rough and hence accompanied by lower cushion pressures and increased trunk drag. Further analysis of such conditions is recommended.

ACRS System. Similar steady state analyses to those discussed above for the ACTS were also made for the ACRS. In general, little difference was observed between ACTS and ACRS results. One reason for this is that only hover conditions were considered, as discussed previously. Figure 64 shows typical results for the ACRS with a 10 knot side wind, which can be
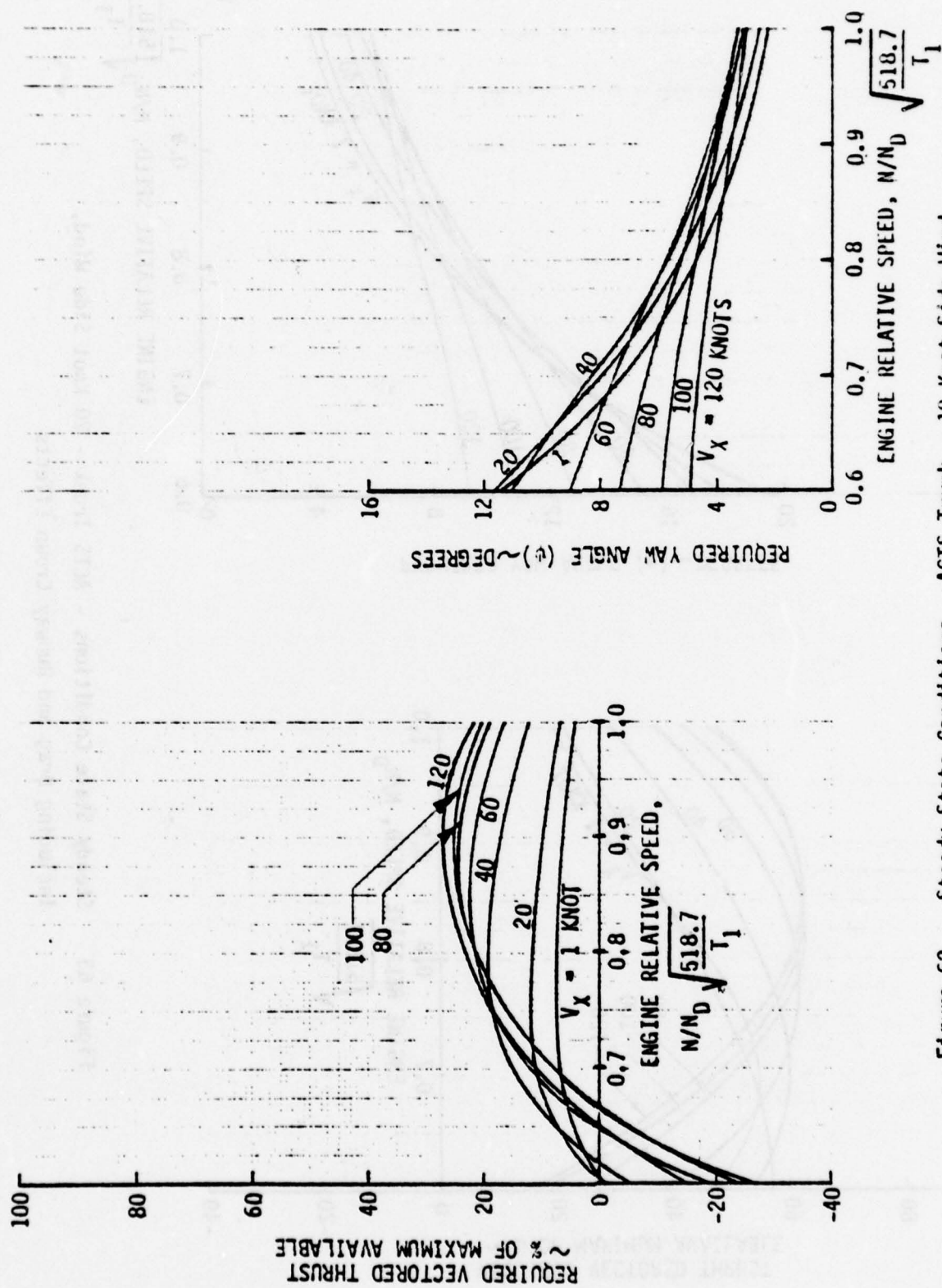
Figure 62   Steady State Conditions – ACTS Trunk – 10 Knot Side Wind.
Including Drag and Runway Crown Effects
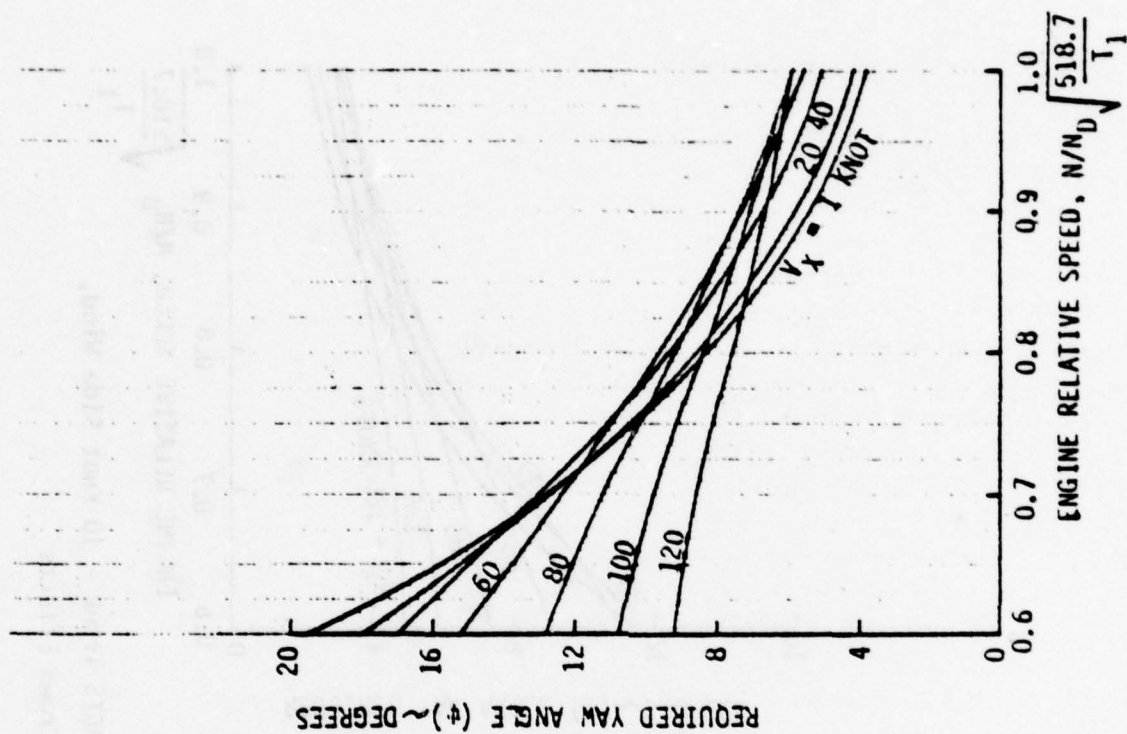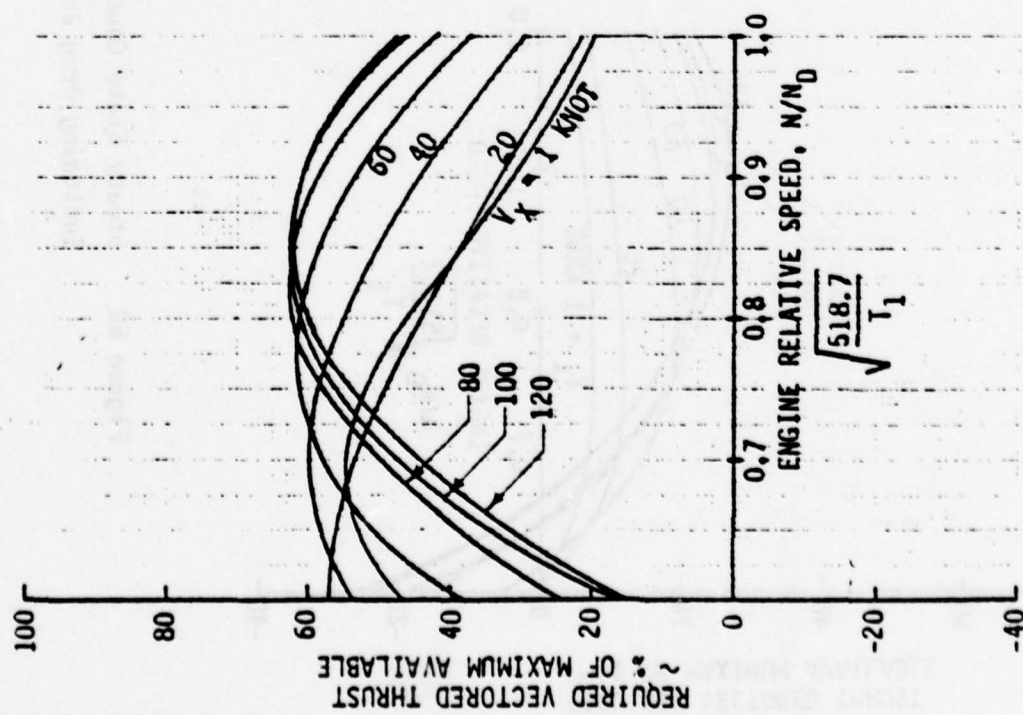
Figure 63   Steady State Conditions - ACTS Trunk - 20 Knot Side Wind,
Including Drag and Runway Crown Effects

REQUIRED YAW ANGLE (ψ) ~ DEGREES

20

16

12

8

4

0

80

~100

60

40

120

20

$V_X = 1$ KNOT

0.6   0.7   0.8   0.9   1.0

ENGINE RELATIVE SPEED, $N/N_D \sqrt{518.7/T_1}$

REQUIRED VECTORED THRUST ~ % OF MAXIMUM AVAILABLE

100

80

60

40

20

60

40

20

100

80

120

$V_X = 1$ KNOT

0.6   0.7   0.8   0.9   1.0

ENGINE RELATIVE SPEED, $N/N_D \sqrt{518.7/T_1}$
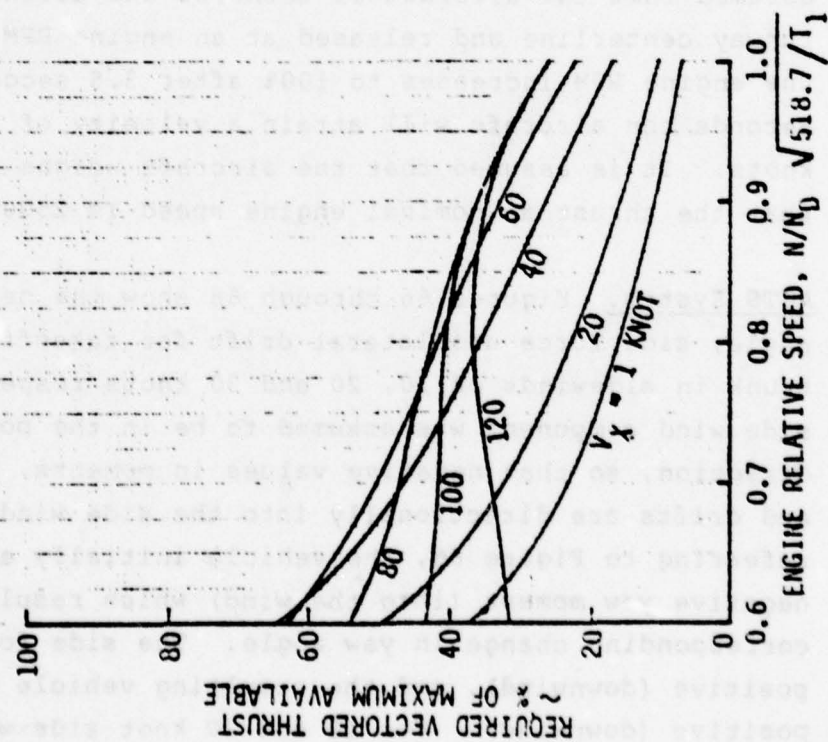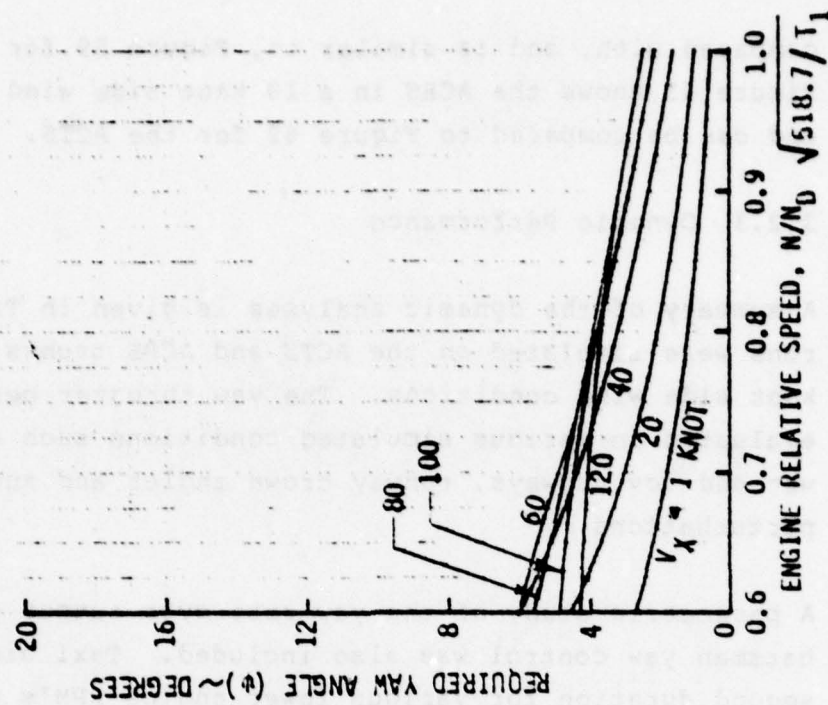
Figure 64   Steady State Conditions - ACRS Trunk - 10 Knot Side Winds.
Including Trunk Drag Effects

compared with, and is similar to, Figure 59 for the ACTS. Figure 65 shows the ACRS in a 10 knot side wind and 2% crown, and can be compared to Figure 62 for the ACTS.

3.2.3 Dynamic Performance

A summary of the dynamic analyses is given in Table 5. Takeoff runs were simulated on the ACTS and ACRS trunks in 10, 20 and 30 knot side wind conditions. The yaw thruster performance was evaluated in various simulated conditions such as wind gusts, wet and icy runways, runway crown angles and sudden yaw perturbations.

A parametric study of the yaw rate gyro output gain and the batsman yaw control was also included. Taxi simulations of 25 second duration for various lower engine RPM's were also made.

In the simulations of the ACTS/ACRS Jindivik takeoff, it is assumed that the aircraft is tethered and aligned with the runway centerline and released at an engine RPM of 87%, and that the engine RPM increases to 100% after 3.5 seconds. In 3.5 seconds the aircraft will attain a velocity of approximately 50 knots. It is assumed that the aircraft weighs 3400 lbs., and that the thrust at nominal engine speed is 2500 lbs.

ACTS System. Figures 66 through 68 show the net yaw moment, yaw angle, side force and lateral drift for takeoff on the ACTS trunk in sidewinds of 10, 20 and 30 knots respectively. The side wind component was assumed to be in the positive Z-axis direction, so that negative values in moments, angles, forces and drifts are directionally into the side wind component. Thus referring to Figure 66, the vehicle initially experiences a negative yaw moment (into the wind) which results in a corresponding change in yaw angle. The side force is initially positive (downwind), and the resulting vehicle drift is also positive (downwind). For 10 and 20 knot side winds (Figures 66
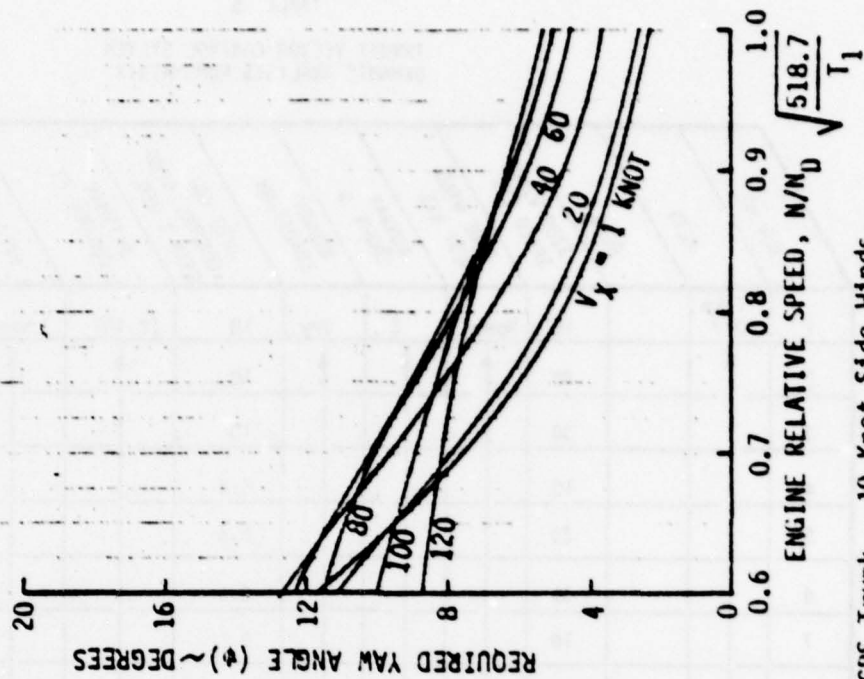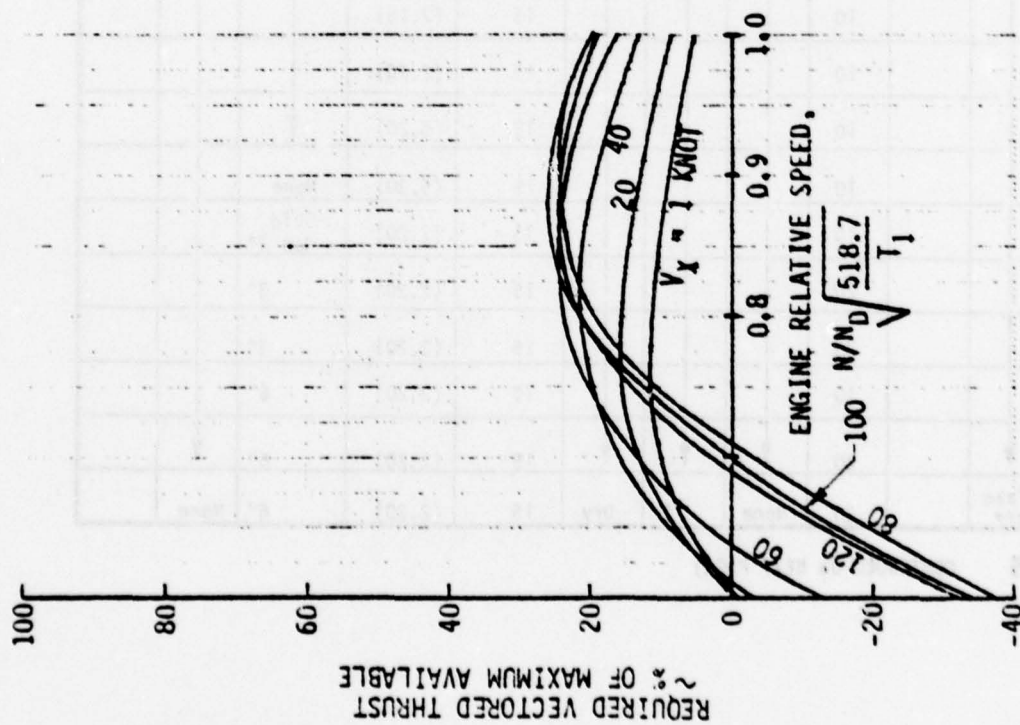
Figure 65   Steady State Conditions - ACRS Trunk - 10 Knot Side Winds,
Including Trunk Drag and Runway Crown Effects

93

TABLE 5

THRUST VECTOR CONTROL SYSTEM
DYNAMIC ANALYSES RUN MATRIX

RUN NO.	ACTS	ACRS	SIDE WIND SPEED KTS	SIDE WIND GUST KTS	RUNWAY CROWN %	RUNWAY CONDITION	AUTO YAW CONTROL GYRO GAIN % DEG.	BATSMAN CONTROL FT	SKID/TRUNK INDUCED YAW MOMENTS	LARGE YAW PERTURBATIONS	FIGURE NO
1	Take Off		10	None	2	Dry	10	(2,10)	None	None	66
2			20				10				67
3			30				10				68
4			10				6.6				69
5			20				6.6				69
6			30				6.6				69
7			10				5				70
8			20				5				70
9			30				5	(2,10)			70
10			10				15	(2,5)			
11			10				15	(2,15)			
12			10				15	(2,20)			
13			10				15	(5,20)			
14			10				15	(5,30)	None		
15			10				15	(2,20)	Skid Gap 3"		
16			20				15	(2,20)	3"		
17			30				15	(2,20)	3"		
18			10				15	(2,20)	6"		
19			20				15	(2,20)	6"		
20	Take Off		30	None	2	Dry	15	(2,20)	6"	None	

(TABLE 5   CONTINUED ON NEXT PAGE)

TABLE 5 - Cont'd

THRUST VECTOR CONTROL SYSTEM
DYNAMIC ANALYSES RUN MATRIX

RUN NO	ACTS	ACRS	SIDE WIND SPEED KTS	SIDE WIND GUST KTS	RUNWAY CROWN %	RUNWAY CONDITION	AUTO YAW CONTROL GYRO GAIN & DEG	BATSMAN CONTROL FT	SKID/TRUNK INDUCED YAW MOMENTS	LARGE YAW PPERTURBATIONS	FIGURE NO.
21	Take Off		10	None	2	Dry	15	(2,20)	Skid Gap 18"	None	
22	↑		20		↑	Dry			18"		
23			30	↓		Dry			18"		
24			10	None		Wet			3"		
25			0	10 Kts 4 SEC		Dry			↑		73
26	↓		0	20 Kts 4 SEC		↑					73
27	Take Off		0	30 Kts 4 SEC							73
28	Taxi 50%RPM		0	10 4 SEC							74
29	Taxi 60%		0	10 4 SEC						↓	74
30	Taxi 70%		0	10 4 SEC						None	74
31	Taxi 60%		0	None					↑	20° 2 SEC	75
32	Taxi 70%		0	↑		↓			3"	20° 2 SEC	75
33		Take Off	10	↓		Dry			6"	None	
34		Take Off	10	None		Wet				↑	
35		Taxi 60%	0	10 4 SEC		Dry	↓	↓			
36		Taxi 70%	0	10 4 SEC		Dry	15	(2,20)			
37	Take Off		10 20 30	None			10	(2,Y)(5,Y)			76
38	Take Off		↑	↑			15	▷1			77
39		Take Off	↓	↓	↓	↓	10		↓	↓	78
40		Take Off	10 20 30	None	2	Dry	15	(2,Y)(5,Y)	6"	None	79

▷ Y, lateral distance at which Batsman signals for full gryo reference angle shift rate was varied as shown in Figures 76 to 79
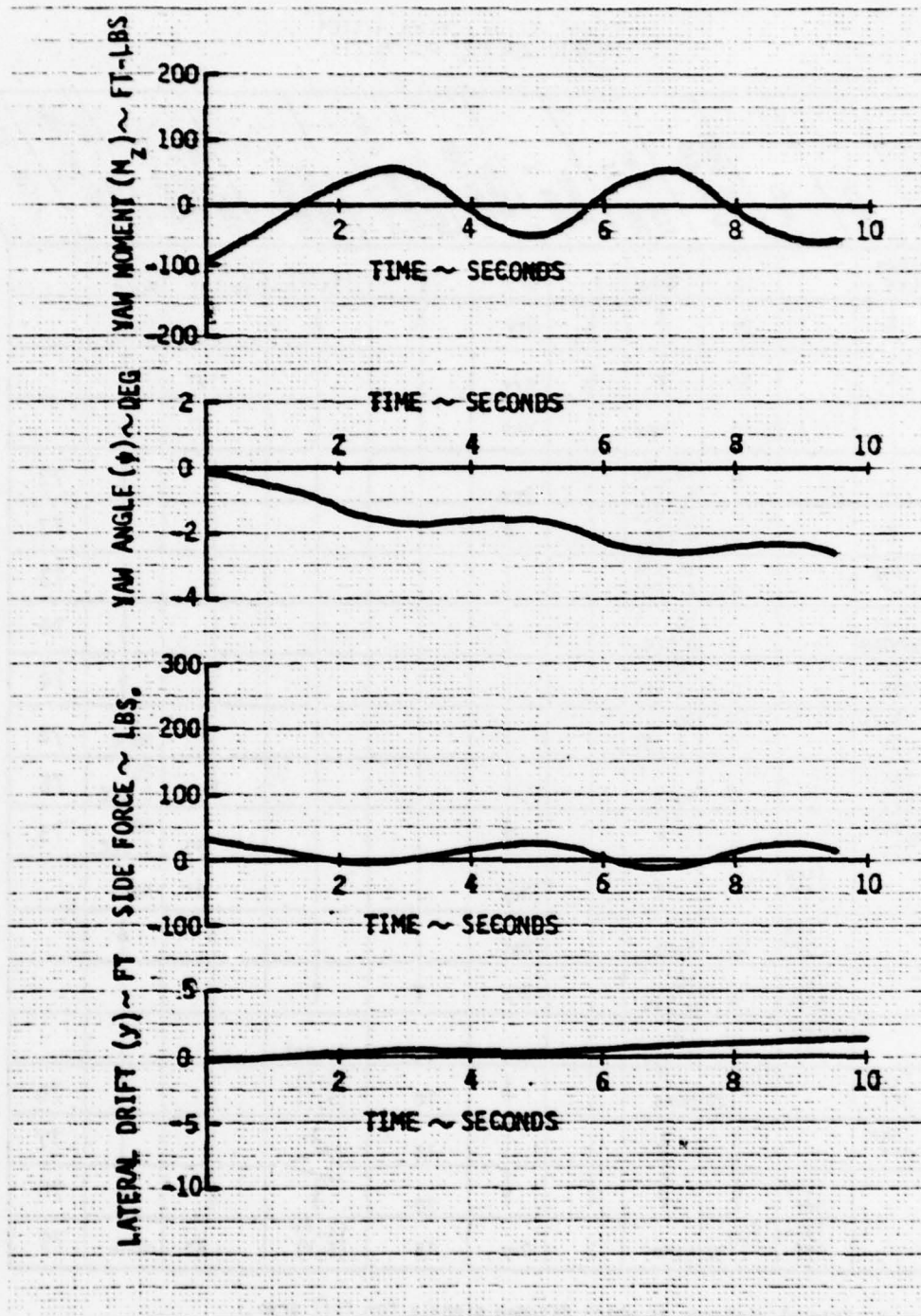
Figure 66   Aircraft Dynamics During Takeoff - 10 Knot Side Wind
            Yaw Gyro Gain 10%/Deg

96
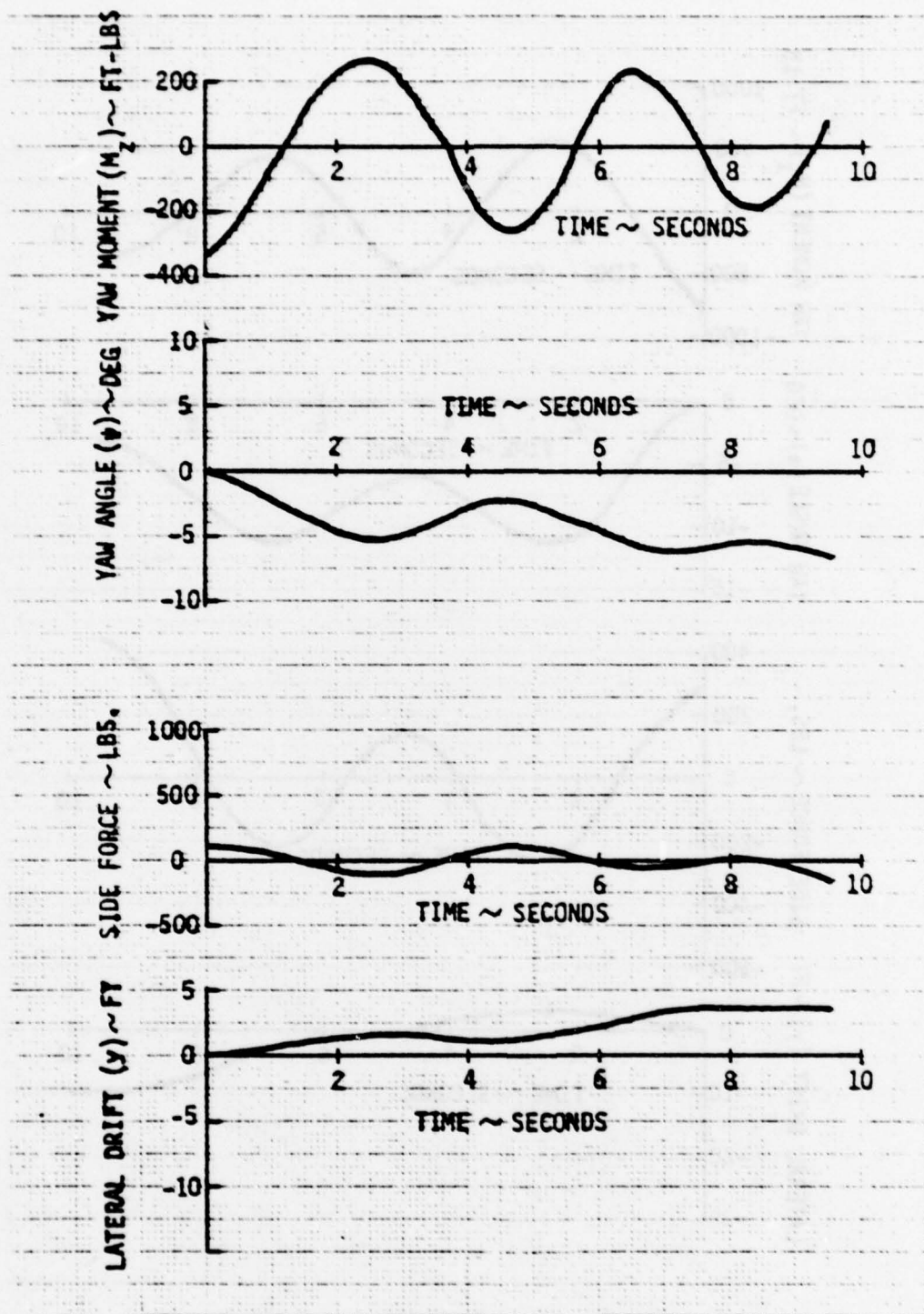
Figure 67   Aircraft Dynamics During Takeoff - 20 knot Side Wind
Yaw Gyro Gain 10%/Deg
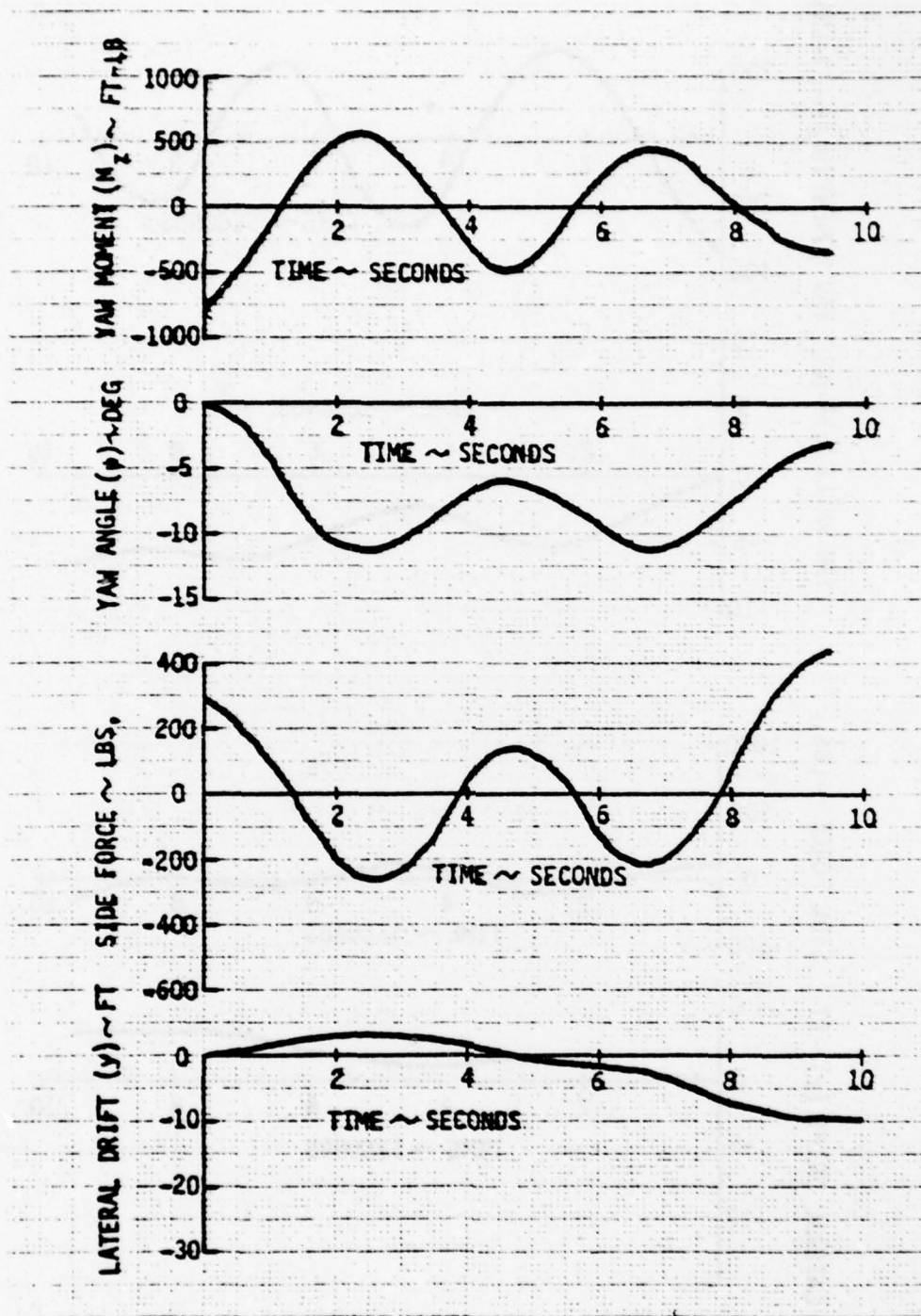
Figure 68   Aircraft Dynamics During Takeoff - 30 Knot Side Wind
Yaw Gyro Gain 10%/Deg

and 67), the vehicle lateral drift is always downwind. However, for the 30 knot side wind (Figure 68), the vehicle initially drifts downwind, but then yaws sufficiently into the wind so that the final (and maximum) lateral drift is upwind. For these cases, the yaw gyro gain was assumed to be 10%/degree, corresponding to maximum thrust vectoring at a yaw gyro reference angle error of 10 degrees. The batsman control was simulated to begin at a drift of $\pm$ 2 feet from the runway centerline, and the gain was set to given the maximum reference angle reset rate at a drift of $\pm$ 10 feet.

Figures 69 and 70 show lateral drifts for 10, 20 and 30 knot side winds when the yaw gyro gain is reduced to 6.6%/degree and 5%/degree respectively. The reduced gain results in a lower output from the yaw thruster as the vehicle yaws into the wind, and thus the tendency to finish on the upwind side of the runway centerline is enhanced. The results, in terms of maximum lateral drifts and yaw angles, are shown in Figure 71. The maximum lateral drift essentially doubles as the yaw gyro gain is reduced from 10%/degree to 6.6%/degree, and doubles again when the gain is further reduced to 5%/degrees. The vectored thrust time histories for these three gyro settings in a 30 knot side wind are shown in Figure 72. The highest setting provides increased vectored thrust during the first 3 seconds and reduces the tendency to yaw into the wind during this period.

Side wind gusts of 10, 20 and 30 knots were simulated for the ACTS takeoff. The gust velocity was programmed to take the shape of the half sine wave cycle and occur in the first 4 seconds. The lateral drift time histories are shown in Figure 73. The yaw gyro gain was simulated at 6.6% vectored thrust per degree. The batsman control was set between 2 and 20 feet of drift. In these analyses, wing tip skid friction and trunk drag induced yaw moments were considered. The lateral drift for the 30 knot gust is less than 10 feet.

99
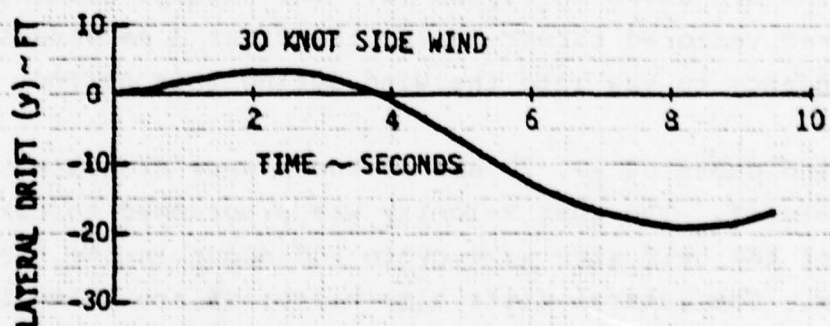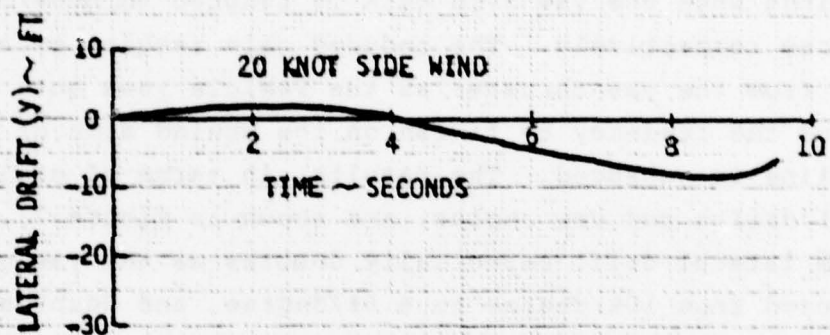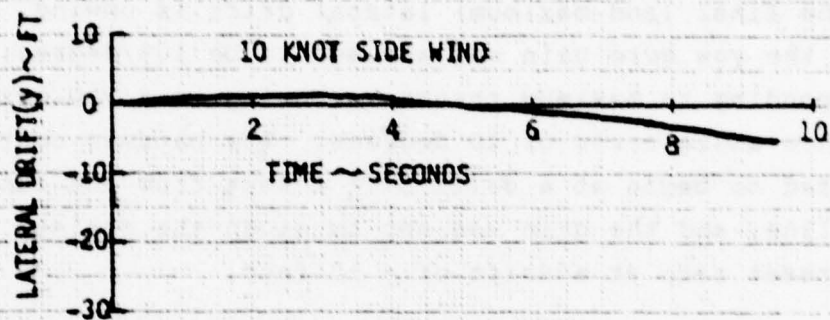
Figure 69   Lateral Drift Time Histories for Takeoff
Yaw Gyro Gain 6.6%/Deg
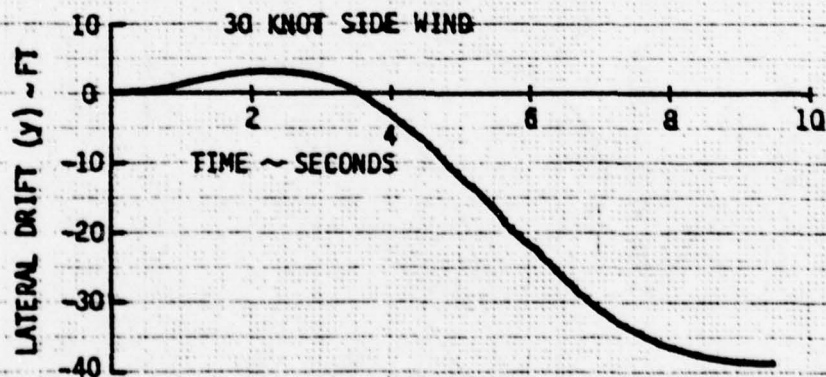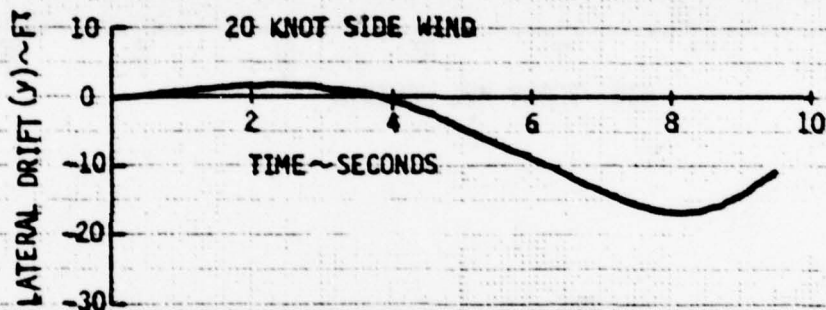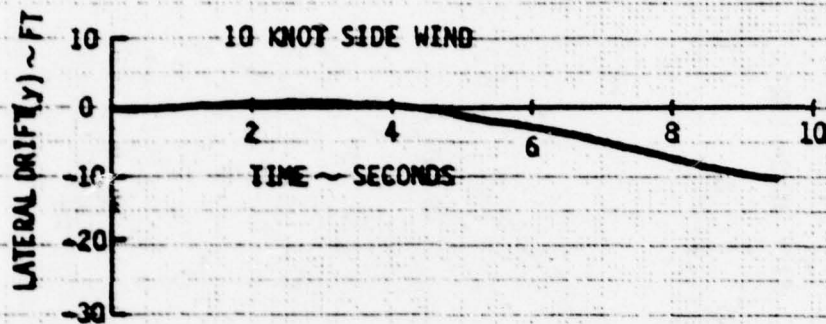
Figure 70   Lateral Drift Time Histories for Takeoff
Yaw Gyro Gain 5.0%/Deg

101
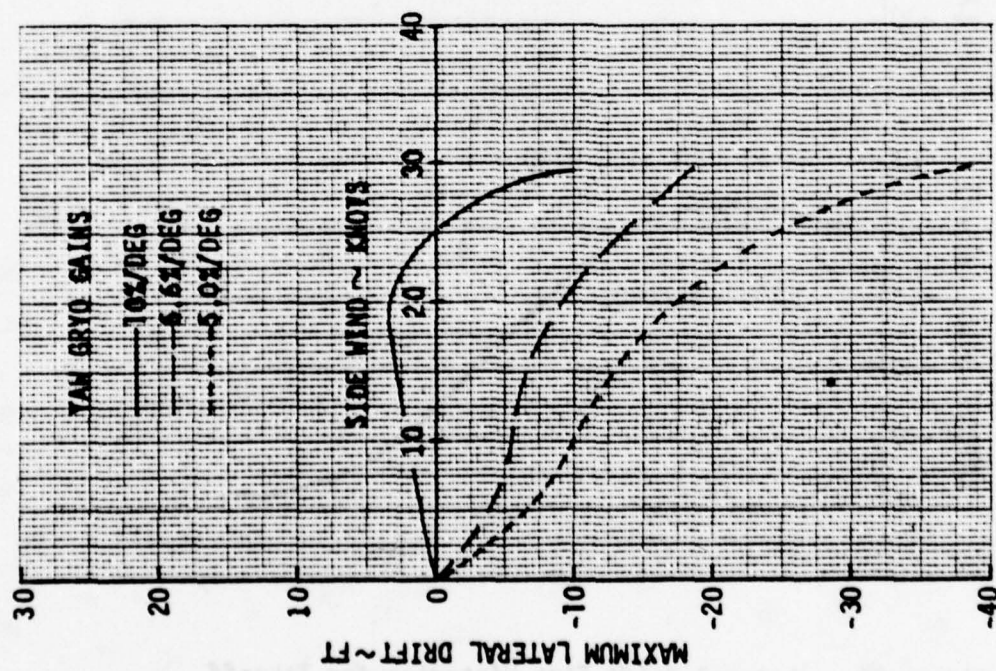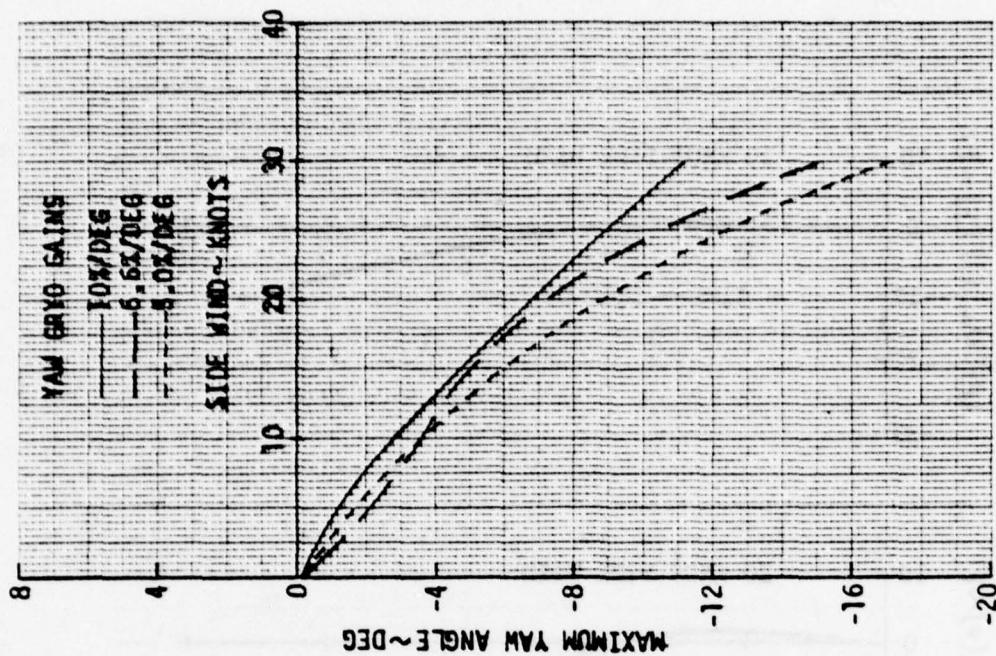
Figure 71 Maximum Lateral Drift and Yaw Angle vs Side Wind Velocity
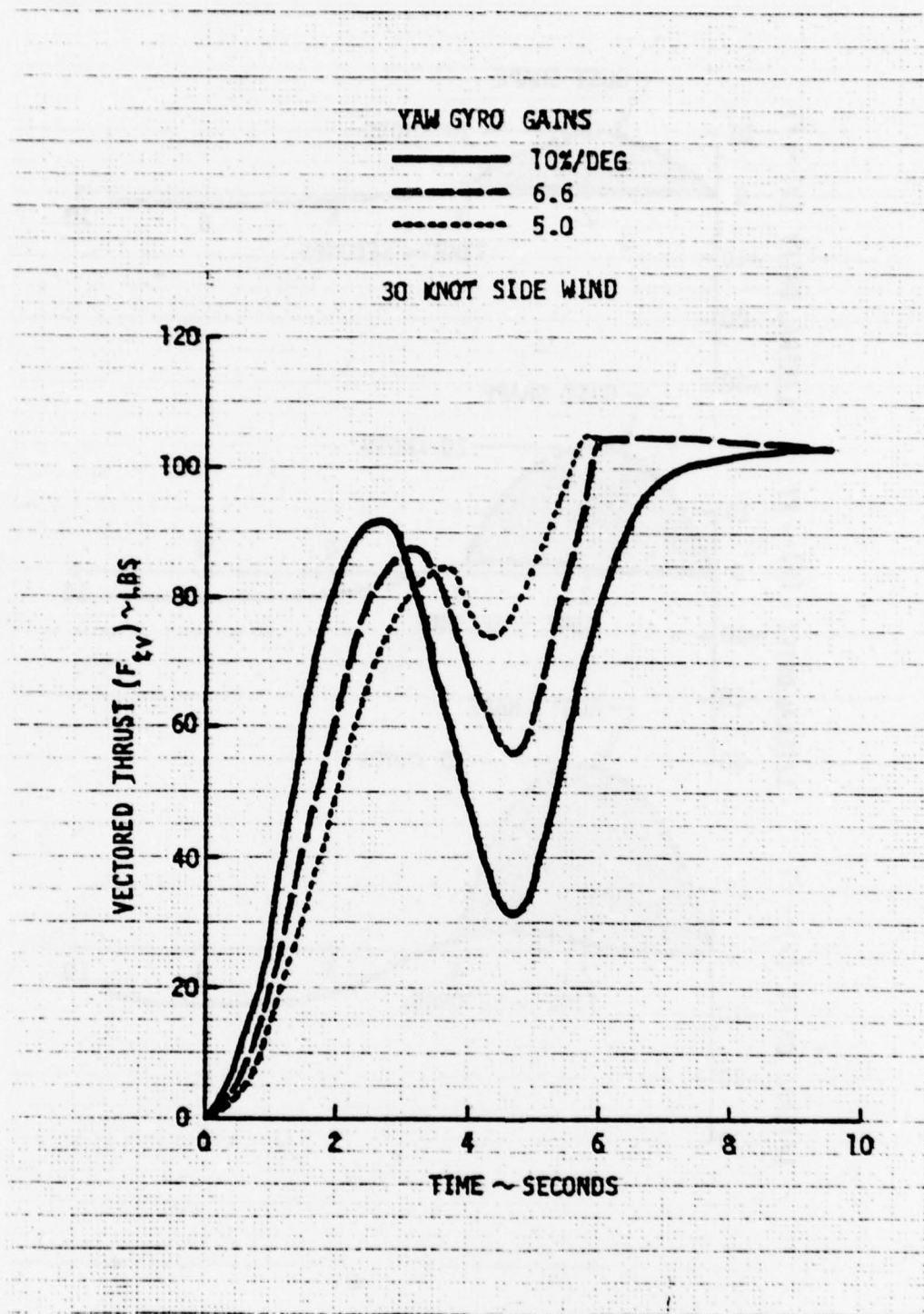
Figure 72   Vectored Thrust Time Histories

103
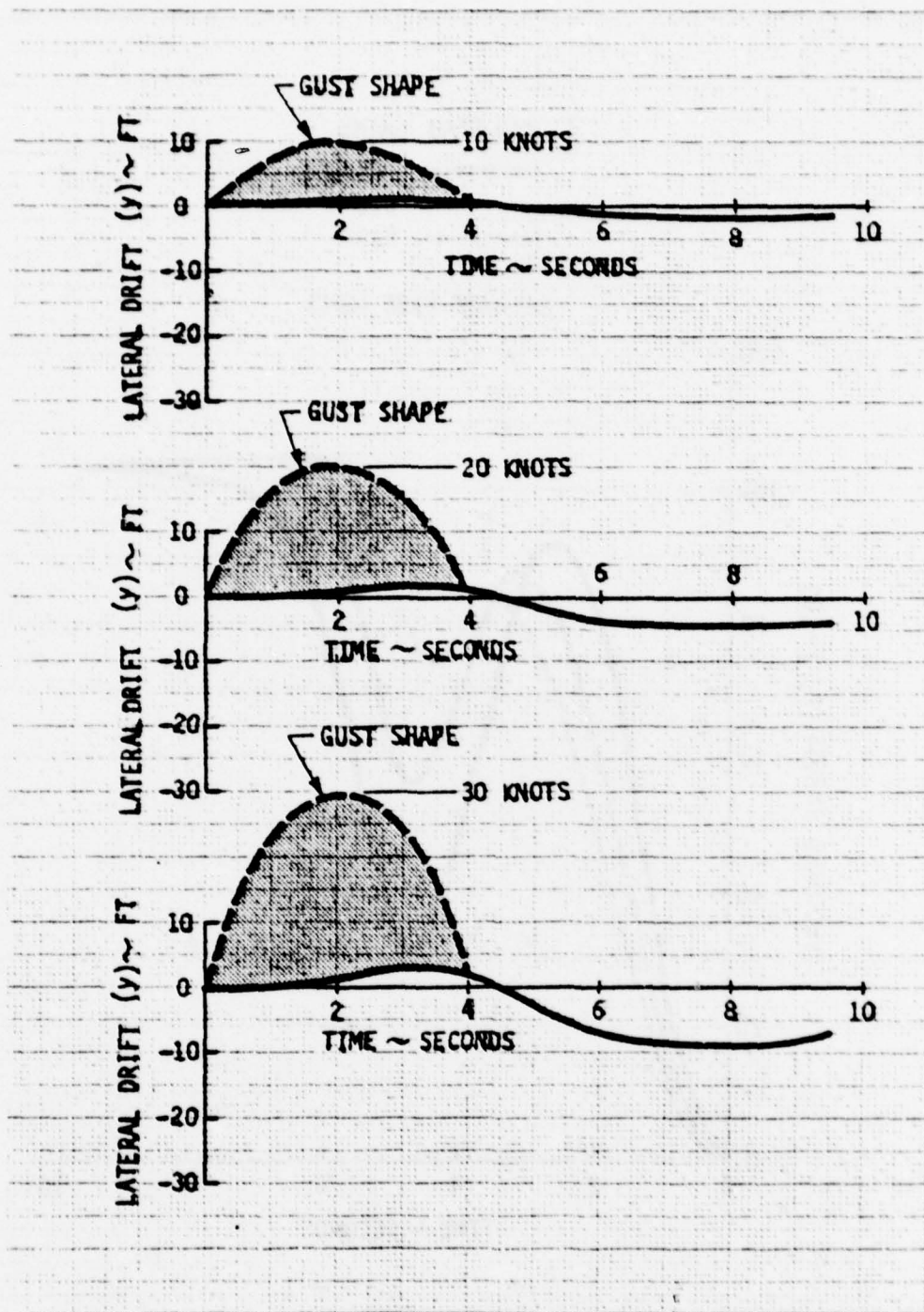
Figure 73   Lateral Drift Time Histories During ACTS Takeoff

The Jindivik ACTS was simulated at taxi conditions with engine RPM's set at 50, 60 and 70 percent. The cushion pressures were assumed to be as in Figure 35. The side wind gust was 10 knots, and asymmetrical trunk drag and skid friction were considered. These simulated taxi runs were for 25 seconds. The lateral drift versus longitudinal distance is shown in Figure 74. With an engine RPM at 50%, the vehicle did not move. At 60% RPM the aircraft traveled 800 feet and reached a velocity of 35 knots. At 70% RPM a distance of 1540 feet and a velocity of 76 knots were attained. In these taxi conditions with a 10 knot side wind gust, lateral drift away from the runway center line was less than 3.0 feet.

A condition corresponding to an externally induced yaw perturbation of 20° occuring linearly over a 2 second period was also simulated. This could occur as a result of wing tip skid contact, and results are shown in Figure 75. The yaw gyro gain was assumed to be 10% per degree, and the batsman control to vary from 2 to 20 feet. The results show the vehicle initially drifting away from the runway centerline in response to the disturbance. However the yaw gyro system and the batsman react to the change in yaw angle and drift respectively, and the vehicle then moves to the other side of the runway centerline. Both yaw gyro and the batsman are in fact over-responding to the disturbance. The results of Figure 75 suggests that a yaw gyro gain of 10% per degree is probably the maximum acceptable value.

The results of a parametric study of the thrust vector control system for takeoff on the ACTS trunk is presented in Figure 76 and 77. In Figures a and b of 76 the auto gyro demand gain for vectored thrust is 10% per degree. In Figure 76a the batsman control begins at a lateral drift of ±2 feet and in Figure 76b batsman control begins at ±5 feet. The batsman control gain was varied as shown on the figures. These data represent the maxima of the positive or negative lateral drift for side wind conditions up to 30 knots during a takeoff run.

105
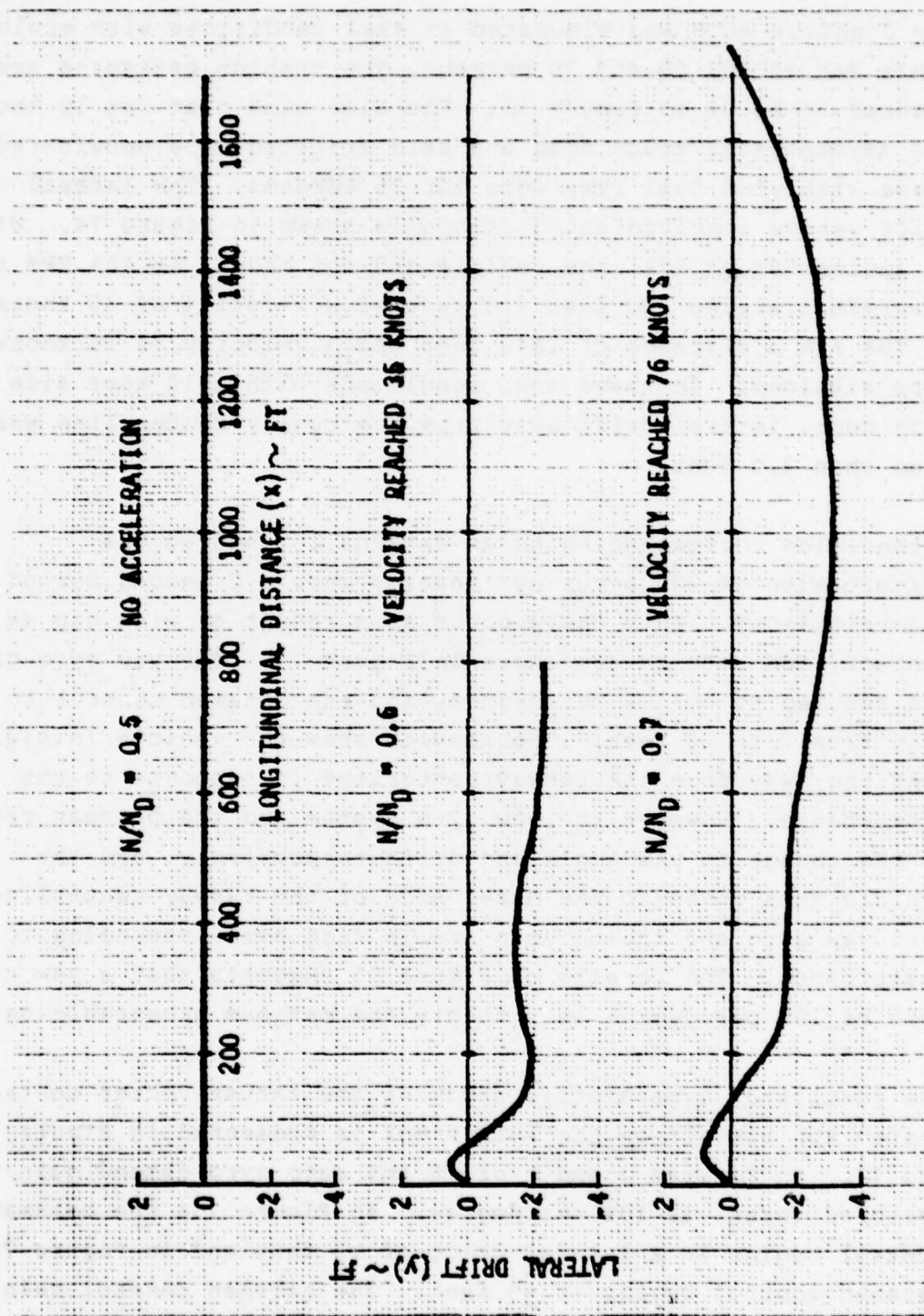
Figure 74   ACTS Taxi Map
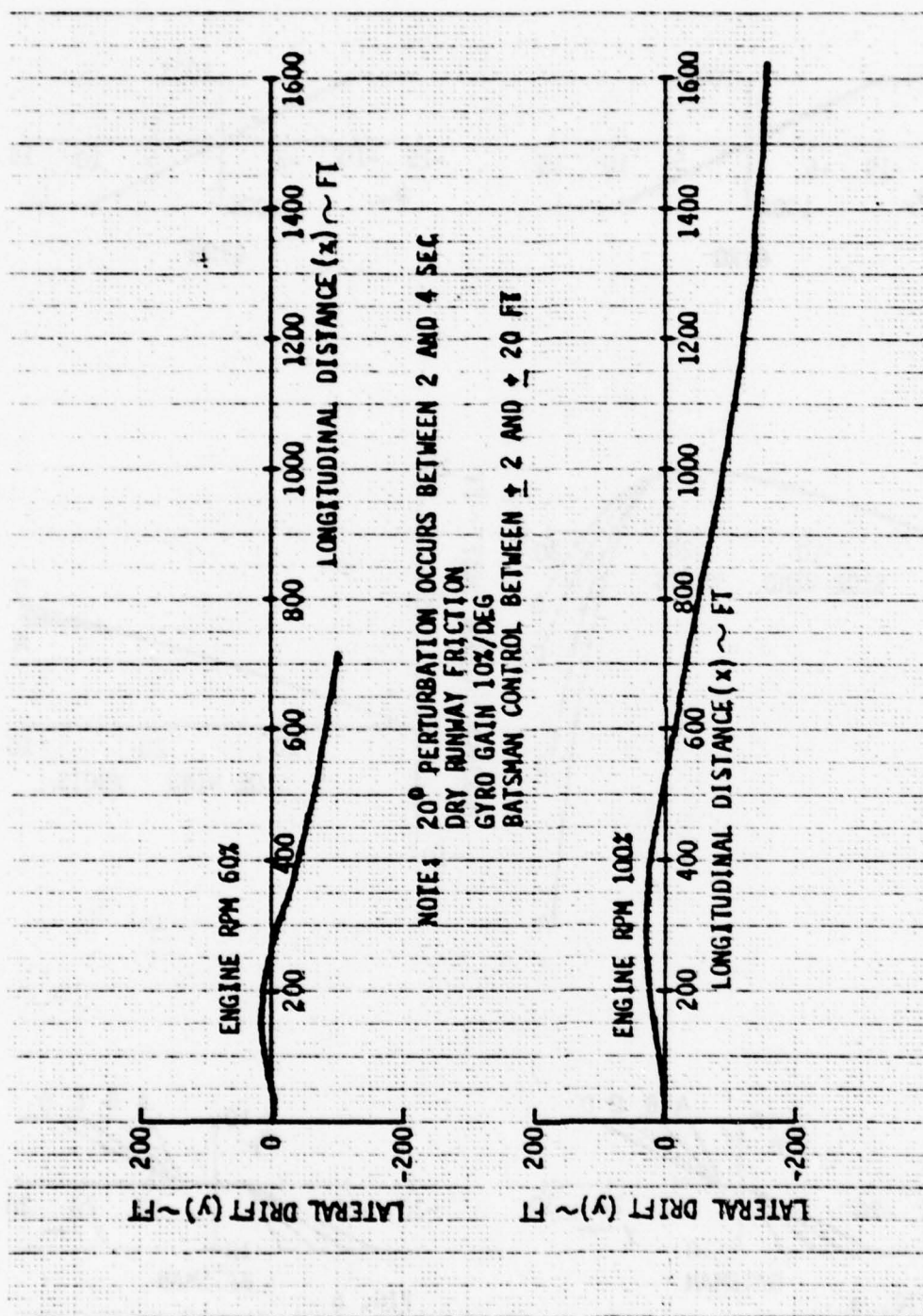
Figure 75   Response to Yaw Perturbation During ACTS Taxi
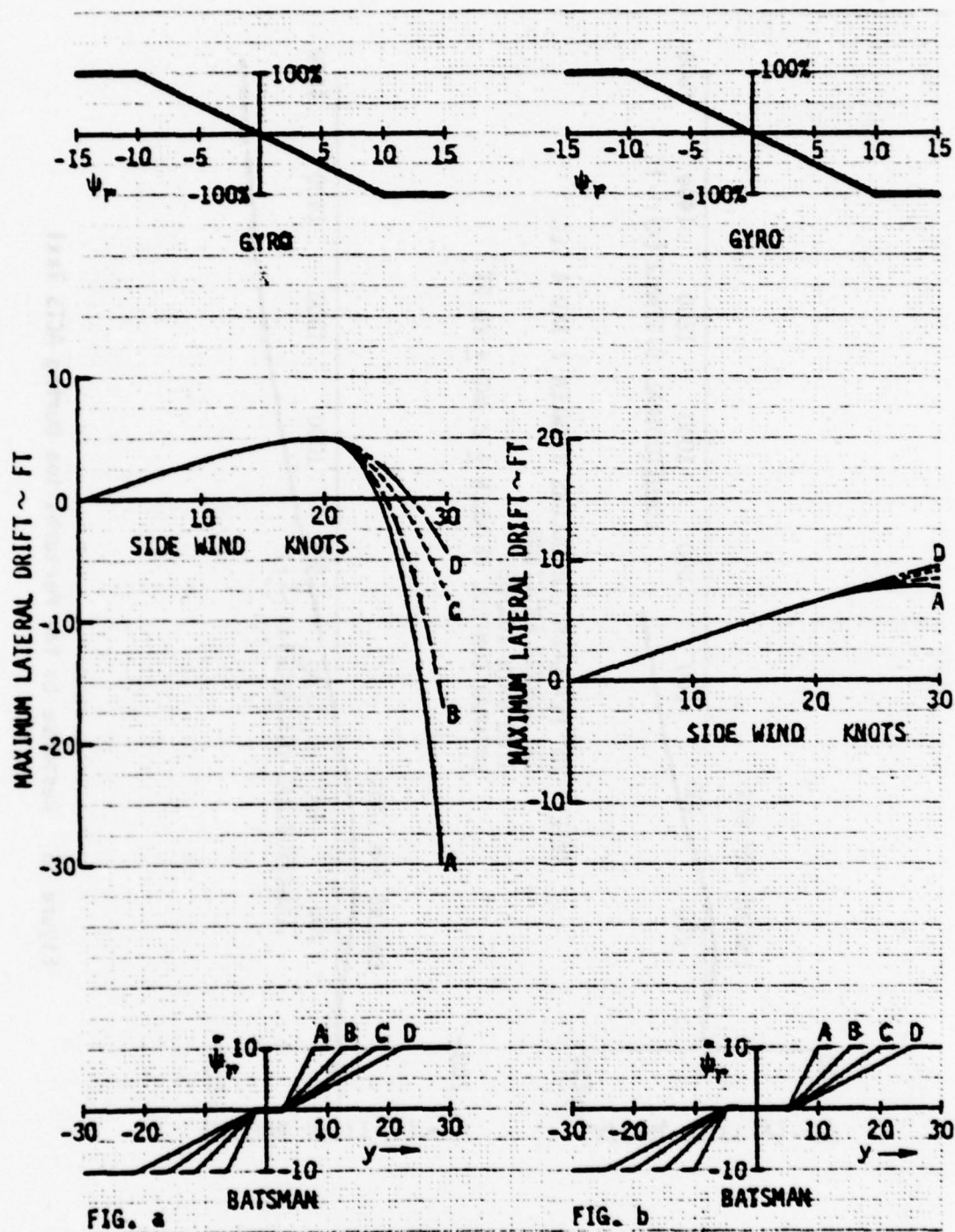
Figure 76   Thrust Vector Control System Parametric Analysis
ACTS Trunk-Auto Gyro Gain 10%/Degree
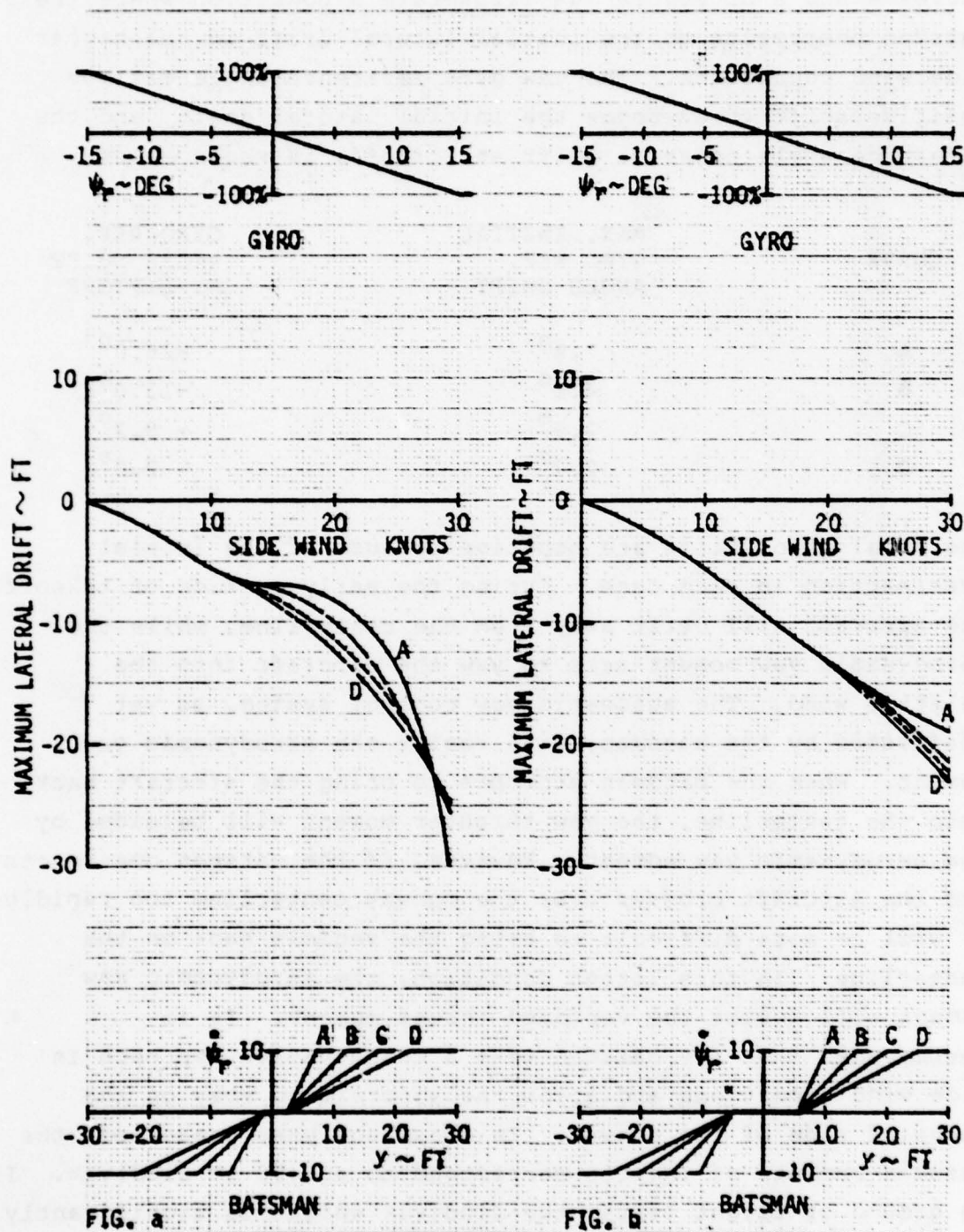
Figure 77   Thrust Vector Control System Parametric Analysis
ACTS Tank - Auto Gyro Gain 6.6%/Deg

Curves A and B of Figure 76a illustrate a condition where the
batsman overreacts to the initial lateral drift in the higher
side wind conditions. The yaw gyro reference angle maximum
positive shift to overcome the initial lateral drift, and the
reference angle negative shift at liftoff, is shown below:

CURVE	MAX. INITIAL GYRO REF. ANGLE SHIFT	GYRO REF. ANGLE SHIFT AT LIFTOFF
A	7.8°	-26.0°
B	4.1°	-13.0°
C	2.9°	- 8.2°
D	2.7°	- 2.0°

The final gyro shifts are negative because of the initial
overreaction in each case. During the early portion of takeoff,
the aircraft will drift away from the centerline, while the
aerodynamic yaw moment acts to yaw the aircraft into the
relative wind. The automatic yaw control system, as yet
unaffected by the batsman, will resist the aerodynamic yaw
moment. When the batsman attempts to bring the aircraft back
onto the centerline, the yaw thruster moment will be aided by
the aerodynamic yaw moment. However, if the batsman overreacts
and the aircraft crosses over the runway centerline too rapidly,
it will be more difficult to bring the vehicle back on the
centerline. In this latter condition, the aerodynamic yaw
moment will resist the vectored thrust moment. It is
recommended that the batsman take a conservative approach in
side wind conditions and allow the aircraft to stay on the
downwind side of the runway. In these analyses presented, the
assumed moments of inertia correspond to a 3400 lb Jindivik. If
in ground or flight tests, the Jindivik weight is significantly
less than 3400 lbs, a side wind will more easily yaw the
aircraft; it is even more important in this case that the
batsman attempt to hold the Jindivik on the down wind side of

the centerline. The Jindivik may easily yawed into the relative wind, but not so easily out of the wind stream.

It should also be pointed out that these data and recommendations are pertinent to a hovering or near hovering condition. During taxi or other lower power conditions, the drag may be considerably greater than assumed for these calculations, affecting the vehicle response.

In Figure 76b the batsman control allows the aircraft to drift 5 feet before attempting to bring the aircraft back to the centerline. In these cases, there is not much demand for batsman control. For example, in the case of a 30 knot side wind, batsman control did not begin until six seconds into the takeoff run, where the aircraft velocity is 68 knots. The data shown below present the effect of the batsman at the 30 knot side wind condition of Figure 76b.

CURVE	GYRO REF. ANGLE AT 6 SEC.	GYRO REF. ANGLE AT LIFTOFF (9.5 SEC)	YAW ANGLE AT LIFTOFF	GYRO SHIFT AT LIFTOFF	LATERAL POSITION AT LIFTOFF
A	-7.5°	-1.5°	-14.8°	12.9°	6.2 ft
B	-7.5°	-3.3°	-11.1°	7.6°	8.1 ft
C	-7.5°	-4.2°	-9.7°	5.3°	8.8 ft
D	-7.5°	-4.7°	-8.9°	4.0°	9.1 ft

In the 3.5 seconds that the batsman control is operating, there is insufficient time for any large changes in motion.

In Figures 77(a) and (b) the lateral drift data is a result of the auto gyro gain set at 6.6% per degree. At this lower gain, the aerodynamic yaw moment causes a greater yaw angle, and consequently the aircraft drives to the upwind side of the runway. The auto yaw control gain of 6.6% is not sufficiently responsive.

111

ACRS System. The results of a parametric analysis of takeoff on the ACRS trunk are shown in Figures 78 and 79. The assumptions are the same as for ACTS takeoff conditions of Figures 76 and 77. Because of the higher drag on the ACRS trunk, the drag induced yaw moment resists the aerodynamic yaw moment and tends to keep the aircraft parallel to the runway centerline. Hence, initially the vehicle drifts downwind. The batsman, following the control algorithm shown in the figures, overreacts to the extent that the autogyro reference angle is shifted nearly the maximum 30 degrees in some cases. As with the ACTS, the vehicle heads into the wind and crosses the runway centerline. It is then more difficult for the thruster to recorrect the vehicle heading since aerodynamic side forces are opposing the yaw thruster moment, and the final lateral drifts are all in the upwind direction.

3.3 SYSTEM EVALUATION

Takeoff Capability. At high engine power settings, the steady state analysis shows the yaw thruster capability adequate for 10 and 20 knot side winds, and for 30 knot winds at power settings above 95%. The simulations of takeoff on the ACTS show that the yaw gyro gain should be set at about 10%/degree. The batsman was assumed to respond to lateral drift, which can be sensed more readily than vehicle heading. Batsman response was varied to give initiation between 2 and 5 feet, and maximum correction between 7 and 25 feet.

In most cases, best response was obtained when the batsman exerted least control, since the batsman tended to overreact and hence yaw the vehicle too far into the relative wind. With a yaw gyro gain of 10%/degree and least batsman control (maximum correction at 25 feet) the vehicle drift was less than 10 feet even with a 30 knot side wind.

112
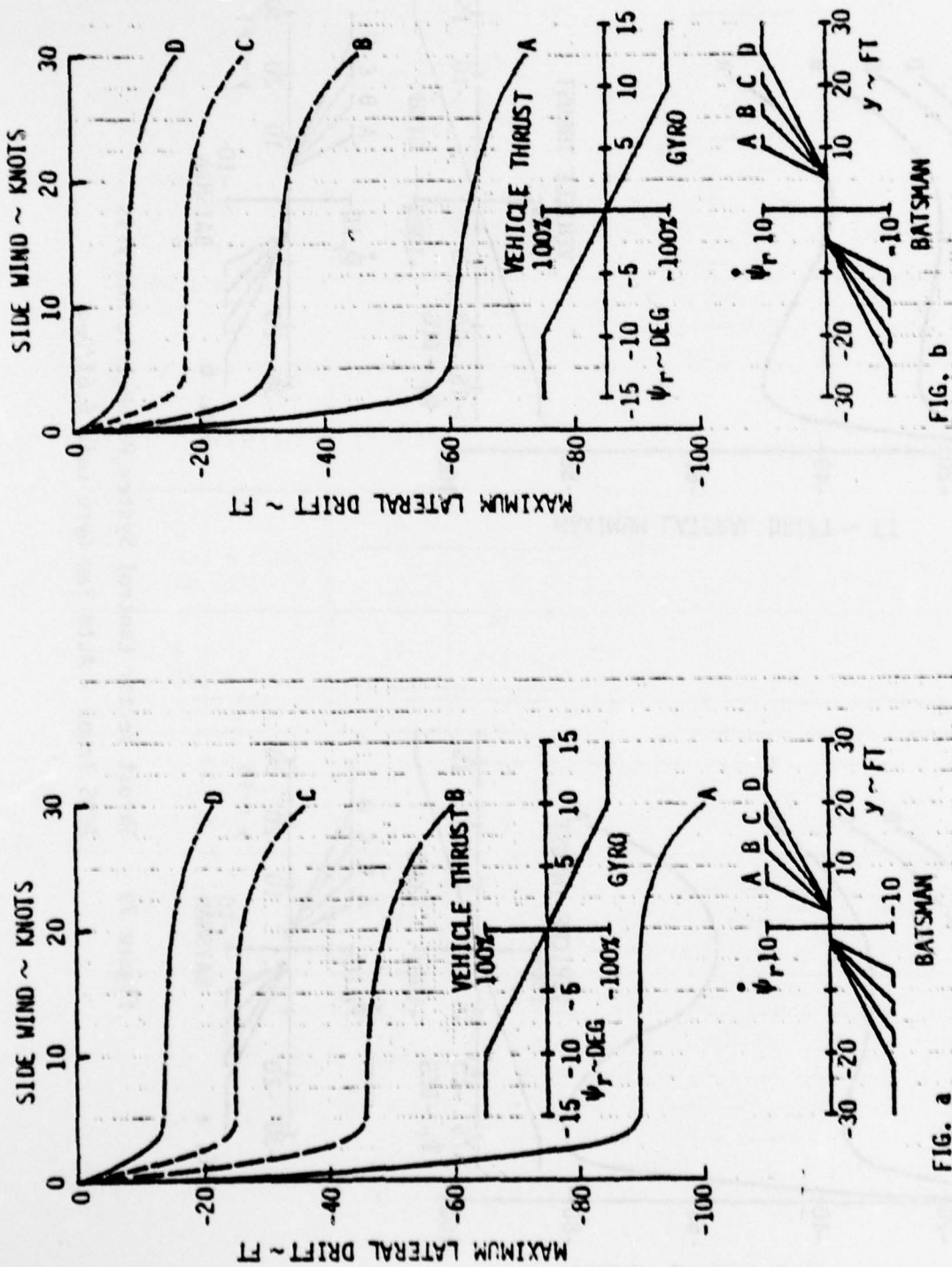
Figure 78. Thrust Vector Control System Parametric Analysis
ACRS Trunk - Auto Yaw Gyro Gain 10%/Deg

113

SIDE WIND ~ KNOTS

MAXIMUM LATERAL DRIFT ~ FT

VEHICLE THRUST

GYRO

BATSMAN

FIG. b

SIDE WIND ~ KNOTS

MAXIMUM LATERAL DRIFT ~ FT

VEHICLE THRUST

GYRO

BATSMAN

FIG. a
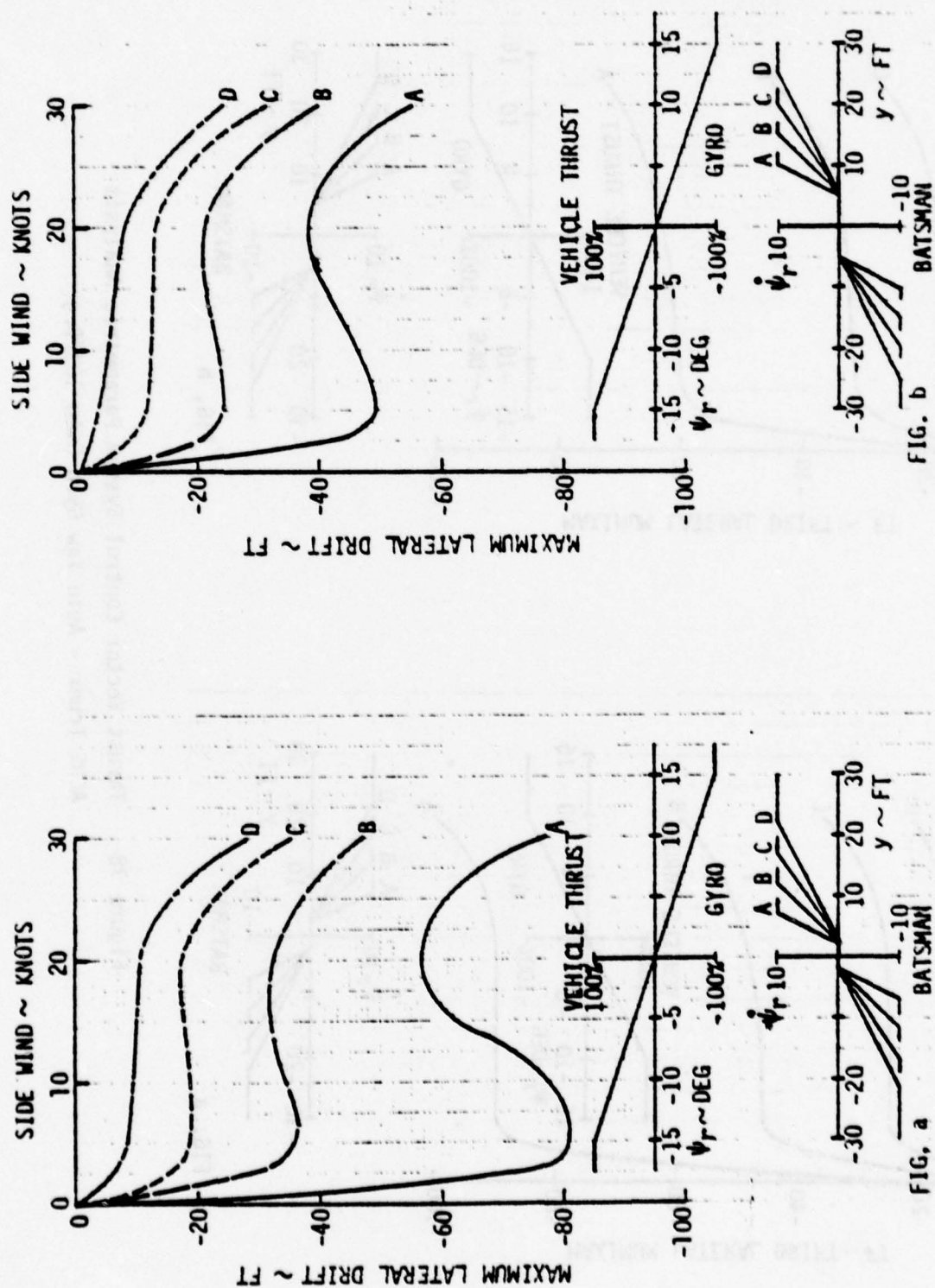
Figure 79   Thrust Vector Control System Parametric Analysis
ACRS Trunk - Auto Yaw Gyro Gain 6.6%/Deg

Takeoff runs were also simulated on the ACRS. Although takeoff
on the ACRS is not currently planned for the Jindivik, the
results are significant in that they show the effect of
increased trunk drag. With the same yaw gyro gain and batsman
control, the drift was about 20 feet with a 30 knot side wind.
The final drift could have been reduced further by allowing the
vehicle to move further downwind before initiating any
corrective action.

As discussed earlier, the trunk drags which can be expected in
future Jindivik testing are not yet known, as they depend on the
resolution of problems in the airflow system. It is possible
that drags will be higher than assumed in this analysis. If so,
the batsman will have to allow substantial downwind drift
and avoid yawing the vehicle too far into the wind.

Taxi Capability. For an idealized case of zero trunk drag, the
steady state analysis shows that there is sufficient vectored
thrust in a 10 knot side wind. In a 20 knot side wind, however,
Figure 57 shows insufficient yaw thruster capability at relative
engine speeds less than about 0.75 and speeds less than 80
knots. The effects of trunk drag are complex. Moderate levels
of trunk drag improve the directional control capability during
taxi for two reasons. Firstly, the friction provides some
directional stability to the vehicle and thus less vectored
thrust is required to prevent weathercocking; secondly, for a
given forward velocity and acceleration, increasing the drag
increases the required engine thrust, which in general improves
the directional control capability. However, as shown by the
takeoff simulations, increasing drag also requires a somewhat
different, and probably more difficult, set of responses from
the batsman.

115

SECTION 4

WIND TUNNEL DATA ANALYSIS

4.1 INTRODUCTION AND SUMMARY

Low speed wind tunnel tests were conducted to determine the effect of an air cushion recovery system (ACRS) on Jindivik lateral-directional stability. The tests were performed at the Aeronautical Research Laboratories, Melbourne, Australia. The wind tunnel model is shown in Figures 80 through 82. Tests were run with and without the ACRS #3 trunk, with fin off, the standard fin (6.52 sq. ft.), and an extended fin (8.64 sq. ft.). The In-Ground-Effect (IGE) shape of the trunk was used for the tests, rather than the Out-of-Ground-Effect (OGE) shape, which is somewhat different. This minor discrepancy is overshadowed by the fact that an entirely new trunk shape is planned for any future flight tests. The proposed trunk and the trunk actually tested are compared in Figure 83. This difference in trunk shape is considered a shortcoming of the test, and tests of the proper trunk should be performed.

Tests were performed with wing flap settings of 1° and 19°. Photos of the model installed in the tunnel appear in Figures 80 through 82, and a summary of test conditions is given in Table 6.

In those figures which present test data, the terminology used on the raw data supplied to Boeing has been retained. Thus "bag" refers to the ACRS trunk, and "pipe" to the external bleed air duct.

4.2 WIND TUNNEL DATA AND ANALYSIS

Figures 84 through 89 summarize the test results. These figures

116

Figure 80   Wind Tunnel Model - Under View

117

FIN
EXTENSION

STANDARD
FIN

BLEED
AIR DUCT
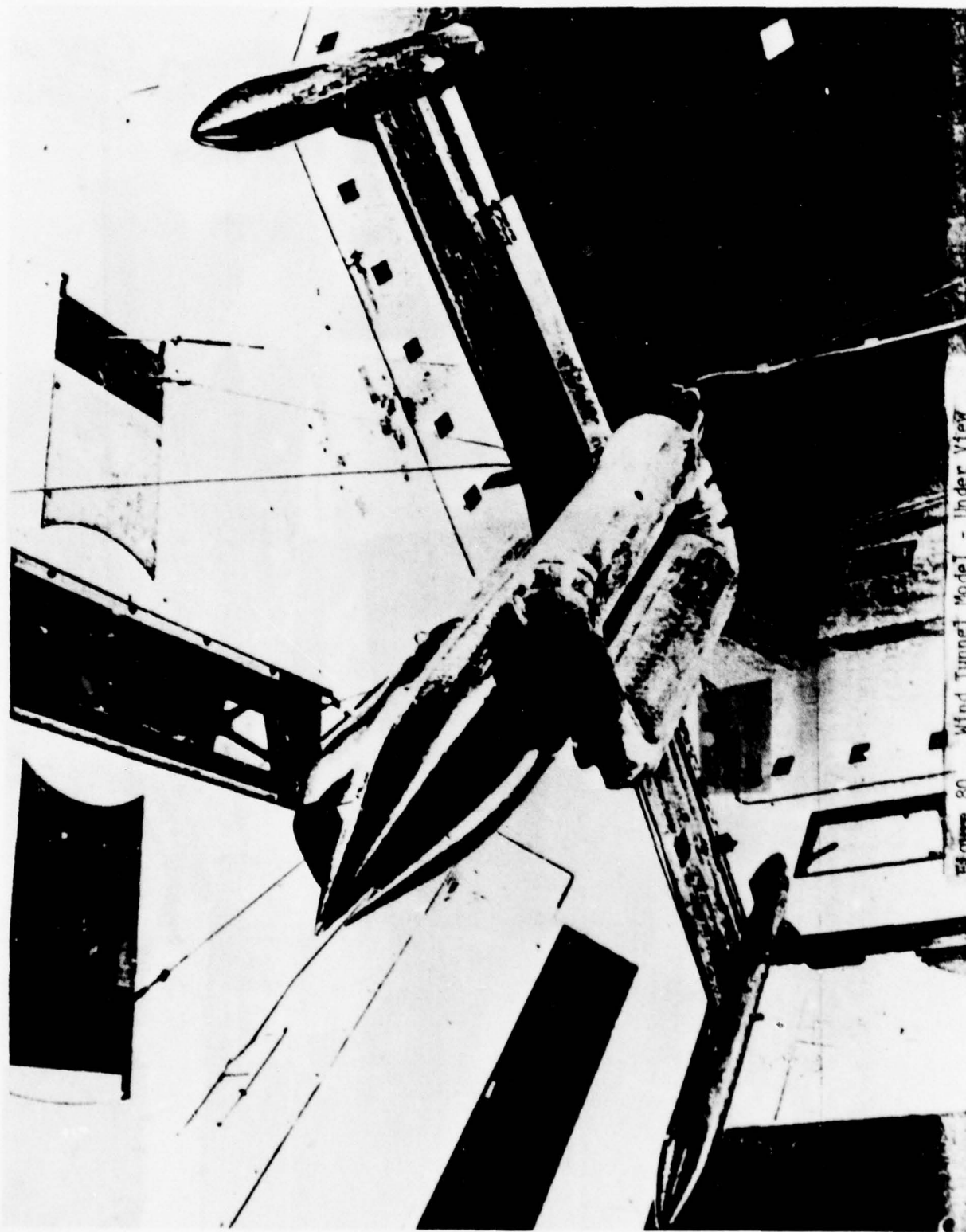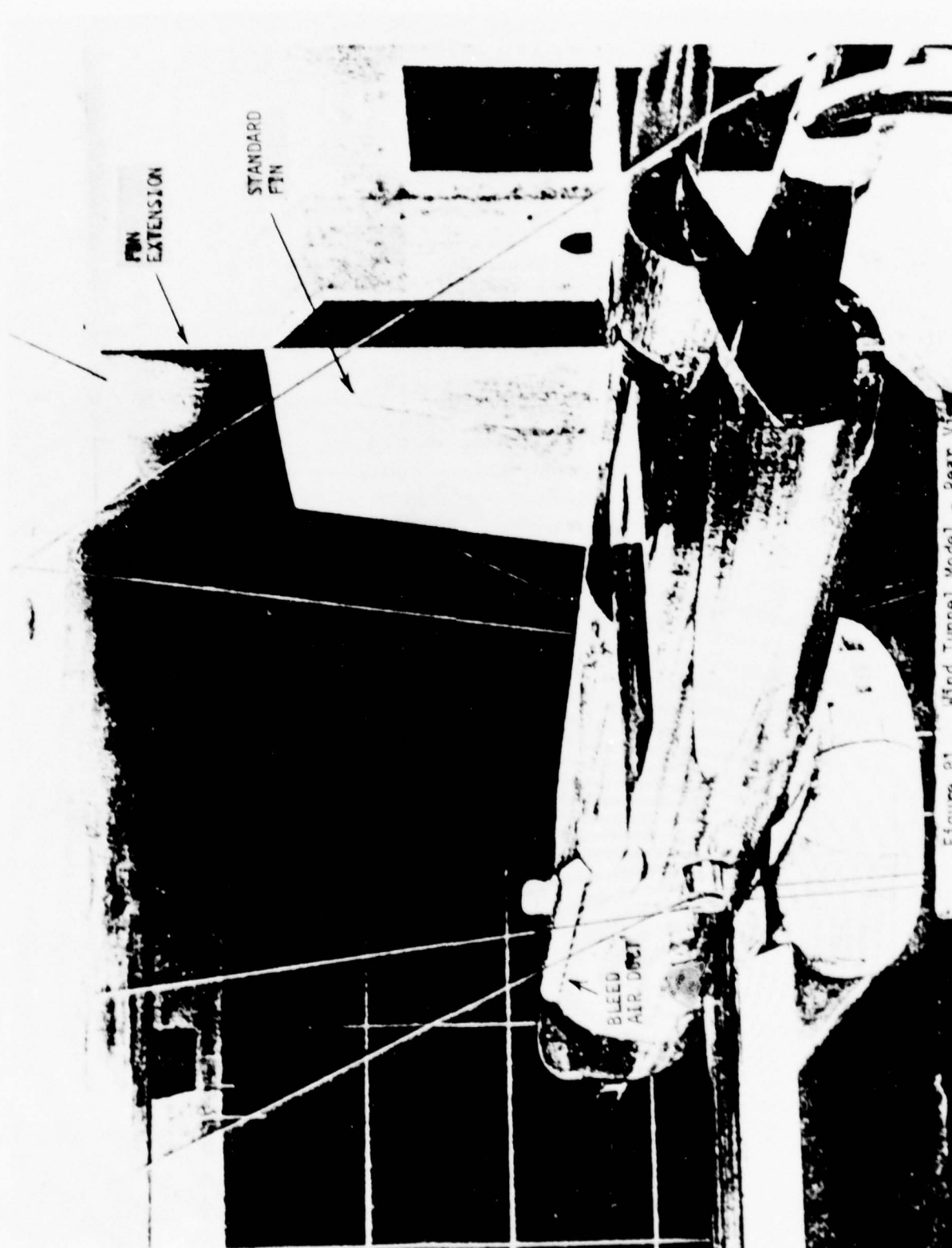
Figure 81   Wind Tunnel Model - Rear View

118
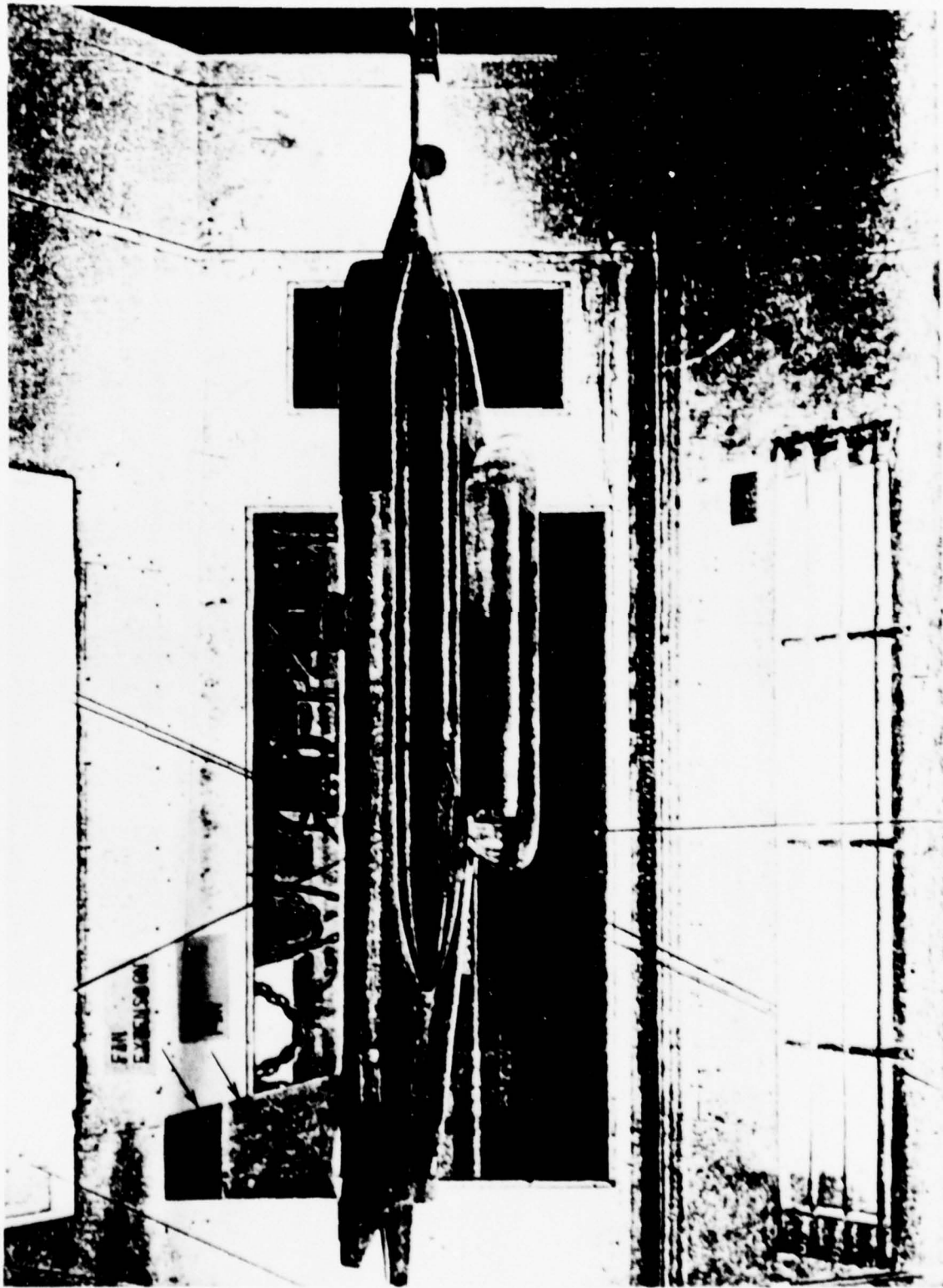
Figure 82   Wind Tunnel Model - Side View

119
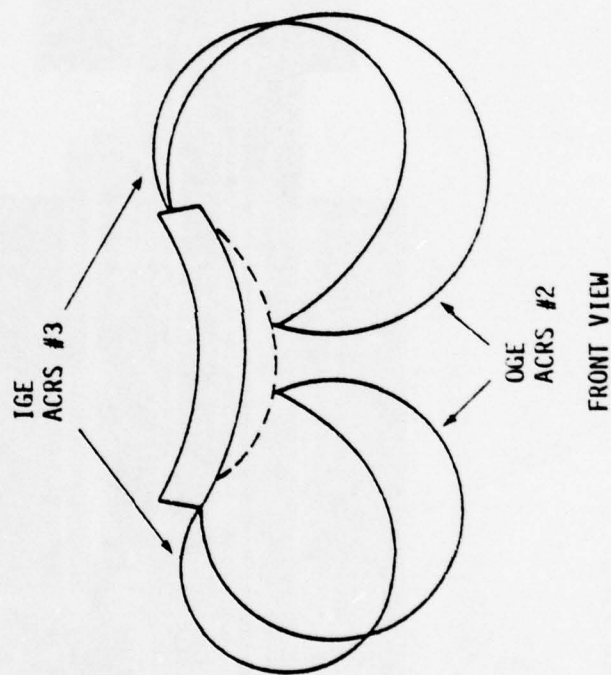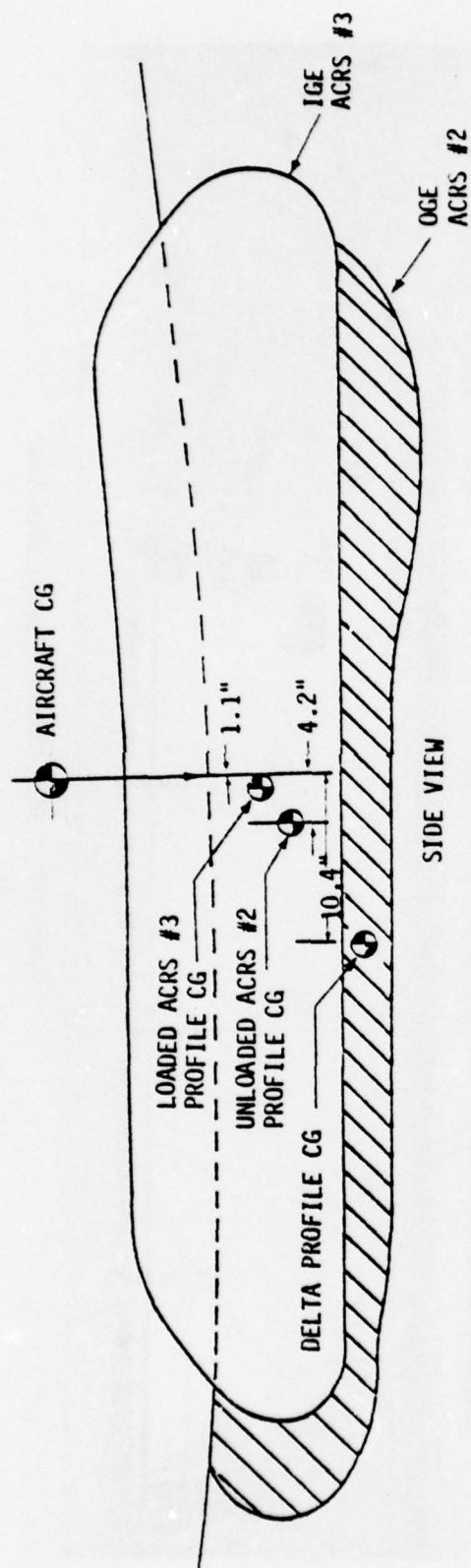
Figure 83   ACRS #2 and #3 Trunk Profiles

120

TABLE 6   WIND TUNNEL TEST CONDITIONS

CONFIGURATION & DESCRIPTION	LATERAL DIRECTION			LONGITUDINAL			
	$\delta_f^{\,o}$	α^o	$\delta_e^{\,o}$	$\delta_f^{\,o}$	α^o	$\delta_e^{\,o}$	β^o
# 1 Ref - Clean	1°, 19°	0°	0°	—	—	—	—
# 2 Bag & Pipe No Tail	1° / 19°	0°, 4° / $4, 0, -2$	N.A.	—	—	—	—
# 3 Bag & Pipe Std. Fin	1° / 19°	$6,4,2,0^o$ / $2,4,0,-2$	0°	1° / 19°	$6,4,2,0$ / $4,2,0,-2$	$+10^o$ 0° -10°	-1°
# 4 Bag & Pipe Extend Fin	1° / 19°	$4,4,2,0^o$ / $4,2,0,-2$	0°	—	—	—	—
# 5 Clean No Tail	1°, 19°	0°	N.A.	—	—	—	—

δ_f = flap deflection (deg.)

δ_e = elevator deflection (deg)

121
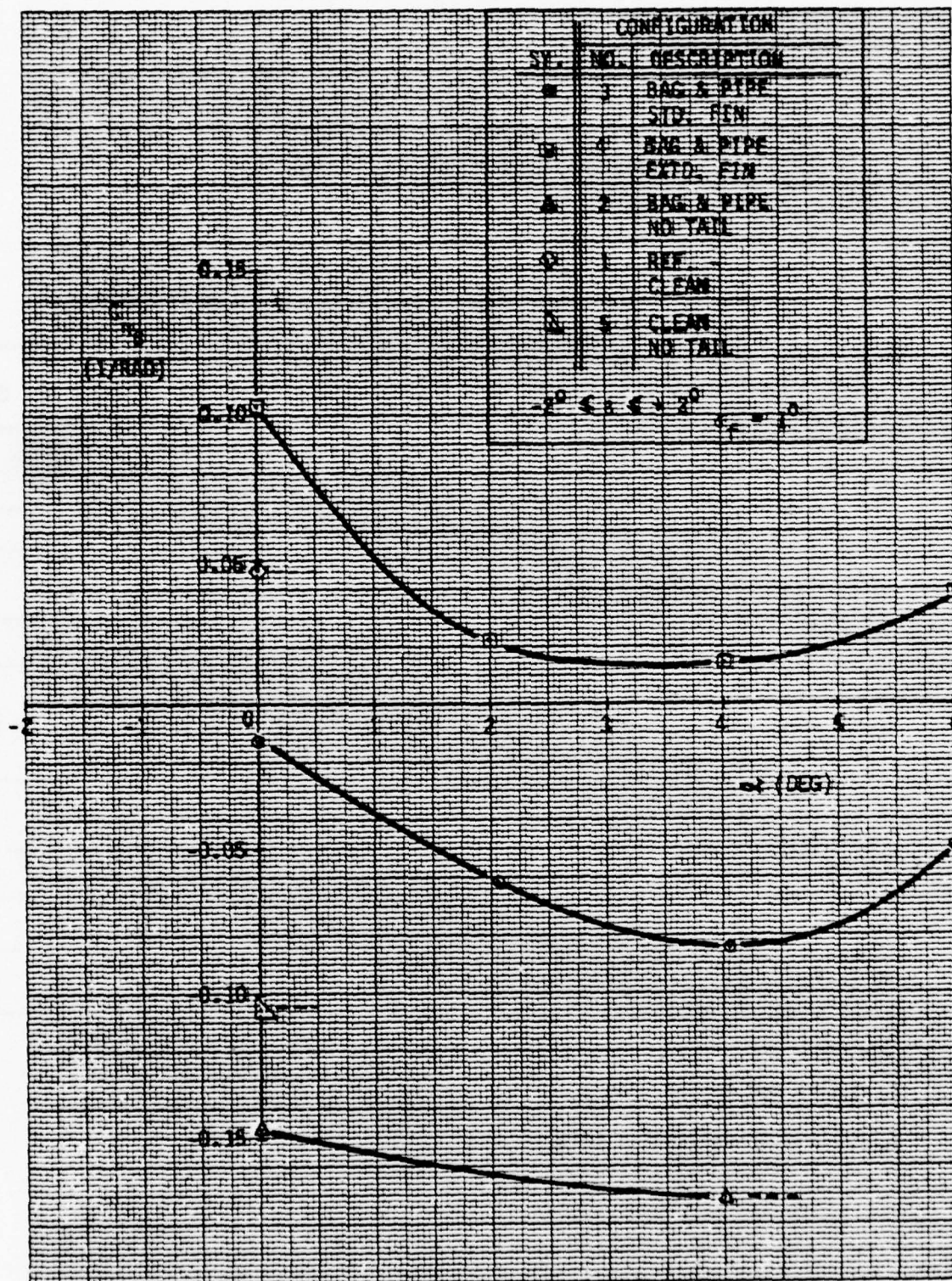
Figure 84   Static Directional Stability Due to Angle of Attach, $\delta_f = 1^o$

122
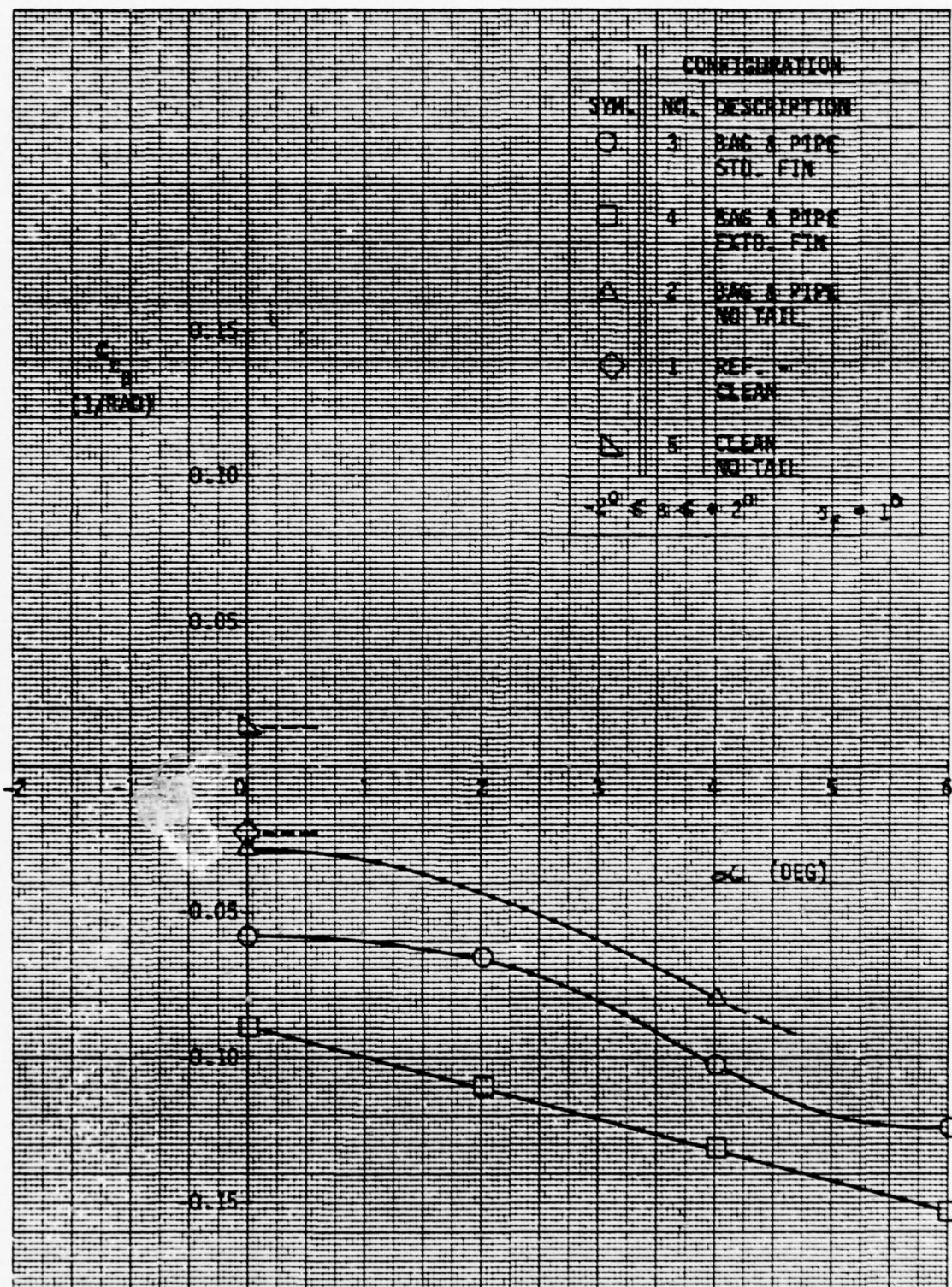
Figure 85   Dihedral Effect Due to Angle of Attack, $\delta_f = 1^\circ$

123
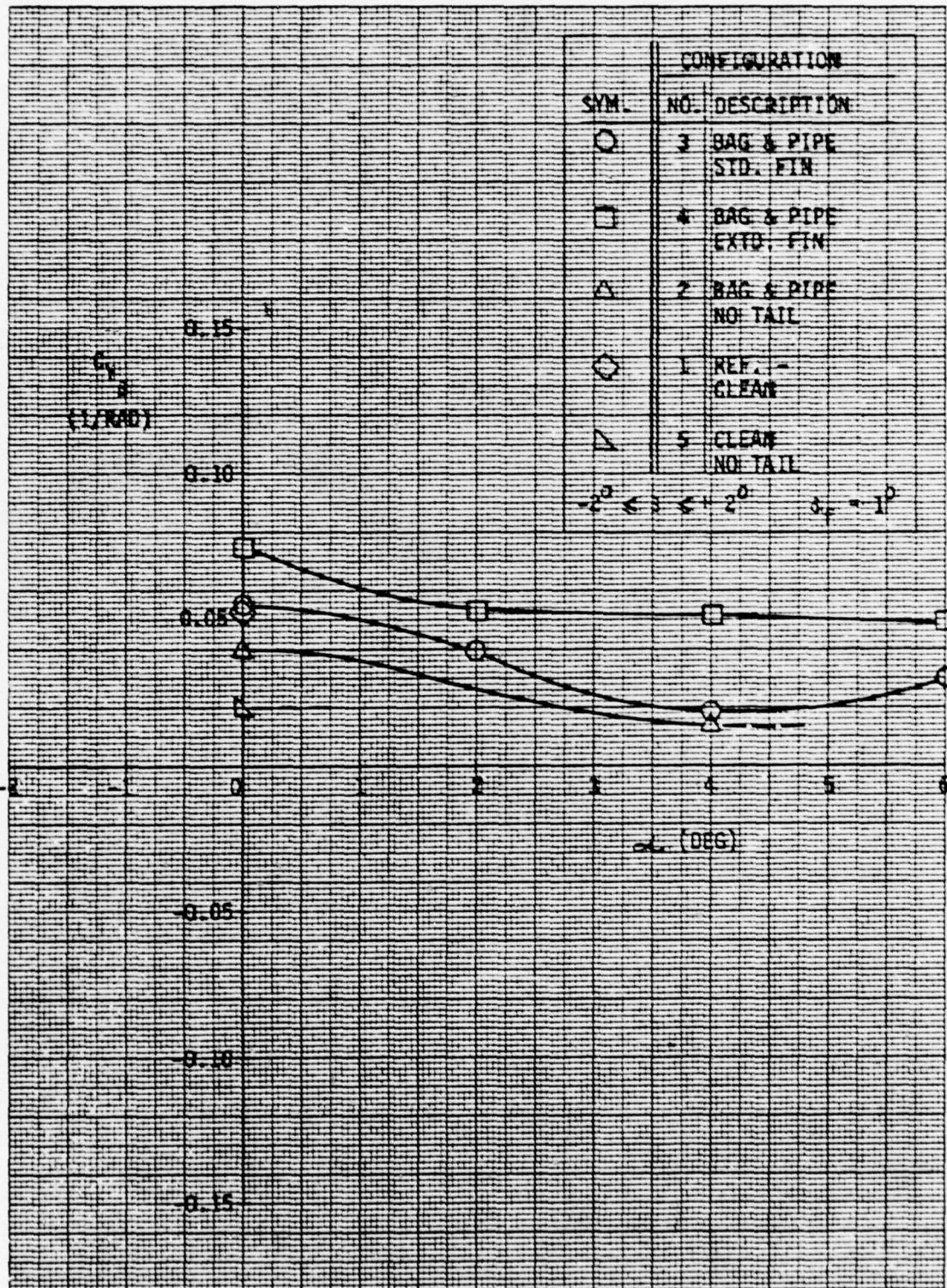
Figure   86   Side Force Due to Angle of Attack, $\delta_f = 1^o$

124
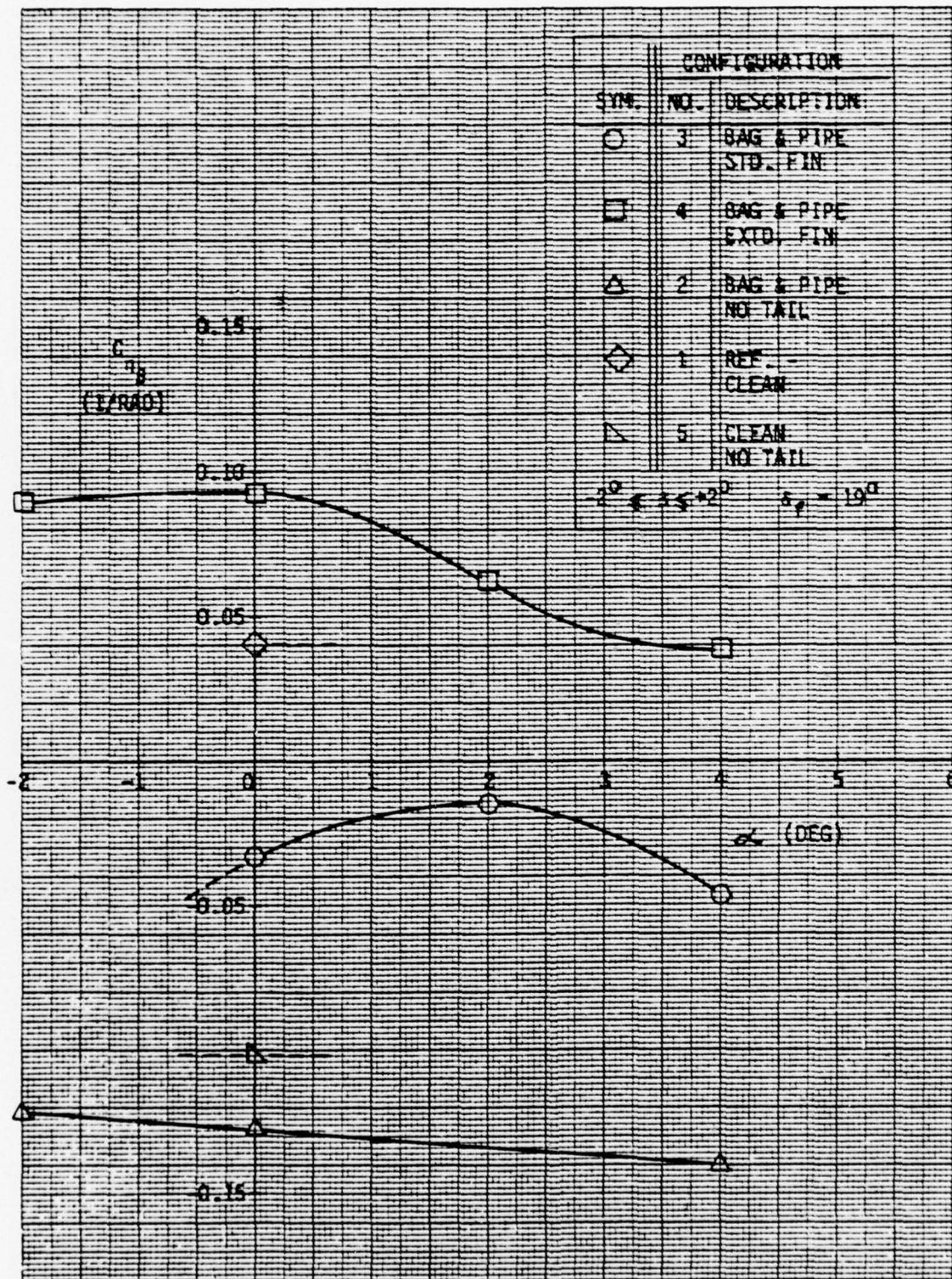
Figure 87   Static Directional Stability Due to Angle of Attack, $\delta_f = 19^0$

125
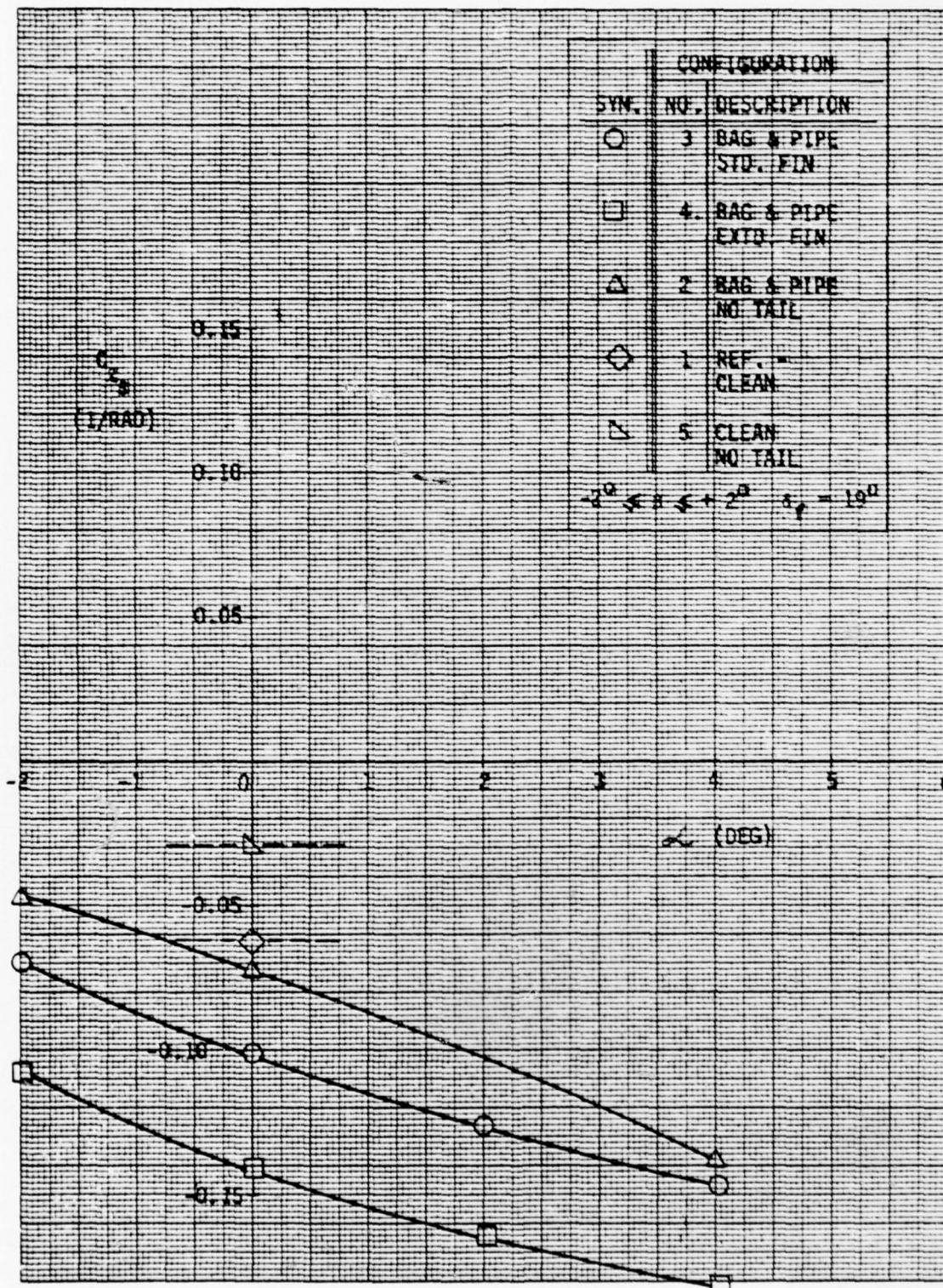
Figure 88   Dihedral Effect Due to Angle of Attack, $\delta_f = 19^o$

126
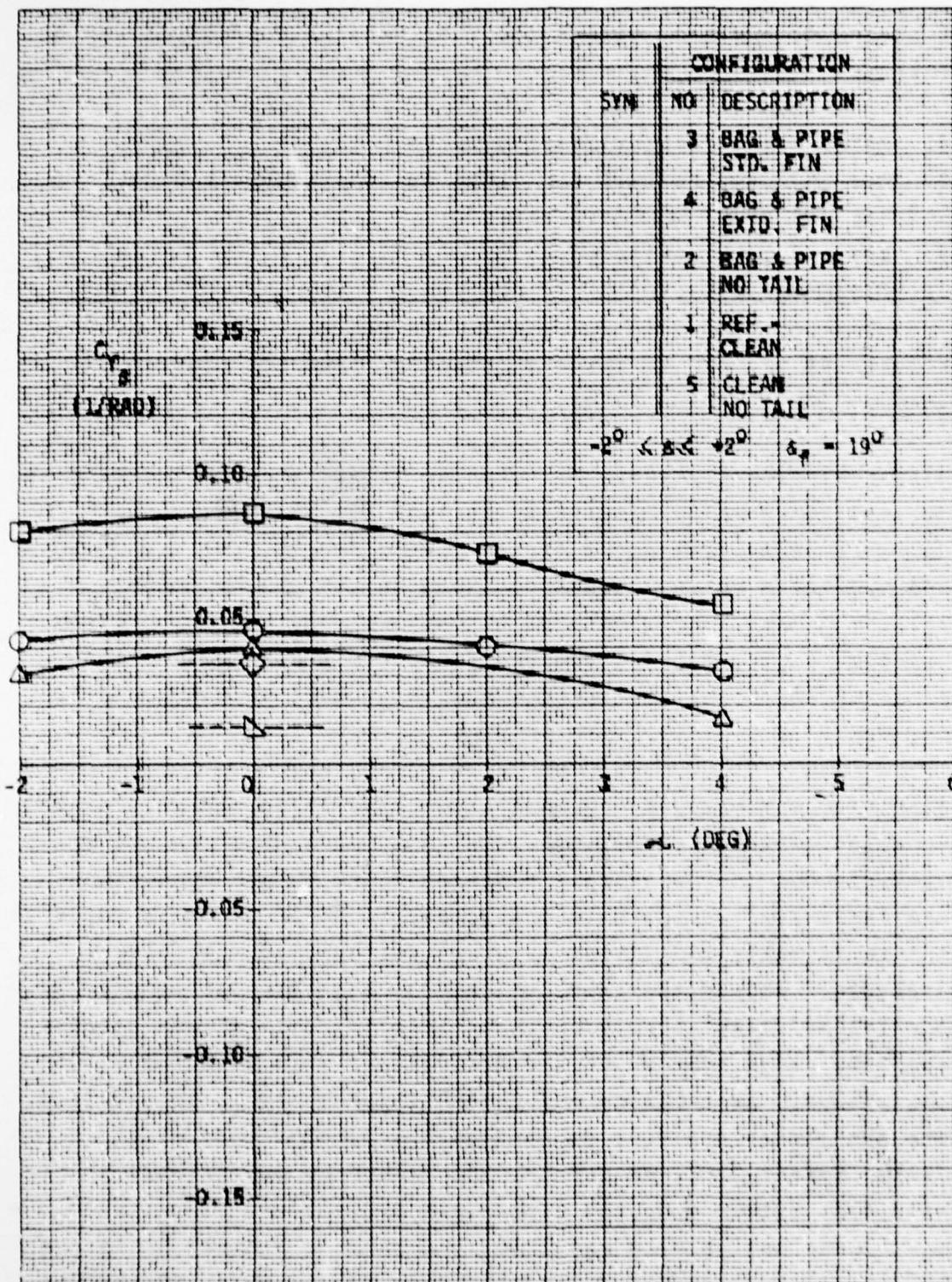
Figure 89   Side Force Due to Angle of Attack, $\delta_f = 19^0$

127

show the stability derivatives C_{n_β}, C_{ℓ_β} and C_{Y_β} plotted as a function of angle of attack for five vehicle configurations as follows:

1. Reference-clean (standard vehicle)
2. Bag and pipe no tail fin (ACRS #3 and bleed air duct)
3. Bag and pipe, standard tail
4. Bag and pipe, extended tail
5. Clean-no tail fin

Figures 84 through 86 present data for flaps 1°, Figures 87 through 89 for flaps 19°.

Note that sideslip angle was limited to $\pm 2^\circ$ when calculating the derivative shown on Figures 84 through 89. Stability derivatives are the slope of the yawing moment, rolling moments, and sideforce versus sideslip. Some of the yawing moment, rolling moment, and sideforce curves are nonlinear with β (see, example, Figure 93). Therefore β was limited to $\pm 2^\circ$ so that a range of applicability for the stability derivatives could be defined.

Stability derivatives are most often used in an analysis of the vehicle's dynamic stability. The analysis methods assume small disturbances in the vehicle's steady state flight conditions, and linearized aerodynamic characteristics. A sideslip range of $\pm 2^\circ$ is normally considered adequate for dynamic stability analysis. Should the calculations for a particular vehicle at a particular flight condition show sideslip oscillations greater than the range over which the derivatives were measured, then the analysis is invalid, and a non-linear analysis is required. The non-linear analysis necessitates a reproduction of the yawing moment, rolling moment, and sideforce curves versus sideslip, rather than the linearized derivative. Thus, should a non-linear analysis be required, the data of Figures 84 through 89 should be disregarded, and the data from Figures 93 through

128

107 used instead.

Static directional stability is shown on Figure 84. The basic Jindivik-plus-ACRS trunk (circle symbols) is unstable at all angles of attack tested. With the extended fin (square symbols), the Jindivik plus trunk is somewhat more stable than the basic Jindivik without trunk at an alpha of zero degrees (diamond symbol, $\alpha = 0^O$ only). The extended-fin Jindivik plus trunk loses stability rapidly as alpha increases, but does not become unstable. The basic Jindivik was tested only at $\alpha = 0^O$, so no comparisons of the trend of changes in angle of attack can be made.

Dihedral effect for flaps 1^O is shown on Figure 85. The basic Jindivik plus trunk (circle symbols) displays a more stable (negative sign is stable) dihedral effect than the Jindivik with trunk off (diamond symbol) at $\alpha = 0^O$. With the extended fin (square symbol), dihedral effect is more stable than with the standard fin. A gradual increase in dihedral effect is shown with increasing alpha, a normal trend. No comparison of a trends can be made with the standard Jindivik since it was tested only at zero alpha.

Side force derivative for flaps 1^O is displayed on Figure 86. Rate of change of side force with sideslip is almost identical for the basic Jindivik with and without the ACRS trunk. With the extended fin, side force is increased slightly, as would be expected. For the extended-fin Jindivik, side force derivative is relatively constant with angle of attack. No alpha variation is available for the basic Jindivik, trunk off.

Figures 87 through 89 summarize the test results for the flaps 19° configuration. As shown on Figure 87, the basic Jindivik-plus-trunk (circles) is directionally unstable at all angles of attack tested. With the extended fin (squares), the Jindivik-plus-trunk is statically stable at all alphas tested,

129

and is more stable than the basic Jindivik at $\alpha = 0^{\circ}$. Again, as with flaps 1°, no variation with alpha is available for the basic Jindivik.

Figure 88 shows dihedral effect at flaps 19°. The results here are essentially the same as at flaps 1°. There is an overall shift to more negative values of $C_{l_{\beta}}$ than at flaps 1°, but the increments between the various configurations are quite similar. Thus, adding the trunk to the basic Jindivik increases dihedral effect (negatively), and adding the fin extension increases $C_{l_{\beta}}$ still further.

Figure 89 presents side force derivative at flaps 19°. Comparison with Figure 86 shows that flap deflection has essentially no effect on $C_{Y_{\beta}}$. Adding the trunk has little effect, but adding the fin extension increases $C_{Y_{\beta}}$ significantly.

Figures 90 and 91 show the vertical tail's contribution to yawing moment as a function of sideslip angle at an angle of attack of 0°. Figure 90 shows data for the clean (i.e. standard Jindivik, no trunk) configuration and the configuration with the ACRS trunk and bleed air duct at flap deflections of 1° and 19°.

Looking first at the upper half of Figure 90, the two curves are almost identical in slope. This indicates that the fin's contribution to directional stability is the same at either flap deflection. There is a slight vertical shift in the curves, probably caused by some slight asymmetry in the model. This small shift can be disregarded.

In lower half of Figure 90, the data show a decided slope change between flaps 1° and 19°, with flaps 19° showing the shallower slope. At flaps 1°, the slope is essentially the same as in the upper portion of the figure. This shows that adding the trunk had no effect on the fin. The reason for lower stability

130
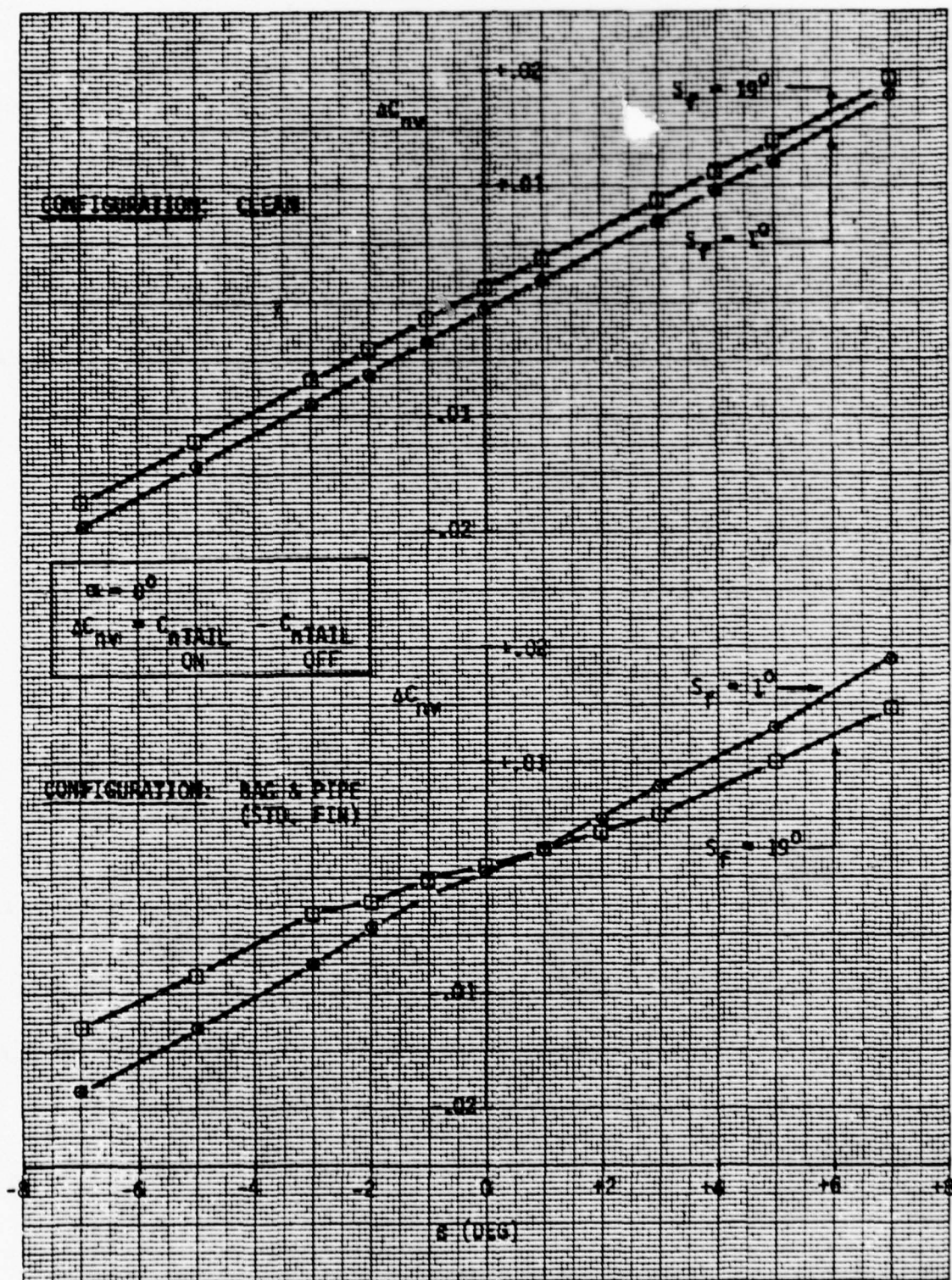
Figure 90   Vertical Tail Contribution to Yawing Moment,
Clean and Standard Fin

131
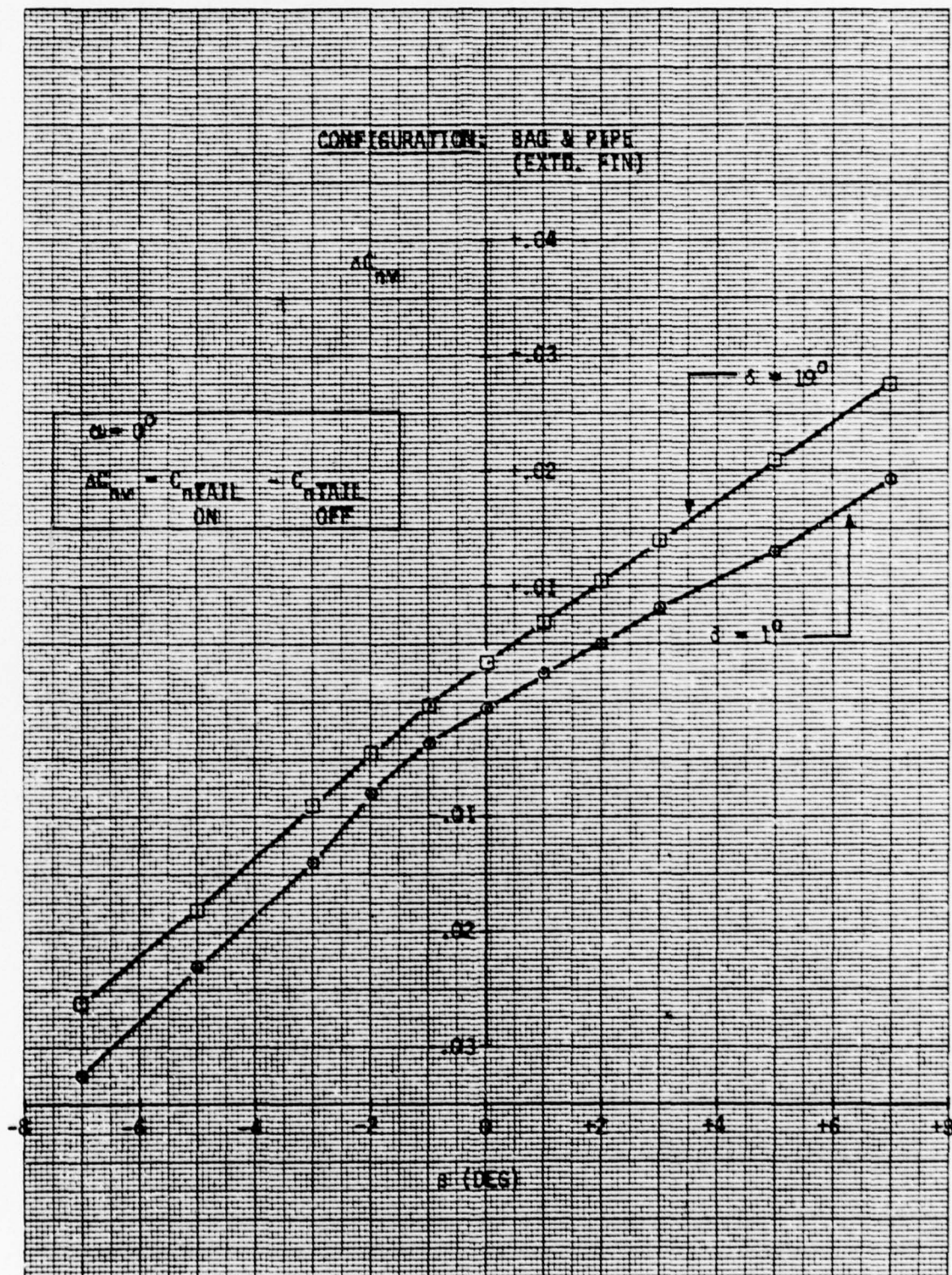
Figure 91   Vertical Tail Contribution to Yawing Moment,
Extended Fin

132

probably is that the wing-body-trunk combination is more unstable than the wing-body alone. For flaps 19°, there may be some interaction between the flaps and the trunk which causes a reduction in fin effectiveness. Another possibility is a wake from the bleed air duct, but this effect should also appear at flaps 1°. Notice at the higher sideslip angles ($\pm5^{\circ}$ to 7°) the slope of the ΔC_{nv} curve is almost back to the nominal value. This may indicate a narrow wake of turbulent air close to the fuslage. At the higher sideslip angles, the fin may emerge from the wake into high-energy air, thus restoring fin effectiveness.

Figure 91 shows the contribution of the extended fin to directional stability. The slopes of the curves are steeper than the basic fin, which is natural. The slope is approximately 50% higher for the extended fin than the standard fin. This is somewhat greater than the area increase (33% larger) of the extended fin and is probably accounted for by the higher aspect ratio of the extended fin. The decrement in tail effectiveness due to flap deflection which was noted in Figure 90 does not appear here. No explanation of this phenomenon has been developed. It is possible that the data for one figure or the other are in error, but no conclusive evidence is available.

Figures 92 through 111 are plots of the basic data obtained in the Jindivik test series. Data were furnished to Boeing in tabular form and were plotted as a preliminary step in the analysis.

Figures 92 through 95 present lateral-directional data at flaps 1°.

Figure 92 shows the standard Jindivik. The vehicle is well-behaved over the sideslip range tested. A slight non-linearity in yaw, roll, and side force occurs near zero sideslip, but this characteristic is common to many aircraft. The rolling moment shows a reasonably large offset at $\beta = 0^{\circ}$.

133
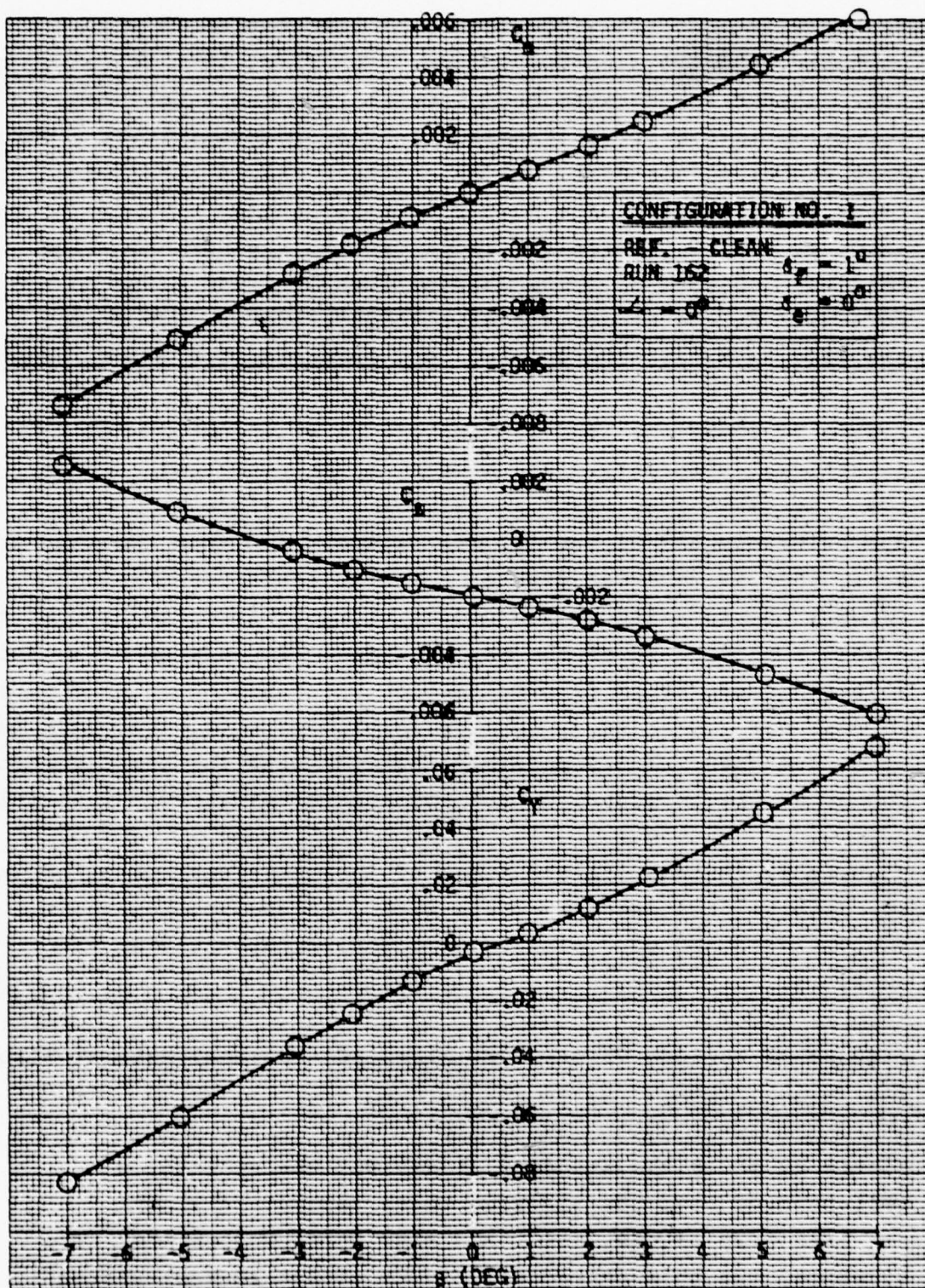
Figure 92   Lateral-Directional Aero Characteristics-
Configuration No. 1, $\delta_f = 1^0$

134
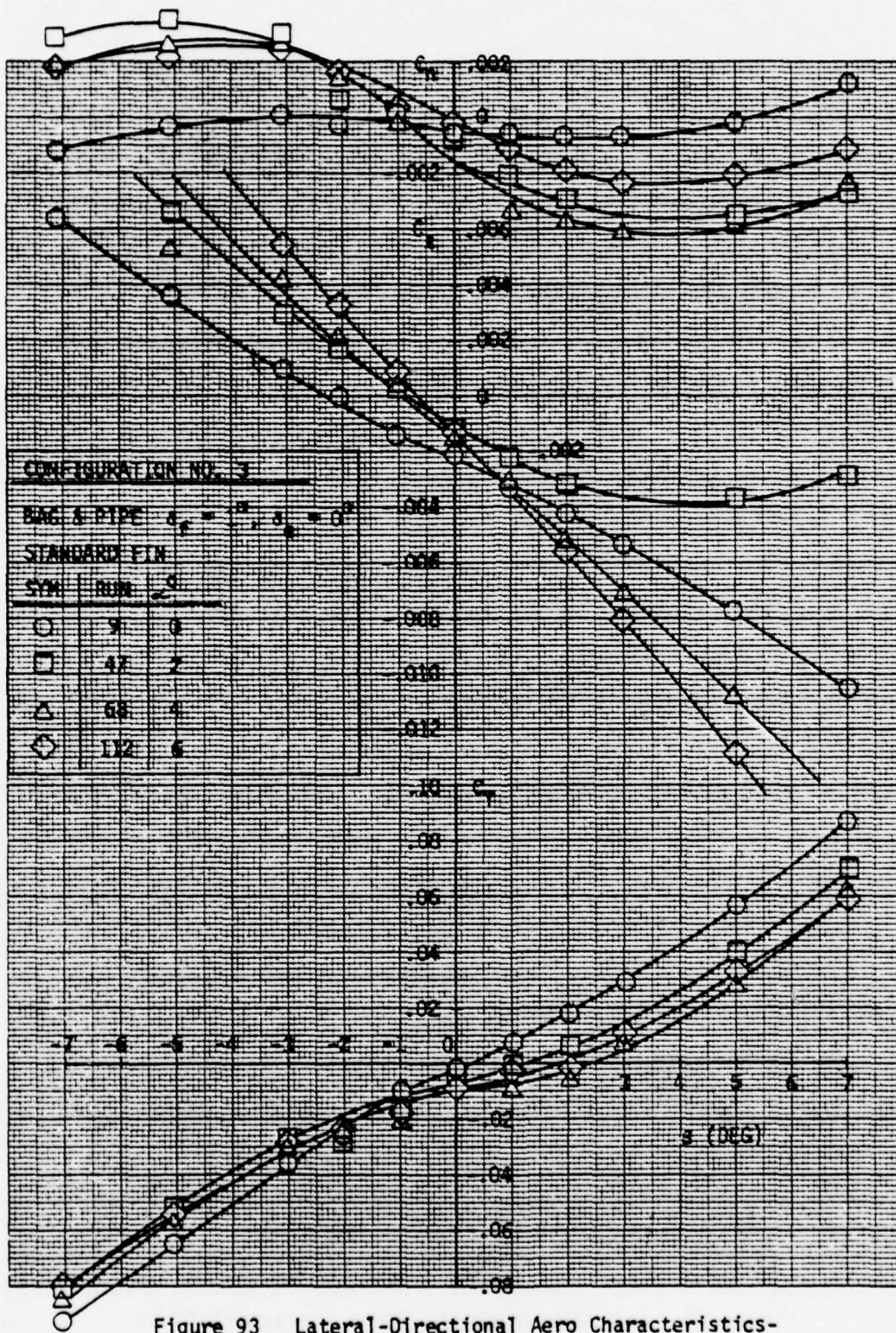
Figure 93   Lateral-Directional Aero Characteristics-
Configuration No. 3, $\delta_f = 1^o$

135
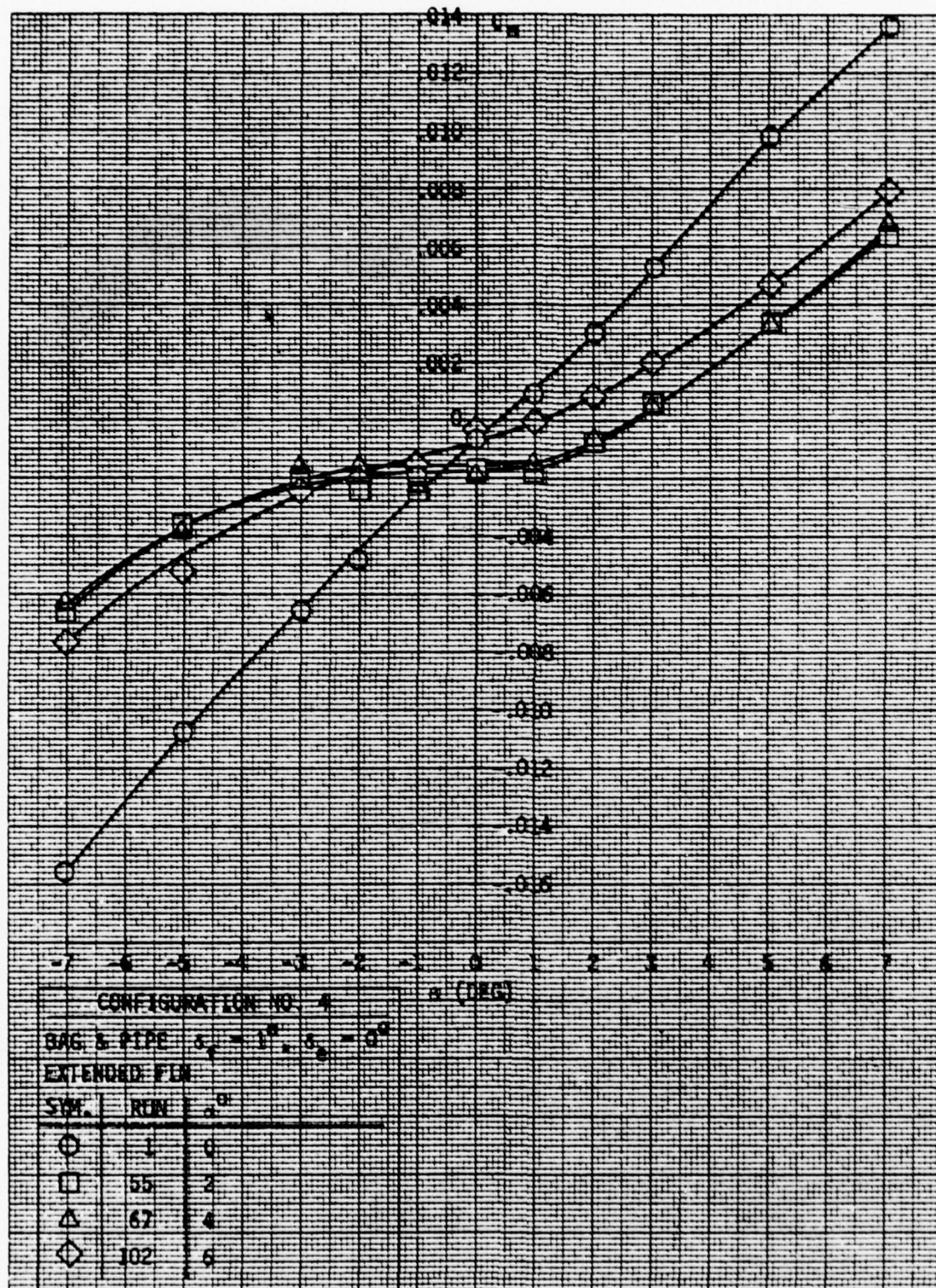
Figure 94   Lateral-Directional Aero Characteristics-
Configuration No. 4, $\delta_f = 1^o$

136
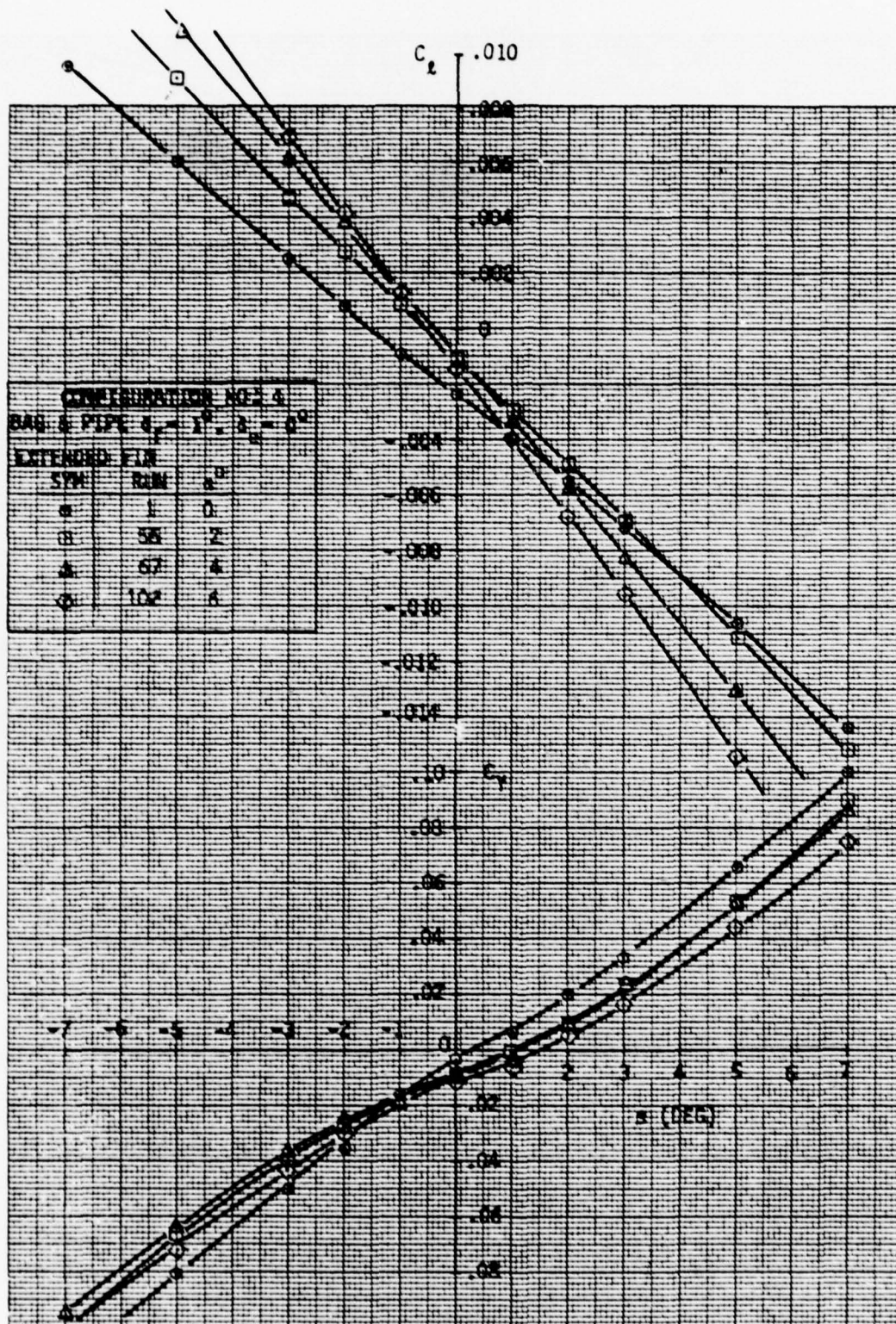
Figure 95   Lateral-Directional Aero Characteristics -
Configuration No. 4, $\delta_f = 1^0$

137
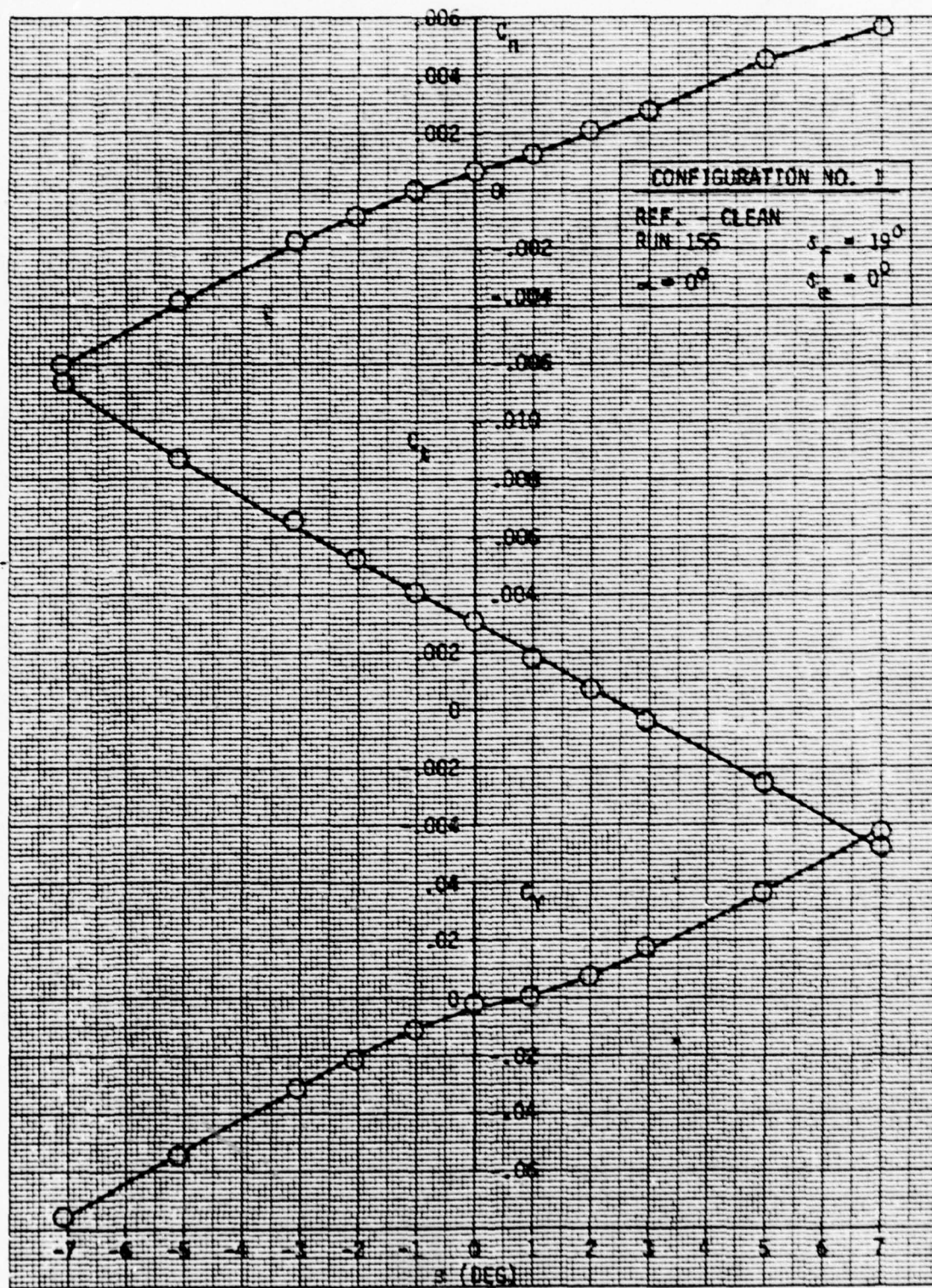
Figure 96   Lateral-Directional Aero Characteristics-Configuration No. 1, $\delta_f = 19^o$

138
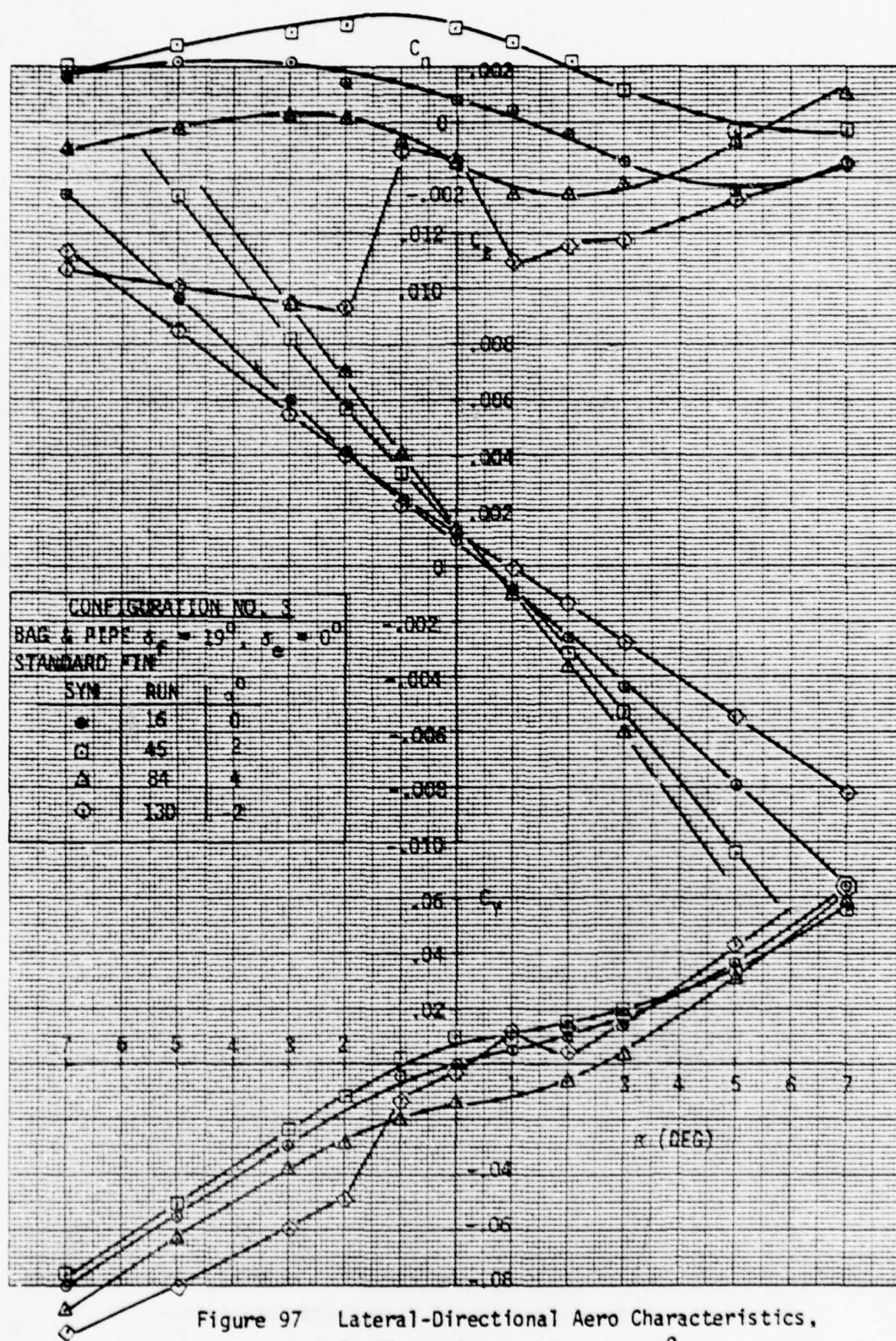
Figure 97   Lateral-Directional Aero Characteristics,
Configuration No. 3, δ_f = 19°

139
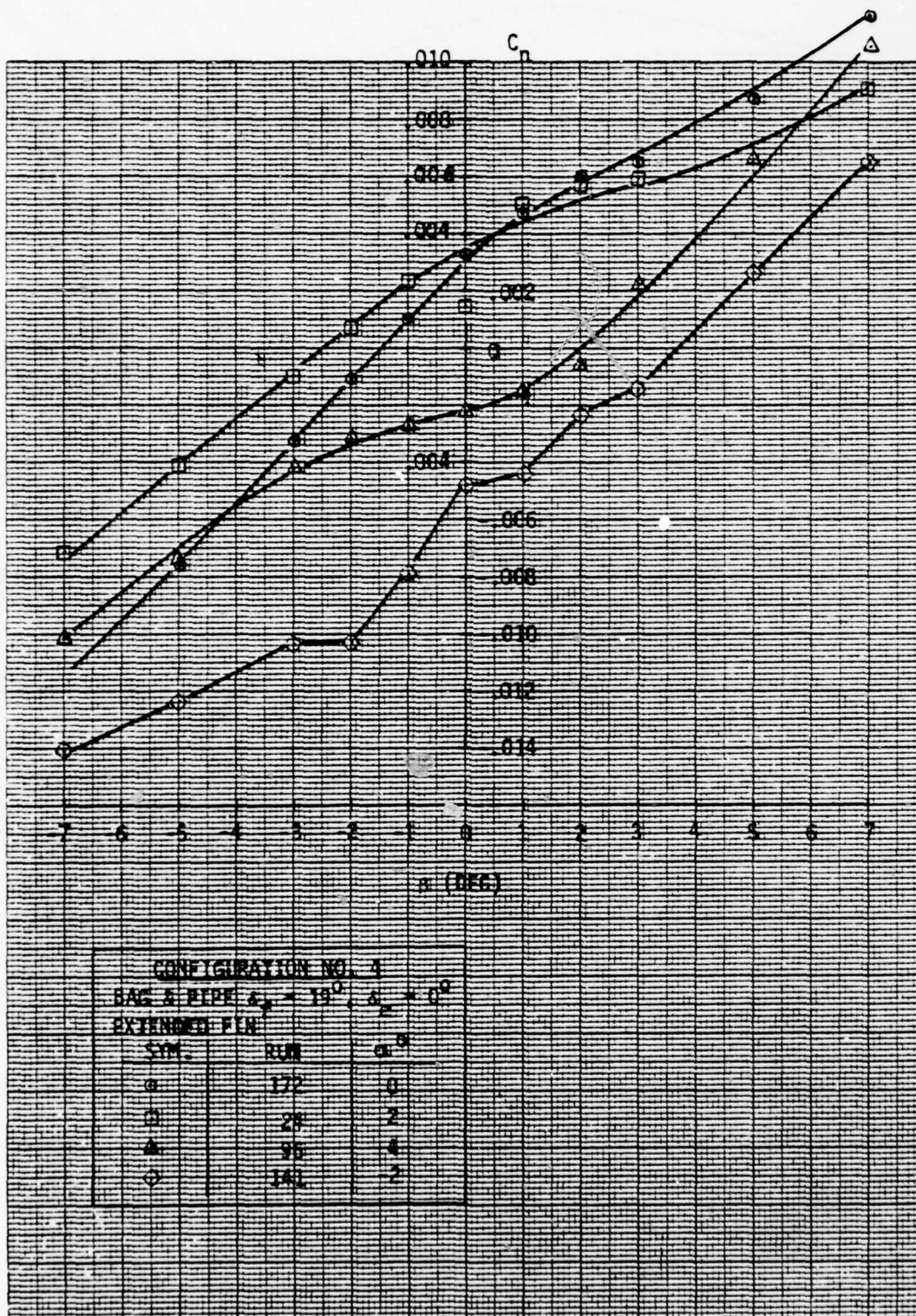
Figure 98   Lateral-Directional Aero Characteristics -

Configuration No. 4, $\delta_f = 19^o$

140
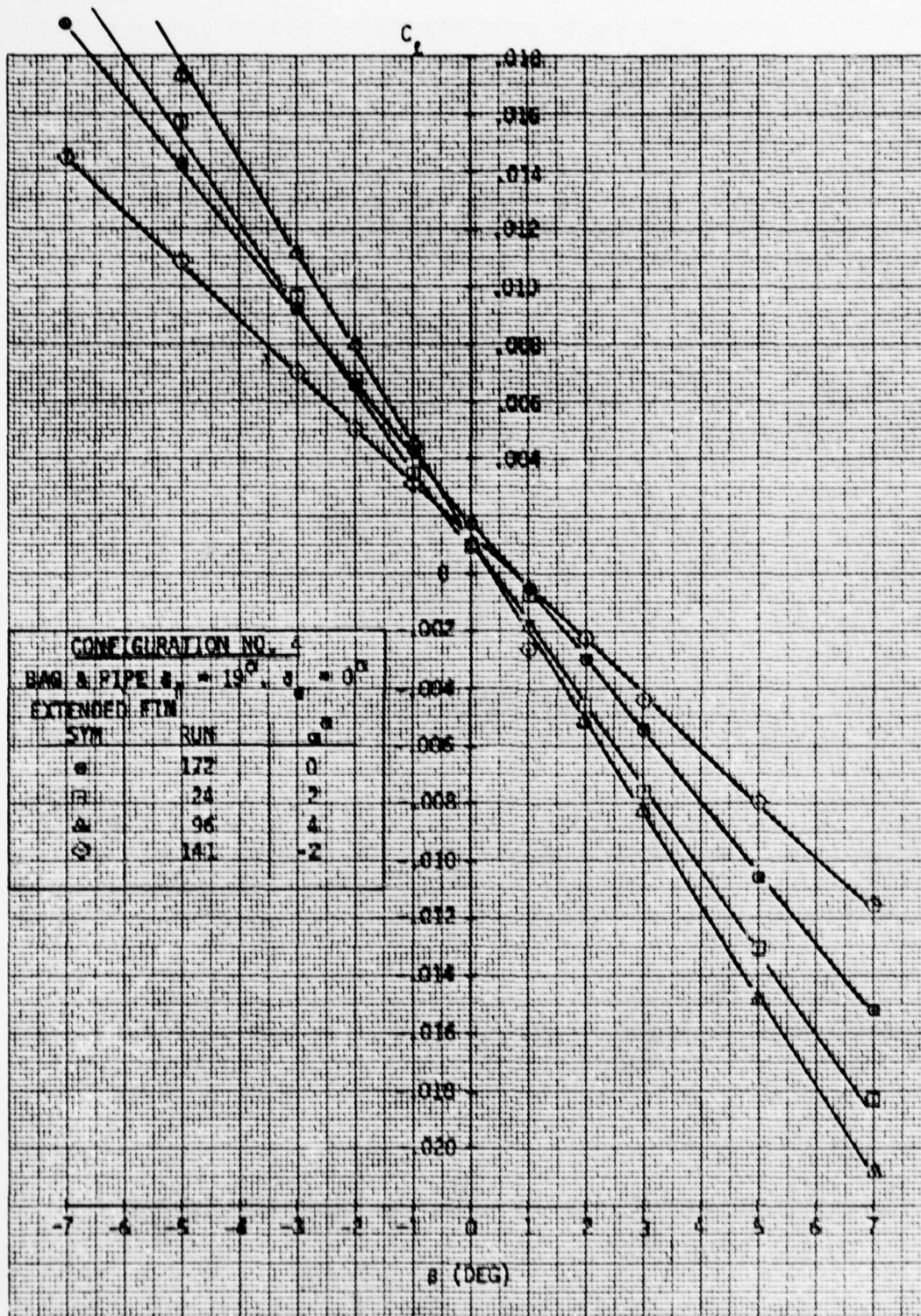
Figure 99 Lateral-Directional Aero Characteristics -

Configuration No. 4, $\delta_f = 19°$

141
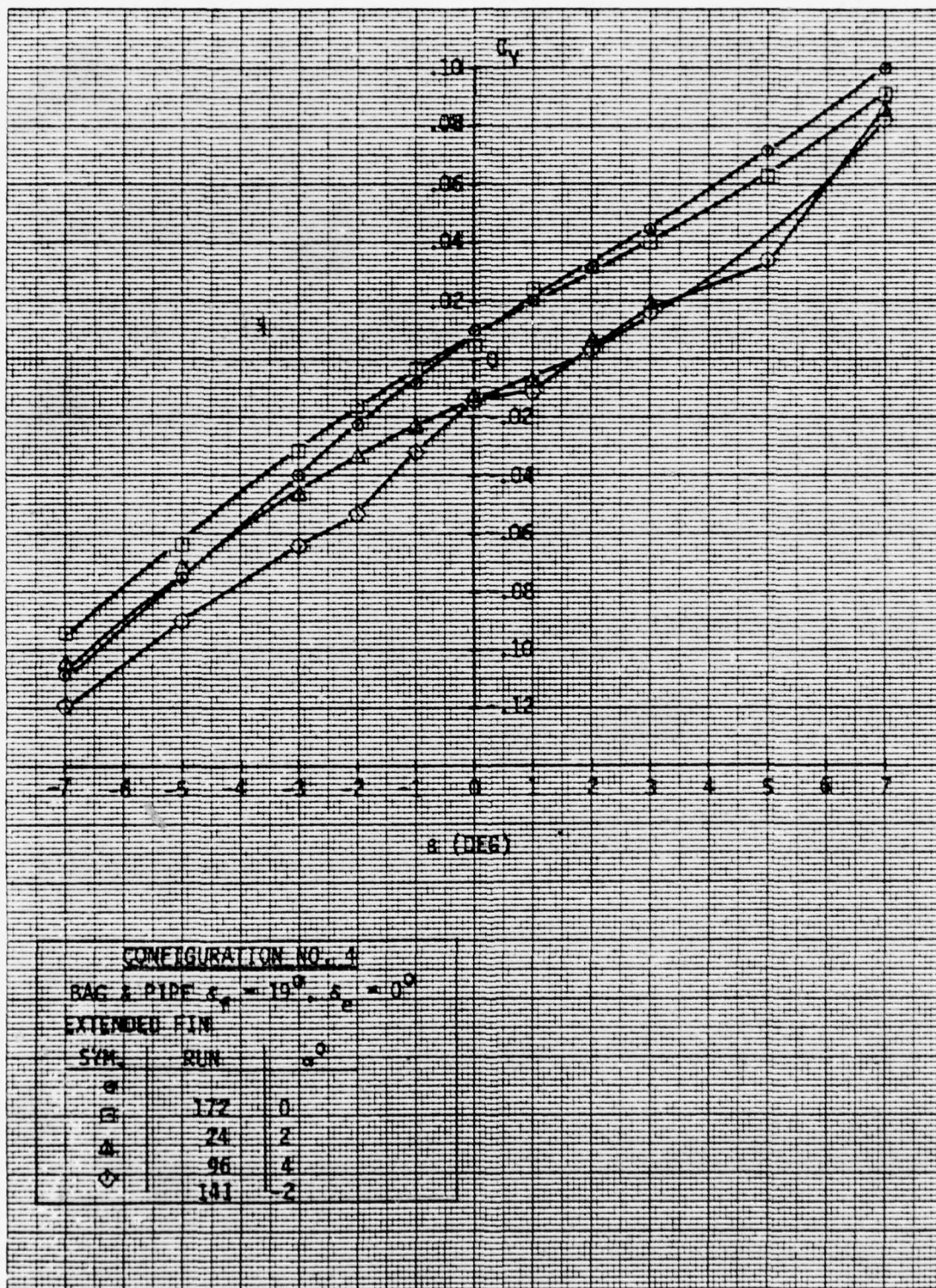
Figure 100   Lateral-Directional Aero Characteristics -
Configuration No. 4, $\delta_f = 19^o$

142
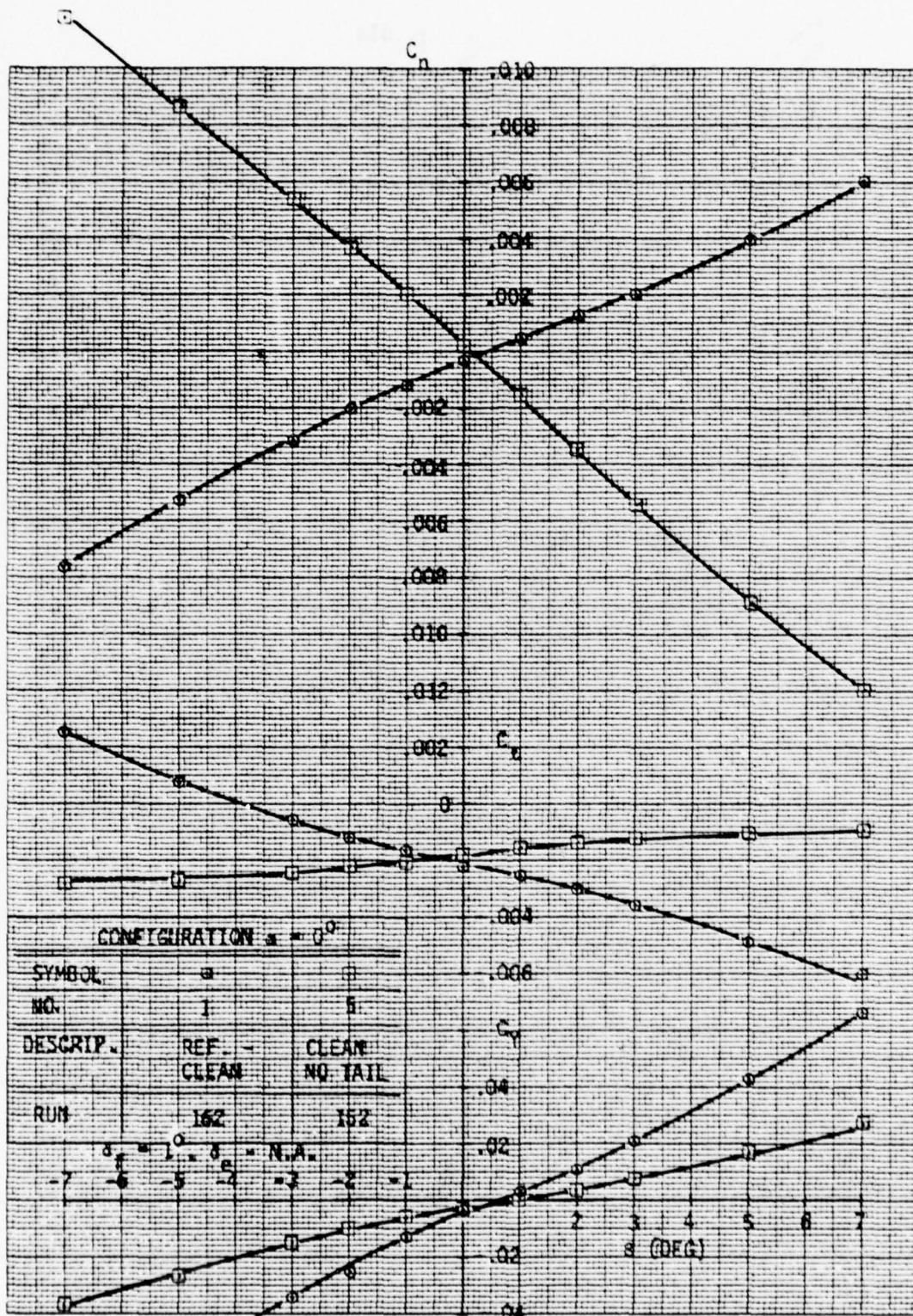
Figure 101   Lateral-Directional Comparison -
Configurations No. 1 and 5, $\delta_f = 1^O$

143

C_n

.018
.016
.014
.012
.010
.008
.006
.004
.002
-.002
-.004
-.006
-.008
-.010
-.012
-.014
-.016
-.018

-7 -6 -5 -4 -3 -2 -1 0 1 2 3 4 5 6 7

β (DEG)

CONFIGURATION $\delta_r = 1°$, $\delta_e = *$

SYMBOL	⊙	⊘	⊙	⊡	△	△
α	0	4	0	4	0	4
RUN NO.	150	128	9	68	1	67
NO.	2		3		4	
DESCRIP.	BAG & PIPE NO TAIL		BAG & PIPE STD FIN		BAG & PIPE EXTD. FIN	
* δ_a	N.A.		0		0	
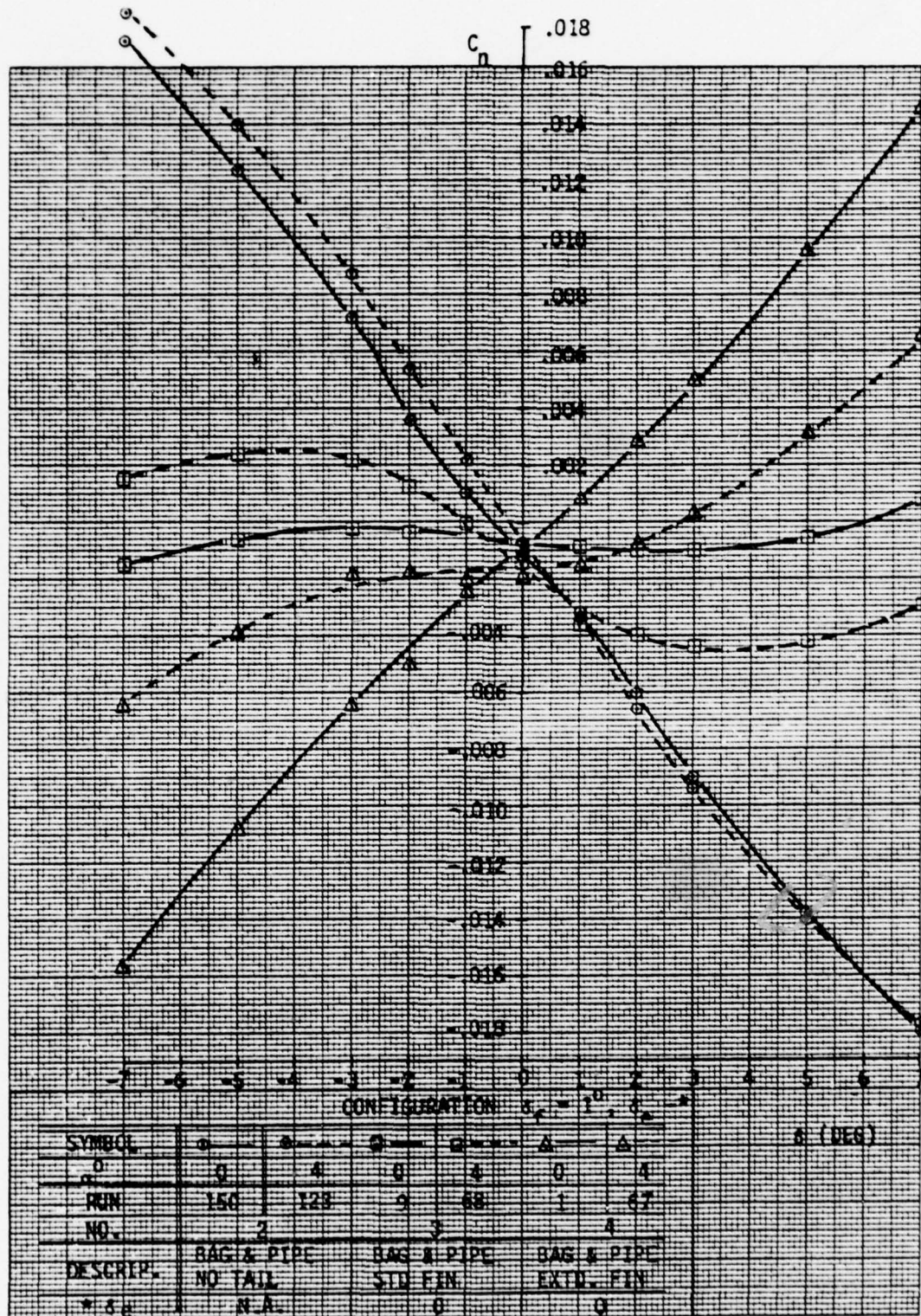
Figure 102   Lateral-Directional Comparison -
Configurations No. 2, 3 and 4, $\delta_f = 1°$

144
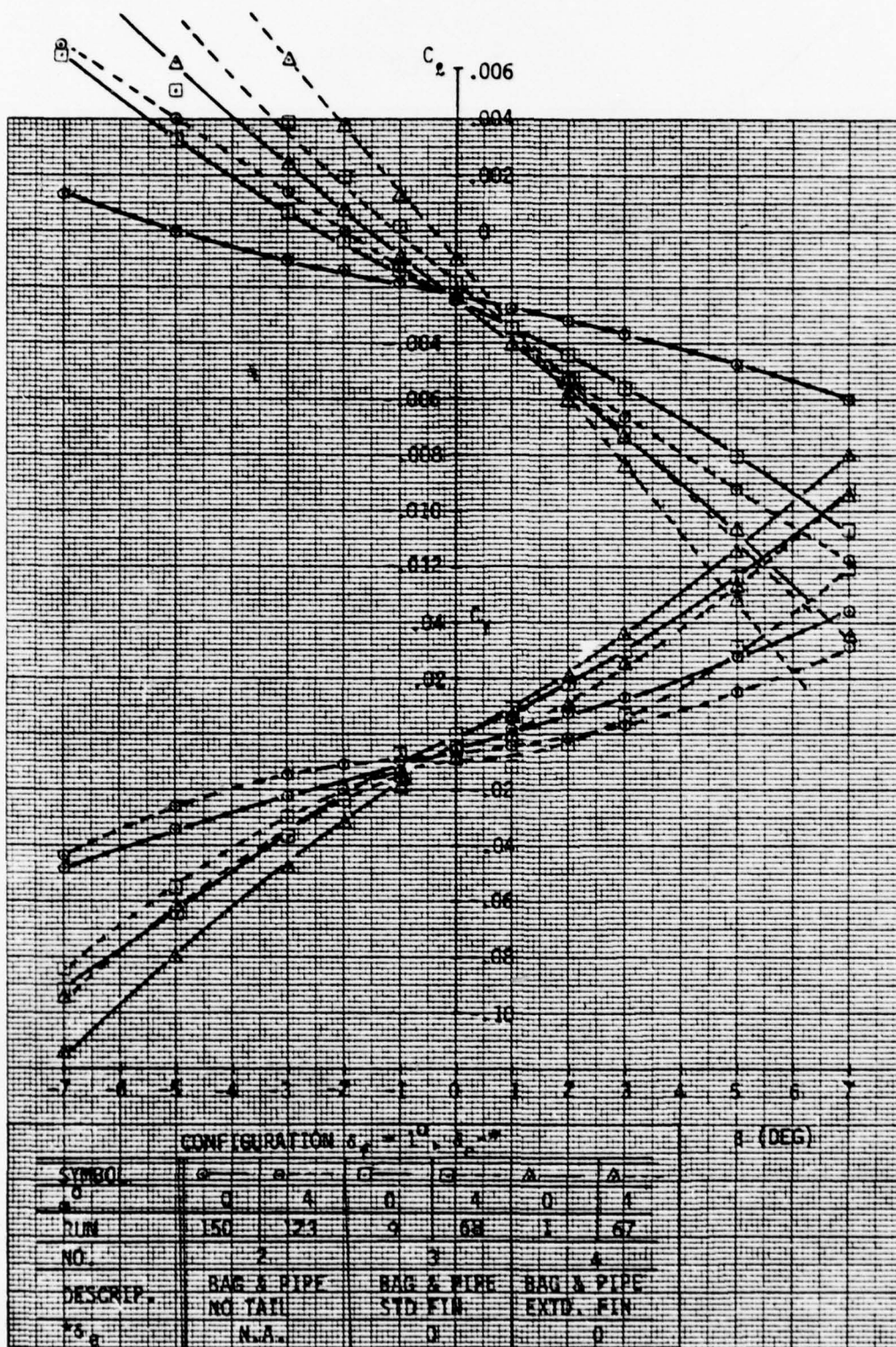
Figure 103   Lateral-Directional Comparison -
Configurations no. 2, 3 and 4, $\delta_f = 1°$

145
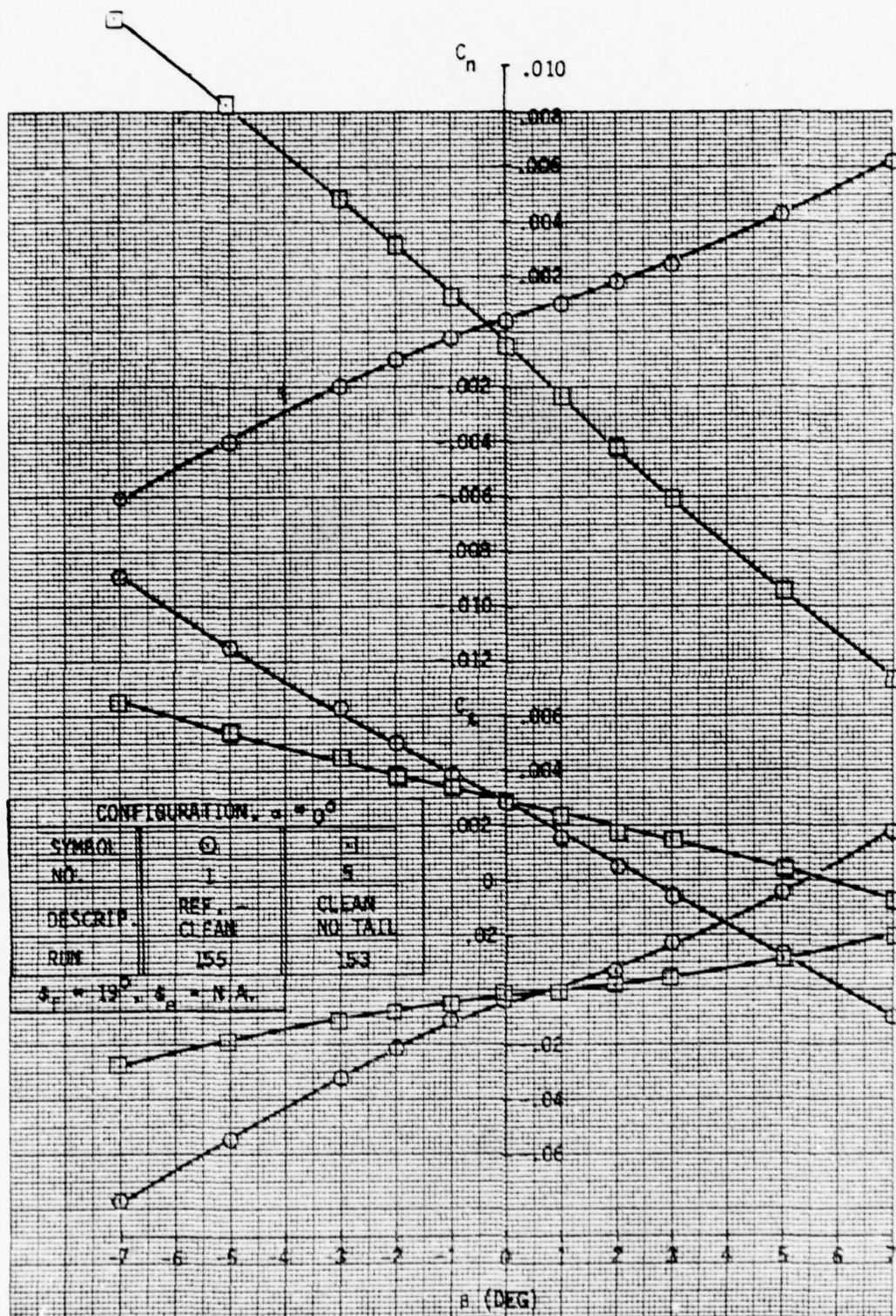
Figure 104   Lateral-Directional Comparison -
Configuration No. 1 and 5, δ_f = 19°

146
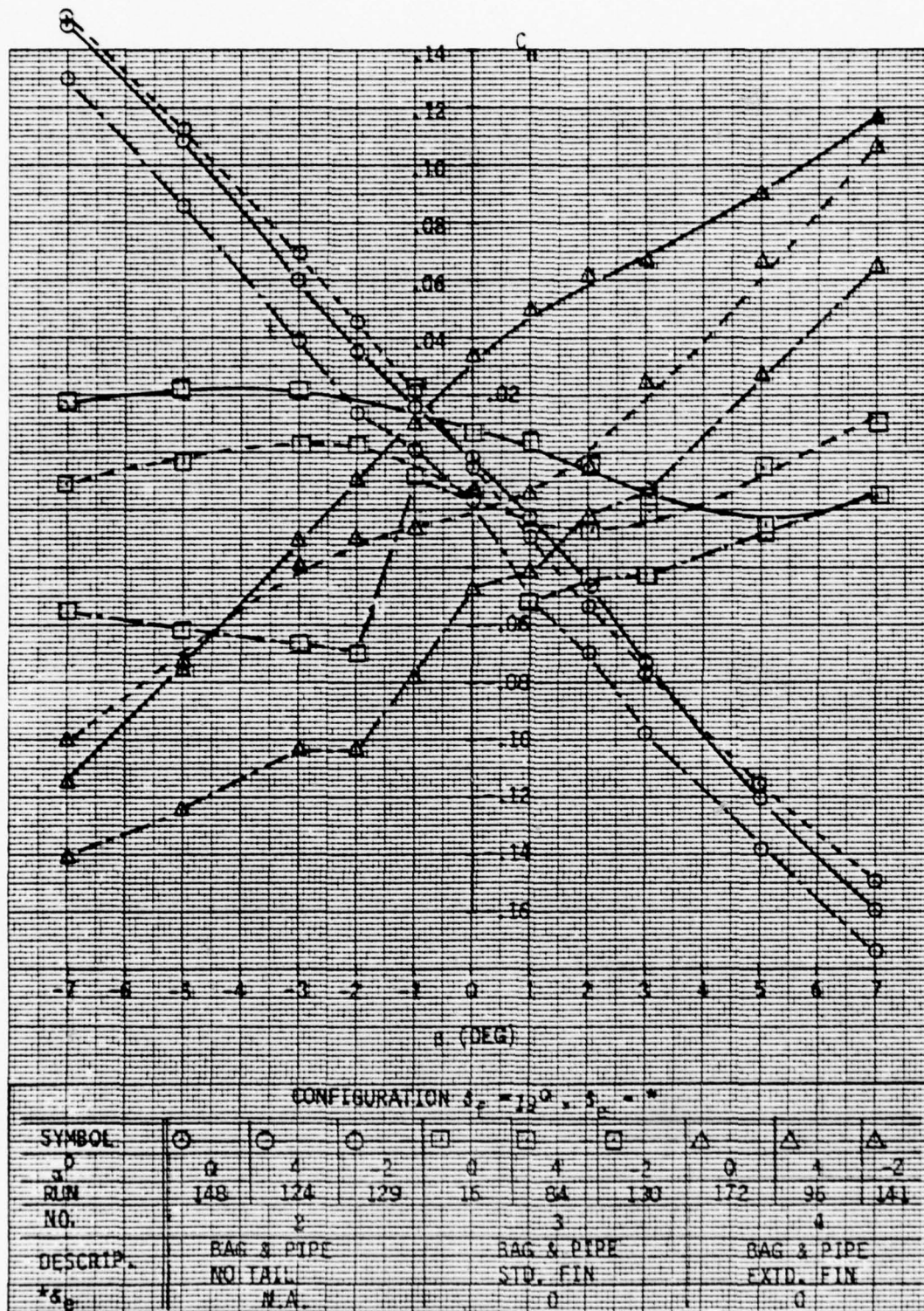
Figure 105   Lateral-Directional Comparison-
Configurations No. 2, 3 and 4, $\delta_f = 19°$

147
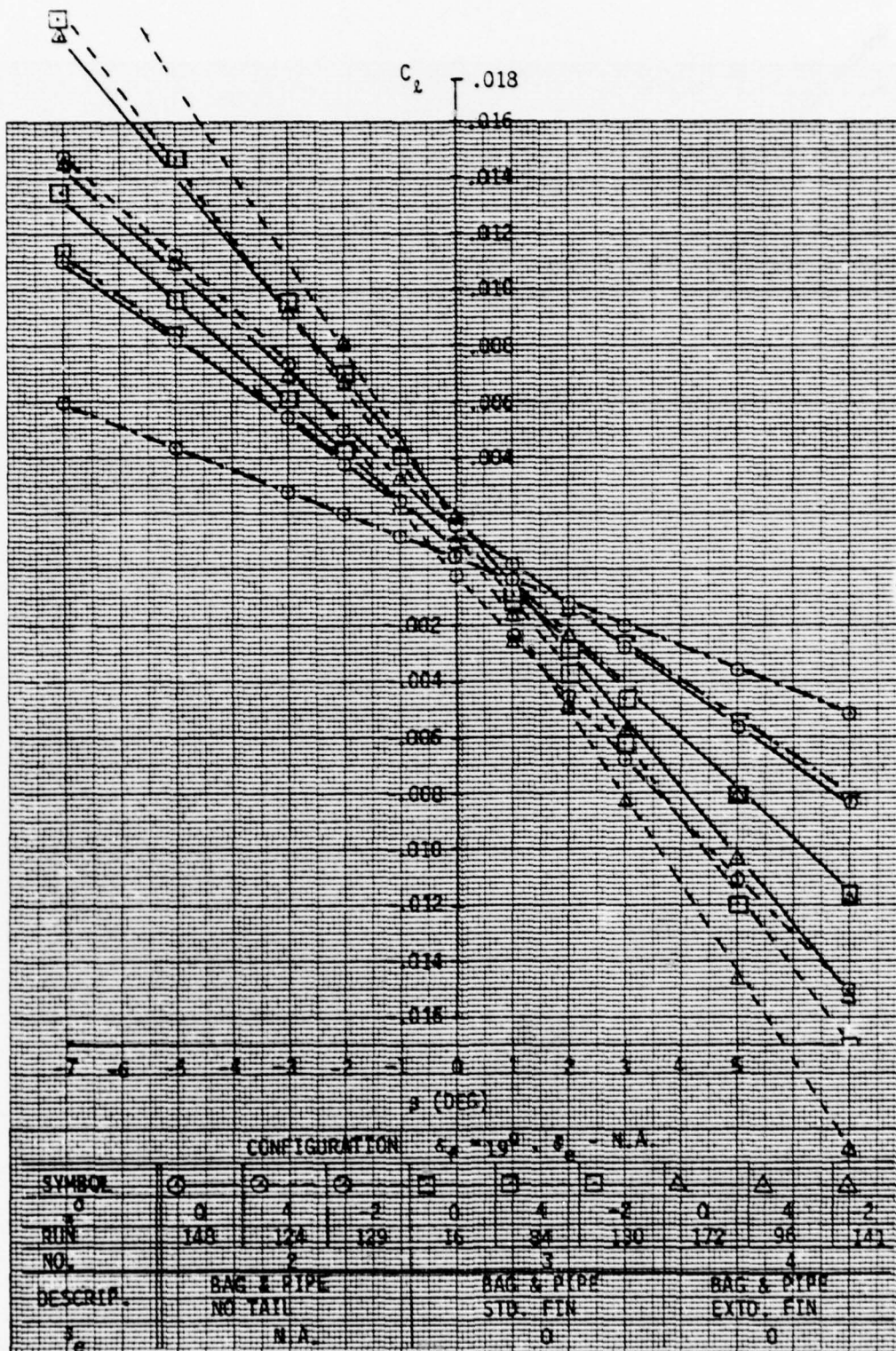
Figure 106   Lateral-Directional Comparison-
Configuration No. 2, 3, and 4, $\delta_f = 19^o$

148
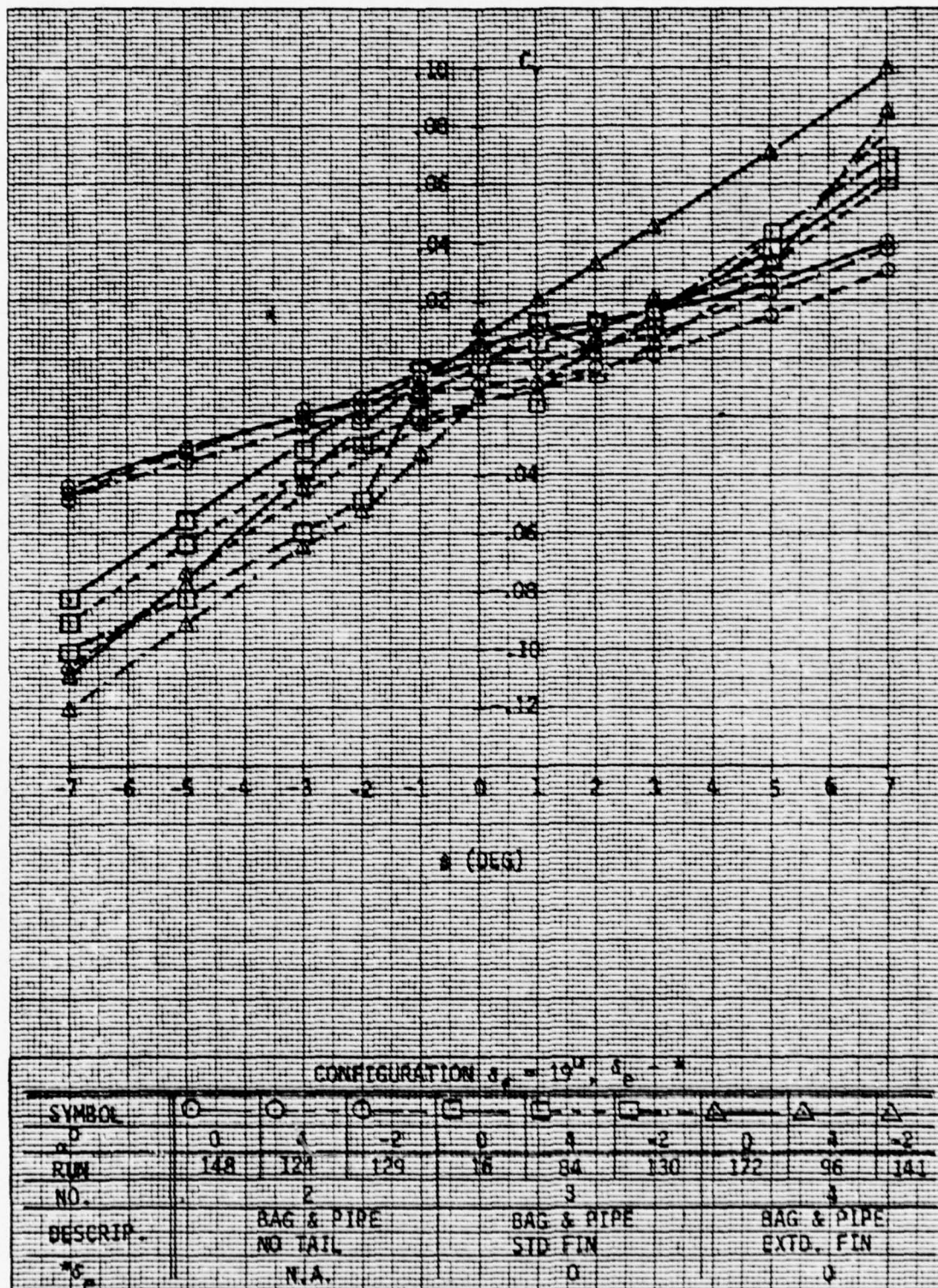
Figure 107   Lateral-Directional Comparison -
Configuration No. 2, 3 and 4, $\delta_f = 19°$

149
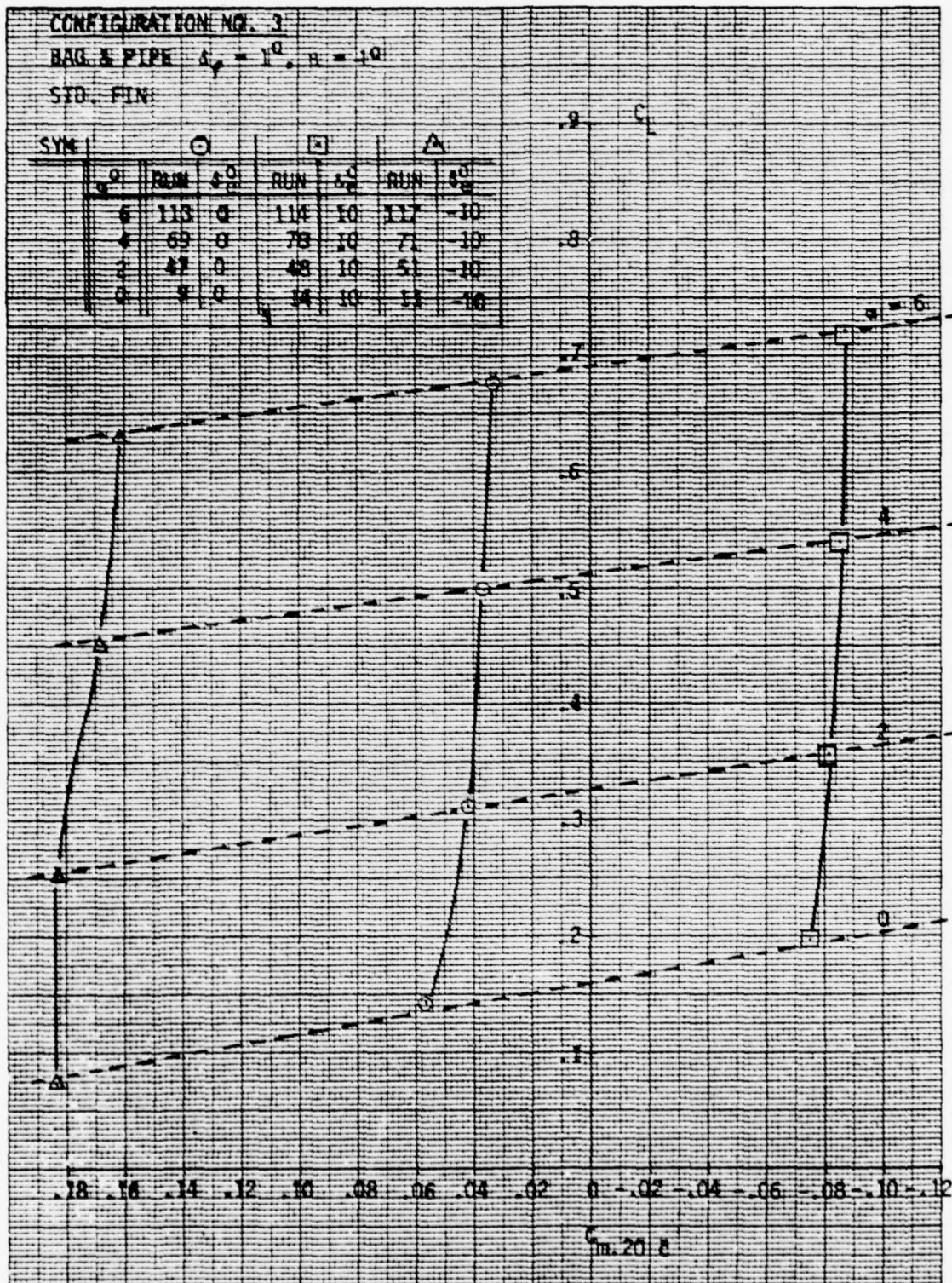
Figure 108 Longitudinal Aero Characteristics -
Configuration No. 3, $\delta_f = 1^o$
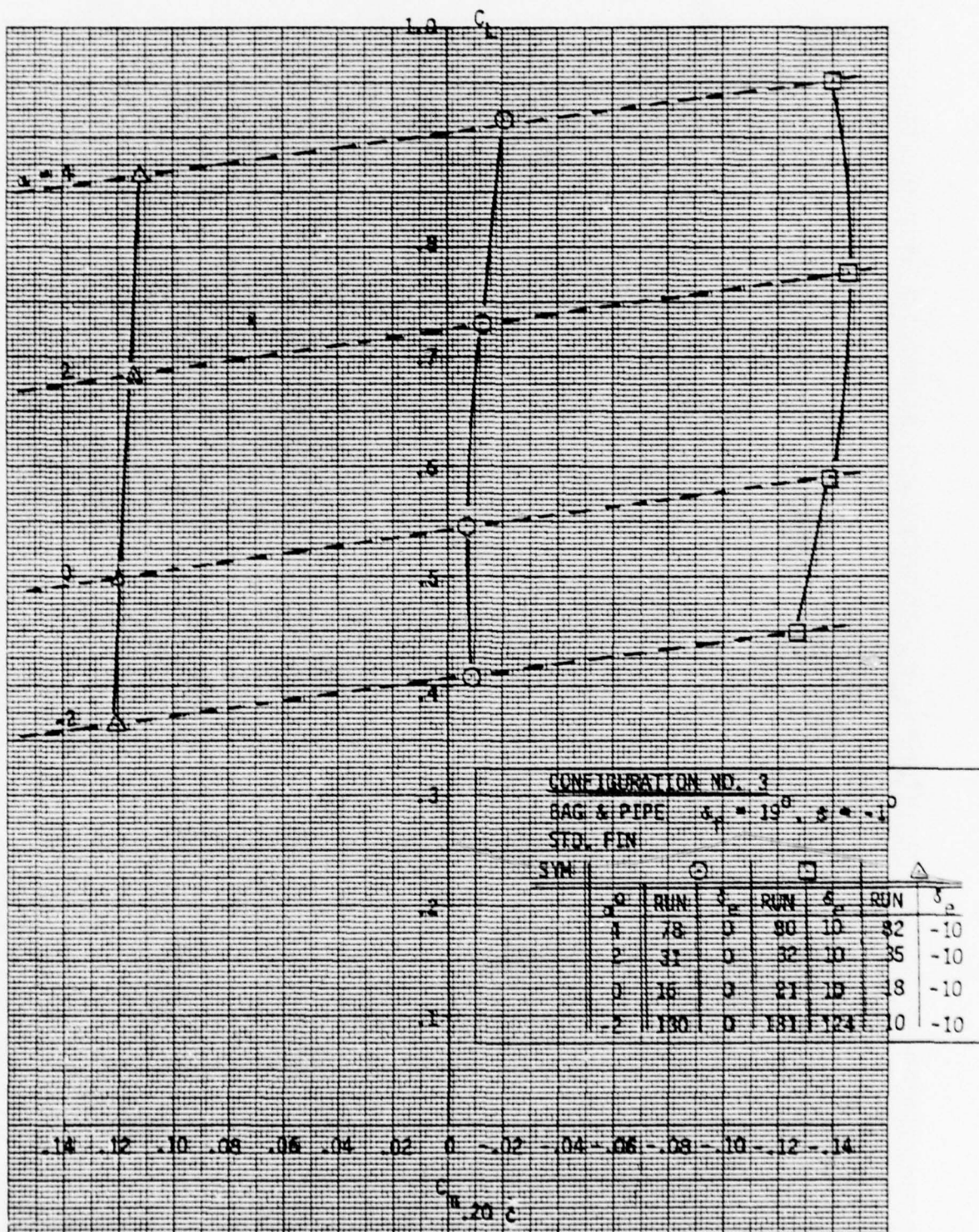
Figure 109 Longitudinal Aero Characteristics -
Configuration No. 3, $\delta_f = 19^o$

151
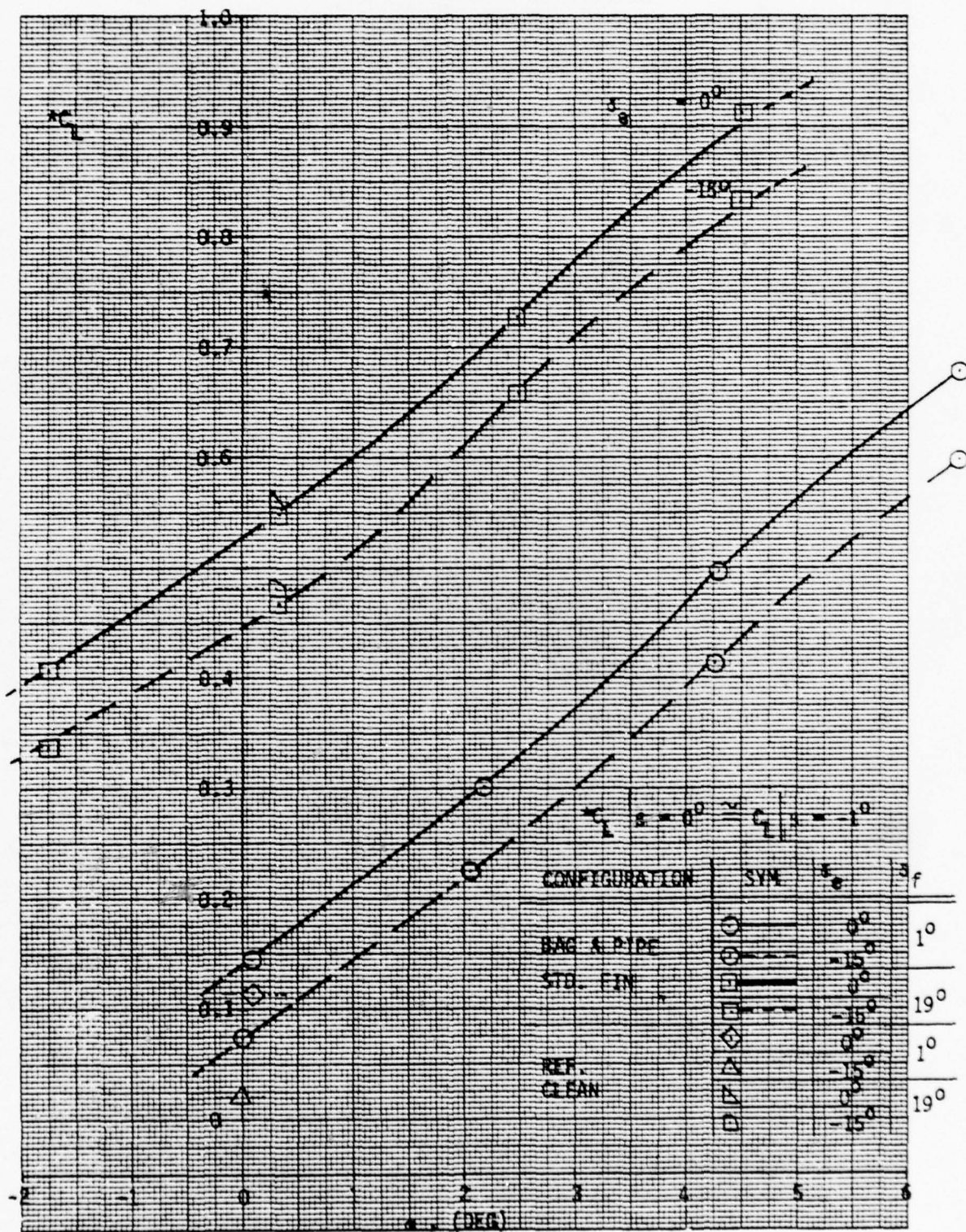
Figure 110   Effect of ACRS, δ_e and δ_f on Coefficient of Lift
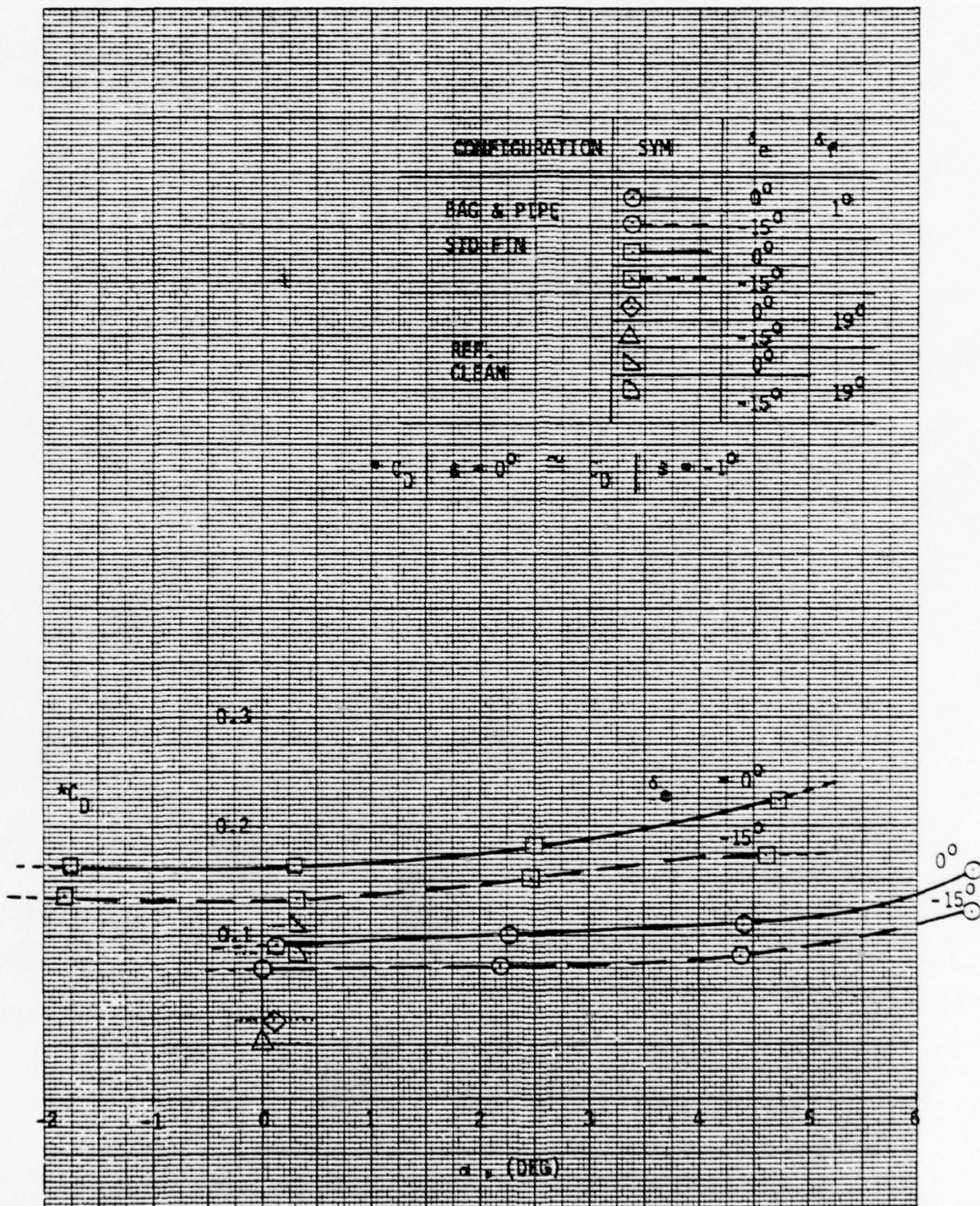
Figure 111   Effect of ACRS, δ_e and δ_f on Coefficient of Drag

This is probably due to a model or tunnel asymmetry, and most likely does not appear in the full scale vehicle. Figure 92 is an important plot, since it serves as the baseline against which modifications to the Jindivik must be judged.

Figure 93 displays the effect of adding the ACRS trunk. Several things should be noted. First, directional stability has been destroyed completely. The vehicle is neutrally stable at $\alpha = 0^\circ$ and is unstable at all higher alphas. This is clearly an unsatisfactory situation. Second, an anomaly occurs in the rolling moment data for $\alpha = 2^\circ$. At large positive sideslip angles, the slope C_{l_β} becomes positive, or unstable. This idiosyncrasy appears nowhere else in the Jindivik data supplied. Consequently, it is assumed that the data points at $\beta = +5^\circ$ and $+7^\circ$ are in error. If the model is ever retested, this $\alpha-\beta$ combination should be checked for repeatability. Third, the side force data for alphas other than zero shows an offset toward negative side force. This might be due to the bleed air duct causing a wake which reduces fin effectiveness, or it may simply be due to tolerance buildup in the test apparatus. The specific test runs involved (9, 47, 68 and 113) were widely separated in time, so the discrepancy may be due only to data scatter.

Figure 94 presents directional stability data for the Jindivik plus ACRS trunk plus the extended-span-fin. There is a large improvement in directional stability, at all α's, when compared to Figure 92. However, there is a possible problem. For angles of attack of 2° and 4°, there is a "flat spot" in the curves between sideslip angles of -3° through $+1^\circ$. This region of essentially neutral stability could cause dynamic stability problems in a full scale vehicle. In particular, a Dutch roll limit cycle could occur. A dynamic stability analysis is required to evaluate whether there is a potential limit cycle and, if so, whether the oscillations would be large enough or severe enough to jeopardize the flight test program.

154

Figure 95 displays the rolling moment and side force data for the Jindivik-plus-trunk-plus-fin-extension configuration. These data are ideal - linear, stable, very little variation with angle of attack.

Figures 96 through 100 show lateral directional data for flaps 19°. Figure 96 shows data for the standard Jindivik. These data are similar to those of Figure 92 in most respects. There are two minor differences, however. The rolling moment data shows no non-linearity through zero sideslip, a small but favorable change. Also, the rolling moment has a large positive offset at zero sideslip, whereas the offset was negative for flaps 1^O. This effect is almost certainly due to a small asymmetry in flap deflection. The left flap is probably deflected slightly more than the right flap, producing a right-wing-down rolling moment.

Figure 97 shows the data for the standard Jindivik plus ACRS trunk. The yawing moment data are very poor. Not only is the vehicle unstable, but there is a wide variation in the yawing moment at zero sideslip as alpha is varied. Also, the curve for $\alpha = -2^O$ is hard to describe. Apparently, there is a severe airflow separation somewhere on the vehicle at $\alpha = -2^O$, which gives rise to the strange behavior of yawing moment. In contrast, the rolling moment and side force data are well-behaved. The $\alpha = -2^O$ side force data does display some peculiar variations, but the general trend is reasonable. The variations occurring in the side force and yawing moment data, when taken together, tend to indicate a separated flow impinging upon the vertical tail. In any event, the flaps 19° characteristics are unacceptable.

Figure 98 displays yawing moment data for Jindivik-plus-trunk-plus-extended-fin. The slopes of the curves indicate satisfactory levels of directional stability, however, the

zero-sideslip intercepts of the curves show the same "wandering" tendency as the vehicle with the standard fin. The tail-off data for this configuration (wing-body-trunk) are shown as the circle symbols on Figure 105. Although there is a small variation with alpha, the yawing moment differences at zero sideslip are considerably smaller than with tail on. The inference is that the fin contribution to yawing moment is strongly dependent upon angle of attack. Since the Jindivik without trunk was tested only at zero alpha, there is no evidence from the test that the configuration with trunk is any different than the basic vehicle. However it is reasonable to assume that the combination of trunk plus 19° flap produces some disturbance to the flow over the fin. In addition to the poor stability, the flow disturbance may produce fin buffet, which might lead to fatigue problems. All in all, the trunk plus 19° flap is an unacceptable configuration, and further configuration development is mandatory.

Figures 99 and 100 show rolling moment and side force versus sideslip. There is some variation in the side force intercept at zero β, tending to confirm the erratic yawing moment behavior. The rolling moment and side force characteristics are probably acceptable, but the yawing moment qualities render the configuration unsatisfactory.

Figure 101 shows the tail-off/tail-on comparisons for the basic Jindivik with flaps 1°. Conclusions to be drawn are that the data are essentially linear and symmetrical, and the vehicle is quite well-behaved.

Figures 102 and 103 show tail-off/tail-on comparisons of the Jindivik-plus-trunk, and both standard and extended fins, with flaps 1°. Angles of attack of 0° and 4° are shown. On Figure 102, note that for tail-off (circles) there is essentially no effect of angle of attack on yawing moment, whereas for tail-on (squares and triangles) there is a reduction in stability as

156

alpha increases. This plot indicates the vertical tail
effectiveness is reduced as alpha increases, probably due to a
flow separation from the trunk (see also Figure 84). Note that
the slope C_{n_β} varies quite drastically as β is increased beyond
$\pm 2^\circ$, which is the limit of applicability of Figure 84. On
Figure 103, all configurations show a relatively constant
increase in C_{ℓ_β} and a decrease in C_{Y_β} with increasing alpha.
This trend has already been depicted on Figures 85 and 86.
Figure 103 is shown to demonstrate the linearity of the results
at sideslip angles beyond $\pm 2^\circ$.

Figure 104 shows the data similar to Figure 101, except that
wing flaps are deflected 19°. Trends indicated on Figure 104
are the same as for flaps 1°, i.e. the characteristics are
linear and symmetrical, and the vehicle is statically stable.

Figures 105, 106 and 107 show tail-off/tail-on comparisons at
flaps 19° of the Jindivik-plus-trunk and standard and extended
fin. The main purpose of these three plots was to compare the
tail-off and tail-on data. A discussion of the yawing moment
tendencies (Figure 105) was given several paragraphs above. To
repeat briefly, the tail-off data are linear and show little
angle of attack effects. The tail-on data are non-linear and
show wide variations in the zero-beta intercept as alpha varies.
Figure 106 shows lateral stability to be well-behaved, both
tail-off and -on. The side force data, Figure 107, show trends
similar to the yawing moment data from Figure 105. That is, the
tail-off data show much less variation with angle of attack than
the tail-on results. It is noteworthy that the tail-on curves
for yawing moment and side force display many similar
non-linearities. For example, examine the configuration with
the standard fin at $\alpha = -2^\circ$. (Squares connected by dot-dash
lines). Both yawing moment and side force show sharp
discontinuities between $\beta = -2^\circ$ and -1°. This behavior tends to
confirm that the discontinuities are real, and not just scatter
in the data. On the whole, though, the side force data are

157

stable and relatively linear.

Figures 108 and 109 present longitudinal stability and control data for a c.g. location of 20% M.A.C. The configuration is standard, but with the ACRS trunk installed. Figure 108 shows flaps 1°, while Figure 109 shows flaps 19°. The data for both figures were measured at -1° sideslip. The stability and control characteristics are excellent. With the c.g. at 20% M.A.C., the aircraft is statically stable and the data are quite linear. Pitch control is also linear, as shown by the even spacing between curves for each elevator deflection. Unfortunately, no data were available for the Jindivik without the trunk. Hence, no evaluation is possible of the trunk's effect on longitudinal stability or control.

Figures 110 and 111 show lift and drag data, respectively, for the standard Jindivik plus the ACRS trunk. Flaps 1° and 19° data appear on each plot. The lift data are quite reasonable. There is a large increase in lift coefficient due to flap deflection and a small decrease due to airplane-nose-up elevator deflection. The drag data are less consistent, however. There is a large increase in drag due to flap deflection, which is normal. The inconsistency occurs when elevators are deflected -15°. There is, at both flap deflections, and for all alphas tested, a substantial drag reduction. Note that this same phenomenon occurs at zero alpha for the basic Jindivik, trunk off. The suspicion arises that there is an error in the drag data at -15° elevator deflection. Note also that Figure 111 shows that the basic Jindivik, at flaps 1°, and elevator -15°, (triangle symbol) has no drag. This point is obviously in error, and together with the inconsistency in drag due to elevator deflection, suggests that the drag data be used with caution.

Figure 112 shows a comparison of yawing moment and rolling data from the latest test with data from an earlier test. The later

NO POD FINS

POD FINS -8°
POD FINS -3°
POD FINS +2°

C_n } PREVIOUS YAWING MOMENT DATA

C_{n1} C_l

C_n NEW YAWING MOMENT DATA

CLEAN CONFIGURATION RUN 162 (1976) $\alpha = 0$

β

-4°   -2°   0   2°   4°

NEW ROLLING MOMENT DATA

0.006
0.004
0.002
0.002
0.004
0.006

C_l

C_1 } PREVIOUS ROLLING MOMENT DATA
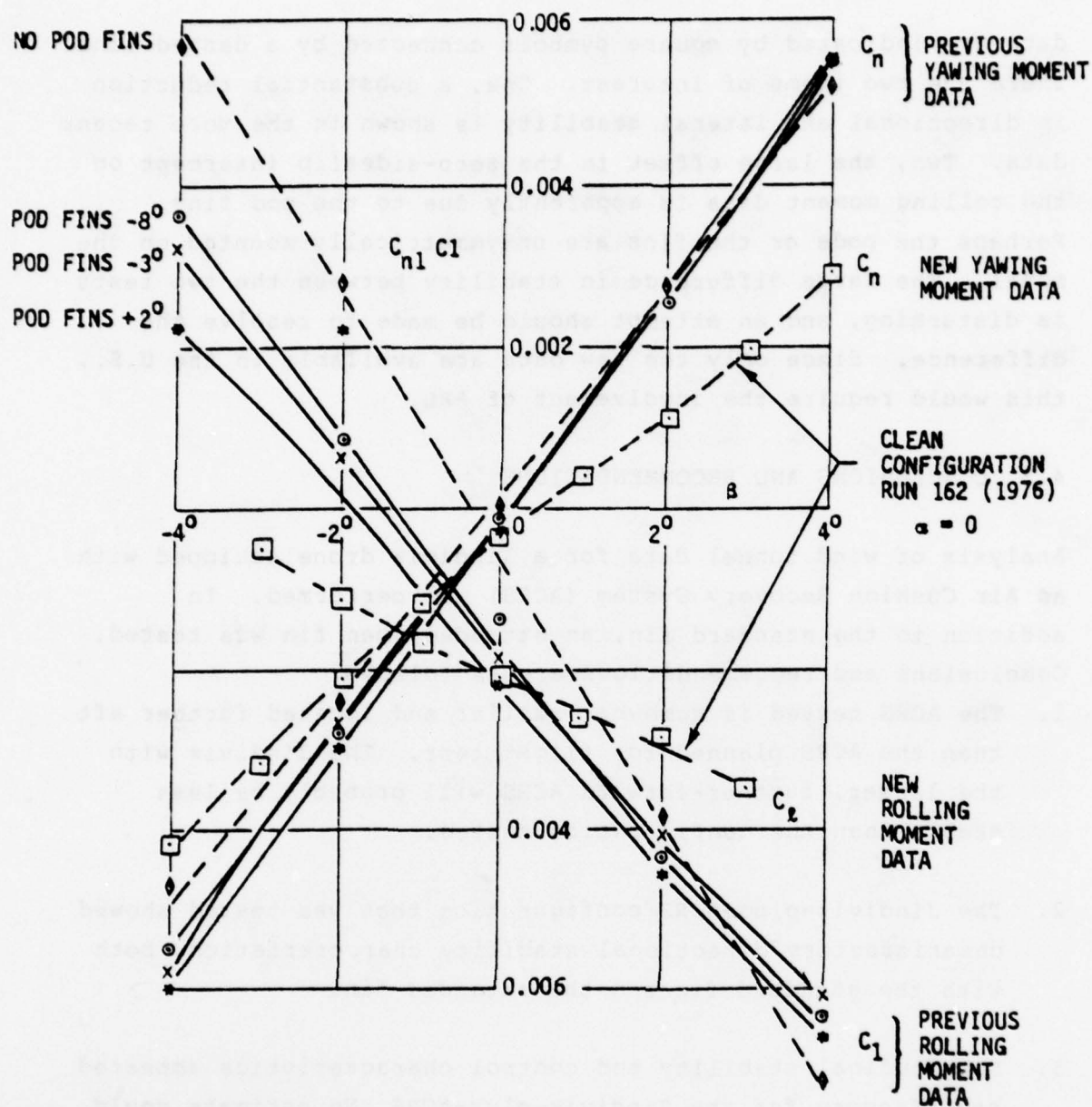
MK 7 PODS   V = 200 F.P.S.

ROLLING AND YAWING MOMENT COEFFICIENT VS ANGLE
OF SIDESLIP AT ANGLE OF ATTACK = 0°

Ref.   Aerodynamics Technical Memorandum 222, Test Data - Low
       Speed Wind Tunnel Tests of Jindivik Mk. 3A Carrying
       Mk. 7 PODS, T. H. TRIMBLE AND M. K. POLITZ, FIG. 20, no date

Figure 112   Comparison of 1976 C_n Data with Older Data

159

data are indicated by square symbols connected by a dashed line. There are two items of interest. One, a substantial reduction in directional and lateral stability is shown in the more recent data. Two, the large offset in the zero-sideslip intercept on the rolling moment data is apparently due to the pod fins. Perhaps the pods or the fins are unsymmetrically mounted on the model. The large difference in stability between the two tests is disturbing, and an attempt should be made to resolve the difference. Since only the new data are available in the U.S., this would require the involvement of ARL.

4.3 CONCLUSIONS AND RECOMMENDATIONS

Analysis of wind tunnel data for a Jindivik drone equipped with an Air Cushion Recovery System (ACRS) was performed. In addition to the standard fin, an extended-span fin was tested. Conclusions and recommendations are as follows:

1. The ACRS tested is somewhat smaller and located further aft than the ACRS planned for flight test. The Jindivik with the larger, further-forward ACRS will probably be less stable than the configuration tested.

2. The Jindivik-plus-ACRS configuration that was tested showed unsatisfactory directional stability characteristics, both with the standard fin and the extended fin.

3. Longitudinal stability and control characteristics appeared satisfactory for the Jindivik-plus-ACRS. No estimate could be made of the ACRS effect upon longitudinal characteristics because the ACRS-off configuration was not tested in pitch.

4. Additional wind tunnel data should be acquired before flight testing of the Jindivik-plus-ACRS. An important point is to test the proper size ACRS trunk. Also, another, still-larger fin extension should be tested. The new fin should have a total area of 10.5 square feet. This fin

160

might be too large, but would provide sufficient difference from the extended fin already tested, so that a correctly-sized fin could be selected by interpolation. It would be prudent to prepare a set of fins to be fitted to the tips of the horizontal tail. These auxiliary fins could be more effective than a body-mounted fin extension because they will be located in an undisturbed airflow. A small amount of data should be obtained with the trunk on but the bleed air duct removed. Some of the existing data shows asymmetries between positive and negative sideslip that may be caused by flow separation from the duct.

5. The concept of using the yaw thruster to maintain directional stability was investigated (see Appendix D) but was found to be unsatisfactory.

LANDING AND SLIDEOUT ANALYSIS

Touchdown and slideout are expected to be the most critical
phases of the Jindivik ACLS flight test. It was originally
intended that a computer simulation of the landing would be made
following completion of ground tests, utilizing data obtained in
those tests. The ground test data, however, were not fully
available prior to completion of this contract.

A preliminary computer evaluation of the landing has been
conducted as described in this section. The analysis should be
updated as soon as ground test data, particularly trunk drag,
stiffness and damping characteristics, become available.

The simulation of the Jindivik recovery on the ACRS trunk
assumes the standard Jindivik procedure for final approach,
touchdown and slideout. In the actual recovery, as currently
envisaged, the ACRS trunk is deployed during the final approach
by inflation with direct engine bleed air. The final approach
speed is 130 knots. The angle of descent is -2.0 degrees, and
the pitch angle is 0.0 degrees. Thus, the angle of attack is
2.0 degrees. The descent rate is 7.67 feet per second. The
Jindivik will be equipped with a ground contact indicator
(sting) which will signal for rapid retraction of the flaps.
The simulation begins just before flap retraction, which occurs
in 0.3 seconds. During touchdown and slideout the engine bleed
air supply to the hub driven turbofan is shut off (Figure 1),
and thus bleed air flows solely to the ACRS trunk. The air
passes out of the trunk through 394 1/8 inch diameter holes at
the trunk-ground interface on the forward third of the trunk,
and also through a pressure relief valve. The peripheral holes
on the forward third of the ACRS trunk provide air lubrication

which reduces the local coefficient of friction, the purpose
being to place the center of frictional drag aft of the aircraft
center of gravity and thus provide directional stability during
slideout. The air flow also reduces the braking pitch moment at
high angles of forward pitch during touchdown and slideout.

Section 5.1 summarizes the method of analysis, and Section 5.2
shows the program verification which was accomplished by
comparing test and analysis for Jindivik drop tests. Section
5.3 presents the results of the simulation of taxi on the ACRS
and of touchdown and slideout. Section 5.4 evaluates the
results and discusses several approaches to improving landing
impact and slideout dynamics.

5.1 METHOD OF ANALYSIS

The evaluation of the dynamic performance of an ACLS system
requires the simulation of the overall aircraft, including
aerodynamic and engine induced forces and moments. The
simulation of the Jindivik ACLS has been conducted using the
Boeing ACLS 6 DOF Computer Program (Reference 14). The
simulations reported herein did not consider side wind or
crabbed landings, or any other effects that might have induced
yaw or roll. Thus effectively only four degrees of freedom were
active. Figure 113 shows the overall structure of this program.
It utilizes a generalized 6 DOF program (Reference 15), to which
are added the unique modules necessary for simulating the
components of the ACLS.

Full details of the program are given in Appendix B. A brief
description of the ACLS modules is given below.

ACLS Trunk Model - The trunk model was developed following
examination of movie films of Jindivik drop tests. The Digges
model (Reference 18), which calculates the shape of a two
dimensional loaded inelastic trunk, is used for the side

163
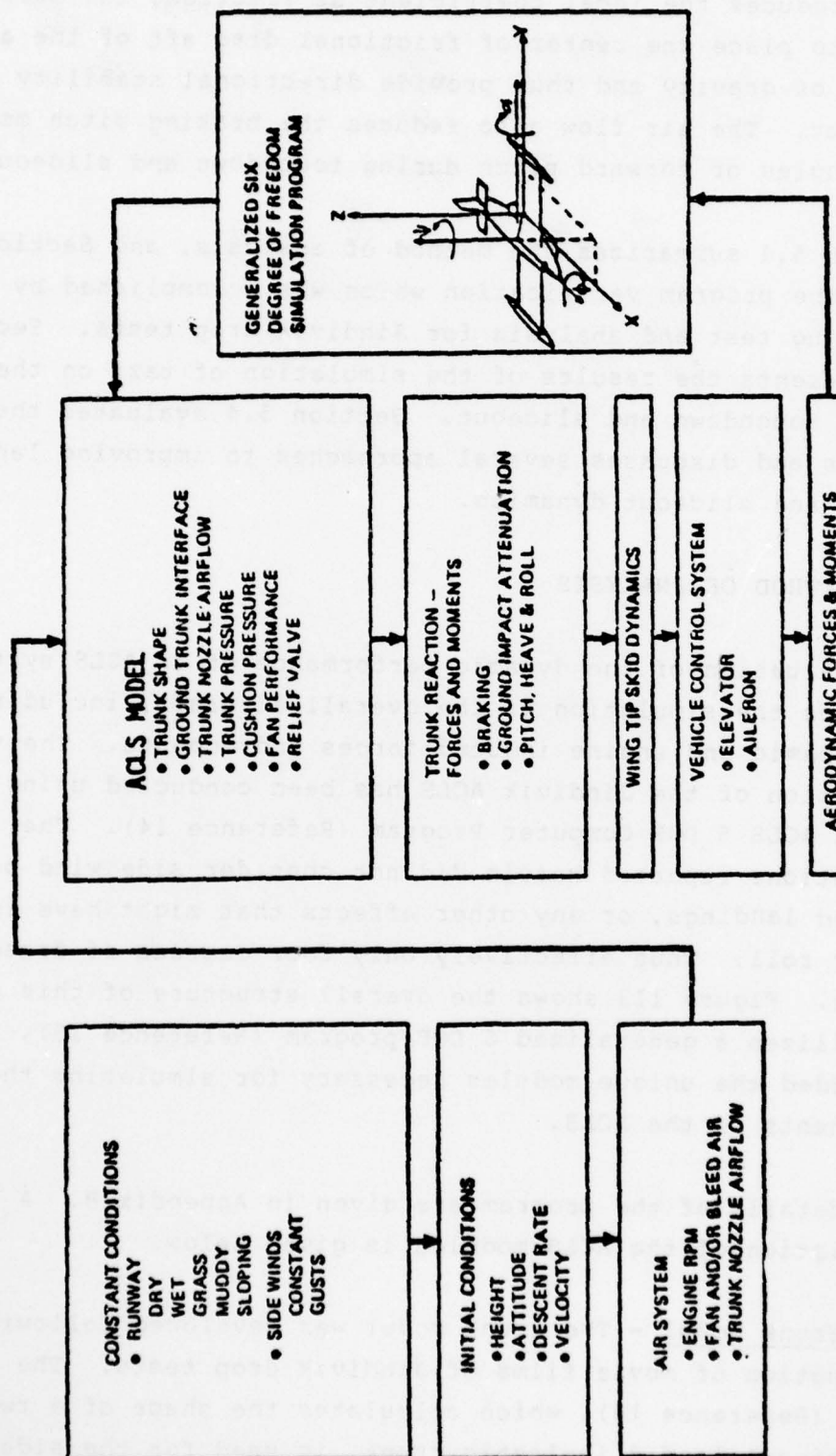
Figure 113 Computer Program Organization

164

elements. For the forward and aft elements, where hoop tension
exerts a significant restraining effect, the segments are
assumed to take the shape of flattened cylinders. Figure 114(a)
shows the subdivision of the trunk into elements, and Figure
114(b) the assumed forward and aft element shape. For the side
elements, the geometry of each element (Figure 114(c)) is
characterized by the cross-sectional area (CA_t), flattened width
(Y_f) and flattened area distance (Y_c), each of which are stored
in the program as functions of relative stroke (Z_o/Z_∞) and
pressure ratio (P_c/P_t).

Air Cushion Volume - Since it is assumed that lateral motion
takes place in the side elements only, the cushion volume is
calculated as a function of side element shape only. The change
in cushion volume resulting from compression of fore and aft
elements was neglected.

Trunk Displacements - The displacement of each trunk element due
to ground contact is calculated geometrically, using the
lowermost point of each trunk which is stored in the form of a
data array.

Airflow System - The airflow into the trunk and cushion is
calculated by storing the corrected airflow as a function of
engine speed and trunk and cushion pressures. Separate curves
were created for ACRS fan-on, ACRS fan-off, and ACTS operation,
but only ACRS fan-off cases were simulated. Outflow between
trunk and ground is determined using the "restrictor flow"
theory (Reference 18). Trunk and cushion pressures are then
obtained by integration. This is a relatively simple model of
the airflow system, since both inflow and outflow (including
relief valve flow) are determined on a quasi steady state basis.
The only dynamic effects are the volume capacitance effects
which determine the trunk and cushion pressures.

Trunk Forces and Moments - For each element in ground contact,

165

TRUNK SEGMENT

FUSELAGE

CROSS
SECTIONAL
AREA CA_t

ΔX

VOLUME = $CA_t \Delta X$

P_t

Y_f

FLATTENED AREA

Y_c

P_c
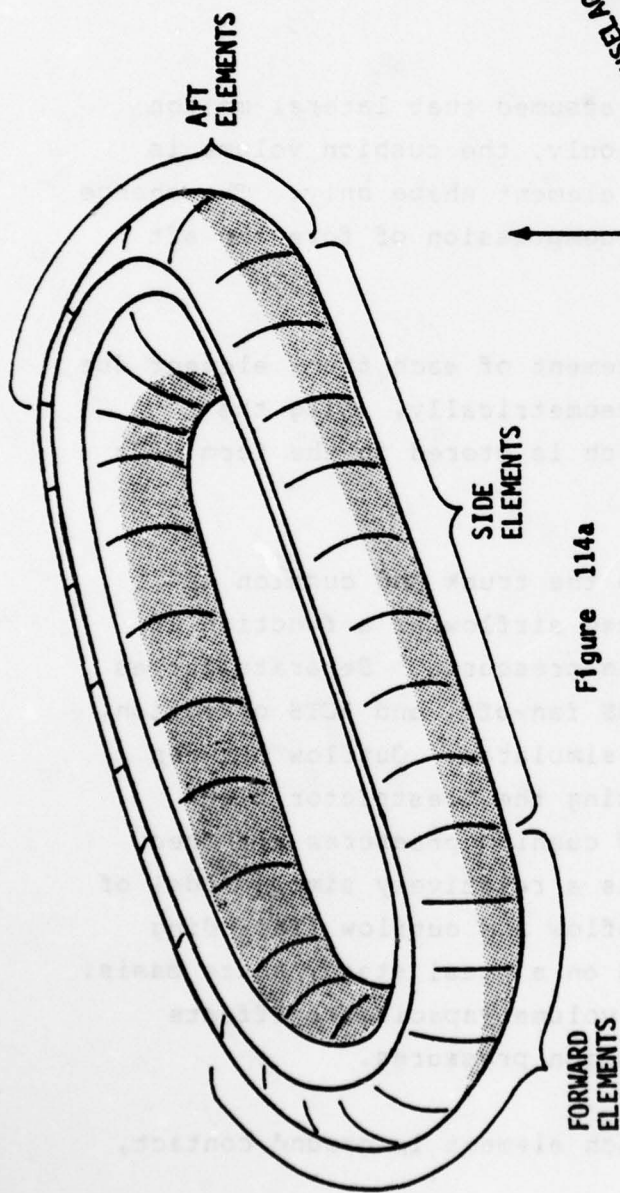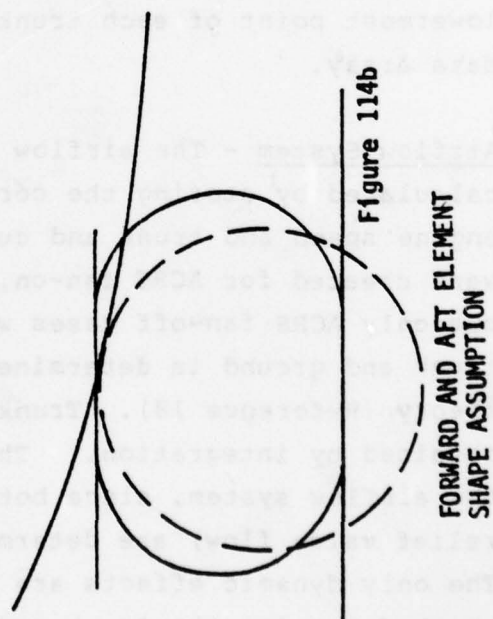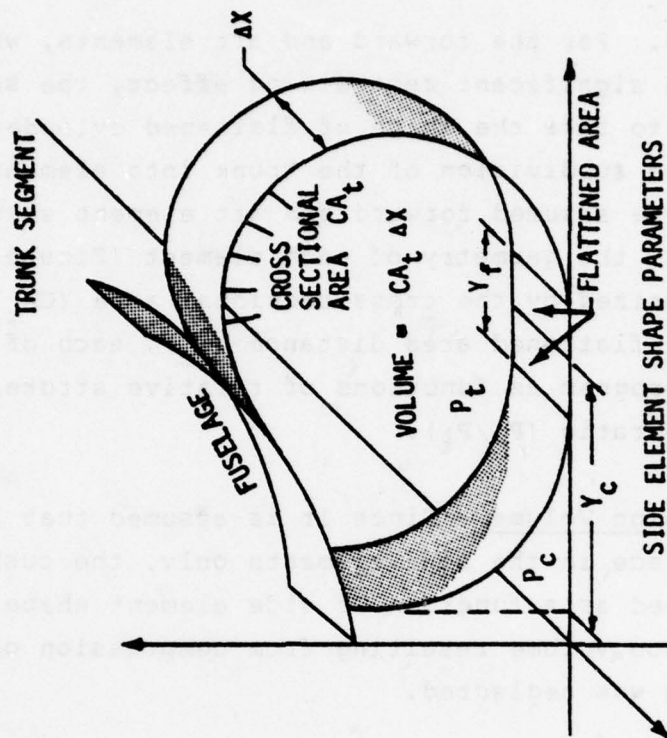
SIDE ELEMENT SHAPE PARAMETERS

Figure 114c

FORWARD AND AFT ELEMENT
SHAPE ASSUMPTION

Figure 114b

AFT
ELEMENTS

SIDE
ELEMENTS

FORWARD
ELEMENTS

Figure 114a

Figure 114 Inelastic Trunk Model

the vertical force is calculated as being the trunk pressure
multiplied by the flattened area. The axial and lateral
components of trunk drag may then be calculated based on the
local (lubricated or unlubricated) components of trunk friction.
The resulting pitch, roll and yawing moments are evaluated.

Aerodynamic Forces - Aerodynamic data is input in the form of
data arrays. Data included in the Jindivik model are:

- drag coefficient C_D
- lift coefficient C_L
- side force coefficient C_Y
- yawing moment coefficient C_n
- pitching moment coefficient C_m
- rolling moment coefficient C_ℓ

Flight Controls - Motion of the elevators and ailerons were not
included in the analysis. This is discussed more fully in
Sections 5.3 and 5.4.

5.2 PROGRAM VERIFICATION

The ACLS 6 DOF program was used to simulate the ACLS Jindivik
drop tests which were conducted at AFFDL. The data correlation
of this simulation provides a checkout of the program and
verification of the method of modeling ACLS.

The Jindivik drop tests configuration is shown in the schematic
of Figure 115. The conditions of the drop test (No. 28) are as
follows:

> Aircraft Weight = 2,614 lbs.
> Moments of Inertia
> $I_{xx} = 1190$ slug ft^2
> $I_{yy} = 1810$ slug ft^2
> $I_{zz} = 2840$ slug ft^2

167

Note 40 lbs. cables removed from tail.

FS162
FS162+
653 lbs.

FS130.25
FS105.5
FS113.5
FS89.5
FS87
180 lbs.
160 lbs.
100 lbs.
1119 lbs.

FS59.7
362 lbs.

FS43
40 lbs
BALLAST
To Trim P/C
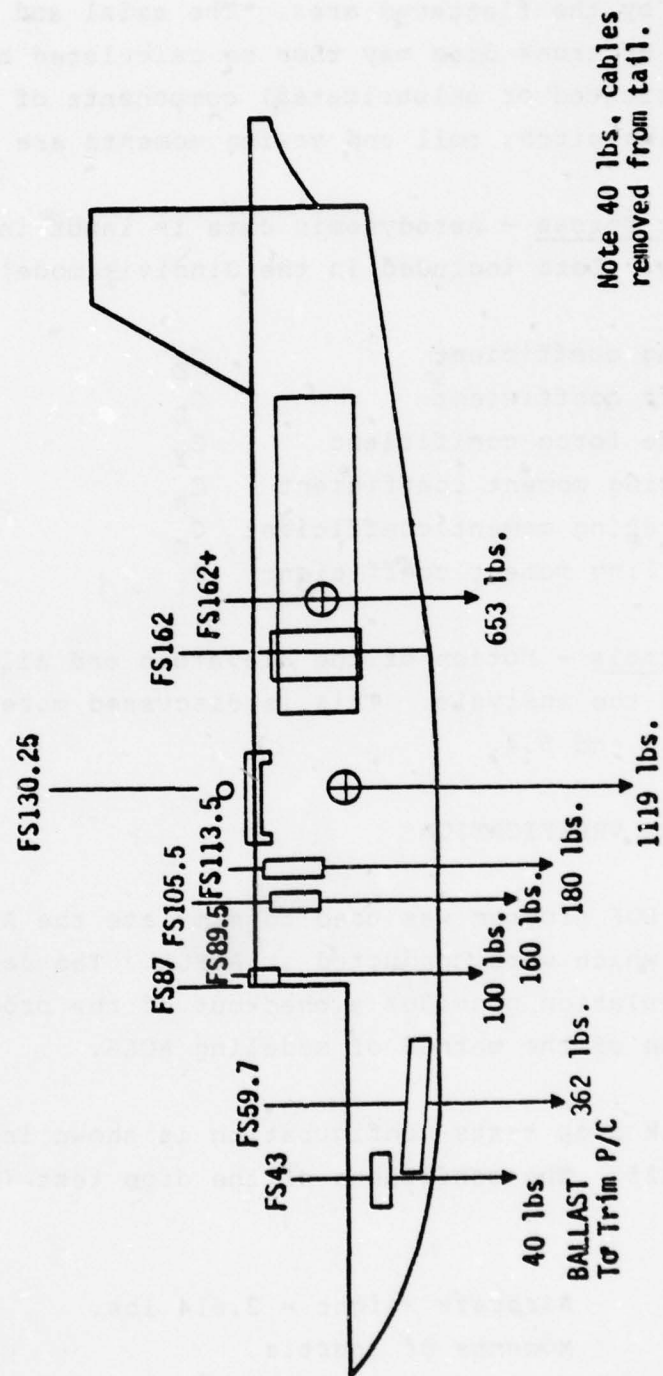
Total Weight 2614 lbs.

Figure 115 Individual Drop Test Configuration

1.0

1.1

1.25 1.4 1.6

2.8 2.5
3.2 2.2
3.6
4.0 2.0
1.8

MICROCOPY RESOLUTION TEST CHART
NATIONAL BUREAU
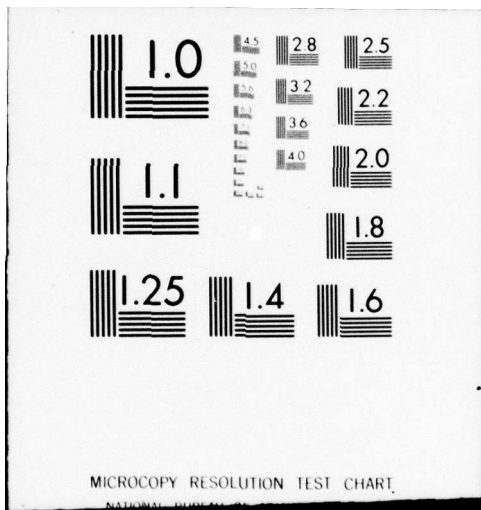
Cross Products of Inertia = 0.
                    cg height = 3.83 ft
                    cg is under lift hook
                    Attitude
                       Pitch = 3.0 deg.
                       Roll = 0.0 deg.
                    Bleed air flow rate = 0.75 lb/sec.
                    Cushion vent area = 0.37 sq. ft.
                    Pitch damping coefficient = 25 ft-lbs-sec/deg.
                       (AFFDL test data for ACRS #2)

Comparisons between test data and analysis are shown in Figures
116 through 119. Figure 116 shows fuselage height, Figure
117 shows pitch angle, Figure 118 shows trunk pressure and
Figure 119 shows cushion pressure. In general, the correlation
is good, with the simulation showing closely similar natural
frequencies and damping characteristics. The calculated peak
cushion pressure is, however, significantly higher than the test
data.

5.3 SIMULATION RESULTS

Taxi tests were conducted with the ACRS #2 and #3 in Australia.
ACRS #3 is 10 inches shorter on the front end than ACRS #2, and
was designed to permit launch on the existing Jindivik trolley.
Simulations were run for both trunks assuming brake tread
coefficients of friction of .8 and .4 for the unlubricated and
lubricated portions of the trunk respectively. This corresponds
to black asphalt, and is a worst case condition.

Figure 120 shows results for ACRS #2. The maximum pitch forward
angle is 5 1/2°, and subsequent pitch oscillations are
reasonably well damped. Figure 121 shows results for ACRS #3,
assuming the same initial velocity of 50 knots. In this case
the maximum pitch forward angle is 6 1/2°.

169
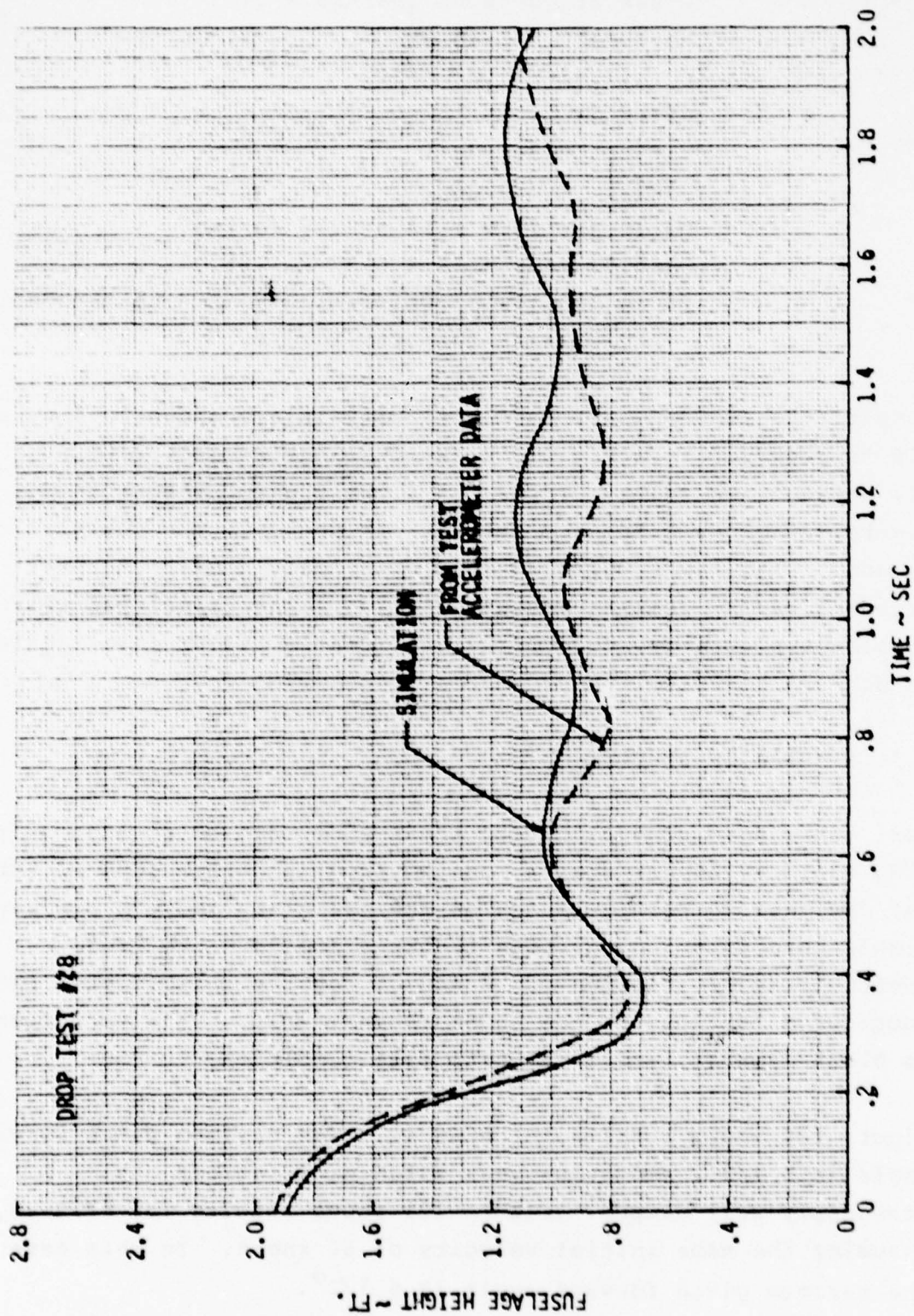
Figure 116   Drop Test-Heave Data Correlation

170
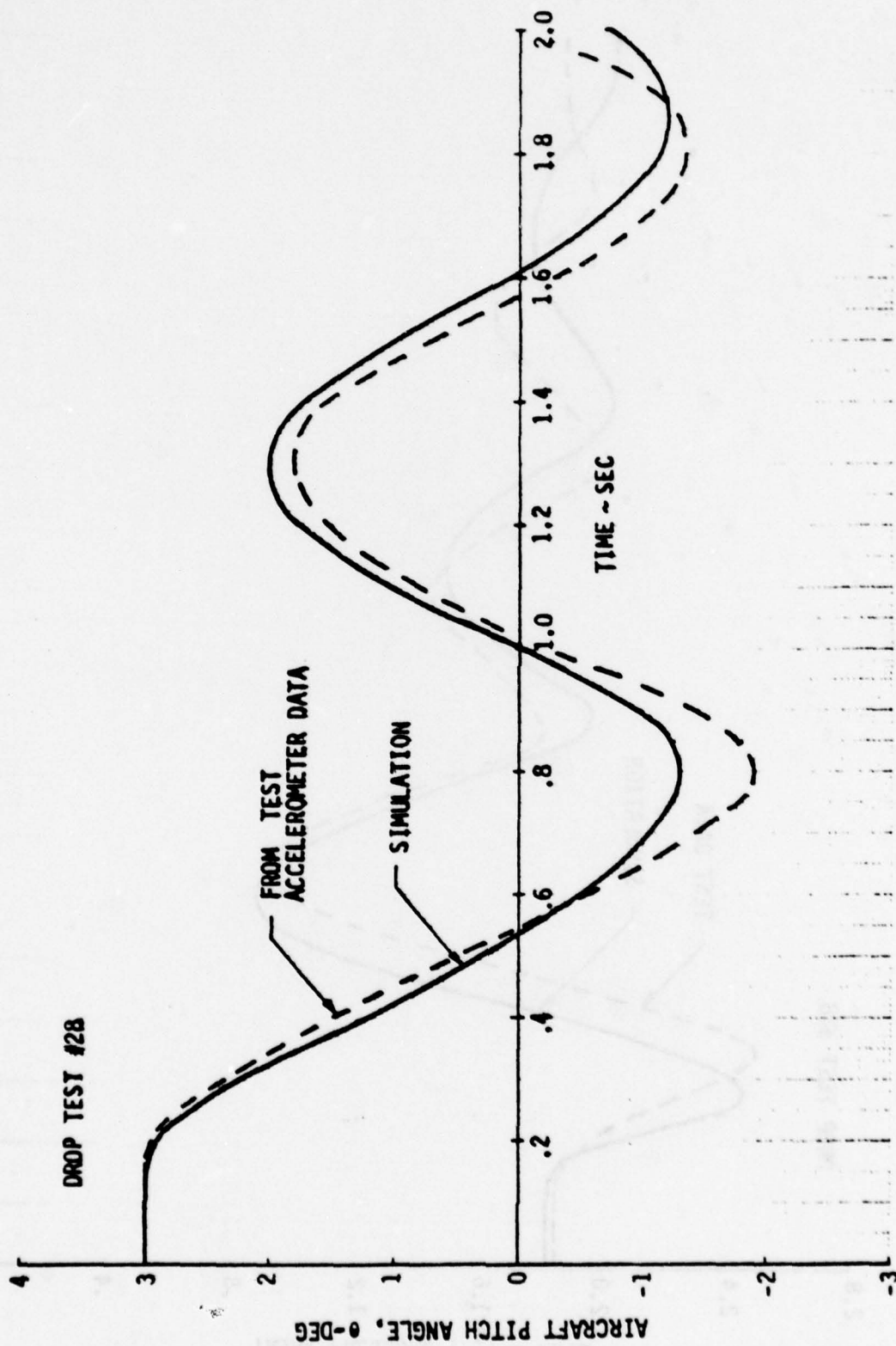
Figure 117 Drop Test-Pitch Data Correlation

171
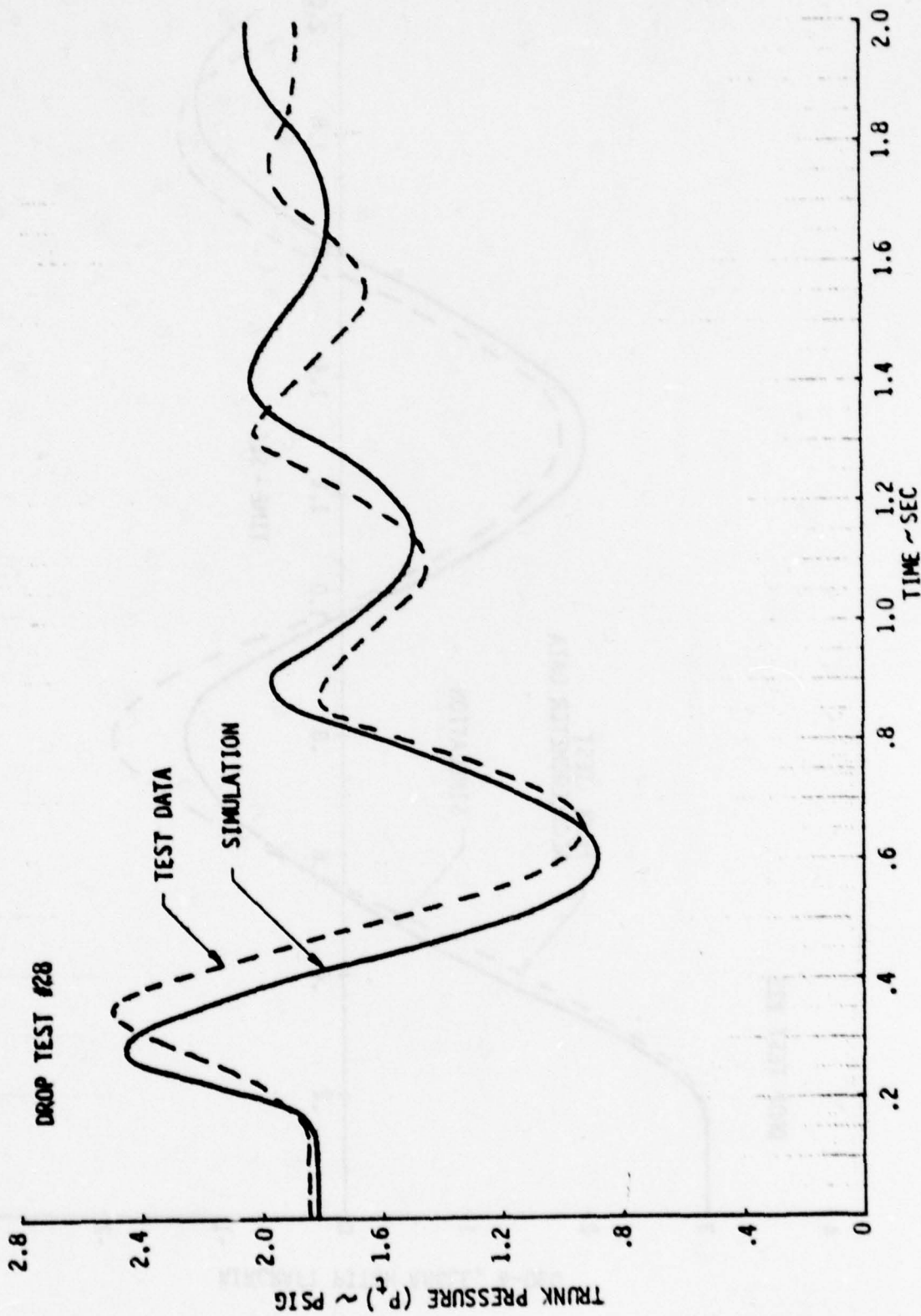
Figure 118 Drop Test-Trunk Pressure Data Correlation

172
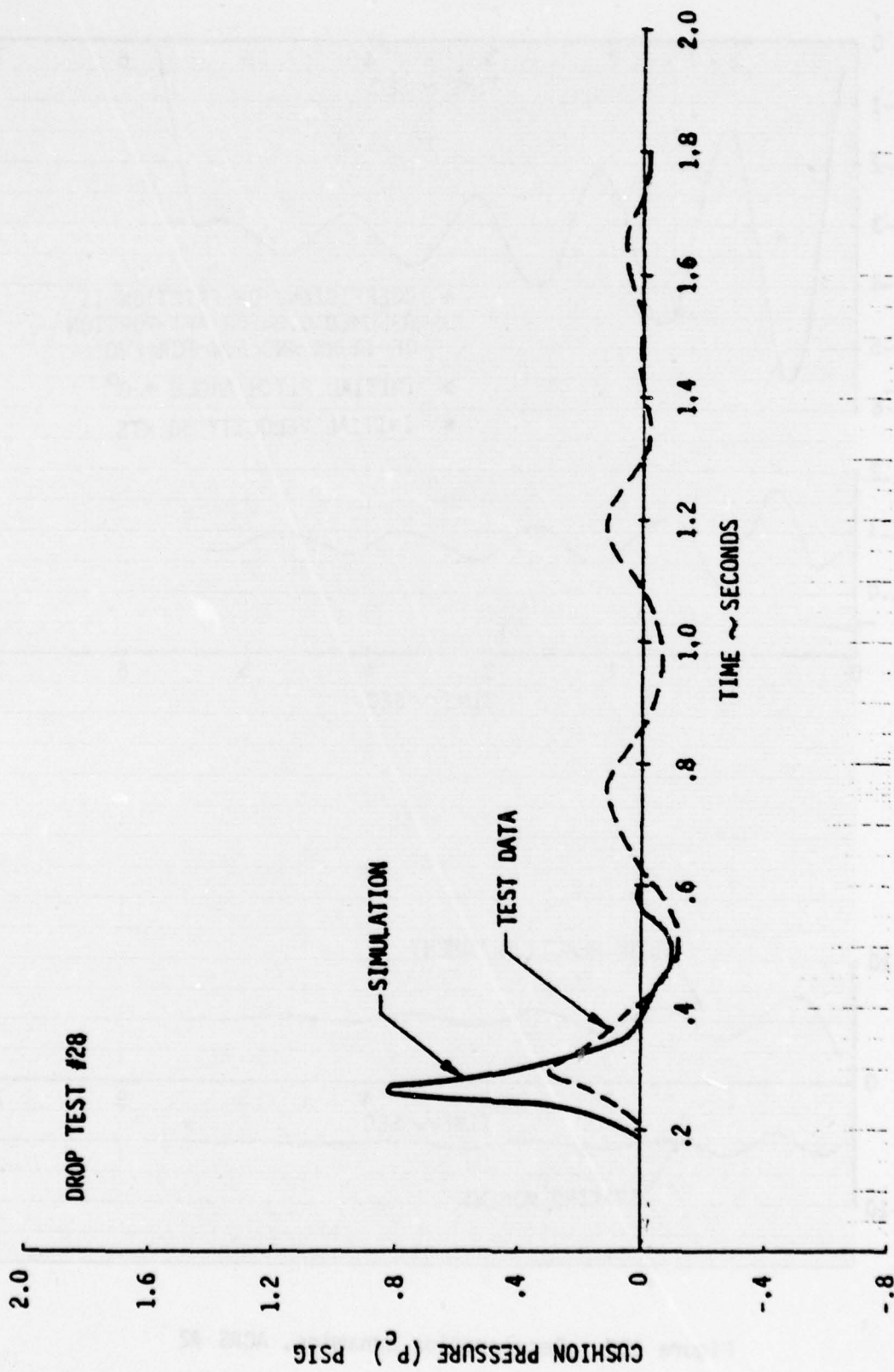
Figure 119 Drop Test-Cushion Pressure Data Correlation

173
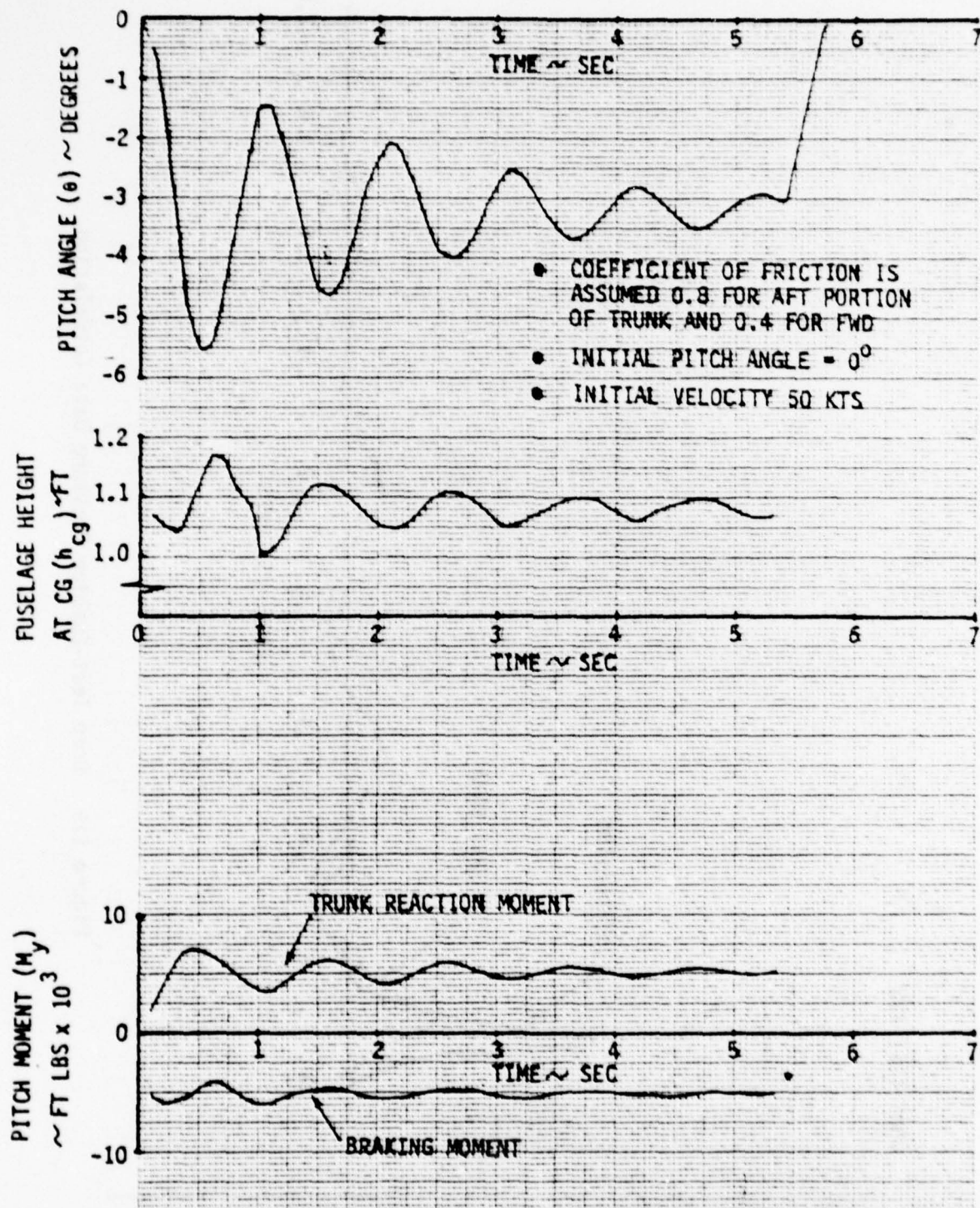
Figure 120   Deceleration Dynamics, ACRS #2
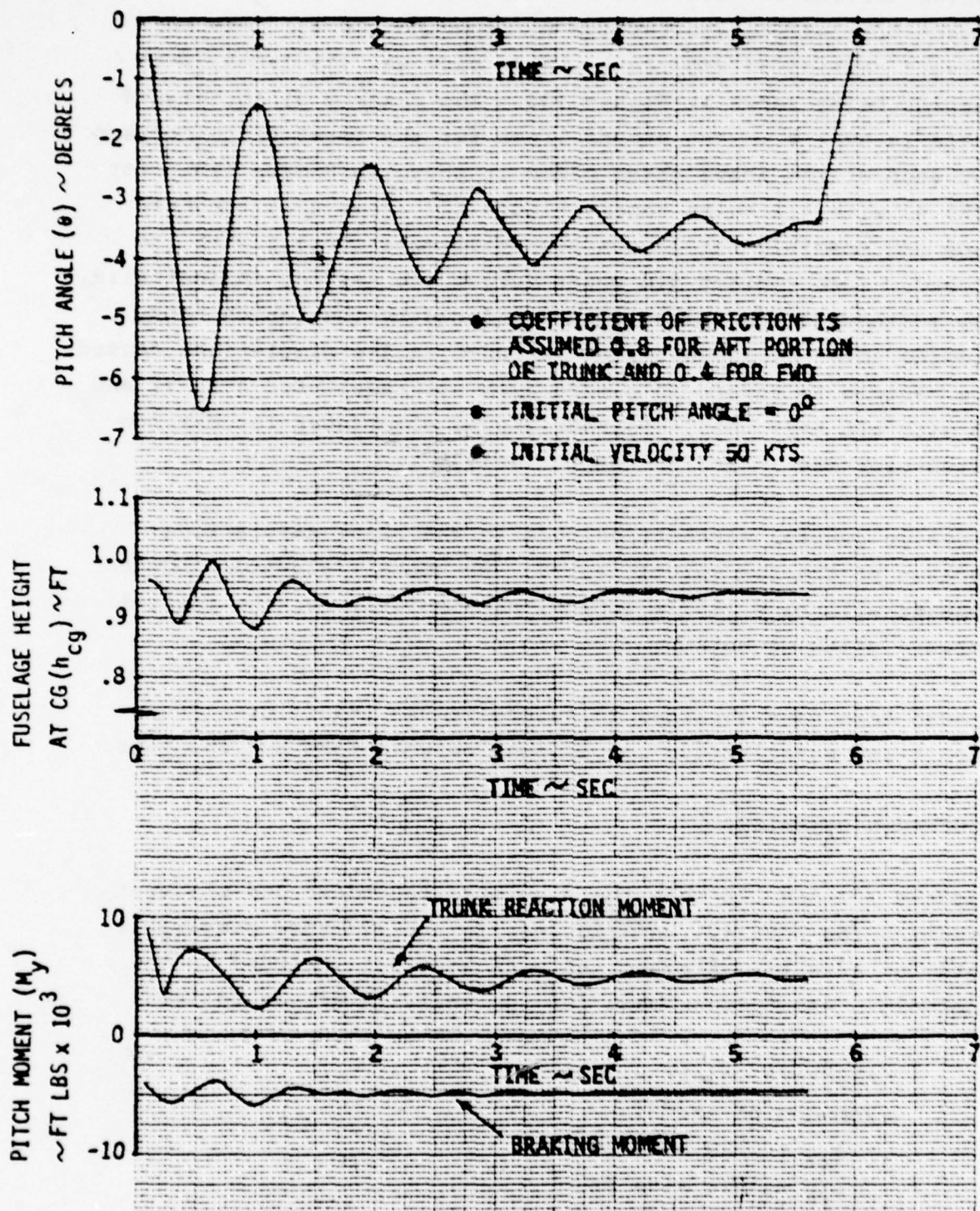
Figure 121   Deceleration Dynamics, ACRS #3

175

During testing in Australia on ACRS #3, an effort was made to divert more air to the cushion by plugging the air jets on the forward portion of the trunk. This case was simulated, with results being shown as Figure 122. The maximum pitch forward angle is over 9°. The ground lines for the first pitch forward for each of the above three cases is shown in Figure 123. For ACRS #3 with all holes taped, Figure 123 shows that the nose boom and possibly the launch hook will make contact with the ground. Such contact did occur during the testing in Australia. The subsequent high pitch moment induced by the launch hook digging into the asphalt (not included in the simulation) caused the vehicle to remain in a nose down attitude. For ACRS #2 and #3 with all jets open, the boom ground clearances for maximum pitch-over are 9" and 5" respectively.

Elevator control was not included in the above simulations. Because of the low velocities (0 - 50 knots), elevator induced moments will have little impact, particularly for the initial forward pitching motion.

Ground test data obtained in Australia was insufficient to permit any quantitative comparisons between test and analysis.

TOUCHDOWN DYNAMICS

Figures 124 and 125 show the simulated touchdown and slideout dynamics for ACRS #2, and Figures 126 and 127 show comparable data for ACRS #3. Elevator effects were not included in the analysis. Assumptions made for the analysis are as follows:

> Aircraft weight = 2700 lbs
> Moments of inertia
> $\quad I_{xx}$ = 1190 slug ft^2
> $\quad I_{yy}$ = 1811 slug ft^2
> $\quad I_{zz}$ = 2840 slug ft^2
> Cross products of inertia = 0

176
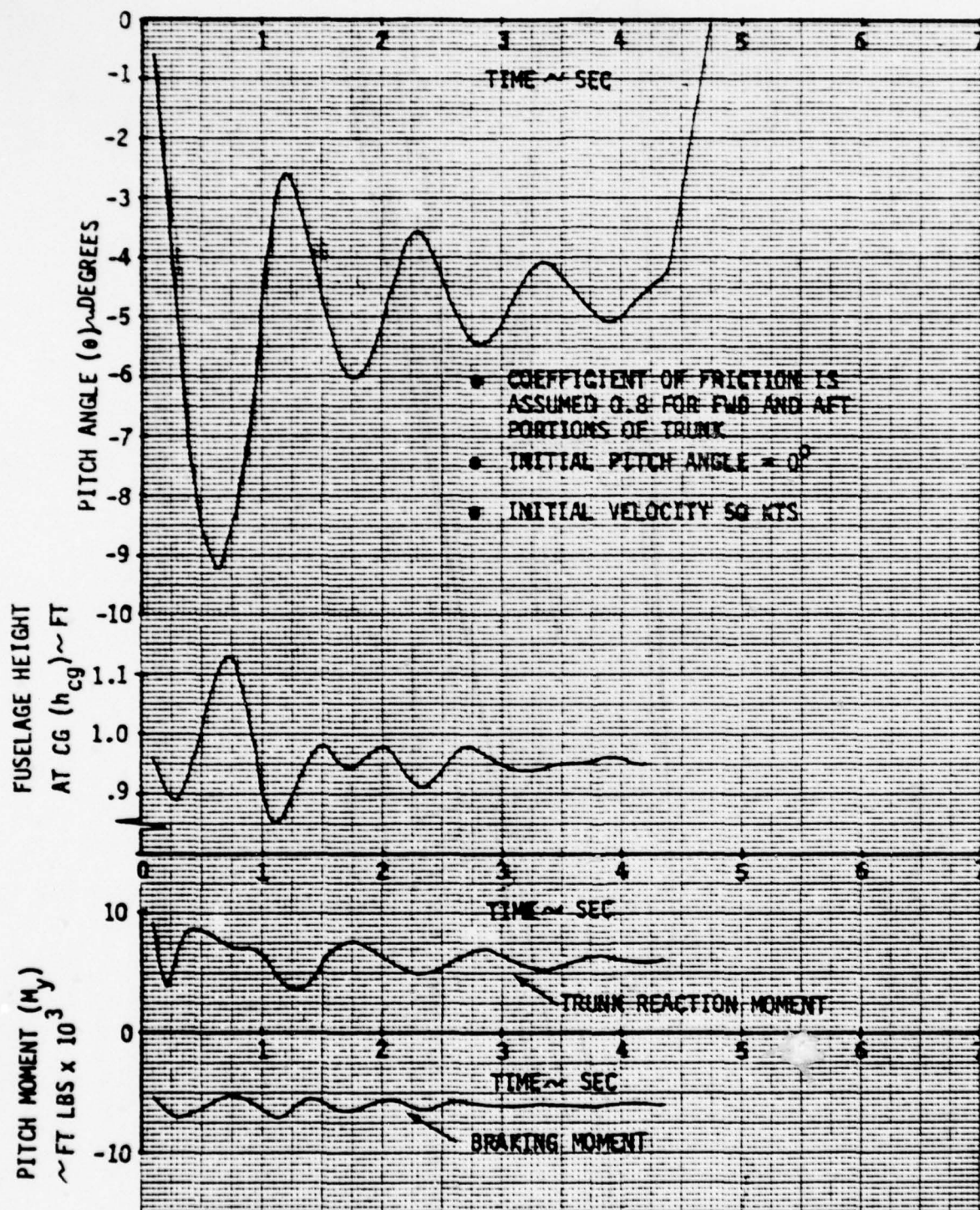
Figure 122   ACRS #3 Deceleration Dynamics With Air Jets Plugged

177

NOTE: SIMULATION OF ACRS #3 JETS
TAPED SHOWS LAUNCH HOOK MAKES
CONTACT WITH GROUND

ACRS #2 - ALL JETS OPEN (-5.6° PITCH)

ACRS #3 - ALL JETS TAPED (-9.2° PITCH) -·-·-

ACRS TRUNK #3

LAUNCH HOOK

ACRS TRUNK #2

ACRS #3-ALL JETS OPEN (-6.5°)
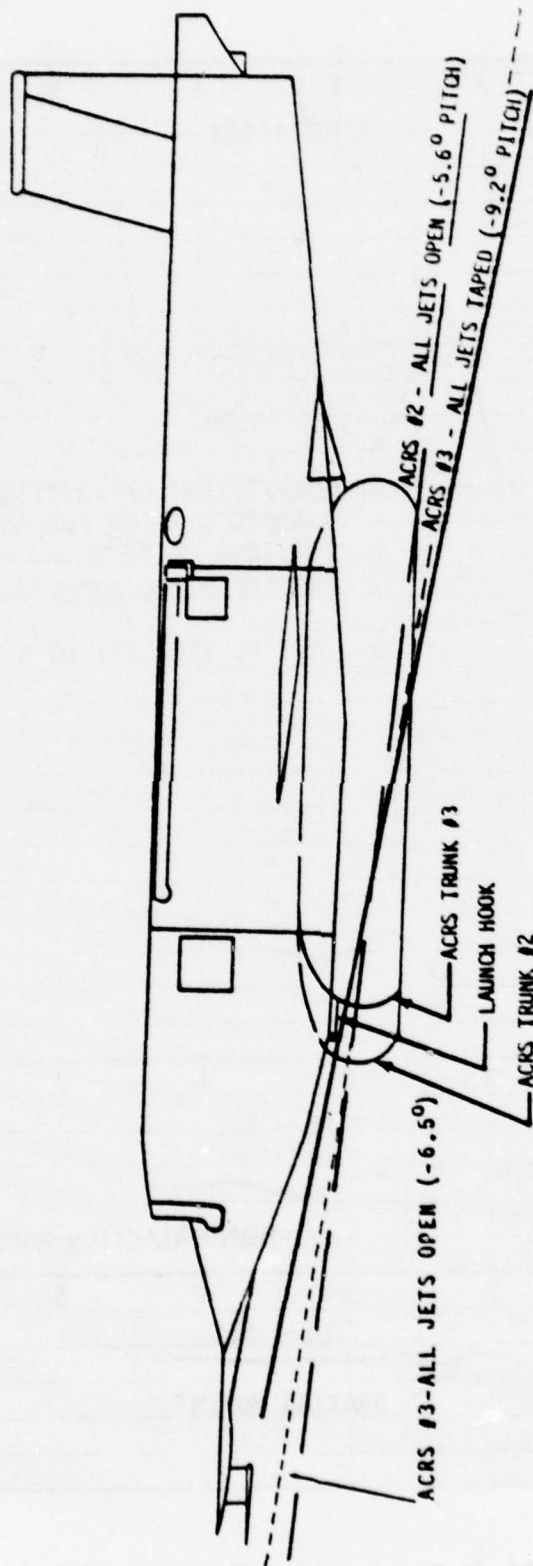
Figure 123   Jindivik Ground Line in Pitch Attitudes

178
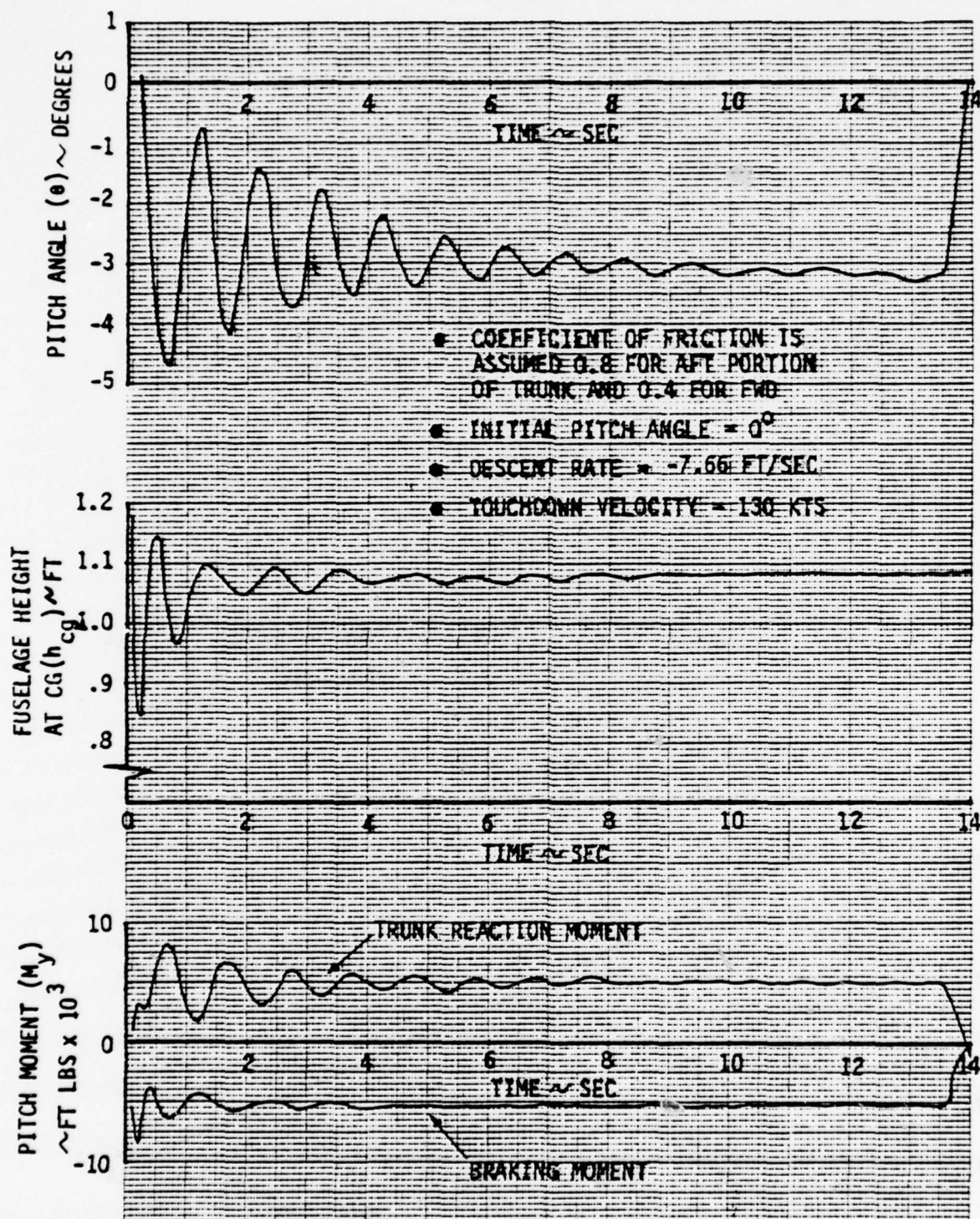
Figure 124   ACRS #2 Touchdown and Slideout Dynamics
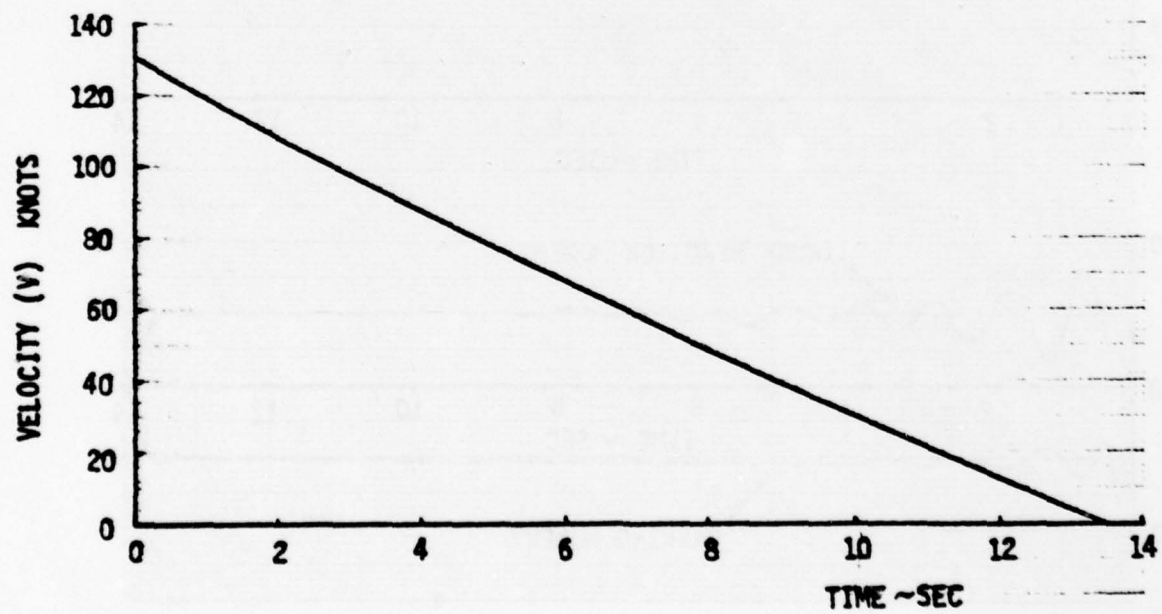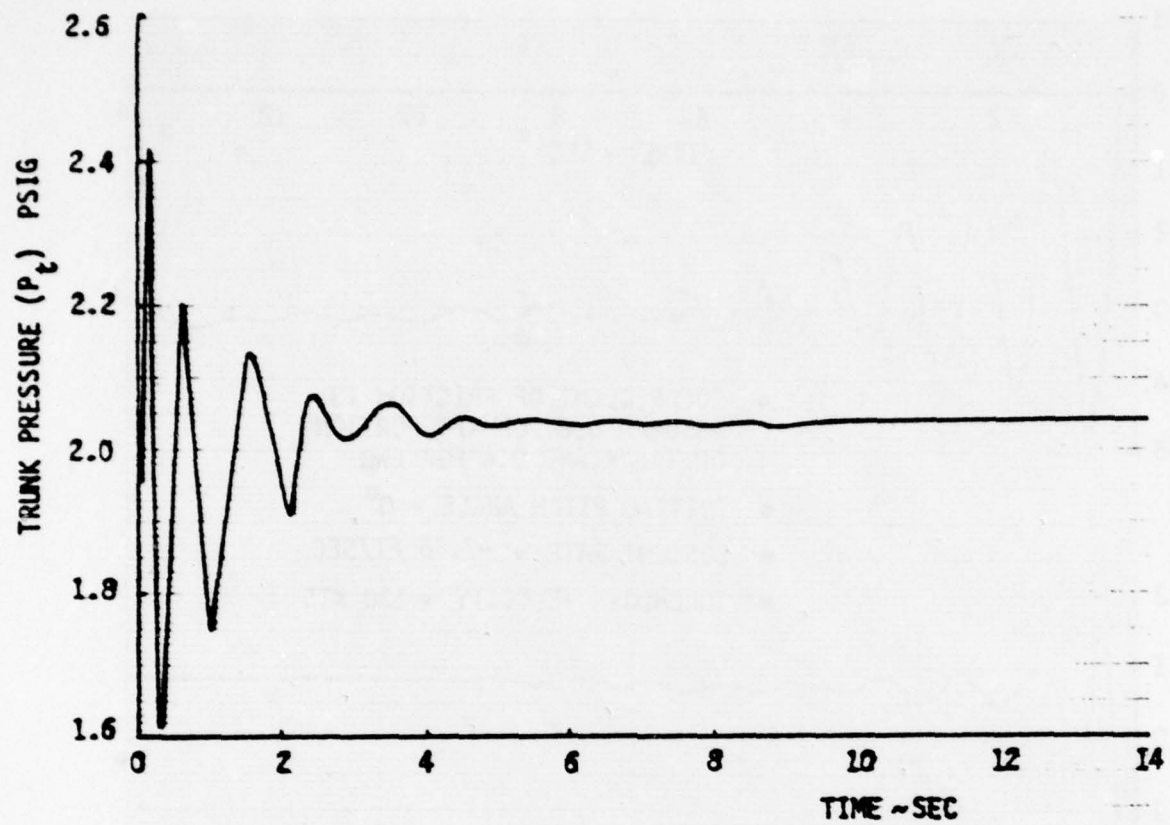
Figure 125   ACRS #2   Touchdown and Slideout Dynamics   (Continued)
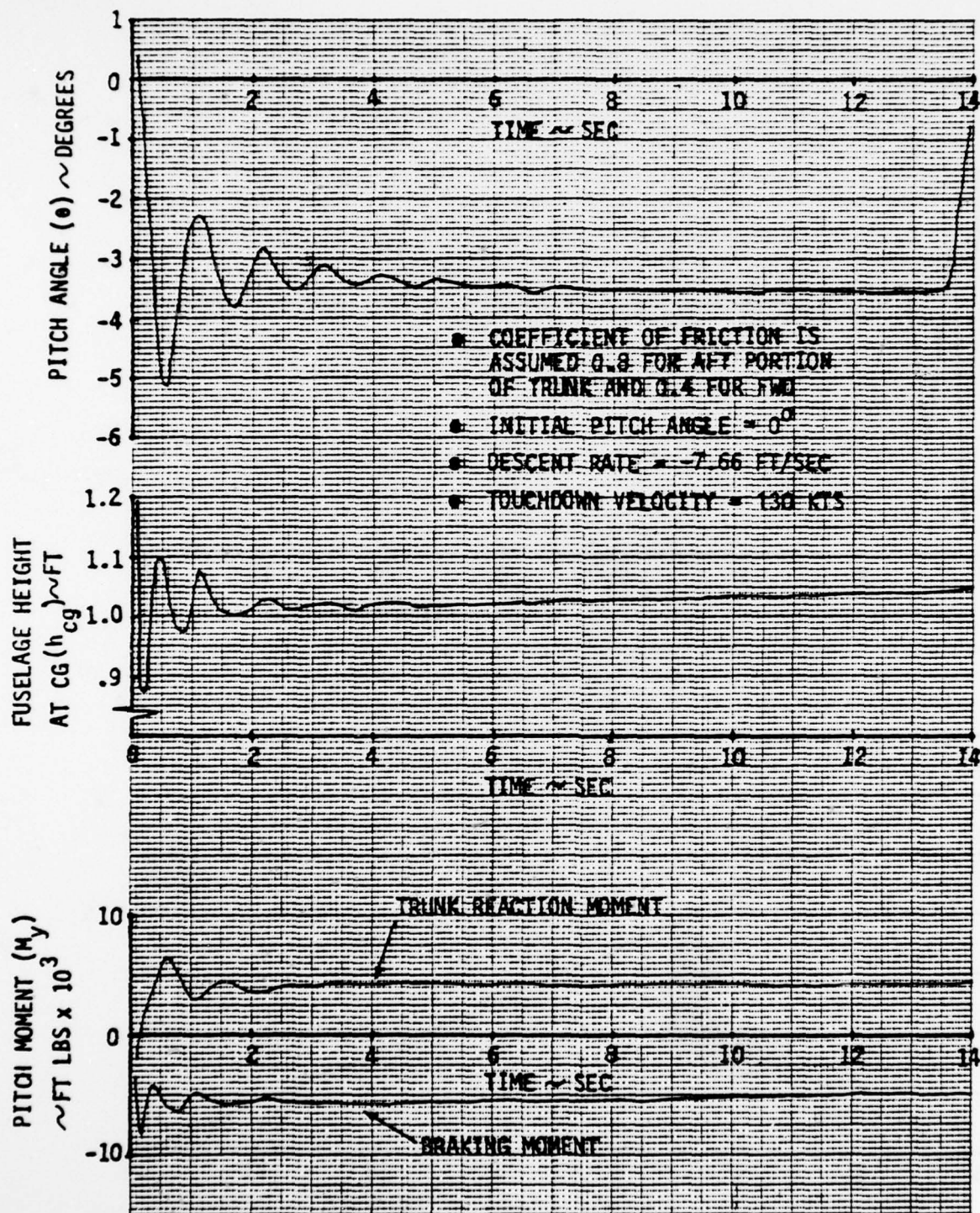
Figure 126   ACRS #3 Touchdown and Slideout Dynamics
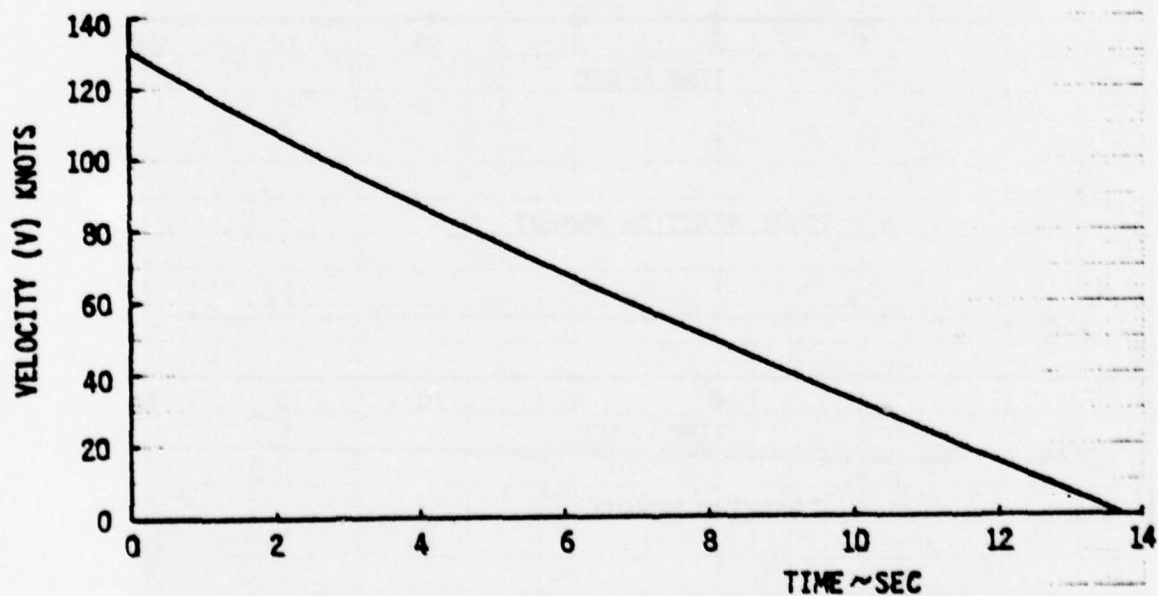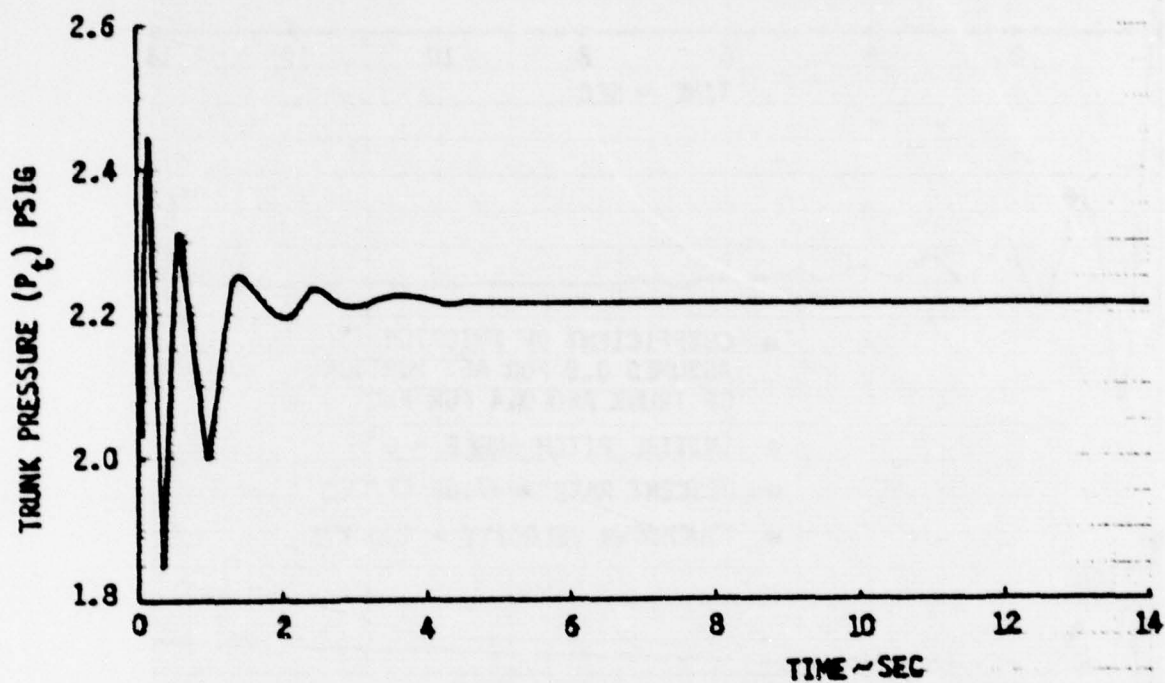
Figure 127   ACRS #3 Touchdown and Slideout Dynamics (Continued)

182

Touchdown speed = 130 knots

Angle of descent = -2°

Pitch attitude = 0°

Rate of descent = 7.66 ft/sec

Flap retraction time = 0.3 sec

Bleed air flow rate = 0.75 lbs/sec

Cushion vent area = 0.21 ft^2 (minimum back flow area
through fan)

Engine idle thrust = 300 lbs

Engine thrust line above cg = 0.375 ft

Engine gyro couple pitch moment = 10.5 σ

Aerodynamic pitch damping coefficient = -.246 sec/rad

Trunk pitch damping coefficient = 25 ft-lbs-sec/deg

Distance of cg aft of lift hook = 0.5 ft.

The initial pitch forward is marginally acceptable and the pitch damping is acceptable. Two factors should, however, be noted:

1. Elevator effects -- The Jindivik elevator is limited to 15 degrees up and 10 degrees down following sting contact with the ground. At a touchdown velocity of 130 knots, the pitch moment at an elevator angle of +15 degrees is 2900 ft-lbs, or approximately 60% of the mean braking moment. Thus, the elevator moment capability is sufficient to have significant impact on pitch amplitude and could reduce the inital pitch forward angle. The elevator servo mechanism rate is 53 deg/sec, and the ratio between servo and elevator is 1.5, giving an elevator rate of 30 deg/sec. The elevator slew time between limits ($\simeq$ .7 seconds) is greater than the half period of the vehicle ($\gtrsim$ .5 seconds). Thus, the possibility of undesirable interaction between the vehicle dynamics and the elevator control system does exist and requires further investigation.

2. The analysis has assumed a trunk damping coefficient obtained from static tests. This coefficient may be higher

183

than in dynamic tests with forward velocity, since with
forward velocity trunk scrubbing effects do not contribute
significantly to overall damping. More test data are
required to assess the importance of this effect.

5.4 EVALUATION OF RESULTS

The results presented in Section 5.3 show marginally acceptable
initial forward pitching. The mechanism for the oscillations is
quite straightforward. The high coefficients of friction
assumed for the unlubricated trunk to asphalt interface
cause large forward pitching moments. When the vehicle pitches
forward, so that a significant portion of the flattened trunk
area is lubricated, the pitching moment is reduced and hence the
vehicle pitches back again. This motion is coupled with heave,
with the latter acting to increase the normal force when the
vehicle is pitched back, and to decrease it when the vehicle is
pitched forward. Also, when the vehicle is in the forward pitch
attitude due to deceleration, there is a loss of heave
stiffness.

The cases which have been analyzed are severe, in that dry
asphalt gives the highest coefficient of friction in the
unlubricated area of the trunk. An area of uncertainty in the
analysis is the mechanism and magnitude of pitch damping due to
the trunk. The trunk damping coefficient obtained in a static
test, where there is no forward speed, may be higher than that
obtained in a dynamic test. The simulations were conducted with
the static test damping coefficient.

Several approaches are available to reduce the pitching problem,
as follows:

1. Trunk Design.

   As a result of the ground tests and analysis, AFFDL has

184

designed a new ACRS trunk which extends further forward under the nose of the aircraft. This new trunk will provide an increase in pitch stiffness.

2. Elevator Pitch Control.

Elevator control has not yet been included in the simulations. For pitch control following touchdown the elevators may be able to reduce pitch oscillations; however, the possibility of undesirable interractions between the vehicle and the elevator servo exists. An elevator servo motor with an increased rate may be required.

3. Airflow System.

As discussed in Section 2, there appears to be the potential to improve the performance of the airflow system significantly. Depending on how many of the recommended changes can be incorporated, it may be possible to land with the fan valve partially or even fully open. This reduces trunk loads and improves lubrication, resulting in significantly lower pitching moments. At the very least, trunk pitch and roll induced moments at low engine power settings can be reduced.

4. Surface Selection.

Friction coefficients can be reduced by landing on grass.

185

SECTION 6

RETENTION/RELEASE SYSTEM DESIGN

6.1 SYSTEM DESCRIPTION

The Jindivik ACLS vehicle utilizes separate trunks for launch and recovery. Bolts attaching the aircraft fuselage to the ACRS trunks provide a positive attachment between the trunk and the vehicle. During taxi and takeoff on the ACTS, the ACRS trunk is stowed close to the fuselage under the ACTS trunk. The ACTS trunk is attached to the fuselage by a velcro strip, as shown in Figure 128. During taxi tests on the ACTS conducted at the GAF Avalon Field facility, non-standard operating procedures caused the velcro attaching the forward part of the trunk to the fuselage to separate, resulting in damage to both the trunk and the aircraft. This particular situation occurred during rapid vehicle deceleration, which caused the aircraft to pitch nose down and hence concentrate the drag loads on the forward attachment region.

The potential of trunk separation at the aft end of the attachment region also exists. During ACTS deceleration, the center of frictional drag may be forward of the CG, and thus the vehicle may end up in a side slip. The aft parking bladder on the slip side will tend to roll under the aircraft, resulting in a load perpendicular to the velcro strip. Velcro resistance to normal loads is quite low, and thus separation is possible.

A further problem in the velcro attachment system was evidenced during testing at NASA/LaRC and AFFDL. The purpose of the NASA tests was to evaluate release of the ACTS. Release is initiated by inflating rubber tubes which cause separation of the velcro in the forward end, and the aerodynamic drag should then be

186
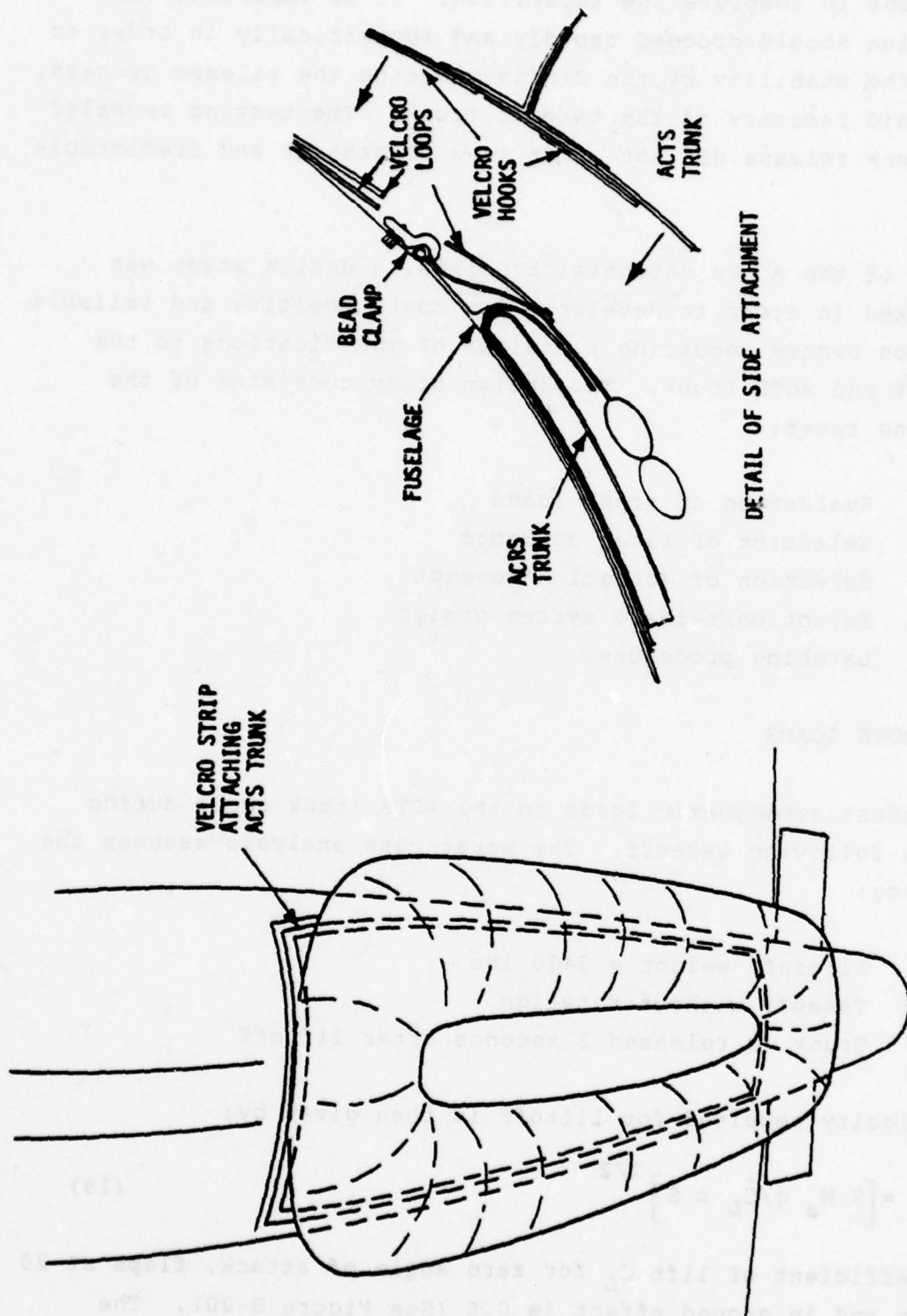
Figure 128 Velcro Attachment of ACTS Trunk

sufficient to complete the separation. It is important that separation should proceed rapidly and symmetrically in order to ensure the stability of the Jindivik during the release process, and to aid recovery of the takeoff trunk. The testing revealed that trunk release did not occur in a consistent and predictable manner.

Because of the above potential problems, a design study was undertaken in order to develop a low cost, positive and reliable retention system requiring a minimum of modifications to the aircraft and ACTS trunk. The design study consisted of the following tasks:

1. Evaluation of trunk loads
2. Selection of latch concepts
3. Selection of actuation concept
4. Retention/release system design
5. Latching procedure

6.2 TRUNK LOADS

The highest aerodynamic loads on the ACTS trunk occur during release following takeoff. The worst case analysis assumes the following:

o   Aircraft weight = 3400 lbs
o   Takeoff without rotation
o   Trunk is released 3 seconds after liftoff

The velocity required for liftoff is then given by:

$$V = \left[2 \ W_a \ g/C_L \ \rho \ S \right]^{1/2} \tag{18}$$

The coefficient of lift C_L for zero angle of attack, flaps at 20 degrees and in ground effect is 0.6 (See Figure B-20). The takeoff velocity is then:

188

$$V_{to} = \frac{(2) \quad (3400) \quad (32.2)}{(.6) \quad (.076) \quad (76)} = 251 \text{ ft/sec} \tag{19}$$

or

$$V_{to} = 149 \text{ knots} \tag{20}$$

Assuming that the trunk is released 3.0 seconds after liftoff, the velocity at the moment of release is given by:

$$V_r = V_{to} + at \tag{21}$$

or

$$V_r = V_{to} + \frac{F_{th}}{W_a} g t \tag{22}$$

The most severe condition for trunk release will be when the velocity at release is a maximum. Thus, assuming takeoff thrust for the three seconds, this velocity is given by:

$$V_r = 251 + \frac{2500}{3400} (32.2)(3) = 322 \text{ ft/sec} = 190 \text{ knots} \tag{23}$$

The dynamic pressure is given by:

$$q = \frac{1}{2} \frac{\rho}{g} V_r^2 \tag{24}$$

For the above condition

$$q = \frac{1}{2} \frac{.076}{32.2} (322)^2 = 122 \text{ PSF} \tag{25}$$

The aerodynamic drag parallel to the aircraft is given by:

$$F_d = C_D q A_f \cos \alpha \tag{26}$$

189

A_f is the frontal area of the trunk and is approximately 8 sq. ft. Assuming the drag coefficient C_D = 0.15, the aerodynamic drag on the trunk is:

$$F_d = (0.15)(122)(8) \, Cos \, \alpha \simeq 146 \, Cos \, \alpha \, (lbs) \qquad (27)$$

If the aircraft is at an angle of attack, aerodynamic lift will reduce the weight of the trunk and may affect trunk separation. The lift force on the trunk is given by:

$$F = C_L \, q \, A_b \, Sin \, \alpha \qquad (28)$$

Where A_b is the effective cross-sectional area of the bottom of the trunk. The geometric area is 16.7 sq. ft. A_b is assumed to be .75 x 16.7 sq. ft., where the factor .75 accounts for wing spoiling effects. $A_b \, Sin \, \alpha$ is the projected area of lift. The lift coefficient C_L is assumed to be equal to 0.5. For the above worst case condition and for the stall angle of attack of 12 deg, the lift force is:

$$F_\ell = (.5)(122)(16.7)(.75) \, Sin \, 12^o = 159 \, lbs \qquad (29)$$

The net perpendicular force acting on the trunk is:

$$F_{\ell_\eta} = C_L \, q \, A_b \, Sin \, \alpha - W_t \, Cos \, \alpha \qquad (30)$$

Where W_t is the weight of the trunk, and is assumed to be 120 lbs. The net parallel force acting on the trunk is given by:

$$F_p = C_D \, q \, A_f \, Cos \, \alpha - \mu F_{\ell_\eta} + W_t \, Sin \, \alpha \qquad (31)$$

Where μ is the coefficient of friction between the ACTS trunk and the ACRS cover. The frictional terms enters only if F_p is positive.

190

Figure 129 shows the net perpendicular force acting on the trunk as a function of angle of attack and vehicle velocity. Assuming a coefficient of friction of 1 for the rubber to rubber interface, the frictional force resisting separation is then numerically equal to the perpendicular force. Figure 129 also shows the net parallel force of aerodynamic drag and gravity. The net tangential force of separation may be determined from Figure 129. For example, at V = 190 knots and α = 12°, the net parallel force is

$$F_p = 168 - 40 = 128 \text{ lbs} \tag{32}$$

The trunk acceleration parallel to the aircraft is then given by:

$$a = \frac{g}{w_t} F_p = \frac{32.2}{120} \ 128 = 34.4 \text{ ft/sec}^2 \tag{33}$$

and the time required to clear the stowed ACRS trunk of 10 ft in length is:

$$t = \left[\frac{2 \times 10}{a}\right]^{1/2} = \left[\frac{2 \times 10}{34.4}\right]^{1/2} = .76 \text{ sec} \tag{34}$$

Figure 129 shows that only at high angles of attack and high speeds will the ACTS trunk be forced up against the fuselage by aerodynamic lift. The analysis is also conservative because the fan air will provide lubrication between the ACTS trunk and the ACRS trunk cover for the first three feet of a shearing separation, which a mechanical latch system allows. At lower angles of attack, the fan will most likely push the forward part of the trunk away from the fuselage, and the peeling of the velcro attachment system will occur. If the aircraft is at a high angle of attack and at a speed greater than 170 knots, the peeling of velcro can not be assured. The velcro attachment will not allow the trunk to separate in shear.

191
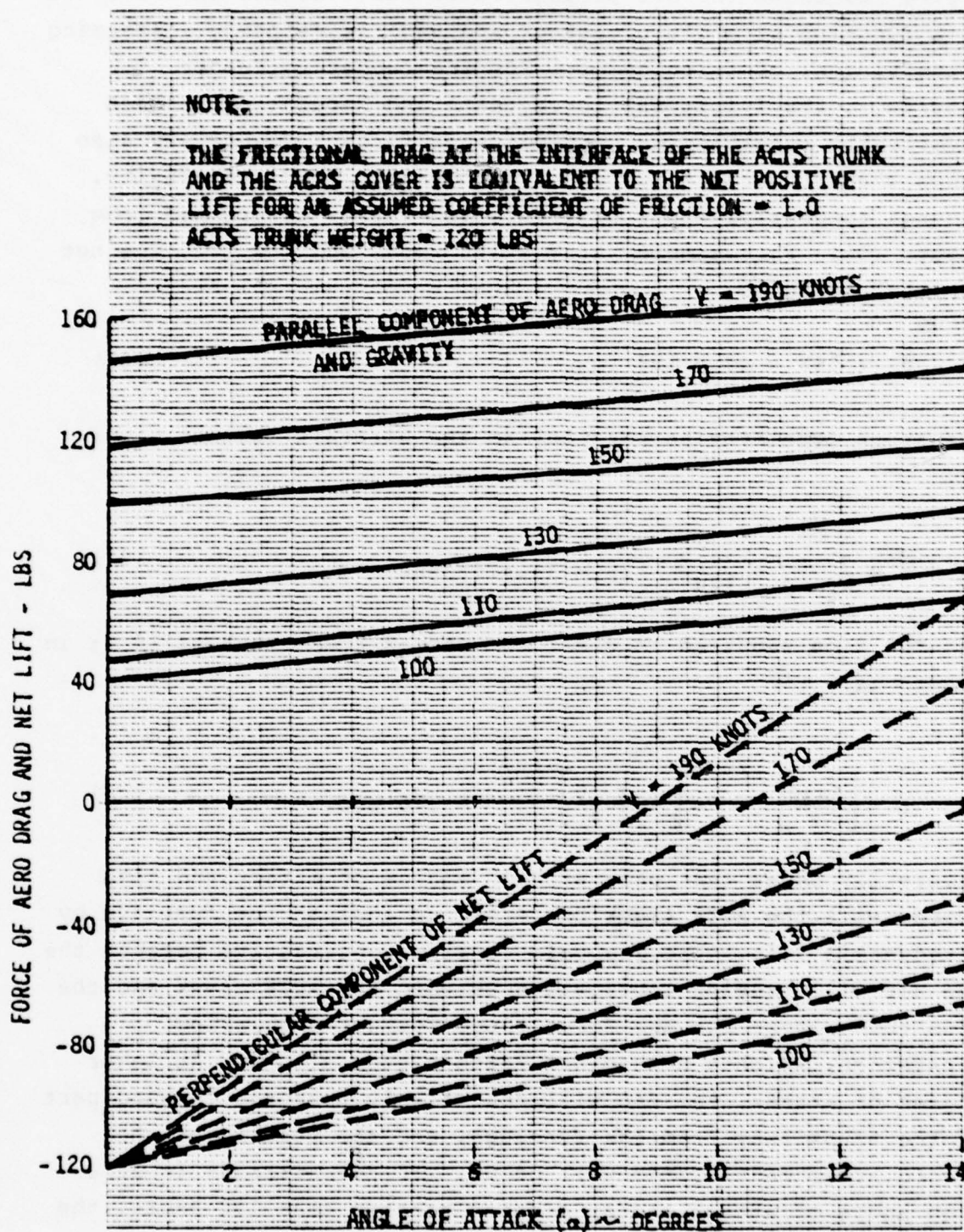
Figure 129   ACTS Trunk Aerodynamic Forces

6.3   SELECTION OF LATCH CONCEPT

Because of the difficulties experienced with the velcro retention/release system discussed in the previous section, it was evident that a positive system that would provide strong retention of the ACTS trunk and also a clean release is required. Two retention/release concepts had been completed, namely the pin and lever latch and the pin and cone latch shown in Figures 130 and 131. These latches were tested at AFFDL and at B. F. Goodrich. The load required to pull the pin versus suspended load for various test specimens is shown in Figure 132.

A search of industry latching devices failed to provide better devices than those already tested. The pin and lever type latch was selected as having more structural integrity than the pin and cone concept.

Several variants of the basic pin and lever type latch were identified as shown in Figure 133. Figure 133a shows a mechanism which simply constrains the cable from vibrating in the airstream after release. Figure 133b shows the original pin and lever device with an ordnance pin puller. Figure 133c shows the lever latch with a bellcrank and cable. Figure 133d shows the bell crank latch installed with internal linkage. The bell crank latch was chosen as providing the cleanest release of the devices while also providing easy adjustment of the cable. The external leakage is considered satisfactory for a demonstration ACLS aircraft, and requires less modifications to the aircraft. Ordnance pin pullers are very expensive, costing $3000 for eight units, and so were considered to be unsatisfactory.

6.3.1   Ground Loads

The highest loads on the ACTS trunk will occur during

193
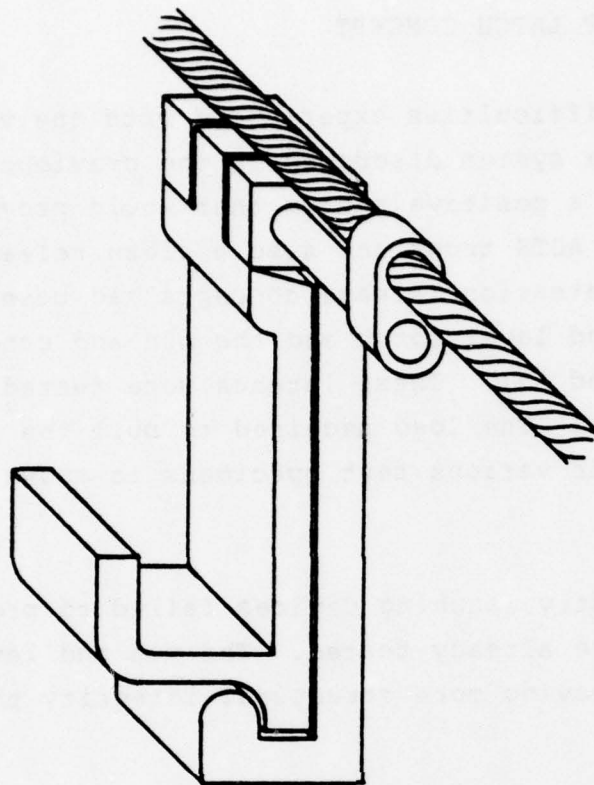
Figure 130   Pin and Lever Latch
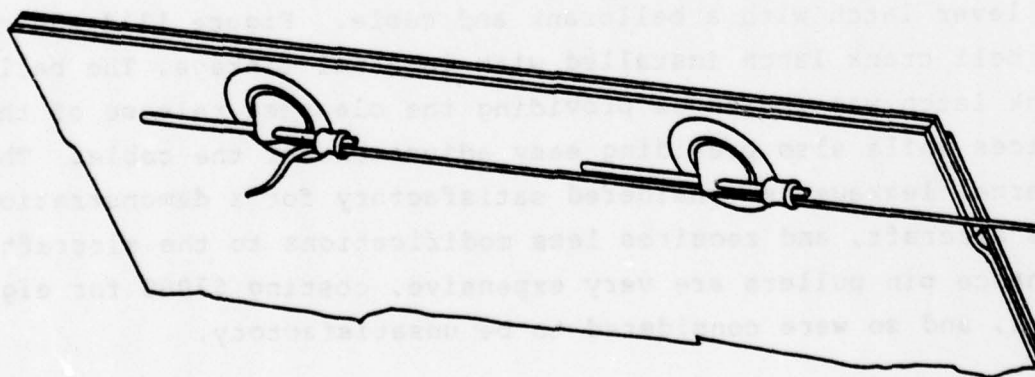
Figure 131   Pin and Cone Latch

194
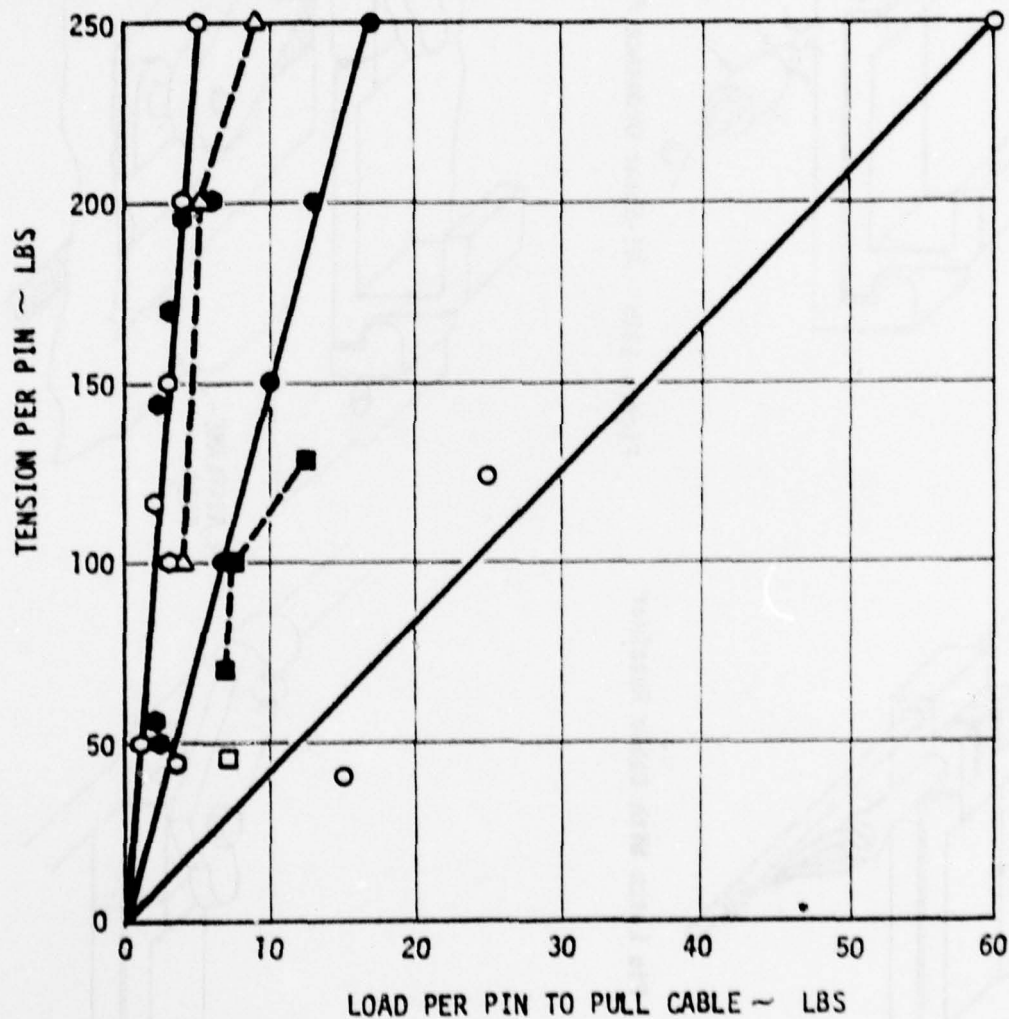
Figure 132   Pin Pull Tests Data

195

PIN PROTRUSION = .34"

.125"
5/16"
.94"

MINIMUM
SIZE PULLER

Figure 133b   Hi-Shear Ordnance Pin Puller on FEM Pin Latch
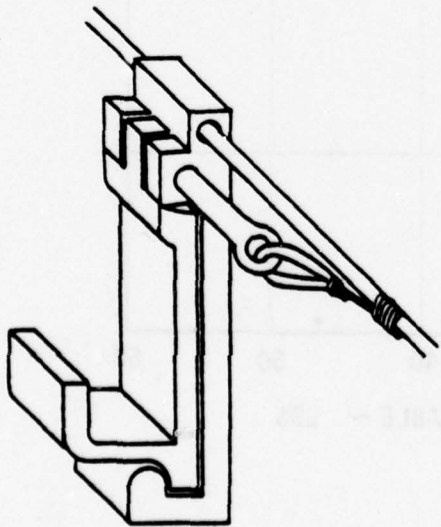
Figure 133a   Pin Latch With Cable Retainer
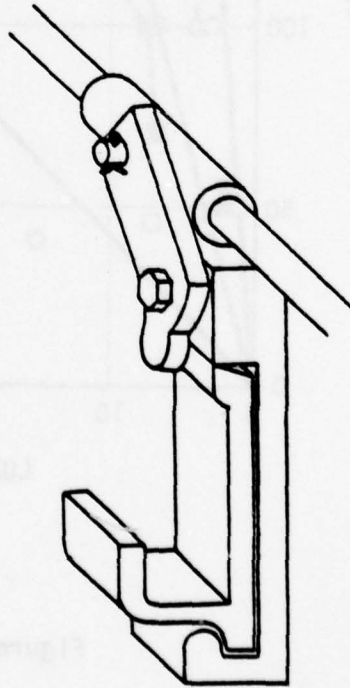
Figure 133c   Swivel Latch

AIRPLANE
SKIN
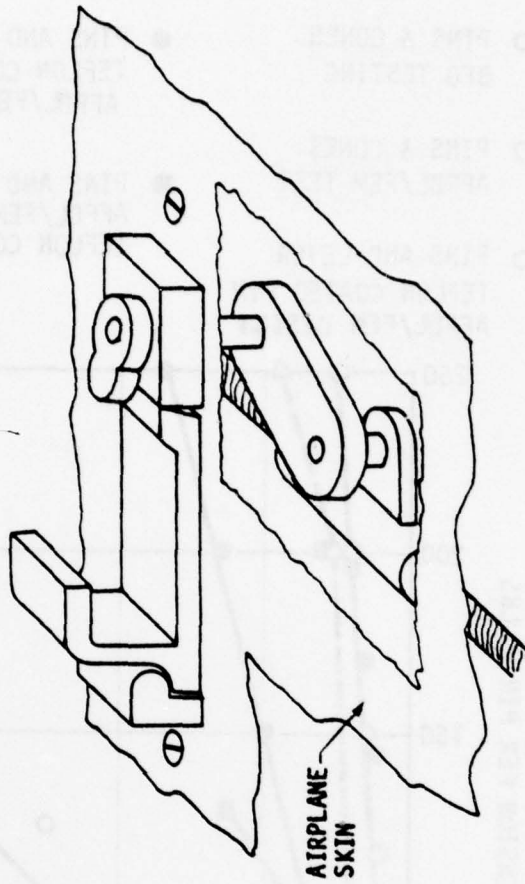
Figure 133d   Swivel Latch With Internal Leakage

Figure 133- Latch Concept

196

deceleration. The worst case condition would be in the event of a fan failure. In this case the Jindivik would pitch forward and load up the frontal portion of the trunk. A total loss of air lubrication would occur. Assuming an aircraft weight of 3,400 lbs with a coefficient of friction of 1.0, and that the drag load is reacted by four retention latches, the load per latch is 850 lbs. Because of the wing tip skids, the degree of roll is limited to a few degrees, and thus the load across the frontal latches can become only slightly unsymmetrical. The maximum possible latch load is assumed to be 1000 lbs. The latches are fastened to the aircraft skin by three No. 10 bolts (0.19 inch diameter) as shown in the layout drawing discussed in Section 6.5. The aft two bolts of the forward four latches pass through the "Z" former. It is recommended that triangular members be attached to the formers just above the latches to react bending moments.

For analysis it is assumed that the 1000 lb latch load is carried by a 2024-T3 skin of 0.04 inches. With three bolts the load per bolt is 333 lbs. For a 0.19 inch diameter bolt and a 0.04 skin the bearing area is:

$$(0.04 \text{ in})(.19 \text{ in}) = .0076 \text{ sq. in.} \tag{35}$$

the bearing stress is then:

$$333 \text{ lbs}/0.0076 \text{ in}^2 = 43,816 \text{ psi} \tag{36}$$

The allowable for 2024-T3 which is a low strength aluminum is 92,000 psi. The margin of strength is greater than 2 to 1.

6.3.2 Retention/Release Actuation Loads

The retention/release latch and the moment model is shown in Figure 134(a) and 134(b). Balancing of the moments about the hook yields:

197
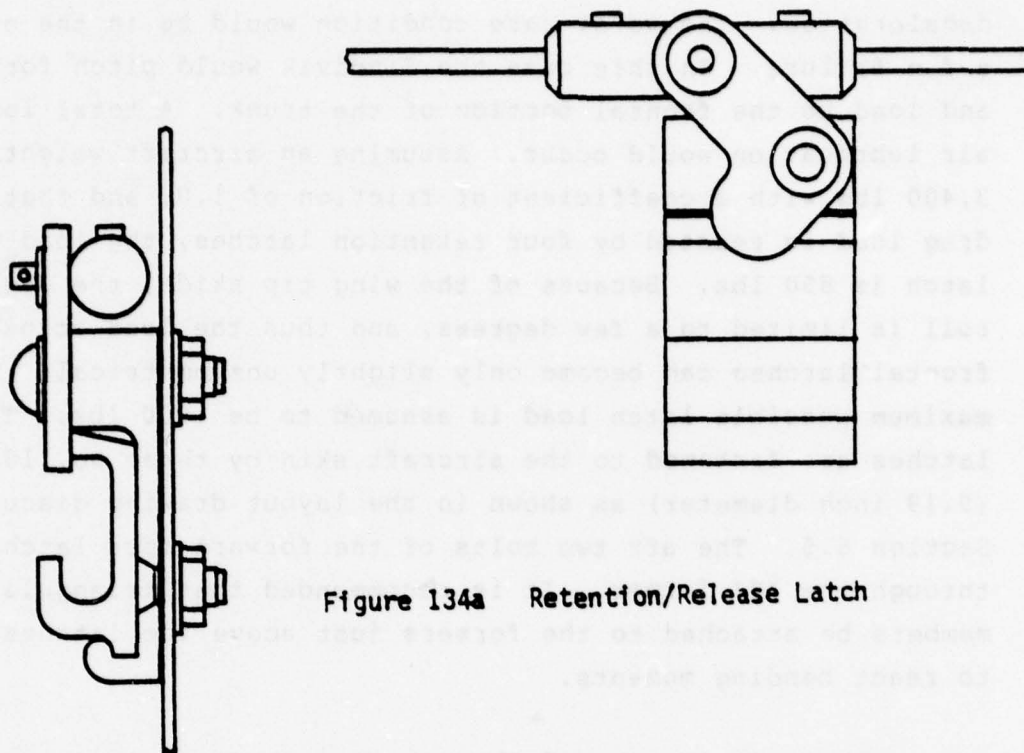
Figure 134a Retention/Release Latch

$F_t l_1 + F_l l_2 = 0$

$F_c l_3 + F_\mu l_4 = 0$

$F_\mu = F_l \mu$

$l_1 = 0.15''$
$l_2 = 1.05''$
$l_3 = 0.55''$
$l_4 = 0.5''$
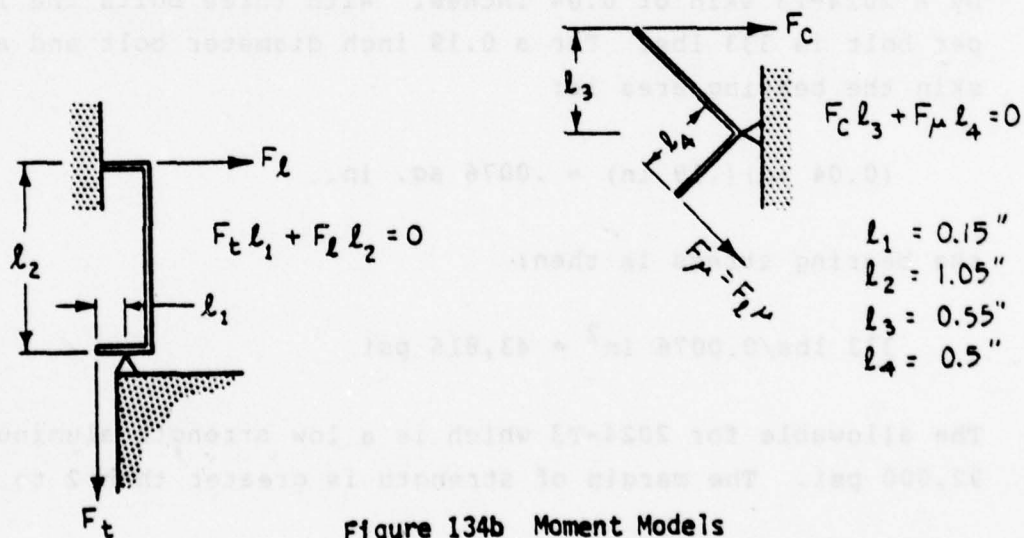
Figure 134b Moment Models

198

$$F_t \, \ell_1 + F_\ell \, \ell_2 = 0 \qquad (37)$$

Balancing out the initial moments for the swivel latch yields:

$$F_c \, \ell_3 + F_\mu \, \ell_4 = 0 \qquad (38)$$

where:

$$F_\mu = \mu F_\ell^{\dot{t}} \qquad (39)$$

and μ is the coefficient of friction between the swivel and the hook. Combining equations 37, 38 and 39 yields the cable tension to release the hook

$$F_c = \frac{\ell_1 \, \ell_4}{\ell_2 \, \ell_3} \, \mu F_t \qquad (40)$$

From the dimensions from Figure 134b the cable force is:

$$F_c = 0.13 \, \mu F_t \qquad (41)$$

The coefficient of friction for various material interfaces is given in the following table. For the worst case condition of aerodynamic drag of 146 lbs (See Equation 27) plus 120 lbs. of trunk weight for α = 0, the actuator load is given as shown in Table 7:

199

MATERIAL INTERFACE	COEFFICIENT OF FRICTION		FORCE	WORST CASE ACTUATOR LOAD (LBS)
	STATIC	SLIDING		
Aluminum-aluminum	1.05	1.47	$.18F_t$	47.8
Aluminum-steel	.61	.47	$.08F_t$	21.3
Teflon-steel	.04	.04	$.005F_t$	1.33
Teflon-teflon	.04	.04	$.005F_t$	1.33

TABLE 7   ACTUATOR LOADS

It is recommended that the catch be made of aluminum and the
swivel of steel. Assuming a cable tension spring on each side
with 10 lbs pull, the maximum actuation load for steel and
aluminum is then:

$$21.3 \text{ lbs} + 20 \text{ lbs} = 41.3 \text{ lbs} \tag{42}$$

6.3.3 Cable Stretch

There being two cables, one on each side of the aircraft, the
cable tension is one half the actuator load plus the cable
tension spring load. In evaluating cable stretch during
actuation, only the differential cable load is considered. The
differential cable load for each side will be 10.65 lbs. For
1/8 inch diameter cable of corrosion resistant steel
(MIL-C-5424), the EA (modulus of elasticity x cross sectional
area) is 106,000 lbs. The cable deflection is given by:

$$d = \frac{P\ell}{EA} \tag{43}$$

200

Assuming a 10.65 lb load at the end of a 150 inch cable:

$$d = \frac{(10.65)(150)}{106,000} = 0.015 \text{ inch} \tag{44}$$

The break strength of this cable is 1,760 lbs and the design strength is 1,495 lbs. Thus standard aircraft control cable is adequate.

6.4 SELECTION OF ACTUATOR

A review of linear actuators for releasing the ACTS trunk was conducted. Linear actuators with sufficient stroke rates are shown in Table 8. The Warner Electric actuator is an industrial unit produced in large numbers and hence very inexpensive. The stroke rate is nearly four times that of the more expensive Plessey aircraft actuator. Providing there is sufficient space in the Jindivik, the Warner actuator is recommended over the Plessey unit.

The Warner Electric actuator is used on helicopters to dump water buckets for putting out forest fires. The manufacturers were consulted in regard to running the 12 volt motor on 28 volts. Their experience shows that there would be no problem for the Jindivik application, where the loads are low and the stroke frequency is nil. However, testing at 28 volts with simulated maximum loads would be required to verify this.

201

TABLE 8 - LIST OF ACTUATORS

ACTUATOR	VOLTAGE	STROKE RATE in/sec	MAX LOADS lbs	WEIGHT lbs	LENGTH in	COST $
Warner Electric Model DCA-5JB (Ball Screw) [1]	12 VDC	1.9 at 50 lbs	500	10-12	15	100
Plessey Industries, Inc.						
Model L12 (1/4 ACME)	26 VDC	.5	150	1.3	7.3	1000
Model R585 (1/4 ACME)	26 VDC	.66	650	2.0	7.5	1000
Motion Controls	28 VDC	.4	?	2.0	6.45	1000
American Standard Wabco Pressure Master	None	[2]	Piston Area 1.5 in²	10	6.0	200 [3]
Wabco Pressure Master [4]	26 VDC	Choice	Piston Area 1.5 in²	10	8.0	1200
Ordnance Pin Pullers and Power Cartridges [5]	26 VDC	1.0	∞	0.1	1.0	3100
Ordnance Clamp Separation	26 VDC	–	–	0.2	–	500
Solenoid Actuators [6]	28 VCC	–	–	?	–	15

[2] Parallel mounted motor version also available
Jindivik Pneumatic System provides 575 psi air. With cylinder actuator piston area of 1.5 in², force will be 860 lbs.

[3] Price includes $100 for cost of 4 way valve for actuating cylinder for ground checkout. It is assumed that existing Jindivik solenoid valves can be used to activate system for jettison of trunk.

[4] Power cartridges from Hi-Shear Corp. testing would be required to ensure proper size of cartridge.

[5] Hi-Shear Corp. price includes testing of 2 items, 6 items would be shipped.

[6] Guardian Corp. – 1.0 inch stroke, 8.0 lb. pull at stroke initiation. 2.0 lbs. at 1/2 inch. Pull drops off rapidly with increasing stroke.

The second choice for an actuator system is pneumatic. The Jindivik utilizes a 575 psi system for flap and skid actuation. Air is stored aboard the Jindivik in a 2000 psi tank, and the required solenoid valves already exist aboard the aircraft. This system would be more aesthetic aboard the Jindivik, and is also low in hardware costs. However, the cost of duplicating the Jindivik pneumatic system for system development could be considerable.

6.5 RETENTION/RELEASE SYSTEM DESIGN

The overall design of the Retention/Release System for the ACTS trunk is shown in Figure 135. The external linkage of the retention hook is somewhat crude in appearance; however, for the Jindivik ACLS demonstration aircraft this is not critical. This system is recommended as having the minimum cost and requiring little modification of the aircraft and ACTS trunk. The required modifications to the Jindivik are:

o   1/2 inch hole on centerline at station 55.0 for cable
     passage through fuselage skin
o   Four 0.2 inch diameter holes in skin above hole to bolt
     on nylon rub blocks
o   Three 0.2 inch diameter holes on each side of fuselage
     to bolt on pulley support bracket
o   66 0.2 inch diameter holes for bolts fastening 22
     latches
o   Four 0.2 inch diameter holes for bolts fastening cable
     tension spring flange
o   Cutout in former for actuator at body station 67
o   Installation of actuator support web between formers of
     body stations 67 and 76.50.
o   Gussets installed at each location of the front four
     latches to react latch moments

203

GUSSET

EXISTING FORMER

VEHICLE SKIN

LATCH BASE

56.35
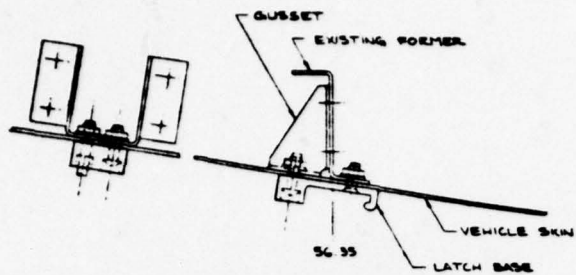
LATCH REINFORCEMENT DETAIL
REQD @ 4 FWD LATCHES ONLY

VEHICLE ℄
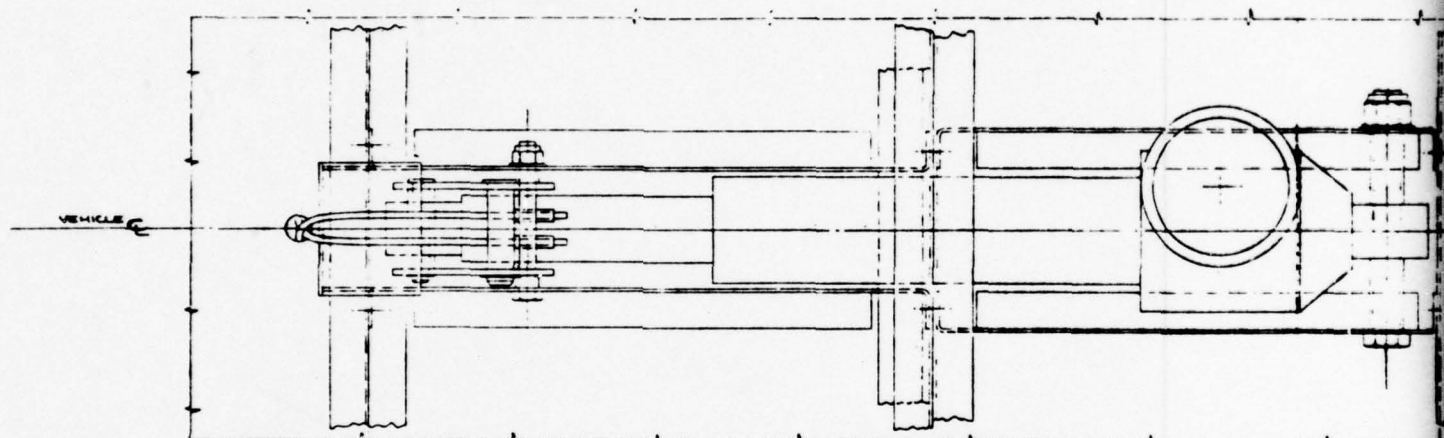
DETAIL E
PLAN VIEW – ACTS ACTUATOR INSTL
FULL SIZE

LEVER (2 REQD)

CONVEX AL CABLE SLIDE

MS 20392 TYPE PIN DRILLED TO ACCEPT CABLE

LEVER SUPPORT WEB (2 REQD)

1" CABLE TRAVEL

ACTUATOR SUPPORT WEB (2 REQD)

2.375 HOLE THRU FORMER

DC LINEAR ACTUATOR
WARNER ELECTRIC DCA-8 J8

SEE DETAIL B-B
FOR CONTINUATION

4" ACTUATOR STROKE

56.35

62.00

VEHICLE SKIN

SLOT TO ENGAGE RETENTION/RELEASE HOOK

HOOK HOLES TO FACILITATE CUSHION INSTL

AL TAB BONDED TO GIRT

GIRT TAB DETAIL
FULL SIZE

⅛" DIA RELEASE CABLE
— FERRULE (⅛" SCH 80 AL PIPE)
— BELLCRANK
— #8 SETSCREW (2 REQD)

#10 RD HEAD MACH SCREW
— ⅛" PIN W/ WASHER & COTTER PIN

FERRULE DRILLED TO INSERT PIN

SPACER

3/16" DIA HOLE THRU
TOP LEG OF BASE

1/16" WIDE SAW SLOT
INTO HOLE

BASE

#10 FLAT HEAD MACH SCREW

HOOK

#10 LOCK NUT (3 REQD)

⅛" DIA ROLL PIN
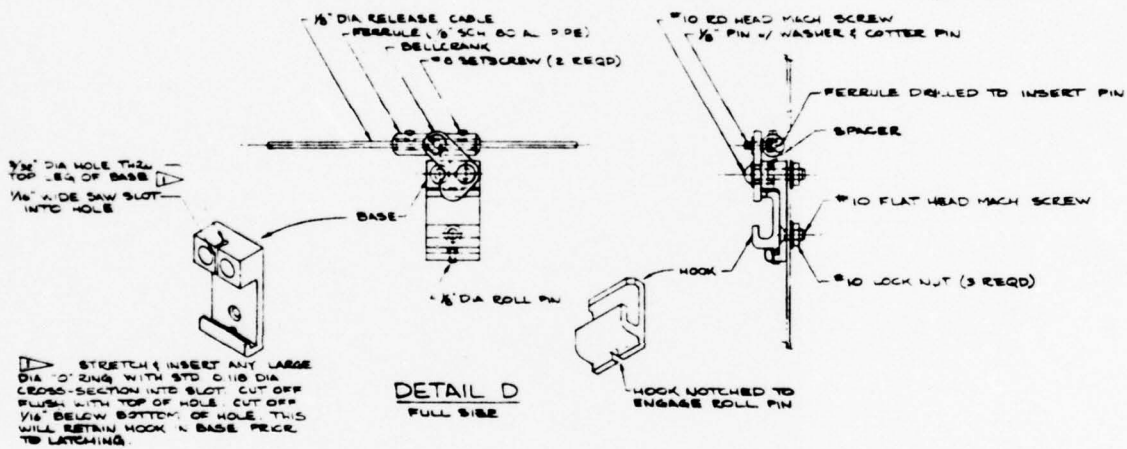
DETAIL D
FULL SIZE

▷ STRETCH & INSERT ANY LARGE
DIA "O" RING WITH STD 0.110 DIA
CROSS-SECTION INTO SLOT. CUT OFF
FLUSH WITH TOP OF HOLE. CUT OFF
1/16" BELOW BOTTOM OF HOLE. THIS
WILL RETAIN HOOK & BASE PRIOR
TO LATCHING.

HOOK NOTCHED TO
ENGAGE ROLL PIN

STA 0.00   16.00   30.7

DETAIL
FULL S

B-B

RUB STRIP

INTERNAL NYLON RUB BLOCK

B-B
FULL SIZE

56.25

76.50

A-A
FULL SIZE

NYLON

2
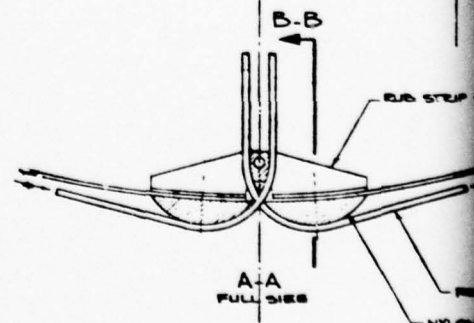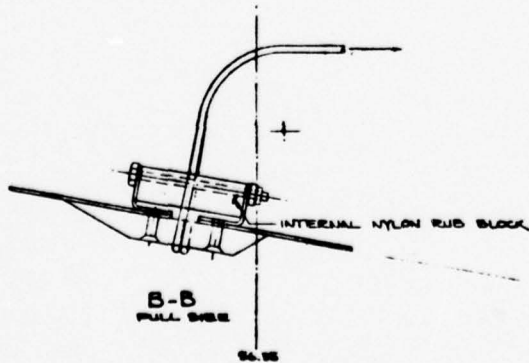
SEE
DETAIL C

SEE
DETAIL D

AL SHEET BONDED TO INSIDE OF
TRUNK GIRT FLAP TO ENGAGE HOOK

LE

3075   4850   5835   6700   7650   8700   10170   12945

PULLEY SUPPORT BRACKET
& FAIRING

SEE DETAIL E FOR ACTUATOR
INSTL IN THIS AREA.

TAKEOFF TRUNK GIRT

DETAIL C
FULL SIZE

A-A

RUB STRIP SUPPORT BRACKET

BOT

RELEASE CABLE

NYLON RUB STRIP

TAKEOFF TRUNK

3

CABLE ROUTED INBD OF FLAP & OUTSIDE OF SKIN.
EXACT CABLE ROUTE (ABOVE VS BELOW FLAP
TORQUE TUBE) TO BE DETERMINED.

TO INSIDE OF
ENGAGE HOOK

FUSELAGE DATUM

2" WIDE VELCRO

LEFT SIDE VIEW
RIGHT SIDE SIMILAR

148.2   162.00   163.50   187.00   214.50   242.00

SECTION @ 148.12

VEHICLE ₵

BOTTOM VIEW

LANDING TRUNK GIRT (REF.)

Figure 135   ACTS Trunk Retention
Release System

205

4

The modifications required for the ACTS trunk are:

o   Removal of the velcro strip

o   The bonding of 22 tabs

The Warner Electric Actuator was chosen primarily for its high
stroke rate of 1.9 in/sec. Figure 135 (detail E), shows the
four inch stroke of the actuator reduced to a one inch stroke
through the lever arm, and thus the stroke rate is reduced to
0.475 in/sec. It is desirable to have the maximum stroke rate
to reduce the risk of or degree of unsymmetrical unlatching.
The Warner Electric actuator stroke could be reduced to 1.0 inch
by installing a limit switch. The cable could then be pulled
directly to provide a stroke rate of 1.9 in/sec.

A potential problem exists that may cause one or more latches to
bind during release. If the opening of one side latch lags the
opening of all the other latches, the total aerodynamic drag
load will be supported by that one latch. The load will be to
the side and will also be coupled with a torque. A single latch
should be built and tested for various load conditions. If
testing shows that binding occurs, the problem may be overcome
by the side latch design shown in Figure 136.

6.6 ACTS LATCH PROCEDURE

The retention/release system design shown in Figure 135 dictates
that the latch hooks be placed and fixed in their receptacles
before the trunk flanges are attached. An alternate procedure
was developed where the hooks are inserted into the trunk first.
This latter procedure provides for a tighter fit. This
procedure for ACTS trunk attachment is described as follows:

a)   The latch hook is inserted into the appropriate slot in
     the trunk flange.

CABLE
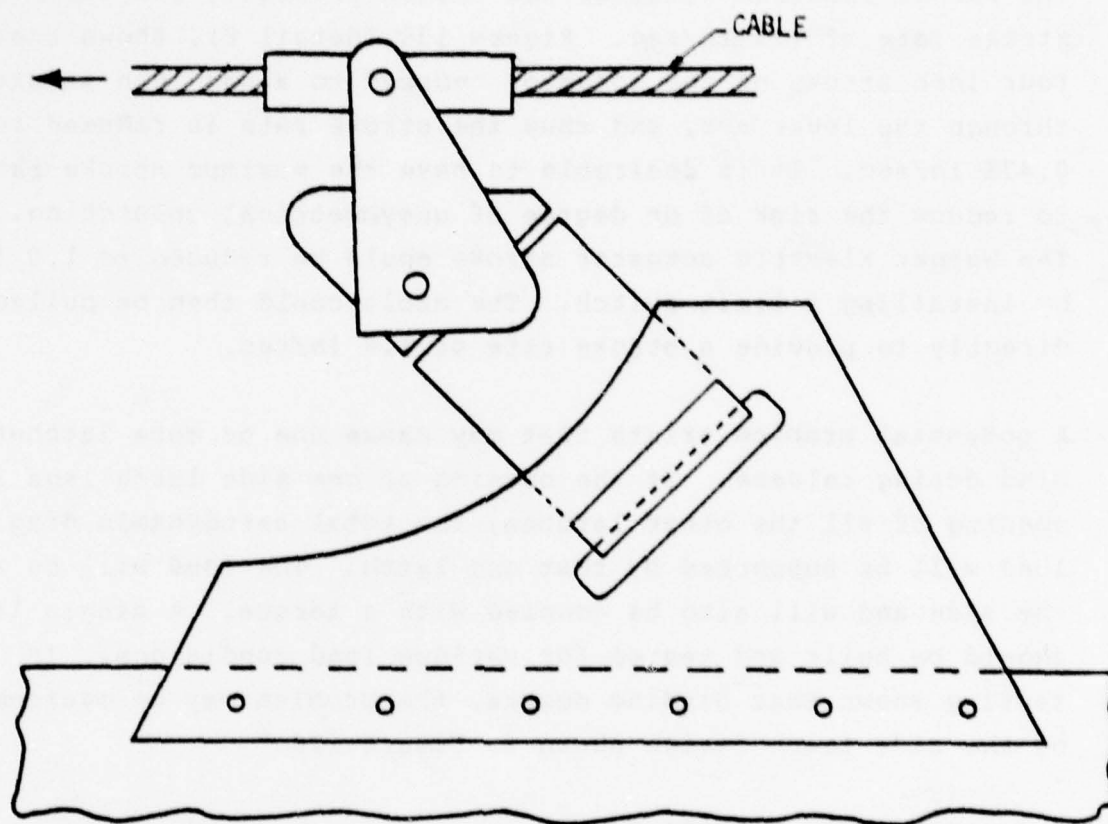
Figure 136 Secondary Side Latch Configuration

b) The special tool shown in Figure 137a is inserted into the hook and flange as shown in Figure 137b.

c) The hook is then placed into the corresponding receptacle as shown in Figure 137c and the tool is used to torque the hook into place.

d) The temporary pin is installed as shown in Figure 137c. This pin should be flagged for visibility, to insure removal before flight.

e) After all latches have been put in place, the actuator is reversed such that the bell cranks lock the latch hooks in place.

f) The temporary pins are then removed.
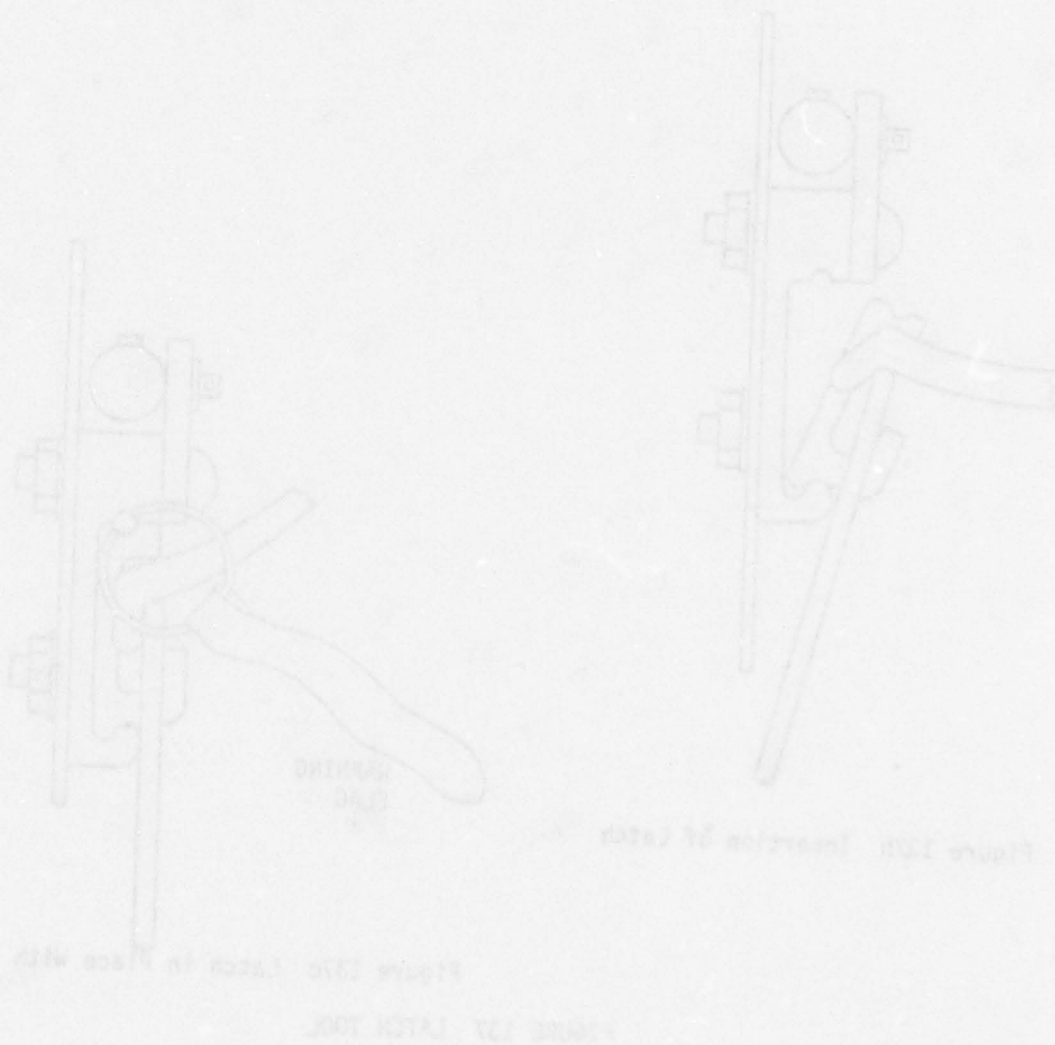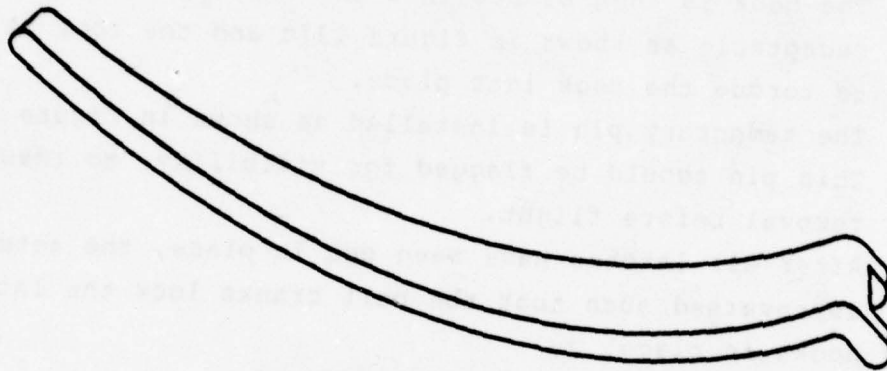
Figure 137a Latch Tool
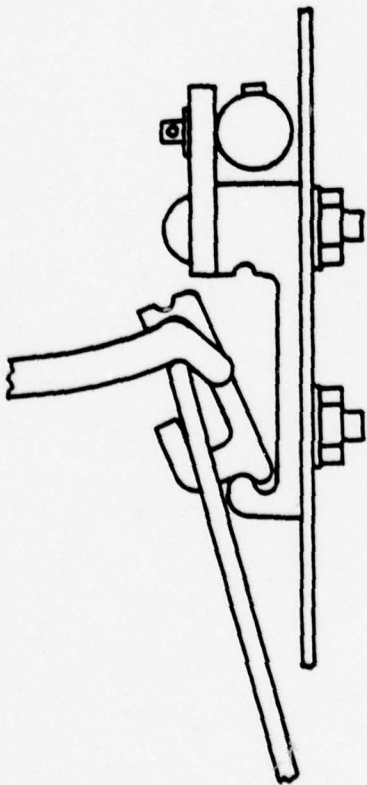
Figure 137b Insertion of Latch

WARNING
FLAG
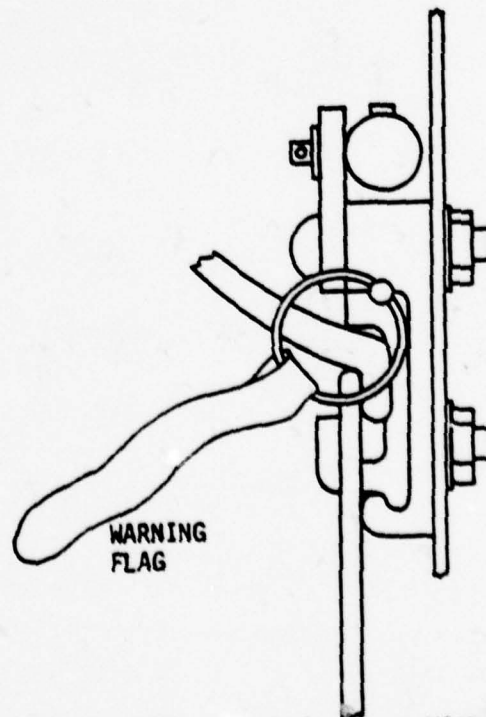
Figure 137c Latch in Place With Temporary Pin

FIGURE 137 LATCH TOOL

210

GROUND TESTS

A series of ground tests were conducted at the GAF Avalon Field
facility. The tests were run by GAF under Contract to AFFDL.
AFFDL representatives were present for the majority of the
tests.

The major objective of these tests was to demonstrate safe,
stable low speed taxi on both the ACRS and ACTS trunks. High
speed taxi tests were to be run at a later date and under a
separate contract. Specific results that were to have been
obtained under this initial contract are as follows:

a. Checkout of the ACLS subsystems and components, namely:

    Air flow subsystem
    Directional control subsystem
    ACRS and ACTS trunks

b. Demonstration, including movie film, of safe, repeatable,
    controllable taxi operation on both trunks and on various
    surfaces.

c. Acquisition of data to determine performance and support the
    analyses of Jindivik lift-off, touchdown, and slideout which
    are an integral part of the flight preparation and flight
    test plans.

The Boeing Company's role in the ground tests was as a technical
consultant. The specific tasks were to analyze test results,
troubleshoot problems through system simulations and recommend
test procedures.

7.1 GROUND TEST EVALUATION

As is usual in the development testing of a new aircraft system,
several unexpected problems arose during the course of the
ground tests. The ground tests were scheduled to have been run
in May and June 1975, but in fact continued intermittently
through calendar year 1976. The major problems encountered
during the testing were as follows:

a. ACRS trunk design

   During initial testing of the ACRS #2 trunk out of ground
   effect, the trunk failed at a normal operating pressure (2
   psig). The ACRS #3 trunk which was used for some subsequent
   testing, and which is approximately 1 foot shorter than the
   ACRS #2 trunk, increases the pitch stability problem which
   is discussed below. Use of a structurally improved ACRS #2
   trunk design is recommended for any further testing.

b. ACTS trunk design

   The velcro attachment and release design was found to be
   unsatisfactory in its ability to hold the leading edge under
   all conditions. A positive retention/release system,
   similar to those discussed in Section 6, is recommended.
   For a production vehicle, the positive system need only
   extend around the leading edge of the ACTS trunk girt. For
   a test vehicle, however, in which deceleration on the ACTS
   trunk will occur, the positive system should extend around
   the whole girt.

c. Airflow system

   As discussed in detail in Section 2, trunk and cushion
   pressures were lower than originally predicted. The effect
   of a low cushion pressure is to cause more load to be

212

carried by the trunk, and hence to increase trunk drag.
This in turn can increase vehicle pitch and roll moments.
The effect of a lower trunk pressure is to reduce the
capability of the ACLS to react pitch and rolling moments.
Potential solutions to this problem are discussed in Section
2. Redesign of the bleed port fitting and flexible ducting
will achieve some improvement at modest cost. A major
improvement could be achieved, at considerable cost, with an
alternate center section on the Viper engine.

d. Pitch and roll stability

Problems were encountered with roll stability, and with
excessive forward pitching during deceleration. These
problems may disappear if the recommendations in the above
paragraphs are adopted, and correct procedures are used. It
is possible that a drogue chute may be required to limit
forward pitching, and ensure directional stability, during
ACTS and ACRS deceleration.

e. Directional control

Some problems were encountered with vehicle directional
control. With the low trunk and cushion pressures
experienced during the tests, activation of the yaw thruster
tended to cause the vehicle to roll. This in turn increased
trunk drag and hence induced yaw moments opposing the yaw
thruster action. In some tests the vehicle roll, induced by
other factors as well as by the yaw thruster, caused wing
tip skid contact. The skids imparted sudden and substantial
yawing moments to the vehicle. This problem was
substantially alleviated by the addition of small wheels
with adjustable brakes to the tip skids.

213

7.2   SUBSYSTEM EVALUATION

AIRFLOW SYSTEM

Initial tests of the Jindivik airflow distribution system at GAF
were run with the system Out of Ground Effect (OGE).   The test
results showed that the performance of the airflow system was
substantially below prediction.   Subsequently, leaks were
discovered at the joint between the girt and the aircraft, and
at the O ring of the trunk relief valve seal.   These were
repaired and the tests were repeated.   Additional tests were run
with the system In Ground Effect (IGE) and low speed taxi
conditions.

Considerable difficulty was encountered in getting repeatable
and consistant data (mainly pressures) in the airflow system
tests.   As discussed in Section 2, it is believed that the drive
(turbine inlet) pressures measured on ACRS #3 are in error.

All tests were run with the valves in the airflow system wide
open or fully closed.   The only changes made to the system
during testing consisted of blocking off some of the holes in
the ACRS trunk and inserting restrictors in the supply line to
the trunk.   Such changes increase cushion pressure and (in some
cases) trunk pressure too, but only at the expense of decreased
lubrication.   The achievement of adequate trunk pressure,
cushion pressure and trunk flow are all necessary to give
satisfactory ACRS and ACTS taxi performance.   Based on test data
obtained at GAF, it does not appear that overall improvements
can be achieved by such means.   If a new Viper center section
were to be installed, then it is probable that the overall
system performance could be improved by modulating the valve in
the trunk line, or alternatively inserting a fixed orifice.
This is discussed more fully in Section 2.

214

THRUST VECTOR SYSTEM

The adequacy of the thrust vector system is hard to assess from the testing carried out to date. No problems were encountered in the control systems for the thruster. The problem discussed in Section 7.1, namely trunk drag induced yaw moments opposing the yaw thruster, is believed to be the result of the unsatisfactory performance of the airflow system rather than the thruster system.

ACTS AND ACTS TRUNKS

The major problems with the trunks were structural, as discussed above. The trunks exhibited good stability, with only minimal flutter. No other unwanted dynamic effects were observed. Two ACRS trunk designs were tested. ACRS #3 was shortened from the original design to give the flexibility to permit launching *Jindivik from the existing trolley system*. This could be desirable in the event that launching on the ACTS was not possible for any reason. However, the decrease in pitch stiffness with the shortened trunk is significant, and thus the original design is recommended.

7.3   TEST PROCEDURES

Details tests procedures for the low speed ground tests on the ACRS and ACTS were developed, and are shown in Appendix C.

SECTION 8

CONCLUSIONS AND RECOMMENDATIONS

1. The major activity in this phase of the development of
    Jindivik ACLS has been the running of a series of ground
    tests by GAF at their Avalon Field facility. The
    difficulties in conducting developmental testing at a
    location so remote from the AFFDL and its contractors are
    self evident. The resulting communication problems, coupled
    with the lack of adequate travel fund authorization, have
    been the major causes of the delays experienced in the past
    eighteen months. Various options are available to avoid or
    minimize these problems, as follows:

    a. Conduct tow tests in the U.S., using a Jindivik shell
        and with a tow vehicle containing an air source,
        electrical power system and data acquisition system.
        This test rig would be used to obtain basic information
        on the airflow system, trunk drag, trunk stiffness and
        damping, and the resulting vehicle dynamics.

    b. Buy or lease the Jindivik test vehicle from GAF and run
        low speed ground tests in the U.S. The test vehicle
        should have sufficient instrumentation to obtain data as
        in a. above.

    c. Conduct further low speed ground tests at Avalon Field,
        with an experienced representative from AFFDL present
        for the duration of the tests, and with adequate spares.

Regardless of the options listed above, it is recommended that
high speed taxi tests and flight tests should be monitored by
GAF because of the availability of experienced crews. It is

recommended that a crew training plan be established by AFFDL and GAF, and implemented by GAF, before high speed taxi and flight tests.

2. The performance of the airflow system is marginal. More test data are still required, but it appears that some improvement could be gained by redesign of the bleed port fitting and by replacement of the flexible ducting. A significant improvement could be obtained by use of a Viper engine with a MK 522 center section. This latter change would permit fan-on landings, and hence reduce the pitch problems (discussed below) and give controllable braking.

3. No significant problems have been encountered with the yaw thruster directional control system. During testing at GAF, outrigger wheels were fitted to the wing tips, with the brakes linked electrically to the heading gyro. This improved directional control during low trunk pressure (high drag) conditions when the vehicle had a tendency to roll.

4. Structural problems were encountered with the ACRS trunk design. It is believed that these problems have since been resolved. The ACRS #2 design is preferable to ACRS #3 because of the increased pitch stiffness exhibited by ACRS #2.

5. The ACTS trunk suffered from parking bladder leakage problems, and from excessive wear in the front of the trunk during deceleration. It is recommended that segmented parking bladders be used, with a high pressure in the front segment; also that the wear strips in the front be extended forward.

6. Trunk vibration is not a significant problem. Some flutter has been observed, but the amplitude of the vibration is acceptable.

217

7. The ACTS retention/release system is unsatisfactory.
   Retention capability is inadequate under certain loading
   conditions, and release tends to be asymmetrical and is not
   repeatable. A bellcrank latching system, released by an
   electrical linear actuator, is recommended.

8. The Jindivik is directionally unstable with the ACRS trunk
   deployed even with the extended tail tested by GAF. It
   should be noted that the wind tunnel data were obtained with
   an IGE trunk shape, which is unrealistic. Further wind
   tunnel tests should be run with an OGE trunk of the latest
   ACRS design. Two additional fin designs should be tested,
   namely a longer fin of 10.5 ft^2, and fins fitted to the tips
   of the horizontal tail. It should be noted that the
   additional fin area will degrade the effectiveness of the
   yaw thruster.

9. Simulation studies show that with the baseline ACRS design,
   a large forward pitching moment occurs at touchdown.
   Depending on the degree of damping, this induces a combined
   pitch-heave oscillation. It is recommended that initial
   landings be on grass, to reduce the coefficient of friction.
   Fan-on landings (see (2) above) might also help. Further
   ground testing is required to evaluate the magnitude of this
   problem.

10. Further simulations of touchdown and slideout, including the
    elevators and associated control system, should be
    conducted.

11. The ACTS has not been designed for braking from high speeds.
    During deceleration the aircraft will pitch nose down, and
    the air lubrication will not be effective on the forward
    portion of the trunk. This may lead to the center of drag
    being forward of the center of gravity, and the vehicle will

be directionally unstable. Consequently, a drogue chute is
recommended for high speed (greater than 20 to 30 knots)
ACTS ground tests.

APPENDIX A

ECSS-X COMPUTER PROGRAM

221

The Environmental Control System Simulator - Extended Version
(Ref. 1) is a digital computer program which solves problems in
the steady-state performance analysis of any fluid flow system.
The program is arranged in a form allowing a series of system
components to be linked together to form a complete system. A
problem oriented language (POL) is used to describe the physical
components and control restraints on the system. A non-linear
equation solver (INWT) is used to solve the system for a given
set of boundary conditions by formulating it as a weight flow
balance of a flow network. By inserting tables of component
performance characteristics, any type of component may be
included.

The program consists of three separate and distinct parts, each
of which is completely independent of the other, viz.,

   o A special purpose precompiler which translates the input
     configuration data into a Fortran program and subroutine.

   o An equation solving algorithm based on the n-dimensional
     Newton-Raphson method "INWT".

   o A set of subroutines simulating the performance
     characteristics of physical system components.

The ECSS system has two executions. The first one is the
preprocessor phase during which the system definition cards are
read in and operated upon to generate a Fortran main program and
a linkage subroutine required to represent the physical system.
The second phase is the execution of the generated program, the
reading in of tables, title cards, execution control cards and
solving the data case using a non-linear algebraic equation
solver. Operating subroutines simulating engineering components
are loaded from a library or magnetic tape. Ancillary user

222

written Fortran subroutines may also be loaded, the program
being designed in an open-ended and modular mode.

The following tables show inputs to the program for typical ACRS
and ACTS simulations. Table A-1 shows the ACRS system
description in POL form. The airflow system is divided into two
sections, each started and terminated by a SEC card. Section 1
goes from the engine to the flow split and thence to the trunk.
Section 2 starts at the flow split and goes to the cushion.
Each POL card within a section results in a call to a subroutine
which models a specific type of component, as described later.
For example, ENG models an engine, POR models an engine bleed
port, and so on. Parameter values can be included in each POL
statement, or can be set (and changed for subsequent cases if
required) as shown in Table A-1. The three SAC cards define the
inputs to the non-linear equation solver INWT in order to
balance out the system. In this case the three unknowns are the
bleed air flow rate Wl (SAC1), the cushion pressure PCUSHG
(SAC2) and the flow split PCT at the Y junction (SAC3). These
quantities are varied in INWT in order to balance the system and
satisfy all the boundary conditions.

Table A-2 shows the input tables for the ACRS, as follows:

TABRV	Relief valve characteristics, area versus pressure.
TABPO	Engine bleed port characteristics, corrected flow versus fractional pressure drop.
TABWTU	Turbine flow characteristics, corrected flow versus pressure ratio.
TABDT	Engine compressor relative temperature rise as a function of engine speed.
TABDP	Engine compressor internal pressure ratio as a function of engine speed.
TABTOT	Fan flow as a function of drive pressure and cushion pressure.

```
SAC1 (WERR,0.,.1,WMIN,WMAX,W1,0.)
SAC2 (WERCU,0.,.1,0.,0.90,PCUSHG,0.)
SAC3 (WA,WT,.1,SPMIN,SPMAX,PCT,0.)


SEC1 (PAMB,TAMB,HAMB,W1)
 ENG (TABOT,TABDP,AMN,SPEED)
 POR  (TABPO)
 LNKT1(AKPF,7.07)
 LNKD1(.59,7.07)
 LNKB1(.478,7.07)
 SPL  (PCT,PA,TA,HA,WA)
LNKD2(.178,7.07)
 LNKV1(1.,AV1)
LNKB2(.015,7.07)
 LNKBA(1.,7.07)
 BAG  (TABRV,ACUSH,AATM,CD,PCUSHG,PAMB,WERR,WIN)
SEC1 (PO1,TD1,HO1,WD1)


SEC2 (PA,TA,HA,WA)
 LNKD3(AK,7.07)
 LNKV2(1.,AV2)
 LNKD4(AK,7.07)
 TRF  (TABWTU,TABTOT,PCUSHG,PAMB,TAMB,WT)
 CUS  (PCUSHH,FLOW1,WIN,PCUSHG,WERCU)
SEC2 ( )


PAMB=14.7,TAMB=519.,HAMB=0.,AMN=0.,ACUSH=2.418,AATM=2.418,CD=0.7,
SPEED=0.4,PCUSHH=0.65,FLOW1=140.
AK=0.4,
W1=40,PCT=50,PCUSHG=0.30,
AV1=6.15, AV2=6.15,
WMIN=20.,WMAX=310.,SPMIN=0.,SPMAX=60.,
AKPF=2.
```

Table A-1 Main Program (ACRS)

```
READ TABLES5
TABRV          1.    4.                          1.
0.    259.2  360.   1000.
0.    0.     21.6   21.6
TABPQ          1.    10.                         1.
0.    76.5   101.   126.   143.   151.   158.   161.   163.   170.
0.    .0476  .0909  .1667  .2308  .2857  .3333  .3750  .4444  .9
TABWTU         1.    13.                         1.
1.00  1.10   1.20   1.30   1.40   1.50   1.60   1.70   1.80   1.90
2.00  2.50   10.00
0.    .925   1.120  1.240  1.325  1.380  1.415  1.430  1.435  1.440
1.440 1.440  1.440
TABDT          1.    11.                         1.
0.    .35    .40    .50    .60    .70    .80    .90    1.0    1.1
1.2
0.    .08    .12    .17    .23    .31    .40    .50    .625   .775
.94
TABDP          1.    11.                         1.
0.    .35    .40    .50    .60    .70    .80    .90    1.0    1.1
1.2
1.    1.19   1.26   1.415  1.660  2.000  2.564  3.100  3.800  4.400
5.00
TABTOT         2.    -24.   -19.                 1.    1.
120.  110.   100.   90.    80.    70.    60.    55.    50.    45.
40.   35.    32.5   30.    27.5   25.    22.5   20.    17.5   15.
12.5  10.    7.5    5.0
15.   15.1   15.2   15.3   15.4   15.5   15.6   15.8   16.    16.2
16.4  16.6   17.2   17.7   18.2   18.7   19.7   22.7   25.7
0.    0.     0.     0.     0.     0.     0.     0.     0.     0.
0.    0.     0.     0.     0.     0.     0.     0.     0.     0.
0.    1.2    1.33   1.68
0.    0.     0.     0.     0.     0.     0.     0.     0.     0.
0.    0.     0.     0.     0.     0.     0.     0.     0.     0.
0.    1.54   1.83   2.04
0.    0.     0.     0.
0.    0.     0.     0.     0.     0.     0.     0.     0.     0.
1.42  1.76   2.04   2.21
0.    0.     0.     0.     0.     0.     0.     0.     0.     0.
0.    0.     0.     0.     0.     0.     0.     0.     0.            1.45
1.80  2.08   2.27   2.42
0.    0.     0.     0.     0.     0.     0.     0.     0.     0.
0.    0.     0.     0.     0.     0.     0.     0.     1.57   1.88
2.16  2.34   2.48   2.60
0.    0.     0.     0.     0.     0.     0.     0.     0.     0.
0.    0.     0.     0.     0.     0.     1.42   1.72   2.06   2.24
2.43  2.57   2.70   2.78
0.    0.     0.     0.     0.     0.     0.     0.     0.     0.
0.    0.     0.     0.     0.     1.60   1.92   2.15   2.36   2.54
2.68  2.80   2.90   2.94
0.    0.     0.     0.     0.     0.     0.     0.     0.     0.
0.    0.     1.70   1.98   2.24   2.43   2.62   2.76   2.89   3.01
3.11  3.19   3.24   3.25
0.    0.     0.     0.     0.     0.     0.     0.     0.     0.
0.    2.16   2.41   2.58   2.73   2.88   3.01   3.13   3.23   3.33
3.42  3.50   3.51   3.52
0.    0.     0.     0.     0.     0.     0.     0.     0.     0.
```

Table A-2 Table Inputs (ACRS)

2.36	2.74	2.88	3.02	3.13	3.25	3.36	3.47	3.55	3.64
3.73	3.76	3.77	3.78						
0.	0.	0.	0.	0.	0.	0.	0.	0.	2.52
2.90	3.16	3.27	3.38	3.49	3.59	3.69	3.78	3.87	3.96
4.02	4.03	4.04	4.05						
0.	0.	0.	0.	0.	0.	0.	0.	2.64	3.04
3.32	3.53	3.64	3.74	3.83	3.92	4.01	4.09	4.13	4.27
4.28	4.29	4.30	4.31						
0.	0.	0.	0.	0.	2.75	3.50	3.70	3.90	4.07
4.23	4.37	4.42	4.47	4.52	4.57	4.63	4.70	4.71	4.72
4.73	4.74	4.75	4.76						
0.	0.	0.	0.	3.0	3.9	4.3	4.55	4.62	4.75
4.88	5.0	5.06	5.12	5.16	5.20	5.25	5.30	5.31	5.32
5.33	5.34	5.35	5.36						
0.	0.0	2.0	3.65	4.20	4.60	4.90	5.10	5.25	5.40
5.5	5.6	5.65	5.7	5.71	5.72	5.73	5.74	5.75	5.76
5.77	5.78	5.79	5.80						
0.	3.50	4.18	4.61	4.93	5.20	5.43	5.55	5.66	5.75
5.85	5.94	5.99	6.04	6.05	6.06	6.07	6.08	6.09	6.10
6.11	6.12	6.13	6.14						
4.9	5.2	5.45	5.70	5.90	6.10	6.28	6.39	6.45	6.55
6.63	6.65	6.67	6.69	6.71	6.73	6.75	6.77	6.79	6.81
6.83	6.85	6.87	6.89						
7.40	7.55	7.68	7.83	7.95	8.07	8.20	8.25	8.30	8.32
8.34	8.36	8.38	8.40	8.42	8.44	8.46	8.48	8.50	8.52
8.54	8.56	8.58	8.60						
9.17	9.30	9.40	9.52	9.63	9.75	9.77	9.79	9.81	9.83
9.85	9.87	9.89	9.91	9.93	9.95	9.97	9.99	10.01	10.02
10.03	10.04	10.05	10.06						

Tables A-3 through A-8 show component subroutines for the ACRS. Subroutine ENG (Table A-3) calculates the engine internal total pressures and temperatures, given the engine speed and vehicle Mach number. Subroutine POR (Table A-4) calculated the engine bleed port pressure drop ($\Delta P/P$) as a function of corrected flow ($W_b \sqrt{T}/P$). Subroutine LNK (Table A-5) calculates the pressure drop in ducting sections, based on an input of the pressure drop K factor ($K = \Delta P/q$, where q is the dynamic head). Subroutine TRF (Table A-6) calculates the turbofan performance, based on steady state performance maps input in tabular form. Subroutine BAG (Table A-7) calculates the inflow and outflow characteristics of the trunk, including outflow to the cushion volume and to ambient through the holes in the ACRS trunk, and also the relief valve flow. Subroutine CUS (Table A-8) calculates the flow characteristics of cushion air under the trunk.

Table A-9 shows the ACTS system description in POL form. The majority of the component subroutines are identical to those for the ACRS, and hence are not repeated. The turbofan, trunk and cushion subroutines are, however, slightly different, and are shown in Tables A-10 through -12 respectively.

```
      SUBROUTINE ENG(TABDT,TABDP,AMN,SPEED)
      COMMON/CURVAL/P,T,H,W/PRNT/PRNT/IO/IO/NOMEN/NOMEN/DEGREE/DEG(3)
      LOGICAL PRNT
C     CALCULATE  TOTAL PRESSURE AND TEMPERATURE AT ENGINE NLET
      PT=P*(1.+.2*AMN*AMN)**3.5
      TT=T*(1.+.2*AMN*AMN)
C     CALCULATE  PRESSURE AND TEMPERATURE AT EXIT FROM ENGINE CCMPRESSOR
      ENC=SPEED*SQRT(519./TT)
      DTOT=TBL(TABDT,ENC,DEG,IER)
      T=TT*(1.+DTOT)
      PR=TBL(TABDP,ENC,DEG,IER)
      P=PT*PR
      IF(PRNT) WRITE(IO,9999) NOMEN,P,T,H,W
 9999 FORMAT(14X,A10,3X2HPT5X,6X2HTT5X,6X1HH6X,6X1HW/21X,4(F10.4,3X)/)
      RETURN
      END
```

Table A-3   Engine Model

228

```
      SUBROUTINE POR(TABPO)
C    TABLE GIVES PORT DPOP=F(CORRECTED FLOW)
      COMMON/CURVAL/P,T,H,W/PRNT/PRNT/IO/IO/NOMEN/NOMEN/DEGREE/DEG(3)
      LOGICAL PRNT
      WCOR=W*SQRT(T)/P
      DPOP=TBL(TABPO,WCOR,DEG,IER)
      P=P*(1.-DPOP)
      IF(PRNT) WRITE(IO,9999) NOMEN,WCOR,DPCP,P
 9999 FORMAT(14X,A10,3X4HWCOR3X,6X4HDPOP3X,6X1HP/21X,3(F10.4,3X)/)
      RETURN
      END
```

Table A-4 Bleed Port Model

```
      SUBROUTINE LNK(AK,A)
      COMMON/CURVAL/P,T,H,W/PRNT/PRNT/IO/IO/NOMEN/NOMEN/SGGGOR/SGG
      LOGICAL PRNT
C    CALCULATES PRESSURE DROP GIVEN K FACTOR AND AREA
C    MACH NUMBER IS FIRST CALCULATED, THEN DYNAMIC HEAD IS DETERMINED (J)
C    OP=K * Q
      P=AMAX1(P,.001)
      GM=W*SQRT(T)/(A*P*SQG)
      AM=TAMGM(GM)
C    AM=MACH NUMBER
      PS=P/(1.+.2*AM*AM)**3.5
      AQ=P-PS
      OP=AK*AQ
      P=P-DP
      IF(PRNT) WRITE(IO,9999) NOMEN,P,T,W,DP
 9999 FORMAT(14X,A10,3X2HPT5X,6X2HTT5X,6X1HW6X,6X2HDP/21X,4(F10.4,3X)/)
      RETURN
      END
```

Table A-5 Ducting Element Model

230

```
      SUBROUTINE TRF(TABWTU,TABTOT,PCUSHG,PAMB,TAMB,WT)
      COMMON/CURVAL/P,T,H,W/PRNT/PRNT/IO/IO/NOMEN/NOMEN/DEGREE/DEG(3)
      DIMENSION S(2)
      LOGICAL PRNT
C     PURPOSE - CALCULATES THE PERFORMANCE OF AN ACLS TURBO-FAN USING
C                     PERFORMANCE MAPS
C     CALCULATE TURBINE FLOW
      PCUSHA=PAMB+PCUSHG
      PCUSHA=AMAX1(PCUSHA,.001)
      PRT=P/PCUSHA
      WTCOR=TBL(TABWTU,PRT,DEG,IER)
      WT=WTCOR*1.55*P/SQRT(T)
C     1.55=SQRT(519)/14.7      WT IS IN LB/SEC
C     WT IS CALCULATED VALUE OF TURBINE FLOW
      S(2)=P
      S(1)=144.*PCUSHG
      W=TBL(TABTOT,S,DEG,IER)
C     W IS TOTAL FLOW FROM TURBOFAN
      IF(W.LE.WT)GO TO 10
      IF(W.EQ.0.)GO TO 10
C     WITH W.LT.WT, WE HAVE REVERSE FLOW THROUGH FAN. HENCE OUTLET
C     TEMP = INLET TEMP
      T=TAMB+WT*(T-TAMB)/W
 10   P=PCUSHA
C     CORRECT FLOW TO LB/MIN
      W=W*60.
      WT=WT*60.
      IF(PRNT)WRITE(IO,9999)NOMEN,PCUSHA,PCUSHG,T,W,WT
 9999 FORMAT(14X,A10,3X2HPA5X,6X2HPG5X,6X2HTT5X,6X1HW6X,6X4HWTUR3X/
     1 21X,5(F10.4,3X)/)
      RETURN
      END
```

Table A-6 Turbofan Model (ACRS)

231

```
      SUBROUTINE BAG(TABRV,ACUSH,AATM,CD,PCUSHG,PAMB,WERR,WIN)
      COMMON/CURVAL/P,T,H,W/PRNT/PRNT/IO/IO/NCMEN/NOMEN/SGGGUR/SCG
      COMMON/DEGREE/DEG(3)
      LOGICAL PRNT
C     CALCULATES OUTFLOW FROM TRUNK
C     OUTFLOW GOES INTO CUSHION CAVITY, TO AMBIENT, AND THROUGH RELIEF VALV
C     AIN= FLOW AREA INTO CUSHION
C     AOUT= FLOW AREA TO AMBIENT
C     AREL= CALCULATED RELIEF VALVE AREA
      AIN=CD*ACUSH
      AOUT=CD*AATM
      PCUSHA=PCUSHG+PAMB
      T=AMAX1(T,300.)
C     CALCULATE RELIEF FLOW
      PREL=144.*(P-PAMB)
      IF(PREL.LE.259.2) GO TO 2
      AREL=TBL(TABRV,PREL,DEG,IER)
      AREL=AREL*0.9
      WREL=CNFLOW(P,T,PAMB,AREL,CCR)
      GO TO 5
    2 WREL=0.
    5 CONTINUE
      IF(PCUSHA.GE.P)GO TO 10
      WIN=CNFLOW(P,T,PCUSHA,AIN,CCR)
      GO TO 20
   10 WIN=P-PCUSHA
   20 IF(PAMB.GE.P)GO TO 30
      WOUT=CNFLOW(P,T,PAMB,AOUT,CCR)
      GO TO 40
   30 WOUT=P-PAMB
   40 WTRUNK=WIN+WOUT+WREL
C     WERR IS TRUNK INFLOW - TRUNK OUTFLOW (=0. AT STEADY STATE)
      WERR=W-WTRUNK
      IF(PRNT) WRITE(IO,9999) NOMEN,P,T,W,WTRUNK,WIN,WOUT
 9999 FORMAT( 14X,A10,3X2HPT5X,6X2HTT5X,6X1HW6X,6X6HWTRUNK1X,6X3HWIN4X,
     16X4HWOUT/21X,6(F10.4,3X)/)
      RETURN
      END
```

Table A-7 Trunk Model (ACRS)

232

```
      SUBROUTINE CUS(PCUSHH,FLOW1,WIN,PCUSHG,WERCU)
      COMMON/CURVAL/P,T,H,W/PRNT/PRNT/IO/IO/NOMEN/NOMEN/DEGREE/DEG(3)
      LOGICAL PRNT
C   CALCULATES OUTFLOW FROM CUSHION.   INFLOW=CUSHION FLOW + PART OF
C   TRUNK FLOW
C   PCUSHG IS VARIED IN SAC CARD UNTIL INFLOW=CALCULATED OUTFLOW
C   PCUSHH IS CUSHION PRESSURE AT WHICH VEHICLE GOES INTO HOVER
C   FLOW1  IS CORRESPONDING FLOW
      T=AMAX1(T,300.)
      DUM=AMAX1(PCUSHG/PCUSHH,0.)
      WOUT=FLOW1*SQRT(DUM)
      IF(PCUSHG.GT.PCUSHH)WOUT=FLOW1+5000.*(PCUSHG-PCUSHH)
      W=W+WIN
      WERCU=W-WOUT
      IF(PRNT)WRITE(IO,9999)NOMEN,W,WOUT,PCUSHG
 9999 FORMAT( 14X,A10,3X1HW6X,6X4HWOUT3X,6X6HPCUSHG/21X,3(F10.4,3X)/)
      RETURN
      END
```

Table A-8 Cushion Model (ACRS)

233

```
SAC1 (W1,WT,.1,0.,240.,W1,0.)
SAC3 (WERR,0.,.1,14.7,20.,PTRUNK,0.)
SAC 3 (WERCU,0.,.1,0.,1.05,PCUSHG,0.)


SEC1 (PAMB,TAMB,HAMB,W1)
 ENG (TABDT,TABDP,AMN,SPEED)
 POR (TABPO)
 LNKT1(AKPF,7.07)
 LNKD1(.59,7.07)
 LNKB1(.478,7.07)
 LNKD3(.4,7.07)
 LNKV2(1.,AV2)
 LNKD4(.4,7.07)
 TRF (TABWTU,TABTOT,PTRUNK,PAMB,TAMB,WT)
 BAG (ACUSH,AATM,CD,PCUSHG,PAMB,WIN,WERR)
 CUS (PCUSHH,FLOW1,WIN,PCUSHG,WERCU)
SEC1 ( )


PAMB=14.7,TAMB=519.,HAMB=0.,  AMN=0.,
ACUSH=57.73,AATM=28.86,CD=0.8,
AV2=6.15,PCUSHG=0.2,PTRUNK=15.0,
PCUSHH=0.7,FLOW1=150.8,
AKPF=2.
```

Table A -9 Main Program (ACTS)

234

```
      SUBROUTINE TRF(TABWTU,TABTOT,PTRUNK,PAMB,TAMB,WT)
C     PURPOSE - CALCULATES THE PERFORMANCE OF AN ACLS TURBO-FAN USING
C                         PERFORMANCE MAPS
      COMMON/CURVAL/P,T,H,W/PRNT/PRNT/IO/IO/NOMEN/NOMEN/DEGREE/DEG(3)
      DIMENSION S(2)
      LOGICAL PRNT
C     CALCULATE TURBINE FLOW
C     PTRUNK IS IN PSIA
      PTRUNK=AMAX1(PTRUNK,.001)
      PRT=P/PTRUNK
      WTCOR=TBL(TABWTU,PRT,DEG,IER)
      WT=WTCOR*1.55*P/SQRT(T)
C     WT IS CALCULATED VALUE OF TURBINE FLOW
      S(2)=P
      S(1)=144.*(PTRUNK-PAMB)
      W=TBL(TABTOT,S,DEG,IER)
C     W IS TOTAL FLOW FROM TURBOFAN
      IF(W.LE.WT)GO TO 10
      IF(W.EQ.0.)GO TO 10
      T=TAMB+WT*(T-TAMB)/W
   10 P=PTRUNK
C     CORRECT FLOW TO LB/MIN
      W=W*60.
      WT=WT*60.
      IF(PRNT)WRITE(IO,9999)NOMEN,PTRUNK,T,W,WT
 9999 FORMAT(14X,A10,3X2HPT5X,6X2HTT5X,6X1HW6X,6X4HWTUR/
     1 21X,4(F10.4,3X)/)
      RETURN
      END
```

Table A-10 Turbofan Model (ACTS)

235

```
      SUBROUTINE BAG(ACUSH,AATM,CD,PCUSHG,PAMB,WIN,WERR)
      COMMON/CURVAL/P,T,H,W/PRNT/PRNT/IO/IO/NOMEN/NOMEN/SQGGUR/SQG
      COMMON/DEGREE/DEG(3)
      LOGICAL PRNT
C     CALCULATES OUTFLOW FROM TRUNK
C     ACTS TRUCK HAS NO RELIEF VALVE
C     AIN= FLOW AREA INTO CUSHION
C     AOUT= FLOW AREA TO AMBIENT
      AIN=CD*ACUSH
      AOUT=CD*AATM
      PCUSHA=PCUSHG+PAMB
      T=AMAX1(T,300.)
      IF(PCUSHA.GE.P)GO TO 10
      WIN=CNFLOW(P,T,PCUSHA,AIN,CCR)
      GO TO 20
   10 WIN=P-PCUSHA
   20 IF(PAMB.GE.P)GO TO 30
      WOUT=CNFLOW(P,T,PAMB,AOUT,CCR)
      GO TO 40
   30 WOUT=P-PAMB
   40 WTRUNK=WIN+WOUT
C     WERR IS TRUNK INFLOW - TRUNK OUTFLOW (=0. AT STEADY STATE)
      WERR=W-WTRUNK
      IF(PRNT)WRITE(IO,9999)NOMEN,P,T,WIN,WOUT
 9999 FORMAT(14X,A10,3X2HPT5X,6X2HTT5X,6X3HWIN4X,6X4HWOUT/
     1 21X,4(F10.4,3X)/)
      RETURN
      END
```

Table A-11 Trunk Model (ACTS)

236

```
      SUBROUTINE CUS(PCUSHH,FLOW1,WIN,PCUSHG,WERCU)
C   ANALYSIS OF CUSHION CAVITY FOR ACTS ONLY
C   PCUSHG IS VARIED IN SAC CARD UNTIL INFLOW=CALCULATED OUTFLOW
C   PCUSHH IS CUSHION PRESSURE AT WHICH VEHICLE GOES INTO HOVER
C   FLOW1  IS CORRESPONDING FLOW
      COMMON/CURVAL/P,T,H,W/PRNT/PRNT/IO/IO/NOMEN/NOMEN/DEGREE/DEG(3)
      LOGICAL PRNT
      T=AMAX1(T,300.)
      DUM=AMAX1(PCUSHG/PCUSHH,0.)
      WOUT=FLOW1*SQRT(DUM)
      IF(PCUSHG.GT.PCUSHH)WOUT=FLOW1+50000.*(PCUSHG-PCUSHH)
      W=WIN
      WERCU=W-WOUT
      IF(PRNT)WRITE(IO,9999)NOMEN,W,WOUT,PCUSHG
 9999 FORMAT(14X,A10,3X1HW6X,6X4HWOUT3X,6X6HPCUSHG/21X,3(F10.4,3X)/)
      RETURN
      END
```

Table A-12 Cushion Model (ACTS)

237

APPENDIX B

6 DEGREE OF FREEDOM ACLS COMPUTER MODEL

The evaluation of the dynamic performance of an ACLS requires the simulation of the overall aircraft, including aerodynamic and engine induced forces and moments. The simulation of the Jindivik ACRS has been conducted using the Boeing ACLS 6 DOF Computer Program (Reference 14). Figure B-1 shows the overall structure of this program. It utilizes a generalized 6 DOF program (Reference 15), to which are added the unique modules necessary for simulating the components of the ACRS. The method of analysis used for these modules is discussed below:

ACRS TRUNK MODEL

The ACRS trunk provides four functions in supporting an aircraft:

a) Acts as a skirt for the cushion air
b) Attenuates landing impact
c) Provides roll and pitch stability
d) Serves as a brake when cushion air pressure is lowered

In order to develop a realistic trunk model, movie films of the ACRS Jindivik drop tests were viewed and frames of the film were enlarged. The trunk shape before the drop is shown in Figure B-2(a). The moment of initial ground contact is shown in Figure B-2(b). The trunk shape at the half way point between initial ground contact and maximum compression is shown in Figure B-2(c), and the shape for maximum compression is shown in Figure B-2(d). An overlay of the trunk shape profiles is shown in Figure B-3. Assuming a camera speed of 24 frames per second, the times of the frames from release are shown on the profiles. It can be seen that the side portions of the trunk show significant upward and outward motion during compression. The forward portion, and likewise the aft portion of the trunk, are restrained from moving upward because of the aircraft fuselage, and are also restrained from moving outward because of the large hoop stresses which develop in the horizontal curvatures.

239
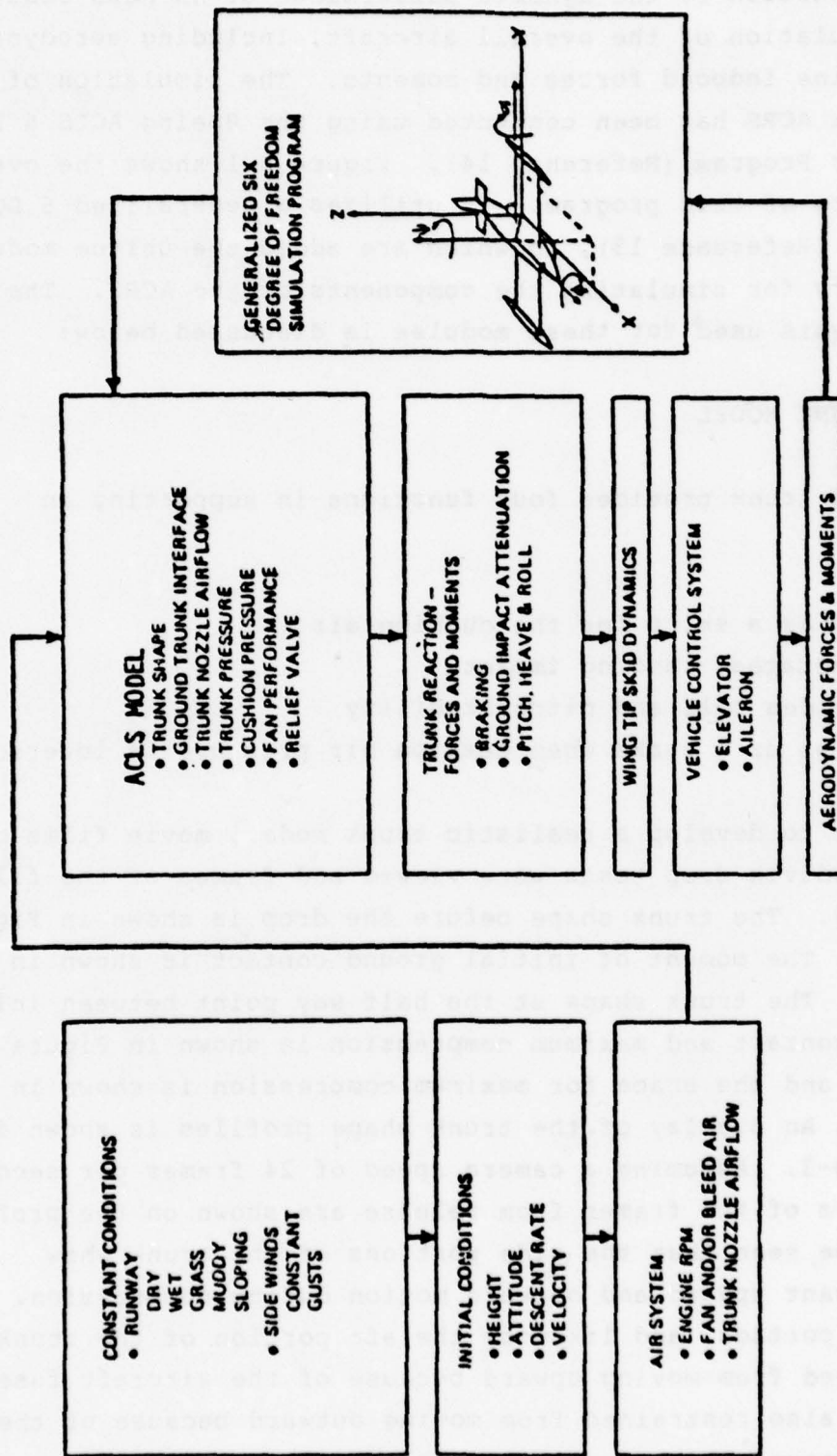
Figure B-2(b) Ground Contact

Figure B-2(d) Maximum Compression

Figure B-2(a) Before Drop

Figure B-2(c) 50 Percent Compression

Figure B-2 ACLS Drop Test Photographs

241

MAXIMUM COMPRESSION 0.75 SECOND

50% COMPRESSION 0.375 SECOND

SHAPE AT INITIAL GROUND CONTACT (0.0 SECOND)
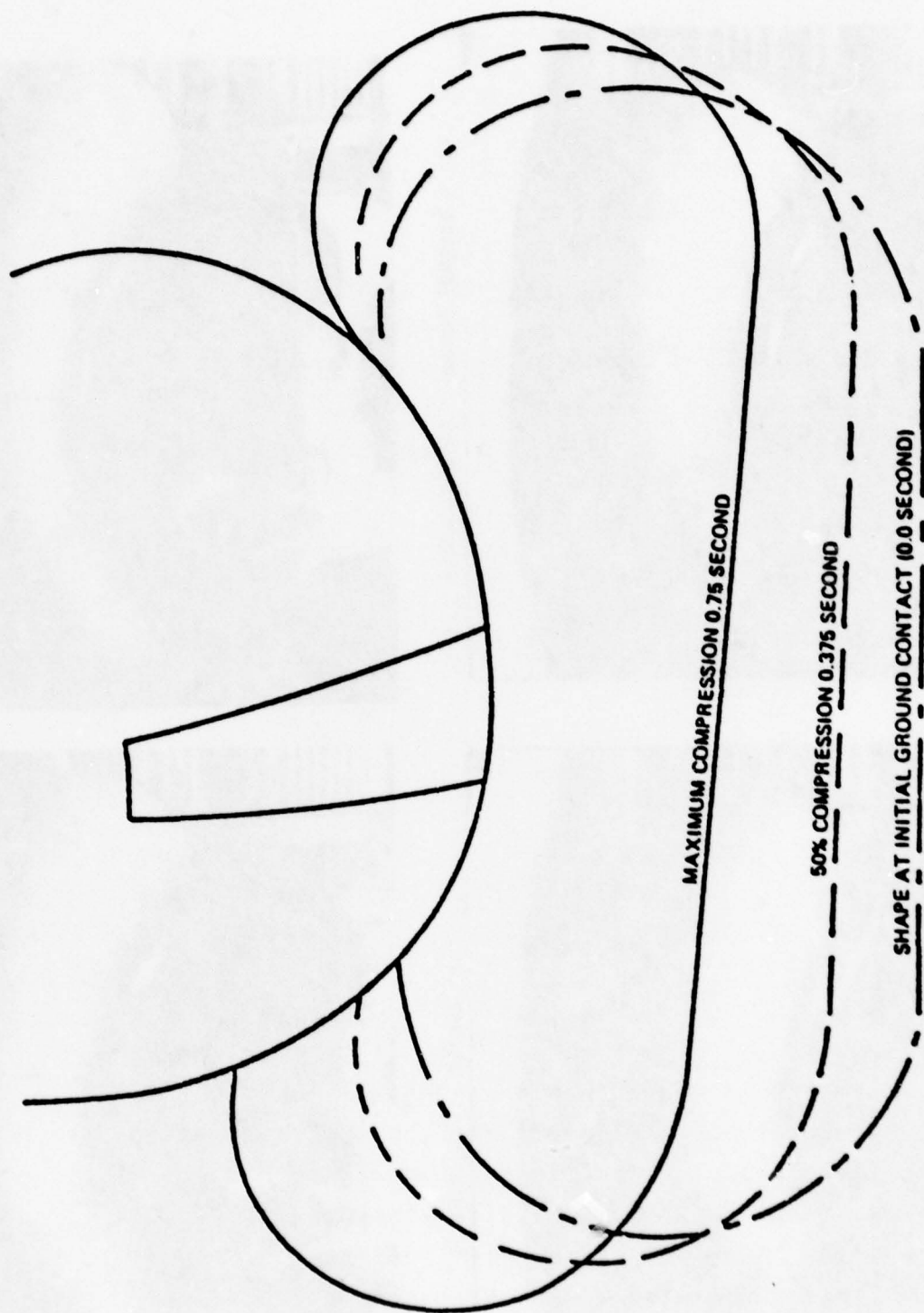
Figure B-3   Trunk Shape Overlay

Several trunk models have already been developed. The Foster-Miller model of Reference 16 (since modified) assumed a "frozen" trunk shape as shown in Figure B-4. Comparison of the frozen model with the drop test shapes of Figures B-2 and B-3 show the model to be unrealistic for this application. For a given trunk stroke the frozen trunk shape model would yield a greater change in volume, which produces a greater change in air pressure, P_t. Also, the flattened area A_t, or foot print, will be larger than reality. Since the reacted vertical load of the trunk is $P_t A_t$, the load error is amplified. This also produces errors in the trunk pitch stiffness and roll stiffness, as well as in the degree of braking which is given by $A_t P_t$.

The Bell model (Reference 17) allows for the effect of hoop tension by adding a simulated spring at each section to restrain outer motion, with the spring constants being required inputs to the model. An iterative calculation is required at each time step.

The Digges model of Reference 18 calculates the shape of a two dimensional loaded inelastic trunk using an iterative procedure. The model is appropriate for the side elements of a trunk, but not for the forward and aft elements where hoop tension effects are signficant.

The selected method utilizes a quasi steady state parametric approach to minimize computer time. The trunk is divided into elements as shown in Figure B-5(a). The two dimensional side element shape parameters for the loaded condition are shown in Figure B-5(c). The Digges program is used to calculate the parametric data for the side elements. The cross sectional area (CA_t), the width of the flattened area (Y_f) and the lateral distance from the lower attachment point to the center of the flattened area (Y_c) are shown plotted in Figures B-6, -7, and -8 as a function of pressure ratio P_c/P_t and stroke ratio Z_0/Z_∞. Z_∞

243

Undeformed Trunk Sector

Trunk Crumpling to Conform with Ground

h_y

E

B

F

K

R_1

ϕ_1

R_2

J

L

D

A(0,0)

$Y_{gh}(i)$

Frozen Trunk Shape

Ground

h_y

E

B

C

H

G

R_1

ϕ_2

R_2

F

D

A(0,0)

$Y_{gh}(i)$
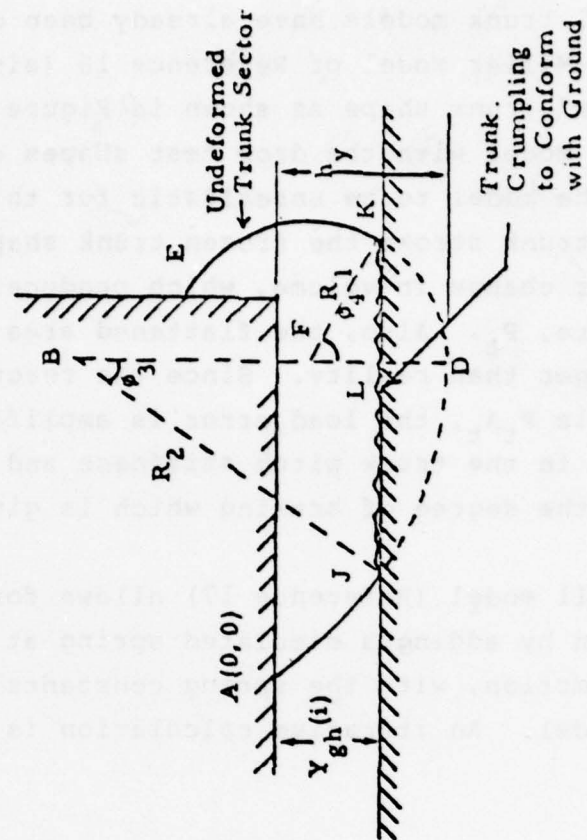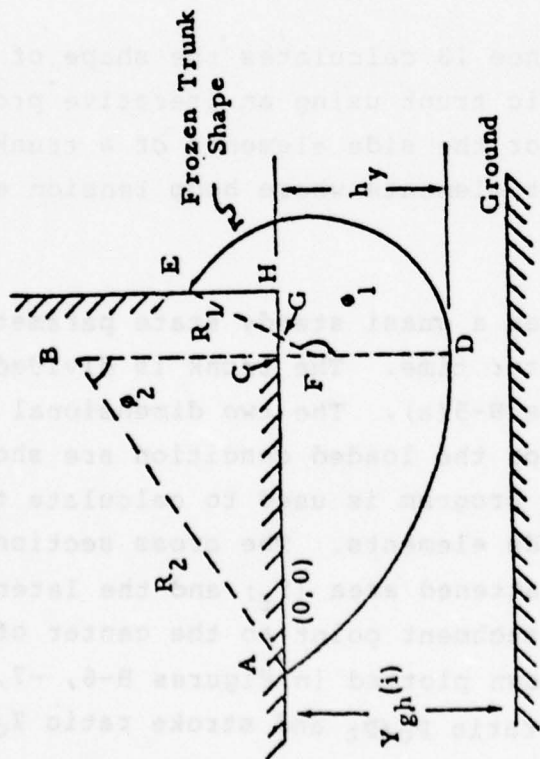
Figure B-4 Frozen Trunk Shape Model

AFT ELEMENTS

SIDE ELEMENTS

FORWARD ELEMENTS

FIG. B-5(a)

TRUNK SEGMENT

ΔX

FUSELAGE

CROSS SECTIONAL AREA CA_t

VOLUME = $CA_t \Delta X$

P_t

Y_f

P_c

Y_c

FLATTENED AREA

SIDE ELEMENT SHAPE PARAMETERS
FIG. B-5(c)

D_1

Y_{f_1}

S_1

FIG. B-5(b)

FORWARD AND AFT ELEMENT SHAPE ASSUMPTION

Figure B-5   Inelastic Trunk Model

245
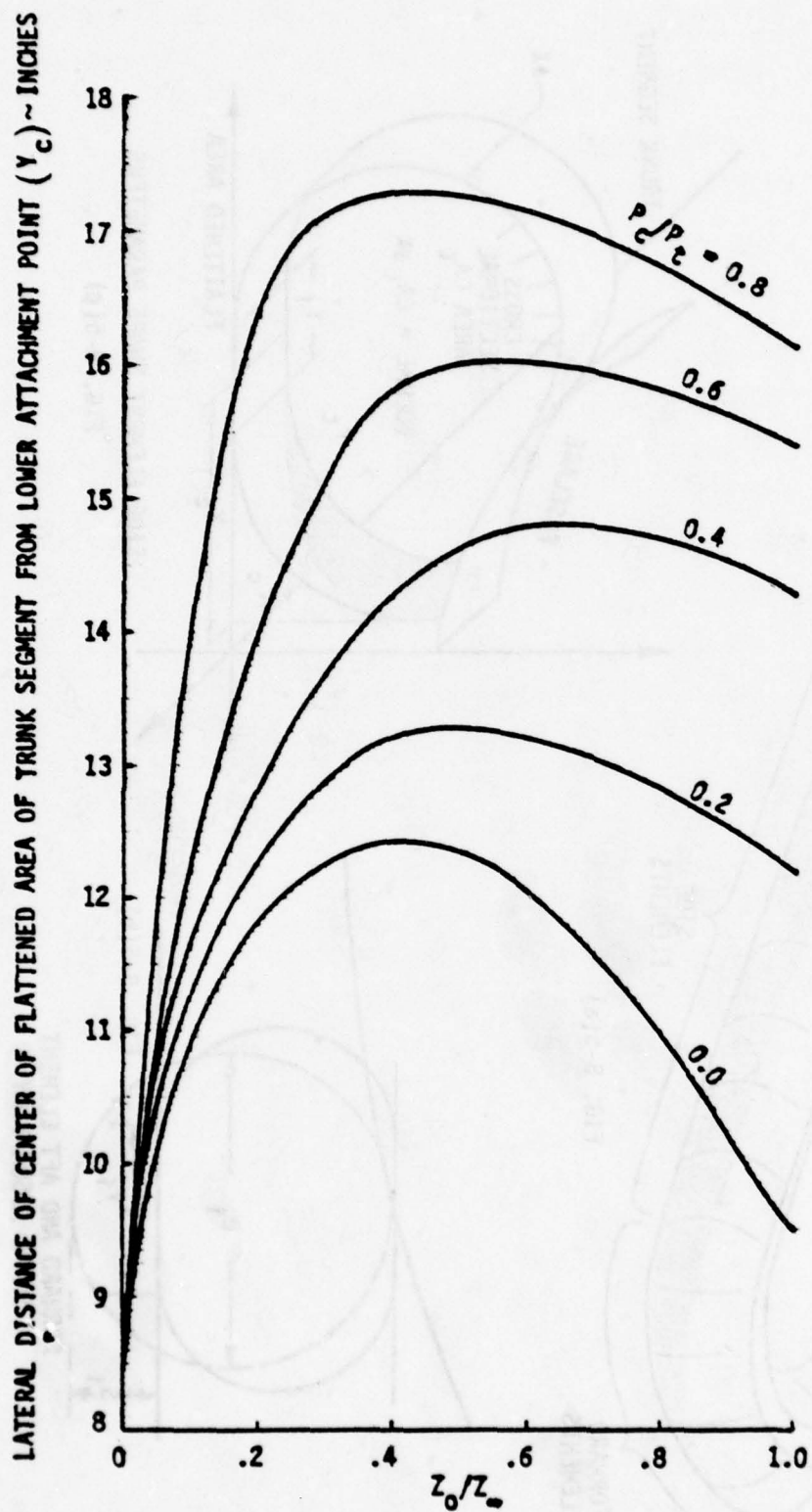
Figure B-6   Distance of Center of Flattened Area of
Trunk Segment vs Percentage Stroke
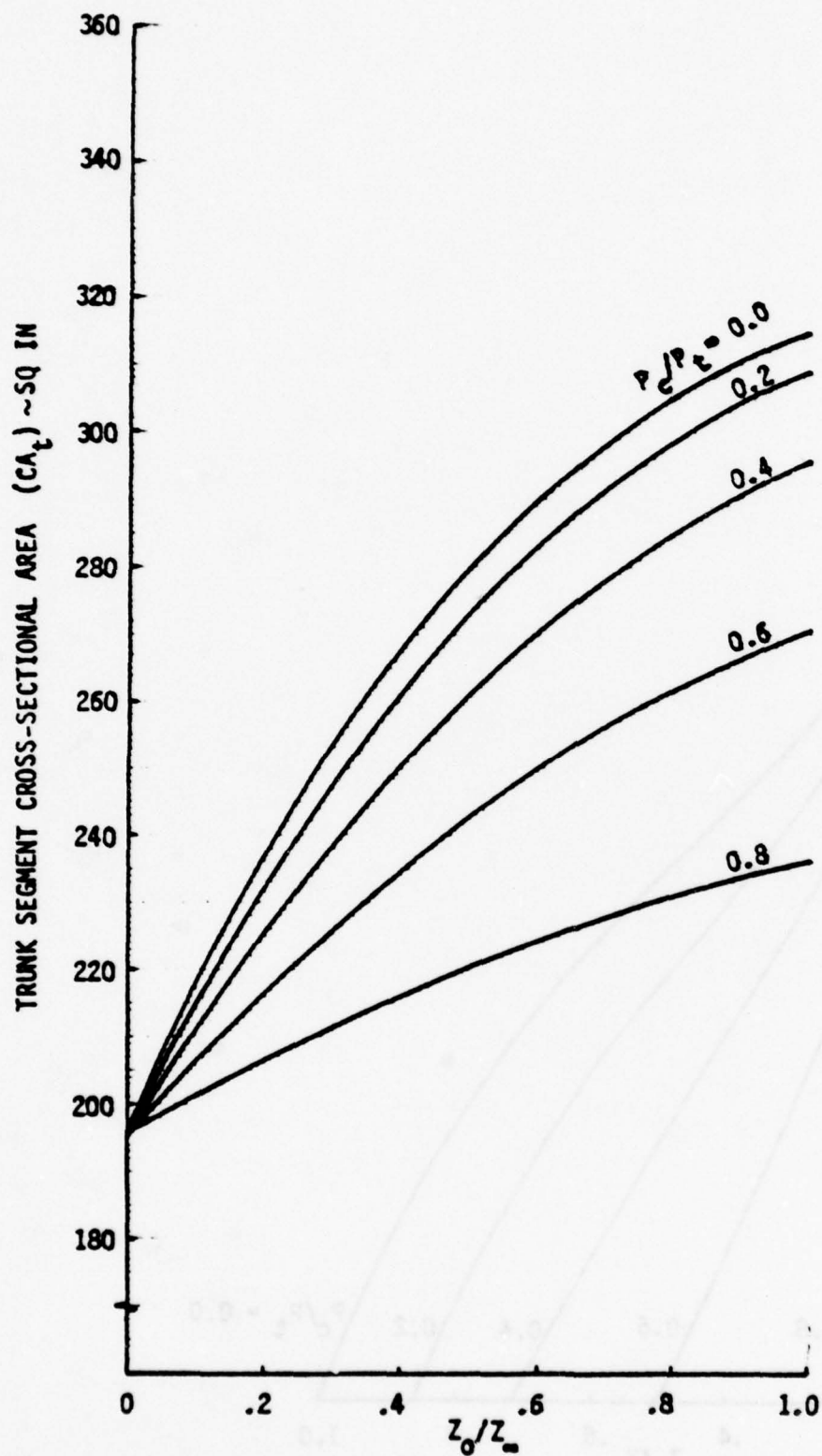
Figure B-7   Trunk Segment Cross-Sectional Area vs
Cross-Sectional Stroke Due to Ground Contact

247
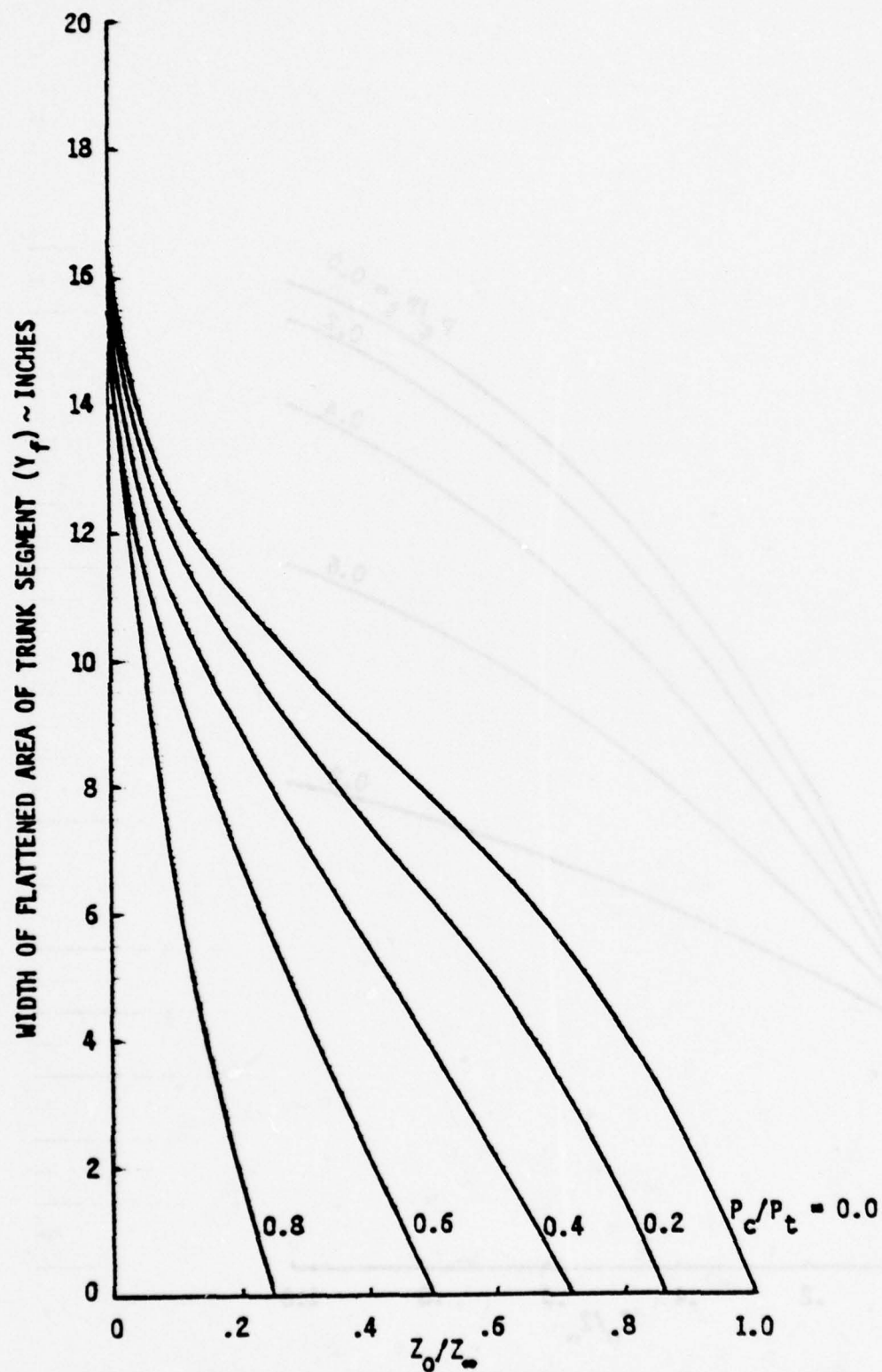
Figure B-8   Width of Flattened Trunk vs Percentage Stroke

248

is the vertical distance between the lower attachment point and the lowermost point of the free shape at a pressure ratio of zero, and Z_o is the vertical distance between the lower attachment point and the lowermost point of the trunk. The volume of a side trunk element is given by the product of the cross sectional area (CA_t) and the length Δx.

The shape of the forward and aft elements is assumed to be restricted by horizontal hoop stress. These segments are assumed to take the shape of a flattened cylinder as shown in Figure B-5(b). For an inelastic bag, the circumference is constant and thus:

$$\pi D_i = 2Y_{f_i} + \pi (D_i - S_i) \qquad \text{B.1}$$

The flattened width of the ith element is then:

$$Y_{f_i} = \frac{\pi}{2} S_i \qquad \text{B.2}$$

The foot print area of the element is then:

$$A_{fp_i} = Y_{f_i} \Delta x_i \qquad \text{B.3}$$

where Δx_i is the mean length of the ith element. The cross sectional area of the element is given by:

$$CA_{t_i} = Y_{f_i} (D_i - S_i) + \frac{\pi}{4} (D_i - S_i)^2 \qquad \text{B.4}$$

substituting Equation B.2 into B.4 and combining terms yields:

$$CA_{t_i} = \frac{\pi}{4} (D_i^2 - S_i^2) \qquad \text{B.5}$$

249

The volume of the ith element is then:

$$V_{t_i} = \frac{\pi}{4} (D_i^2 - S_i^2) \Delta x_i \qquad \text{B.6}$$

The total trunk volume is then obtained by summing the volumes of both side and fore and aft elements, giving:

$$V_t = \sum_{i=1}^{n} V_{t_i} \qquad \text{B.7}$$

AIR CUSHION VOLUME

Since it is assumed that lateral motion only takes place in the side elements, the cushion volume is primarily a function of side element shapes. Figure B-9 depicts the cushion volume geometry.

An approximation of the trunk element radius is:

$$r_i = (1 + P_c/P_t)(Z_0/Z_\infty) r_{d_i} \qquad \text{B.8}$$

where r_{d_i} is the out of ground effect radius. The chord length is given by:

$$C = \left[(Y_{c_i} - Y_{f_i})^2 + (Z_{t_i} - S_i)^2 \right]^{1/2} \qquad \text{B.9}$$

The angle subtending the chord is:

$$\theta_c = 2 SIN^{-1}(C/2r_i) \qquad \text{B.10}$$

the area of the sector shown shaded in Figure B-9 is then:

250
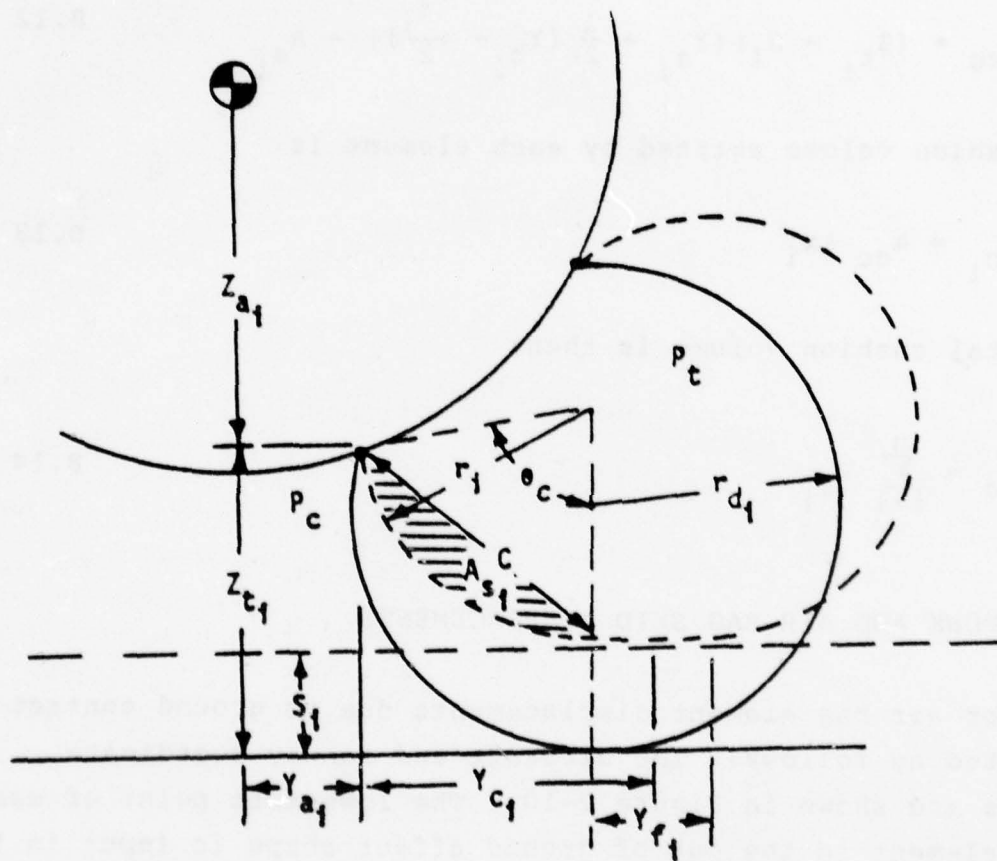
Figure B-9   Cushion Volume Geometry

$$A_{s_i} = (\frac{\partial_c}{2} - \frac{SIN\ \partial_c}{2})\ r_i^2 \qquad\qquad\qquad B-11$$

Finally the cushion cross sectional area skirted by each side element is:

$$A_{cc} = (Z_{t_i} - S_i)(Y_{a_i} + \frac{1}{2}(Y_{c_i} - \frac{Y_{f_i}}{2})) - A_{s_i} \qquad\qquad B.12$$

The cushion volume skirted by each element is:

$$V_{c_i} = A_{cc}\ \Delta x_i \qquad\qquad\qquad\qquad\qquad B.13$$

The total cushion volume is then:

$$V_c = \sum_{i=1}^{n} V_{c_i} \qquad\qquad\qquad\qquad\qquad B.14$$

ACLS TRUNK AND AIR BAG SKID DISPLACEMENTS

Trunk or air bag element displacements due to ground contact are evaluated as follows: The aircraft and runway coordinate systems are shown in Figure B-10. The lowermost point of each trunk element in the out of ground effect shape is input in the form of a subscripted data array $(X_{t_i}, Y_{t_i}, Z_{t_i})$. The X and Y coordinates are relative to the aircraft center of gravity and the Z coordinates are relative to the element lower attachment point. Referring to Figure B-9, an array of element stroke ratios is defined as:

$$(Z_o/Z_\infty)_i = (Z_{t_i} - S_i)/Z_{t_i} \qquad\qquad\qquad B.15$$

x — NOSE
y — RIGHT WING
z — DOWN

DIRECTION OF
RELATIVE WIND

SIDE
WIND

HEADING

RUNWAY C_L

COURSE

DR — DOWN RANGE
CR — CROSS RANGE
RR — RADIAL RANGE

RR

DR

CR

$(X_{t_1}, Y_{t_1}, Z_{t_1})$
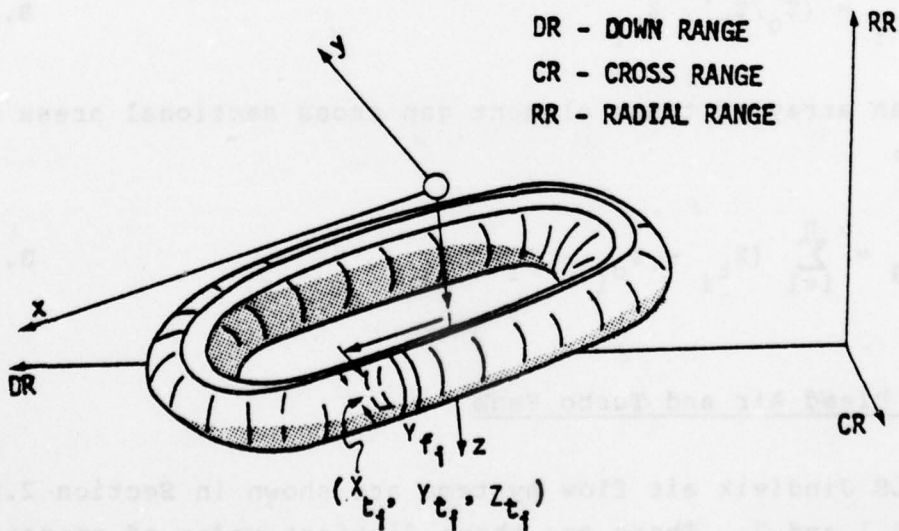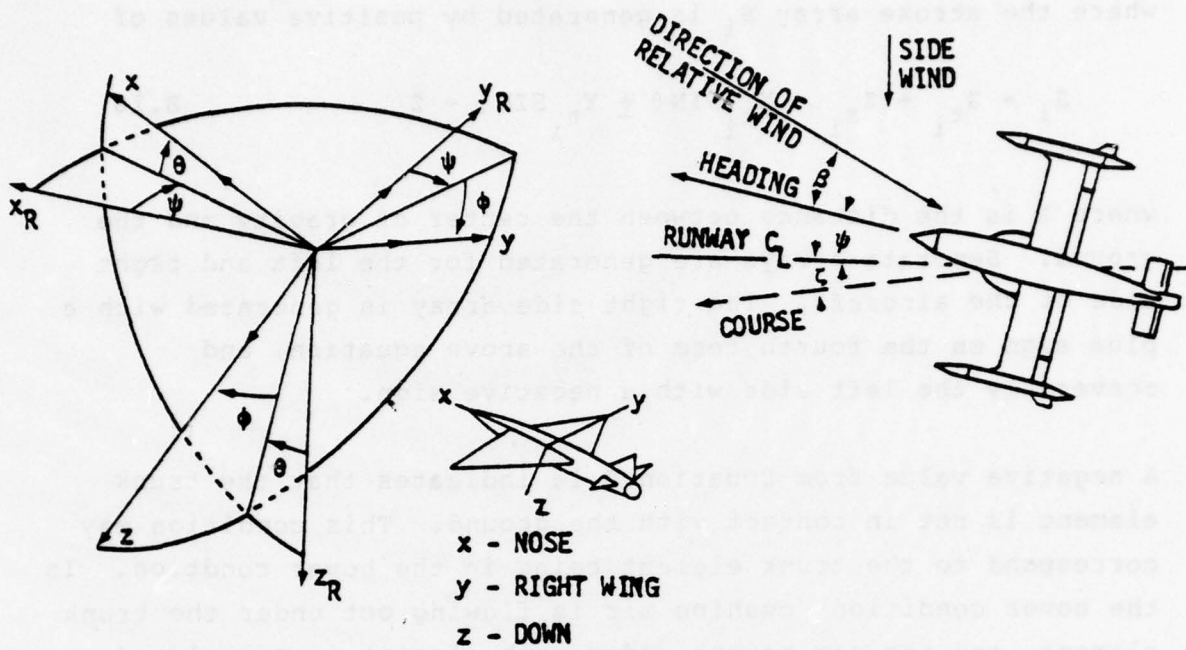
Figure B-10 Coordinate Systems

253

where the stroke array S_i is generated by positive values of

$$S_i = Z_{t_i} + Z_{a_i} - X_{t_i} \sin\theta \pm Y_{t_i} \sin\phi - Z \qquad \text{B.16}$$

where Z is the distance between the center of gravity and the ground. Separate arrays are generated for the left and right side of the aircraft. The right side array is generated with a plus sign on the fourth term of the above equation, and conversely the left side with a negative sign.

A negative value from Equation B.16 indicates that the trunk element is not in contact with the ground. This condition may correspond to the trunk element being in the hover condtion. In the hover condition, cushion air is flowing out under the trunk element, and the gap height under each element is calculated first by obtaining the hover stroke ratio as a function of P_c/P_t by interpolation from Figure B-11. This curve is obtained from Figure B-8 by cross plotting Z_o/Z_∞ versus P_c/P_t for Y_f equal to zero. The extension for each trunk element is given by:

$$Z_{o_i} = (Z_o/Z_\infty)_i \, Z_{t_i} \qquad \text{B.17}$$

Thus, an array of trunk element gap cross sectional areas may be summed:

$$A_g = \sum_{i=1}^{n} (Z_{t_i} - Z_{o_i} - S_i) \, \Delta x_i \qquad \text{B.18}$$

Direct Bleed Air and Turbo Fans

The ACLS Jindivik air flow systems are shown in Section 2.0, Figures 1 and 2. There are three distinct modes of operation.

1) Referring to Figure 1, the ACTS air supply system operates

254

Figure B-11   Trunk Gap Model

255

with valve (2) open and valve (1) closed such that the turbo fan supplies air to the trunk. The air flows out of the trunk th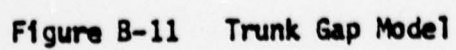rough peripheral jets, lubricating the trunk-ground interface. The cushion volume is pressurized from the peripheral jets.

2) The ACRS system in the recovery mode operates with valve (2) closed and valve (1) open such that the fan is bypassed and the trunk is inflated by direct bleed air. The air flows out of the trunk through peripheral jets on the forward third of the trunk, which serves to place the center of frictional drag aft and thus produce directional stability. During touchdown impact attenuation, the trunk air pressure is relieved through a relief valve. Air entering the cushion volume from the frontal peripheral jets is vented through the turbofan such that there is no buildup of cushion pressure during slideout braking. Rapid compression of the cushion volume during the touchdown impact, however, will result in a cushion pressure buildup which assists the attenuation.

3) The ACRS system in the taxi mode operates with both valves open. The trunk is supplied with direct bleed air and the cushion air is supplied by the turbofan.

The three modes of operation were simulated with ECSS-X computer program, as described in Appendix A. Parametric data was produced for the 6 DOF quasi steady state treatment of the air supply system. The air supply rates as a function of engine RPM and trunk or cushion pressure are shown in Figures B-12 through B-15. The quasi-steady state treatment of dynamic air flow systems assumes that the dynamic effects associated with air inflow and outflow from the trunk and cushion are insignificant compared with the volume capacitance effects of the trunk and cushion. For fan off operation, a comparison of the time constants associated with the supply ducts to those associated
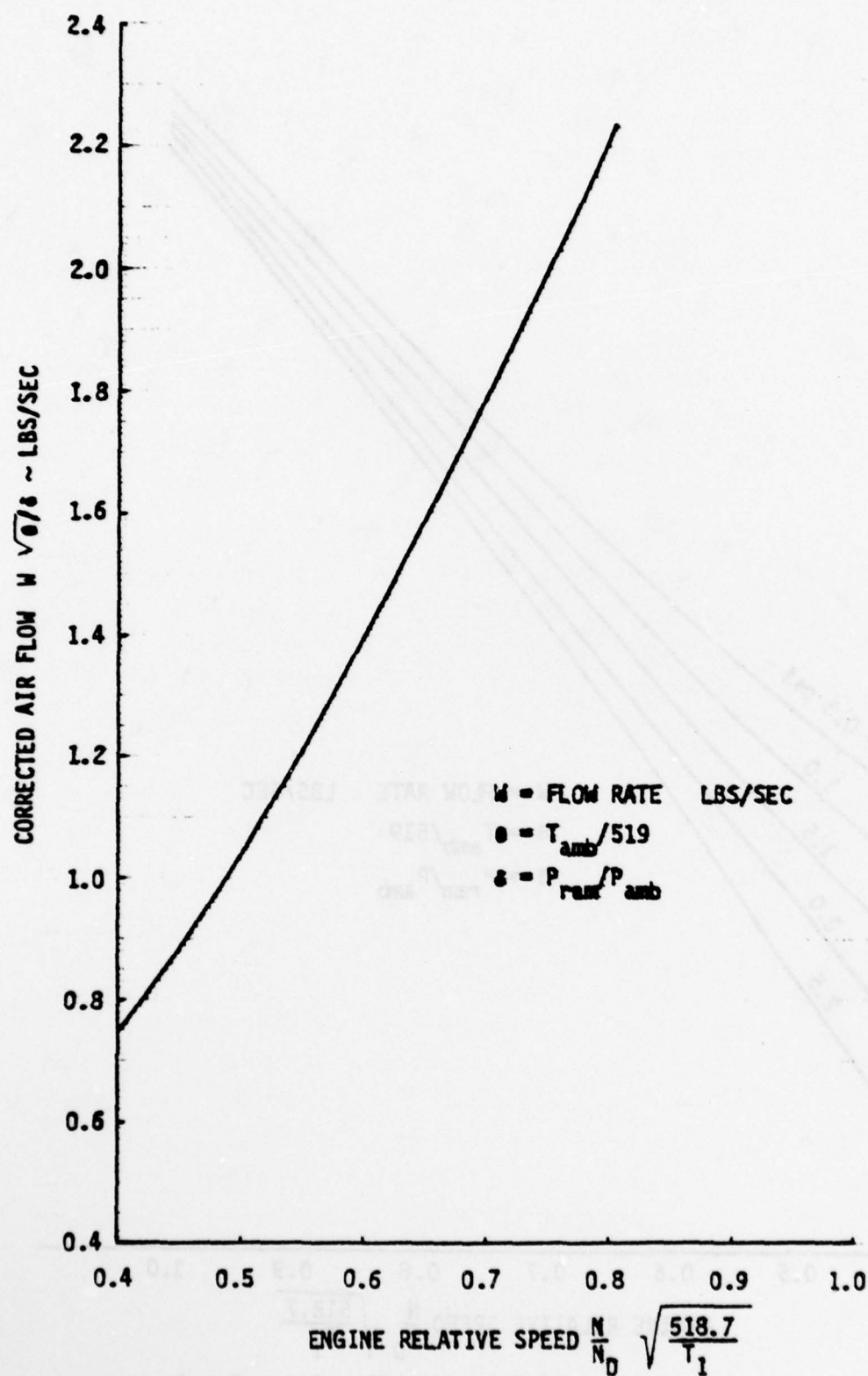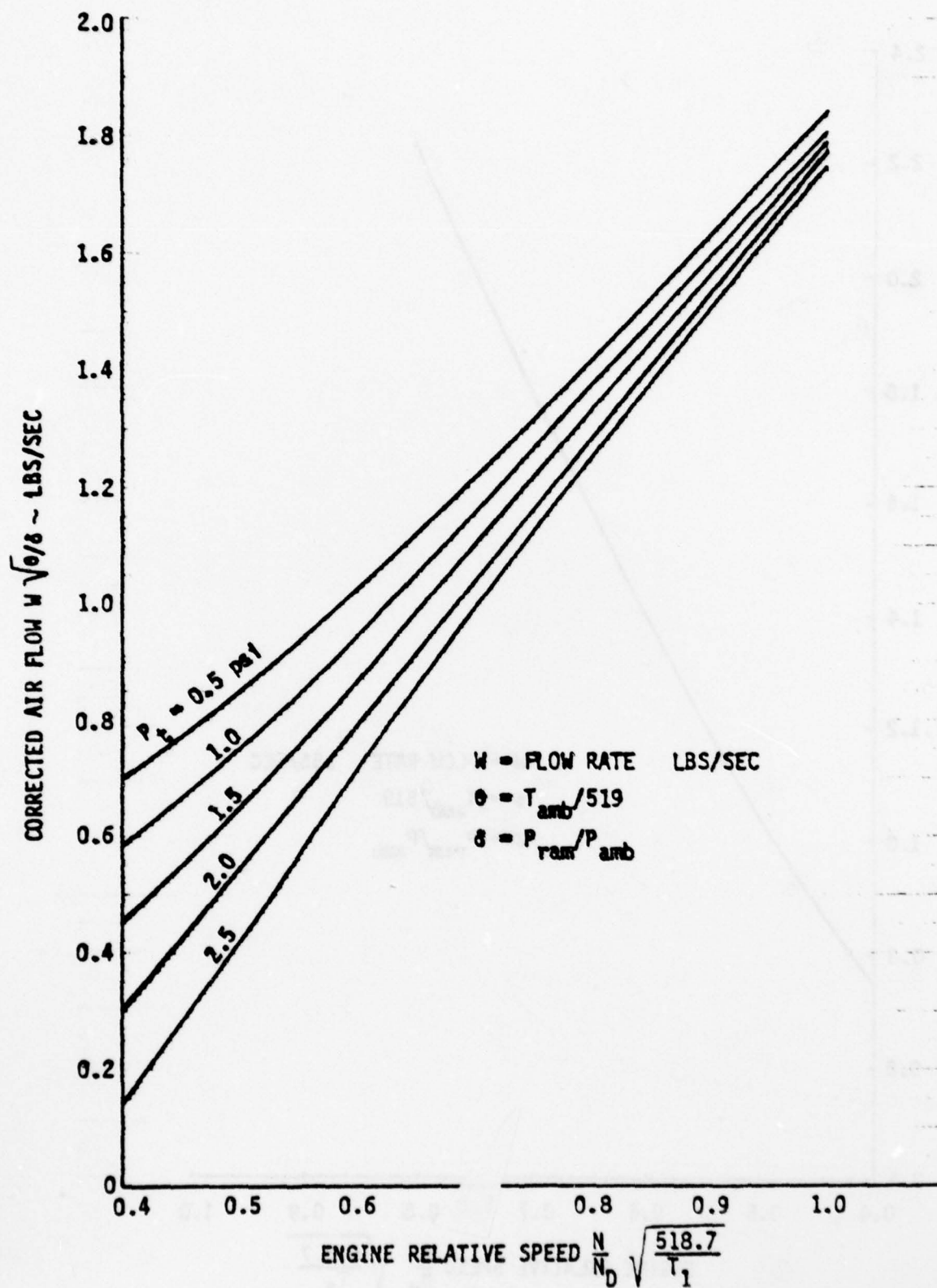
256

Figure B-12   ACRS Trunk Air Flow Rates-Fan Off

257

Figure B-13   ACRS Trunk Air Flow Rates-Fan On

258
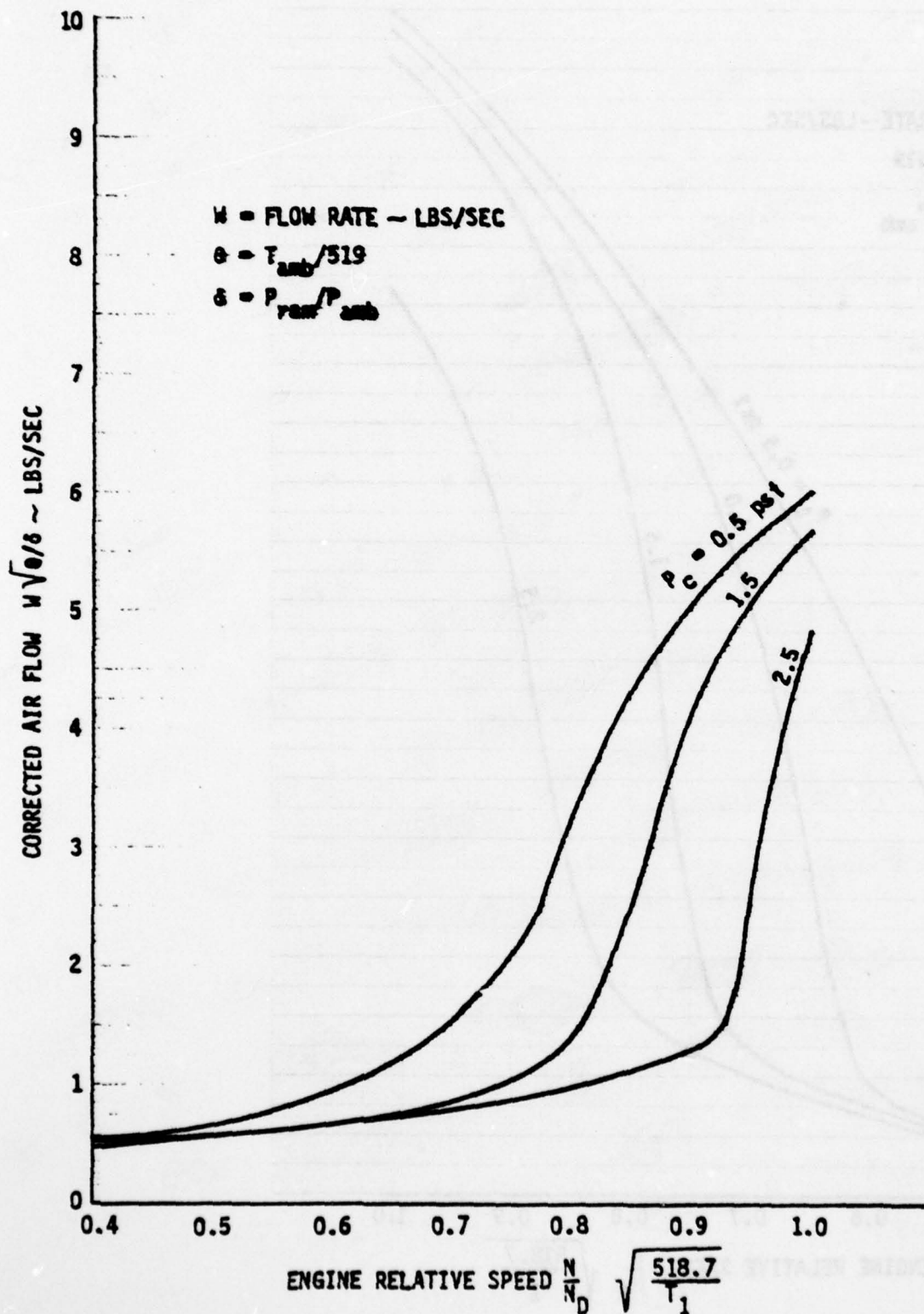
Figure B-14   ACRS Cushion Air Flow Rates-Fan On

259
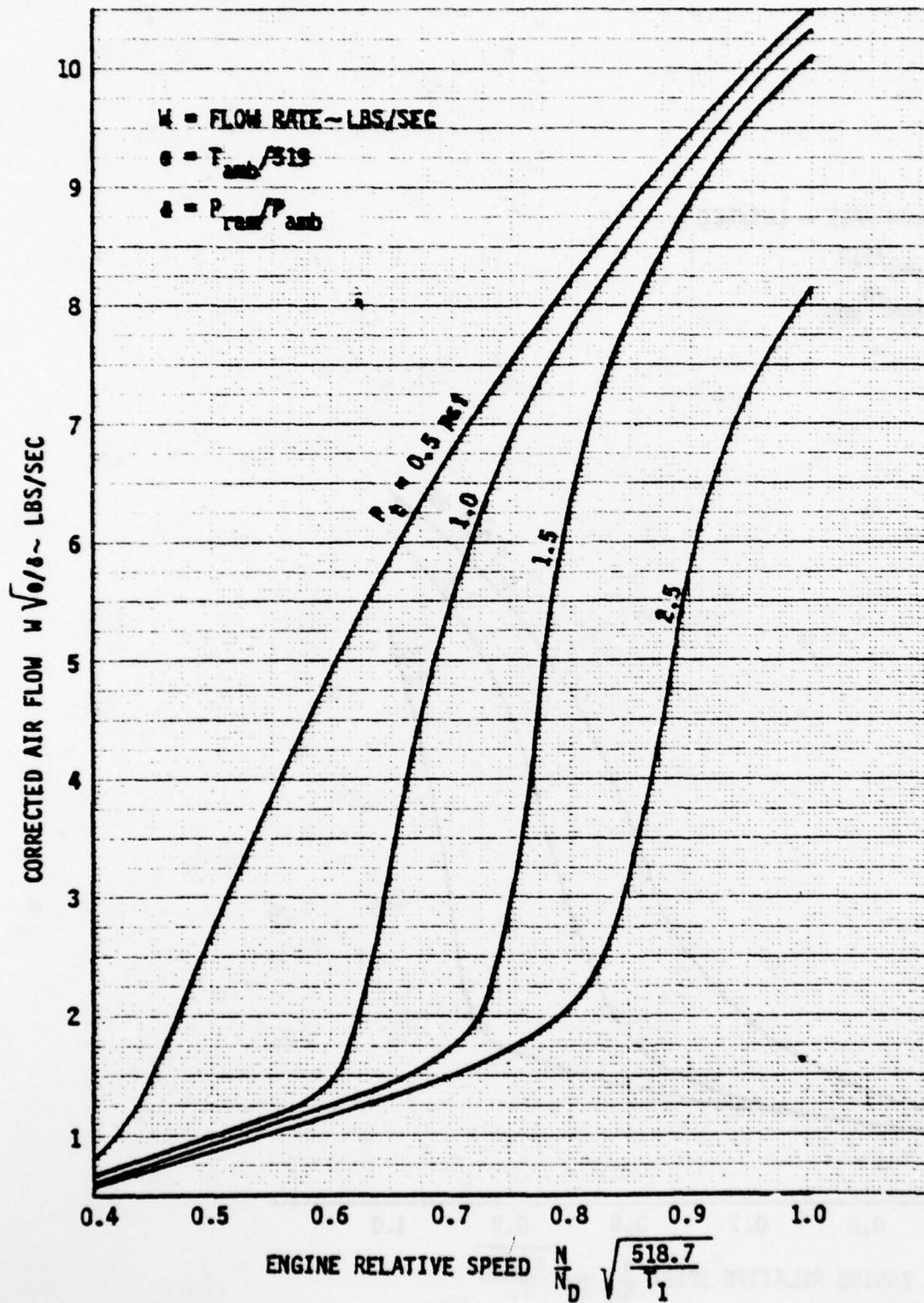
Figure 8-15 ACTS Air Flow Rates

260

with the trunk and cushion shows that this is justified. The results presented in the document are all for this fan off case. For fan on operation, the stall dynamics of the turbofan could be significant and should be included once the stall characteristics of the fan are known.

Relief Valve

The Jindivik ACRS system relief valve area and assumed hysteresis versus trunk pressure are shown in Figure B-16. The relief valve flow rate is given by the standard orifice flow equation:

$$W_{rel} = \rho C_D A_{rel} \left[\frac{2g}{\rho} (P_t - P_{amb}) \right]^{1/2} \qquad \text{B.19}$$

where C_D was assumed to equal 0.9.

Cushion Gap Air Flow Rate

The cushion air gap flow model is depicted in Figure B-17. The size of the air gap is evaluated as previously discussed. It is assumed that the peripheral air jets on the cushion side of the ground tangent plane exit to the cushion volume. The cushion inward air flow rate is then given by:

$$W_c = \rho \left[\frac{2g}{\rho} (P_t - P_c) \right]^{1/2} \left[C_{D_o} \sum_{i=1}^{n} f_{m_i} A_{j_{o_i}} + \frac{C_{D_f}}{2} \sum_{i=1}^{n} A_{j_{f_i}} \right]^{B.20}$$

where $A_{j_{o_i}}$ is the jet area in the non-flattened region of the ith trunk element, $A_{j_{f_i}}$ is the jet area in the flattened region of the ith trunk element, and f_{m_i} is a flow distribution factor. If the trunk element is in the hover condition, f_{m_i} is assumed

261
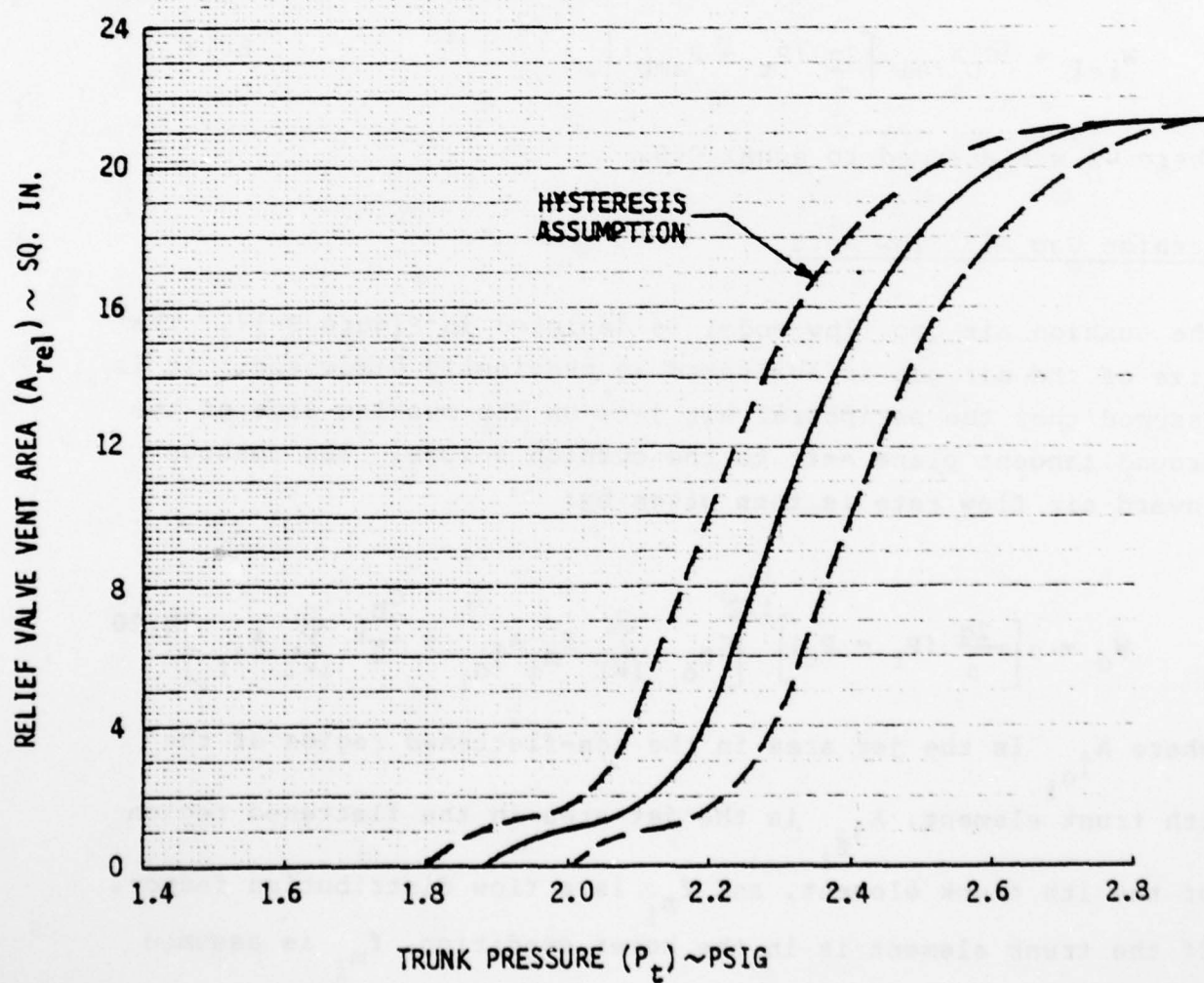
Figure B-16   Jindivik Relief Valve Vent Area
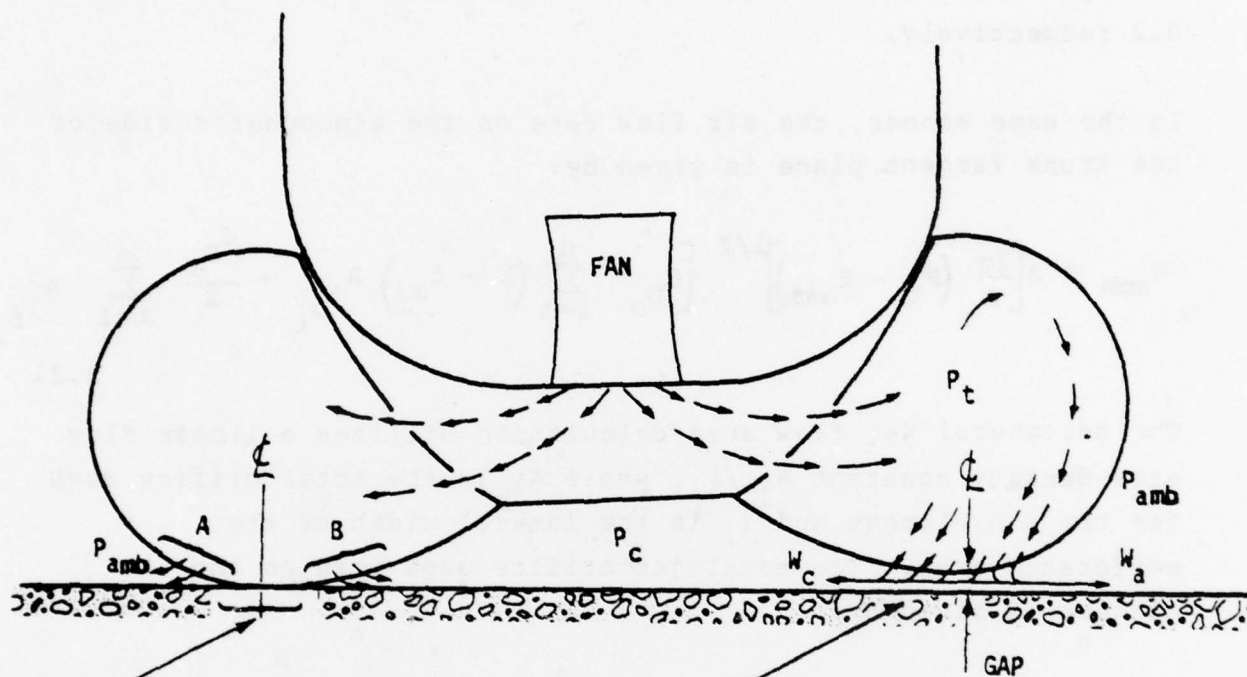
FLATTENED REGION
  o ORIFICE COEF., C_{D_f} = 0.2

  o FLOW EVENLY SPLIT

HOVER CONDITION
  o 60% OF FLOW VENT TO P_c
  o 40% OF FLOW VENT TO P_{amb}
  o P_c VENTS TO P_{amb} THROUGH GAP

FLATTENED REGION
  o ORIFICE COEF., C_{D_f} = 0.2

  o FLOW EVENLY SPLIT
  o NO CUSHION AIR FLOW
REGION A
  o JETS VENT TO P_{amb}
  o EXPOSED JETS, C_{D_o} = 0.6

REGION B
  o JETS VENT TO P_c
  o EXPOSED JETS, C_{D_o} = 0.6

Figure B-17   Restrictor Flow Theory

263

to be 0.6. If the trunk element is flattened, f_{m_i} is set at 0.5. C_{D_o} and C_{D_f} are the discharge coefficients of the jets in the open and flattened regions, and are assumed to be 0.6 and 0.2 respectively.

In the same manner, the air flow rate on the atmospheric side of the trunk tangent plane is given by:

$$W_{amb} = \rho \left[\frac{2g}{\rho}\left(P_t - P_{amb}\right)\right]^{1/2} \left[C_{D_o} \sum_{i=1}^{n}\left(1 - f_{m_i}\right) A_{j_{o_i}} + \frac{C_{D_f}}{2} \sum_{i=1}^{n} A_{j_{f_i}}\right]$$

B.21

The peripheral jet flow area calculation utilizes a linear flow area density constant A_{j_i}/ℓ_i, where A_{j_i} is the total orifice area for the ith element and ℓ_i is the lateral width of the perforated area. The total jet orifice area open on the ith element is given by:

$$A_{j_{o_i}} = \frac{A_{j_i}}{\ell_i}\left(\ell_i - Y_f\right) \quad \left(\ell_i \geqslant Y_f\right)$$

B.22

where Y_f is the flattened width of the trunk. The total jet orifice area in the flattened region of the ith element is:

$$A_{j_{f_i}} = A_{j_i} - A_{j_{o_i}}$$

B.23

ACLS AIR BAG FORCES AND MOMENTS

The method of modeling ACLS system forces and moments is shown in the schematic of Figure B-18. The elemental bag shape model as discussed previously produces the flattened area of each segment depending on the height and attitude of the aircraft.

264

1.0

28

25

1.1

22

20

18

1.25

1.4

1.6

MICROCOPY RESOLUTION TEST CHART

DR – DOWN RANGE
CR – CROSS RANGE
RR – RADIAL RANGE

$F_{l_i} = A_{FP_{l_i}} P_t$ (left side elements)

$F_{D_i} = \mu F_{l_i}$
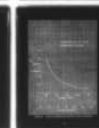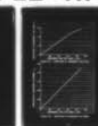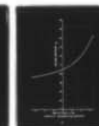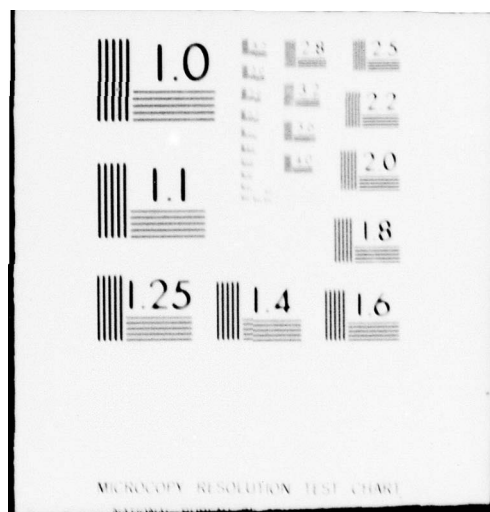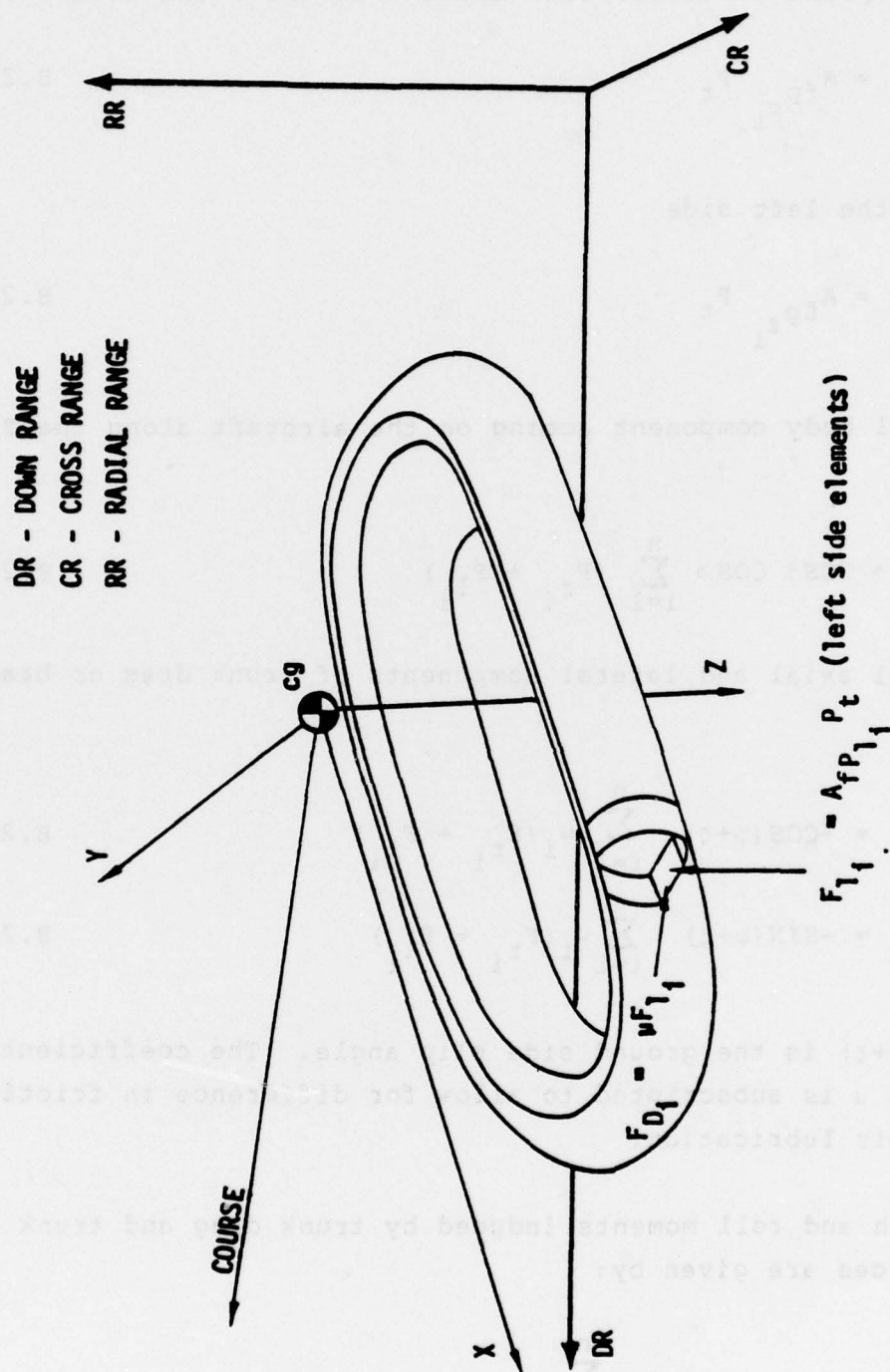
Figure B-18   Trunk Drag Forces

The foot print force for each element on the right side is:

$$F_{r_i} = A_{fp_{r_i}} P_t \qquad \text{B.24}$$

and for the left side

$$F_{l_i} = A_{fp_{l_i}} P_t \qquad \text{B.25}$$

The total body component acting on the aircraft along the Z axis is:

$$F_z = \cos\theta \, \cos\phi \sum_{i=1}^{n} (F_{r_i} + F_{l_i}) \qquad \text{B.26}$$

The total axial and lateral components of trunk drag or braking are:

$$F_{d_x} = -\cos(\psi+\zeta) \sum_{i=1}^{n} \mu_i (F_{r_i} + F_{l_i}) \qquad \text{B.27}$$

$$F_{d_y} = -\sin(\psi+\zeta) \sum_{i=1}^{n} \mu_i (F_{r_i} + F_{l_i}) \qquad \text{B.28}$$

where $(\psi+\zeta)$ is the ground side slip angle. The coefficient of friction μ is subscripted to allow for difference in friction due to air lubrication.

The pitch and roll moments induced by trunk drag and trunk foot print forces are given by:

$$M_y = F_{d_x} Z_{cg} + \cos\theta \sum_{i=1}^{n} X_{t_i} (F_{r_i} + F_{l_i}) \qquad \text{B.29}$$

$$M_x = F_{d_y} Z_{cg} + \cos\phi \sum_{i=1}^{n} Y_{t_i} (F_{l_i} - F_{r_i}) \qquad \text{B.30}$$

The yaw moment induced by trunk drag is given by:

$$M_z = \cos(\psi + \zeta) \sum_{i=1}^{n} u_i (F_{r_i} - F_{l_i}) Y_{t_i} \qquad \text{B.31}$$

$$+ \sin(\psi + \zeta) \sum_{i=1}^{n} u_i (F_{r_i} + F_{l_i}) X_{t_i}$$

AERODYNAMICS

The 6 DOF computer program which serves as the basis of the ACLS Simulation Program has built-in aerodynamic modules. Standard equations are used and expressed in Fortran statements by the user in a subroutine reserved for aerodynamic modeling. The aerodynamic drag is:

$$F_d = C_D q S \qquad \text{B.32}$$

The aerodynamic lift is:

$$F_z = C_L q S \qquad \text{B.33}$$

The aerodynamic side force is:

$$F_s = C_Y q S \qquad \text{B.34}$$

The aerodynamic yaw moment is:

$$M_z = C_n q S b \qquad \text{B.35}$$

The aerodynamic pitch moment is:

$$M_y = C_m q S c \qquad \text{B.36}$$

267

The aerodynamic roll moment is:

$$M_x = C_\ell qSb \qquad\qquad\qquad \text{B.37}$$

where S is the wing reference area, b is the reference wing span
and c is the mean aerodynamic chord. The corresponding
aerodynamic coefficients assumed for simulation are shown in
Figures B-19 through B-24, and were obtained from Reference 11.

The primary contribution to aerodynamic pitch damping for a
straight wing aircraft, such as the Jindivik, is due to the
tail. The pitch damping moment caused by a pitch rate is:

$$\frac{dC_m}{dq} = C_{m_{q_H}} \left(\frac{c}{2V}\right) \qquad\qquad \text{B.38}$$

where q, c and V are respectively the pitch rate, mean
aerodynamic chord, and the aircraft air velocity. The damping
coefficient due to the tail is given by (Reference 19):

$$C_{m_{q_H}} = -2C_{L_{\alpha_H}} \; \eta_H \; \bar{V}_H \; \frac{X_H}{c} \qquad\qquad \text{B.39}$$

The dynamic pressure pressure ratio η_H for the horizontal tail
may be assumed to be in the range:

$$0.9 < \eta_H < 1.0$$

X_H is the distance between the tail and the aircraft center of
gravity. The horizontal tail volume coefficient is given by:
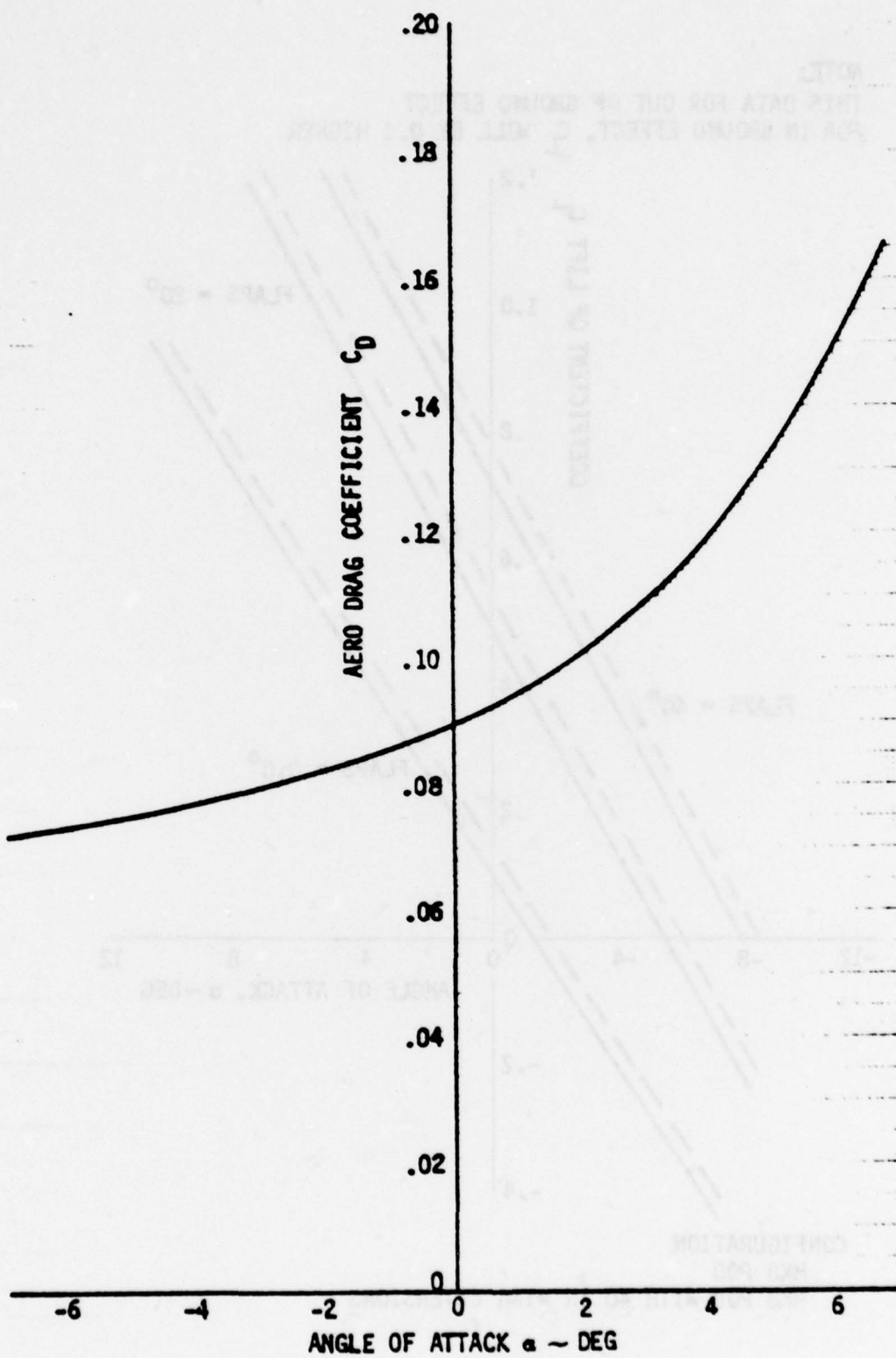
Figure B-19   Aerodynamic Drag Coefficient
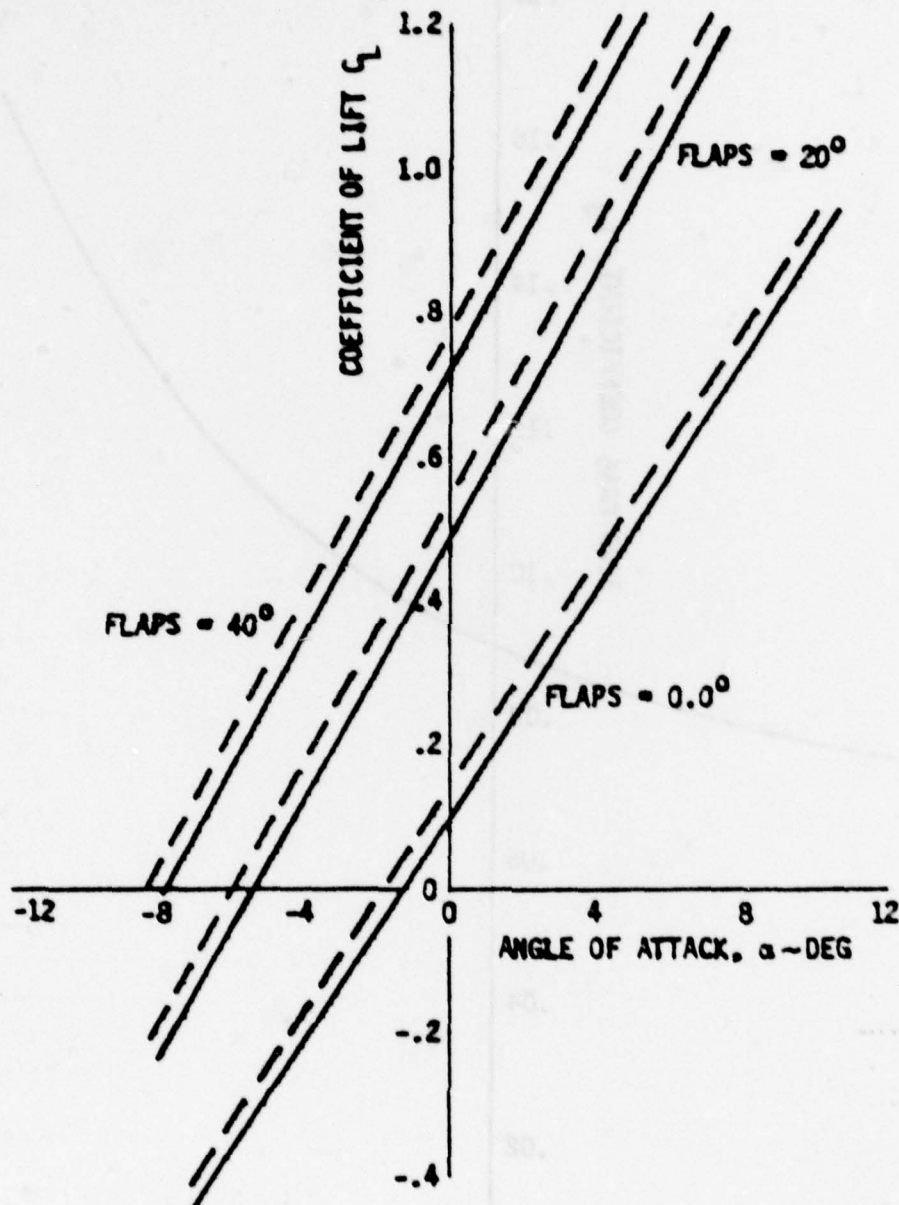
Figure B-20 Coefficient of Lift vs Angle of Attack
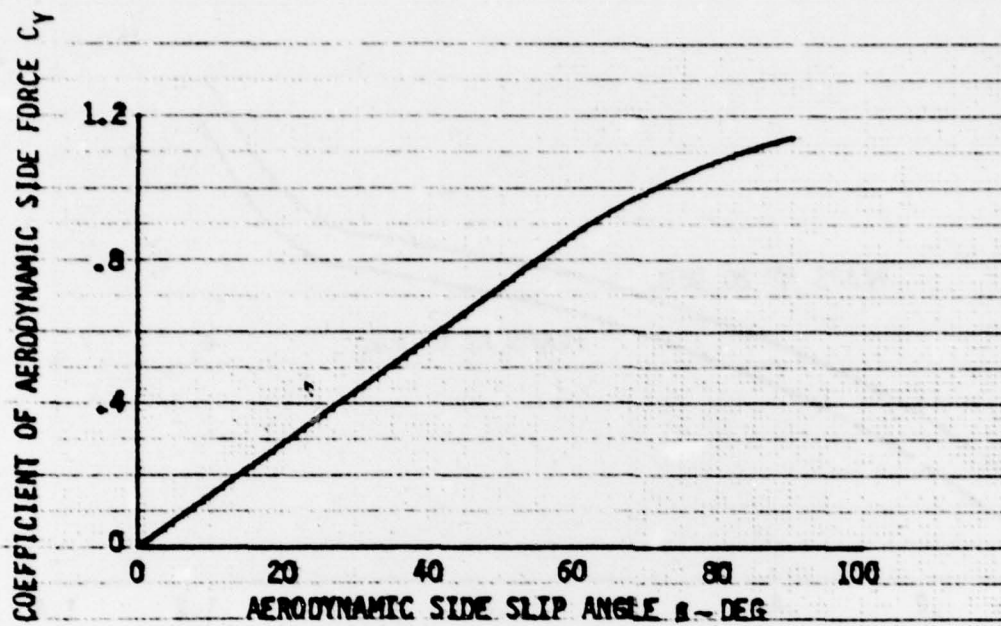
Figure B-21   Coefficient of Aerodynamic Side Force
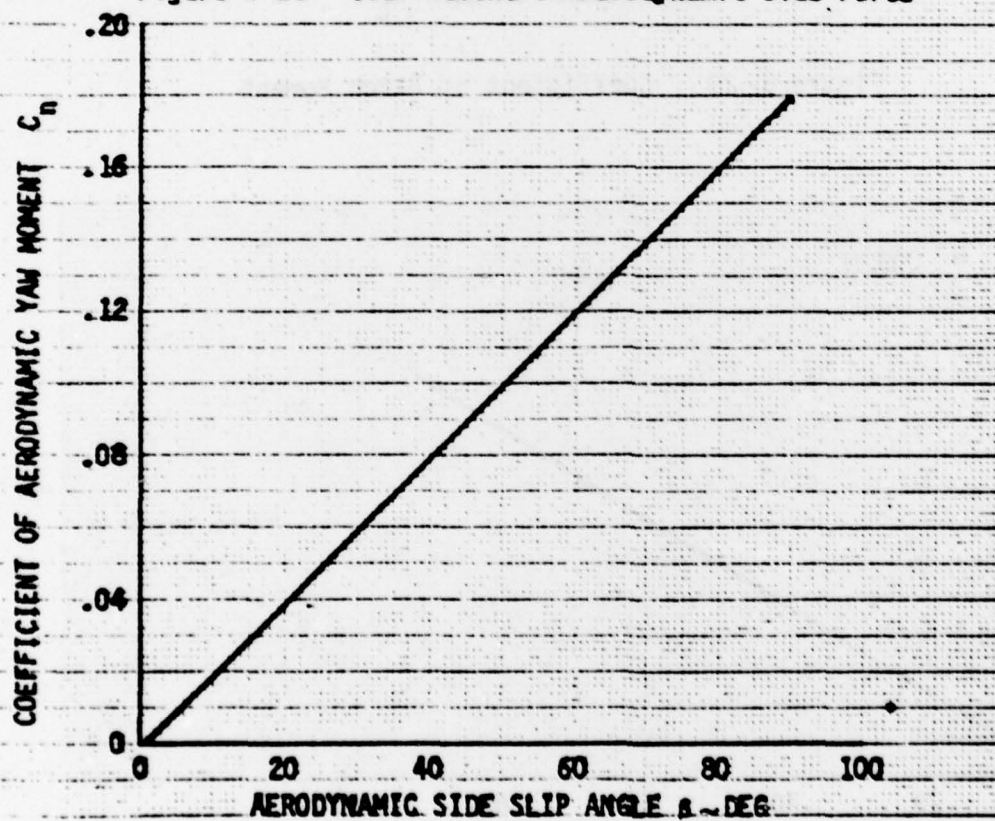
Figure B-22   Coefficient of Aerodynamic Yaw Moment

271
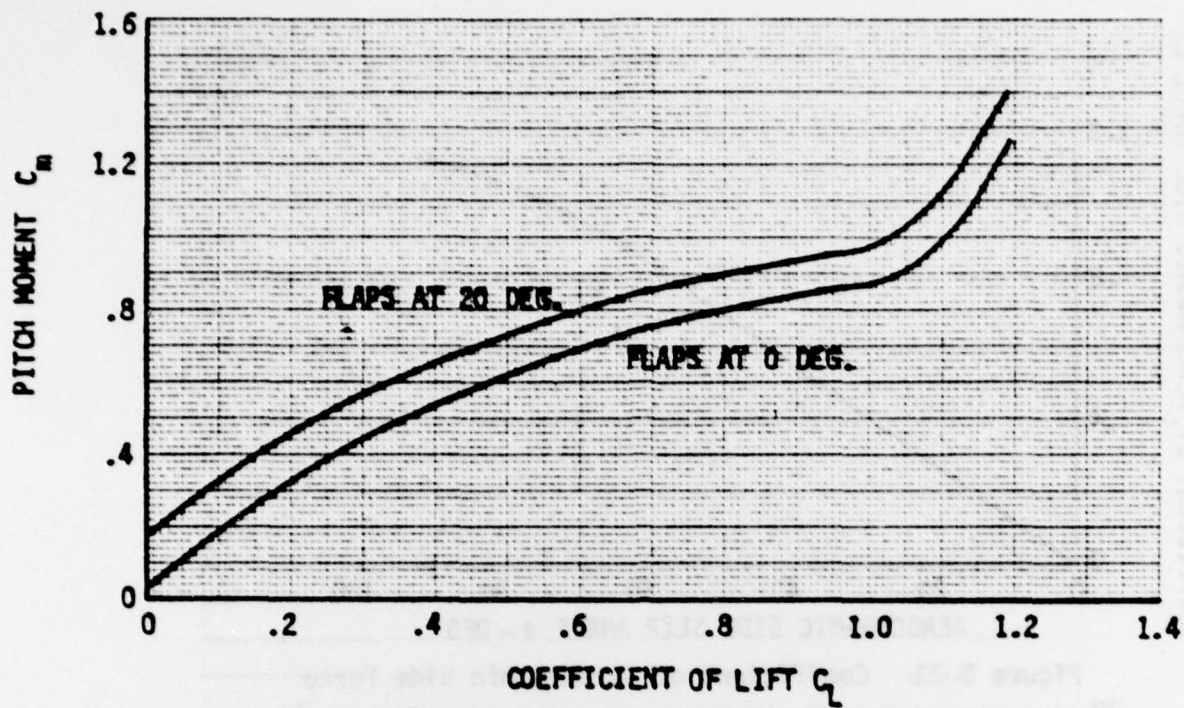
Figure B-23   Coefficient of Pitch Moment
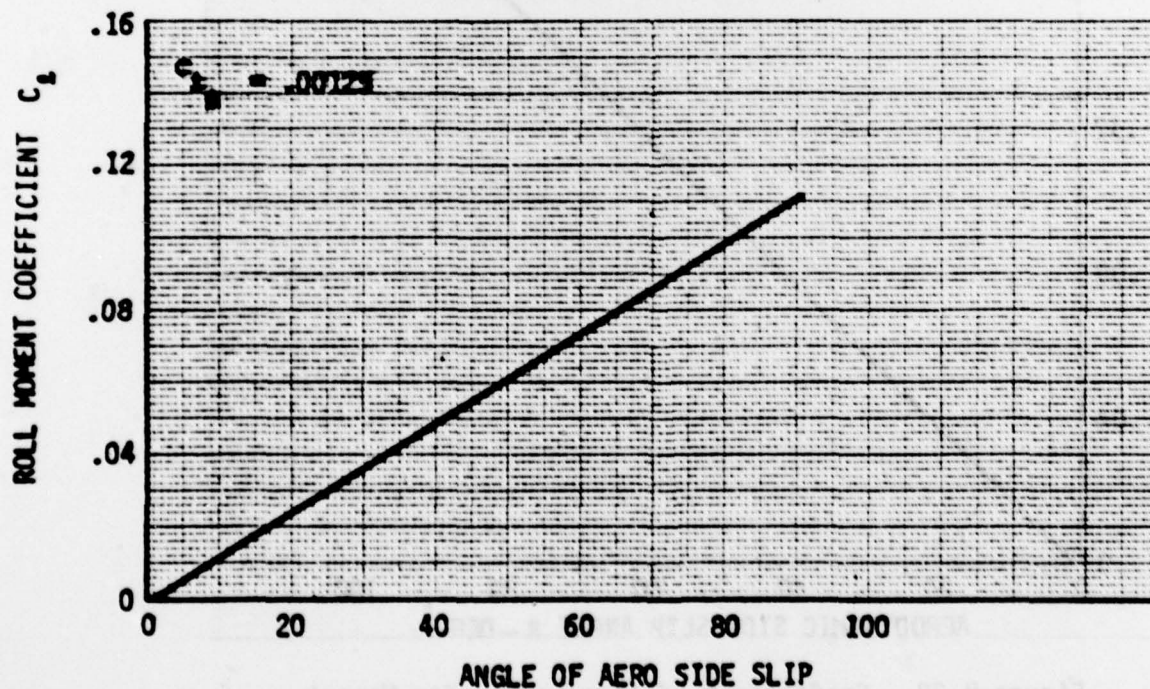
Figure B-24   Coefficient of Roll Moment

$$V_H = \frac{X_H S_H}{cS}$$

or   B.40

$$V_H = \frac{(9.8)(14.6)}{(4)(76)} = 0.47$$

The Jindivik tail aspect ratio is 3.3, the sweep angle Λ is zero, and thus, using data from Reference 19, $C_{L\alpha_H}$ = .061/degree for low Mach numbers and an efficiency of 1. From Equation B.30:

$$C_{m_{q_H}} = -2(0.061)(0.9)(0.47)\frac{9.8}{4} = -0.127/deg.$$

The damping contribution from the tail is provided by Equation B.38:

$$\frac{dc_m}{dq} = -0.127 \frac{4}{2V} = \frac{0.254}{V} \ sec^2/ft-deg$$

APPENDIX C

RECOMMENDED GROUND TEST PROCEDURES

275

TEST PROCEDURES

ACRS System Tests

A. OUT OF GROUND EFFECT

    1. Trunk Pressure Proof Test to 3.0 psig
    2. Bleed Port Static Pressure Check
        Both Valves Closed (no air flow)
        Engine speed 40%
        Engine speed 50%
        Engine speed 60%
    Pressure not to exceed allowable pressure in
    flexible ducts
    3. Landing approach Conditions
        Fan Valve Closed
        Engine speed 40%
        Engine speed 45%
        Engine speed 50%

        RECORD: Trunk pressure, bleed port pressure,
                  and relief valve opening
    4. ACRS Fan
        Both valves fully open
        Engine speed 40%
        Engine speed 50%
        Engine speed 60%

        RECORD: Trunk pressure, bleed port pressure,
                  turbine inlet pressure, fan speed,
                  relief valve opening

B. IN GROUND EFFECT (Tethered)

    1. Landing Slideout Conditions
        Fan valve closed
        Engine speed 40%
        Engine speed 45%
        Engine speed 50%

        RECORD: Trunk and cushion pressures, bleed port
                  pressure and relief valve opening
    2. Taxi Conditions
        Both valves fully open
        Engine speed 40%
        Engine speed 50%
        Engine speed 60%

        RECORD: Trunk and cushion pressure, bleed port
                  pressure, turbine inlet pressure, fan
                  speed, relief valve opening

3. Drop Tests (Landing Impact)
        Fan valve closed
        Engine speed 40%
            sink speeds 4, 6, 8 ft/sec
        Engine speed 45%
            sink speeds 4, 6, 8 ft/sec
        Engine speed 50%
            sink speeds 4, 6, 8 ft/sec

        RECORD: Trunk and cushion pressure, bleed port
                  pressure, relief valve opening
4. Drop Tests (Taxi Dynamics)
        Both valves open
        Engine speed   sink speed
            50%   1 ft/sec
            50%   2 ft/sec
            60%   1 ft/sec
            60%   2 ft/sec

        RECORD: Trunk and cushion pressure, bleed port
                  pressure, turbine inlet pressure, fan
                  speed, relief valve opening

C. TAXI TESTS

    1. Trunk Drag (Breakaway Tests)
        Both valves open
        Slowly increase engine speed to breakaway on:
            dry runway
            wet runway
            grass
            soil

        RECORD: Engine speed at breakaway trunk and
                  cushion pressure, bleed port pressure,
                  turbine inlet pressure, fan speed, relief
                  valve opening
    2. Trunk Drag (Steady State Velocity)
        After breakaway backoff slowly on throttle and
        attempt to maintain velocity 5 to 10 knots on:
            dry runway
            wet runway
            grass
            soil
        Repeat at a velocity of 30-40 knots

        RECORD: Engine speed, trunk and cushion pressure,
                  bleed port pressure, turbine inlet
                  pressure, fan speed, valve opening
    3. Batsman Control
        With the aircraft at a steady state velocity of 10 to 20
        knots, the batsman will test the response of the thrust
        vector control system by negotiating an "S" shape man-
        euver about the runway centerline, with an amplitude of

277

5 to 10 feet. The distance required to perform this
maneuver should be measured. This test should be per-
formed first with no wind, and then with a side wind of
10 to 15 knots. In the side wind condition, as
discussed in paragraph 6.3.8 of Reference 10, the
aircraft will respond rapidly to a yaw maneuver into the
side wind and sluggishly to a command to yaw out of the
side wind. The Batsman should gain a good feel for the
response of the thrust vector control system in these
conditions. The above tests should be repeated at a
vehicle velocity of 20 to 25 knots.

    RECORD: Distance required to perform "S" maneuver
          and the yaw gyro reference time history.

4. Braking Tests
    Both valves initially open
    Release tether with engine RPM at 70%
    Accelerate to test velocity (see below)
    Turn fan valve off
    Back throttle off to engine idle (40% RPM)
        Test Velocity 20 Knots
        Test Velocity 30 Knots
        Test Velocity 40 Knots
        Test Velocity 50 Knots
        Test Velocity 60 Knots
        Test Velocity 70 Knots

    RECORD: Acceleration and deceleration distances,
          trunk and cushion pressure, bleed
          pressure, aircraft pitch time history.

D. OUT OF GROUND EFFECT

  1. Parking Bladder Proof Test
      3.0 psi
  2. Fan Tests
      Engine Speed 40% RPM
      Engine Speed 50% RPM
      Engine Speed 60% RPM
      Engine Speed 70% RPM
      Engine Speed 80% RPM
      Engine Speed 87% RPM

    RECORD: Trunk pressure, bleed port pressure,
          turbine inlet pressure, fan speed.

E. IN GROUND EFFECT (Tethered)

1. Fan Tests
   Engine Speed   40% RPM
   Engine Speed   50% RPM
   Engine Speed   60% RPM
   Engine Speed   70% RPM
   Engine Speed   80% RPM
   Engine Speed   87% RPM

   RECORD: Trunk pressure and cushion pressure,
             bleed port pressure, turbine inlet
             pressure, fan speed.

F. TAXI TESTS

   Release tether with engine RPM at 87%
   Accelerate to test velocity (see below)
   Release drogue chute
   Back throttle slowly to 50% RPM
      Test Velocity   10 Knots
      Test Velocity   20 Knots
      Test Velocity   30 Knots
      Test Velocity   40 Knots
      Test Velocity   50 Knots
      Test Velocity   60 Knots
      Test Velocity   70 Knots

   RECORD: Time to accelerate to test velocity,
             trunk and cushion pressure, fan speed,
             bleed port pressure, aircraft pitch
             time history.

APPENDIX D

EVALUATION OF YAW THRUSTER CAPABILITY TO

MAINTAIN DIRECTIONAL STABILITY

A simplified feasibility analysis was made of the potential use
of the yaw thrusters to alleviate the directional instability
discussed in Section 4. The analysis shows that the yaw
thrusters are inadequate to perform the task. A description of
the analysis technique is given below.

First, it was assumed that side thrust could be generated as a
linear function of sideslip. A maximum side thrust of 20 pounds
was assumed (typical of an approach condition), to be reached at
a sidslip angle of 5 degrees. Five degrees was chosen by
reference to Figure 97, which shows that the yawing moment curve
is about neutrally stable at sideslip angles near 5 degrees.
Figure 97 was used because it is the worst case. A sketch of
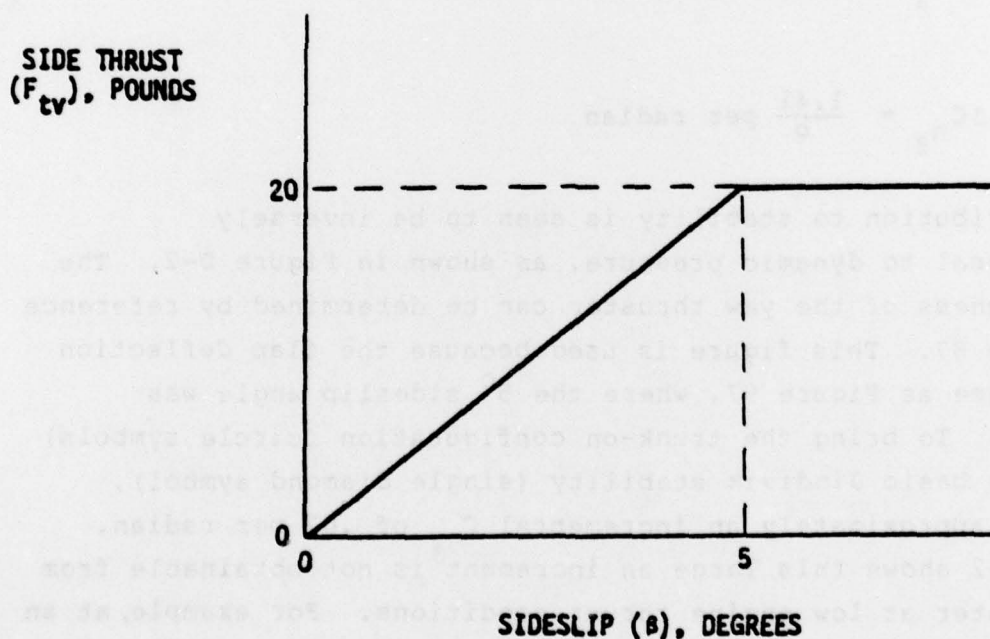the assumed thrust variation is shown below:

Figure D-1.   Assumed Side Thrust Versus
Sideslip Characteristic

281

The thruster was estimated to be 10.6 feet aft of the center of
gravity. Hence, the yawing moment generated by the thruster is
10.6 times the thrust in pounds. The increment to directional
stability produced by the thruster is then

$$\Delta C_{n_\beta} = \frac{\text{THRUST} \times 10.6}{q\,S\,b}$$

where q = dynamic pressure, psf
S = wing area, sq. ft.
b = wing span, ft.

Substituting the various constants and converting degrees to
radians, we have

$$\Delta C_{n_\beta} = \frac{20 \times 10.6 \times 57.3}{q\,(83)(20.75)(5)}$$

or

$$\Delta C_{n_\beta} = \frac{1.41}{q}\ \text{per radian}$$

The contribution to stability is seen to be inversely
proportional to dynamic pressure, as shown in Figure D-2. The
effectiveness of the yaw thruster can be determined by reference
to Figure 87. This figure is used because the flap deflection
is the same as Figure 97, where the 5° sideslip angle was
selected. To bring the trunk-on configuration (circle symbols)
up to the basic Jindivik stability (single diamond symbol),
requires approximately an incremental C_{n_β} of .07 per radian.
Figure D-2 shows this large an increment is not obtainable from
the thruster at low engine thrust conditions. For example, at an
approach speed of 130 knots, the available increment of C_{n_β} is
only .025 compared with the requirement of 07. Thus the
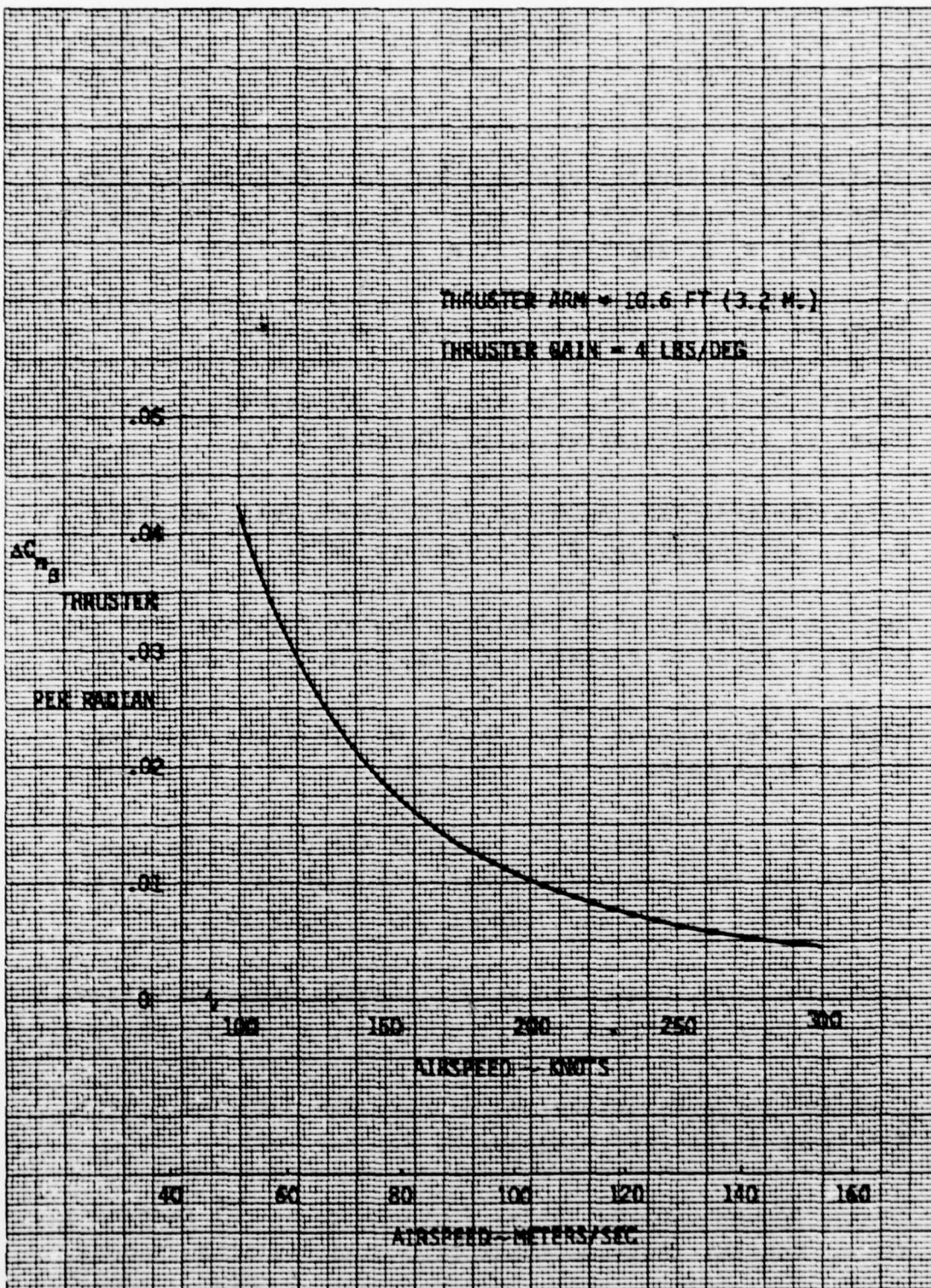concept of using the yaw thruster to stabilize the vehicle is
not feasible.

282

Figure D-2   Stability Augmentation Available From Yaw Thrusters

REFERENCES

1. Environmental Control System Simulator, Extended Version
   Computer Program, TEM-185, Boeing Document D6-58414-1,
   Matheson, N. R. and Lyons, J. R., December 1970.

2. Viper 11 Turbojet Engine, TC502/2, April 1963.

3. Private Communication, Davies, E. R. to Zeeben, J. P.,
   Viper 11 Bleed Characteristics, October 1972.

4. AFFDL-TM-75-42-TEM, ACLS Fan Performance Test, Balster,
   D. J., and Lopiccolo, R. C., January 1975.

5. Interim Technical Report-Airflow System Analysis (Task 1),
   Jindivik ACLS, D180-18862-1, Lloyd, A. J. P., June 1975.

6. ACLS Fan Performance Test, Report No. TR76-103, Balster,
   D. J., March 1975.

7. AFFDL-TR-74-64, Laboratory Tests of Air Cushion Recovery
   System for the Jindivik Aircraft, Vaughan, J. C.; Steiger,
   J. T.; Pool, D. J.; and Campbell, S.; April 1975.

8. AFFDL-TR-74-38, Design of an Air Cushion Recovery System
   for the Jindivik Drone Aircraft, Ryken, J. M., March 1974.

9. Chandler Evans Report No. 937-75-52, Yaw Thruster Control
   Electronics Package, Drapeau, D. L., May 1975.

10. Boeing Document D180-18862-2, Interim Technical Report- Yaw
    Thrust Control Analysis (Task II), Jindivik ACLS, McAvoy,
    J. J., June 1975.

11. Australian Aeronautical Research Laboratories Aerodynamic Note 159 "Investigation of Ground Effect on the Jindivik Target Aircraft", December, 1955.

12. GAF Publications GAF/B3B/1, Books 1 and 2, "Jindivik General and Technical Information.

13. Aerodynamics Technical Memorandum 222, Test Data-Low Speed Wind Tunnel Tests of Jindivik MK. 3A Carrying MK. 7 Pods, Trimble, T. H., and Politz, M. K., Figure 20, (no date).

14. Boeing Document D180-20123-1, ACLS Six Degrees of Freedom Simulation Program, McAvoy, J. J., October 12, 1976.

15. Boeing Document D2-125231-1, Generalized Six Degrees of Freedom Simulation, Engineering Description, Patha, J. T., April 10, 1968.

16. NASA CR-2530, Dynamic Heave-Pitch Analysis of Air Cushion Landing Systems, Captain, K. M., Boghani, A. B., and Wormley, D. N., Foster Miller Associates, May 1975.

17. AFFDL-TR-72-4 Part 1, Air Cushion Landing System CC-115 Aircraft, Coles, A. V., May 1972.

18. AFFDL-TR-71-50, Theory of an Air Cushion Landing System for Aircraft, Digges, K. H., June 1971.

19. Method for Estimating Stability and Control Derivatives of Conventional Subsonic Airplanes, Roskam, J., Professor of Aerospace Engineering, University of Kansas, 1971.